Bond Behaviour of Beams Reinforced with Near Surface Mounted Carbon Fibre Reinforced Polymer Rods under Fatigue Loading

by

Noran Abdel Wahab

A thesis

presented to the University of Waterloo

in fulfilment of the

thesis requirement for the degree of

Doctor of Philosophy

in

Civil Engineering

Waterloo, Ontario, Canada, 2011

AUTHOR'S DECLARATION

I hereby declare that I am the sole author of this thesis. This is a true copy of the thesis, including any required final revisions, as accepted by my examiners.

I understand that my thesis may be made electronically available to the public.

Abstract

Over the past decade, extensive research has been conducted on the strengthening of reinforced concrete (RC) structures using externally bonded fibre reinforced polymer (FRP). More recently, near-surface mounted (NSM) FRP reinforcement has attracted an increasing amount of research as well as practical applications. In the NSM method, grooves are first cut into the concrete cover of an RC element and the FRP reinforcement is bonded inside the groove with an appropriate filler (typically epoxy paste or cement grout). The FRP reinforcement is either prestressed or non-prestressed depending on the required level of strengthening. In all cases, the bond between an NSM bar and the substrate material plays a key role in ensuring the effectiveness of NSM strengthening.

The present work investigated experimentally the bond behaviour of non-prestressed and prestressed beams reinforced with near surface mounted carbon fibre reinforced polymer (CFRP) bars under monotonic and fatigue loading. Forty concrete beams were cast and tested in seven groups. The test variables considered in this study were: presence of internal steel reinforcement or not, the type of CFRP rod (spirally wound or sand coated) and the prestressing force (non-prestressed or prestressed). Twenty eight beams were strengthened with non-prestressed CFRP rods; fifteen beams without internal steel reinforcement and thirteen beams with internal steel. Ten beams with internal steel were strengthened with prestressed CFRP rods. The beams were tested in four point bending. In each group, one beam was loaded monotonically. The remaining beams were loaded under different fatigue load levels. The minimum load was kept constant for all beams at 10% of their monotonic capacity and the peak load was varied from one beam to another (denoted as a percentage of the peak load level).

Twenty eight beams were strengthened with non-prestressed CFRP rods. Bond failures for the beams with and without internal steel, strengthened with CFRP rods and tested under monotonic or fatigue loads was by debonding between the CFRP rod and the epoxy that started at the loading point and as the load was increased or cycled, the debonding spread towards the support until failure occurred. A comparison of the fatigue life curves for the beams with and without steel, strengthened with CFRP rods revealed that the sand coated rod had better bond characteristics than the spirally wound rod (at the same load range the beam strengthened with sand coated rod had a longer life than the beam strengthened with spirally wound rod). Beams with internal steel, strengthened with CFRP rods and tested under fatigue loading failed in bond at high load levels (short fatigue lives) and by rupture of the steel rebar at low load levels (long fatigue lives).

Ten beams with internal steel were strengthened with prestressed CFRP rods. The CFRP rods were prestressed to a force of 62 kN which corresponds to 45% and 40% of the monotonic capacity of the spirally wounded and sand coated rods, respectively. Almost all the beams with internal steel that were strengthened with prestressed CFRP rods failed by slipping between the CFRP rod and the epoxy that started at the support and propagated inwards towards the loading point. The exception to this was the beam strengthened with prestressed sand coated rod and tested under monotonic loading that failed by debonding between the CFRP rod and the epoxy that started at the loading point and propagated towards the support. Comparing the load range (kN) versus life curve for the beams with steel, strengthened with prestressed spirally wound

and sand coated rods that failed in bond, shows that the beam strengthened with sand coated rod has longer fatigue lives than beam strengthened with spirally wound rod.

A model was used to describe the progress of the debonding crack until excessive slipping occurred. The model predicted the number of cycles until excessive slipping between the CFRP rod and the epoxy occurred and the forces in the CFRP rod at all locations in the shear span at the onset of failure with reasonable accuracy.

Acknowledgments

I would like to express my sincere thanks and gratitude to my parents, family and friends who encouraged and supported me during the completion of this work. I doubt that I will ever be able to convey my appreciation fully, but I owe them my endless gratitude. Mum and Dad without your love, guidance, encouragement and influence on my life, I would not have made it that far. My sister Nayera, I am blessed to have you in my life.

I offer my sincerest gratitude to my supervisors, Professors Khaled Soudki and Timothy Topper from Civil Engineering at the University of Waterloo, who have supported me though out my thesis with their patience and knowledge whilst allowing me the room to work in my own way. Their expertise and understanding added considerably to my graduate experience. I am very grateful to them for the time and effort they dedicated to me. Their technical and editorial advice was essential to the completion of this dissertation and has taught me innumerable lessons and insights on the workings of academic research in general.

I would also like to acknowledge and thank Ken Bowman, from the Civil Engineering Laboratories at the University of Waterloo, for his technical assistance during the experimental phase. I would also like to thank Douglas Hirst, Richard Morrison, Terry Ridgway and Robert Sluban from the Civil Engineering Laboratories, Andy from the Mechanical Engineering Laboratories, and all the technicians from the Engineering Machine Shop, especially John Boldt, whose expertise and skills added a lot to my work. Their assistance during the experimental phase of this program is greatly appreciated. Also, I would like to thank Bonnie Neglia and Marguarite Knechtel from Civil and Environmental Engineering for their guidance and assistance.

I would also like to thank my colleagues Rania Al Hammoud, Adham El-Menoufy, Ayman Shihata, Rizwan Azam, Slamah Krem and Martin Noel in the Civil Engineering Research Group for their support and useful discussion. I would also like to express my gratitude to Isis Canada and the government of Ontario for their financial support.

Table of Contents

List of Figures

List of Tables

Chapter 1: Background and Research Objectives

1.1 General

Rehabilitation and strengthening of reinforced concrete (RC) structures is a major concern. Extensive research has been conducted using various strengthening techniques. Initially, strengthening was achieved via externally bonded steel plates, and then with the evolution of fibres, research on externally bonded fibre reinforced polymer (FRP) reinforcement was carried out. The FRP strengthening system can be prestressed or non-prestressed. An advantage of external prestressing for strengthening reinforced concrete (RC) structures is that it can provide active control of stresses and deflections for an existing structure. In addition, prestressing the FRP permits a much greater material efficiency.

Recently, near surface mounted (NSM) reinforcement has attracted an increasing amount of research that resulted in practical applications. In the NSM method, grooves are first cut into the concrete cover of an RC element and the FRP reinforcement is bonded inside the groove with an appropriate filler (typically epoxy paste or cement grout). The FRP reinforcement is either prestressed or non-prestressed depending on the required level of strengthening. The near surface mounted technique of installing FRP reinforcement has the advantage that the FRP reinforcement is embedded inside the cross section and thus protected from the surrounding environment. In addition, NSM FRP has improved bond characteristics compared to the externally bonded FRP. Also, NSM could be used in the negative moment regions of concrete slabs.

The first NSM application was in northern Sweden in 1948, when a bridge slab was strengthened in the negative moment zone (Asplund 1948). Steel bars were placed in the concrete cover and bonded with a cement grout. Before the actual strengthening was carried out, four test slabs were strengthened with the same technique and loaded to failure. The results showed that the NSM method works well for strengthening, and by March 1948 more than 600 m of steel bars were bonded in the concrete cover. (Nordin and Taljsten 2006)

In a more recent NSM application, stainless steel bars were used for the strengthening of masonry buildings and arch bridges (Garrity 2001). In addition, NSM FRP applications and research work for strengthening of reinforced concrete structures have been documented (ACI 440.2R-08). The advantages of FRP versus steel as NSM reinforcement are its better resistance to corrosion, the increased ease and speed of its installation due to its lightweight, and a smaller groove size than that for steel bars due to its higher tensile strength and a better corrosion resistance.

The near surface mounted strengthening technique appears to suit various strengthening situations and loading conditions. The structural member may be subjected to monotonic or fatigue loads. The bond of the FRP reinforcement to the concrete plays a major role in the effectiveness of NSM reinforcement. It is responsible for transferring the forces between the FRP reinforcement and the surrounding concrete, so that the section acts as

one unit. Thus, bond of the FRP reinforcement determines whether NSM is a suitable strengthening technique or not.

The performance of the bond depends on a number of parameters including; the rod cross-sectional shape and surface configuration, the groove dimensions, the shear strength of the groove filler, the degree of roughness of the groove surface, the test method and whether the applied loading is monotonic or fatigue. For prestressed systems, an additional variable is the level of prestressing force.

1.2 Components of NSM FRP system

1.2.1 FRP reinforcement

In most studies, carbon FRP (CFRP) NSM reinforcement was used to strengthen concrete structures. The tensile strength and elastic modulus of CFRP are higher than those of GFRP, so for the same tensile capacity; a CFRP rod has a smaller cross-sectional area than a GFRP rod and requires a smaller groove. This in turn leads to easier installation, with less risk of interfering with the internal steel reinforcement, and with savings in the groove-filling material.

FRP rods can be manufactured in a virtually endless variety of shapes. A variety of cross-sectional shapes (round rods, square bars and strips) are available each of which offers advantages for given practical applications. In practical applications, the choice of cross section shape depends on the constraints of the specific situation, such as the depth of the

cover, and the availability and cost of a particular type of FRP rod. Round rods are readily available and are easy to anchor in prestressing operations.

FRP rods are manufactured with a variety of surface textures, which affect their bond behaviour as NSM reinforcement. Their surface can be smooth, sand coated, or roughened with a peel-ply surface treatment. Round rods can also be spirally wound with a fibre tow, or ribbed (ACI 440.2R-08).

1.2.2 Groove filler

The groove filler is the medium for the transfer of stresses between the FRP rod and the concrete. The groove filler could be cement paste (mortar) or epoxy. In terms of structural behaviour, its most relevant mechanical properties are the tensile and shear strengths (De Lorenzis and Teng, 2007). The tensile strength is especially important when the embedded rods have a deformed surface, which produces high circumferential tensile stresses in the cover formed by the groove filler as part of the bond action.

The use of cement paste as a groove filler was explored in an attempt to lower the material cost, reduce the hazard to workers, minimize the environmental impacts and achieve better resistance to higher temperatures. The cement paste has a lower tensile strength than the epoxy paste. In pull out tests, specimens filled with cement mortar failed at a lower ultimate load than that of epoxy-filled specimens. (De Lorenzis et al., 2002)

The most common groove filler is a two-component epoxy. Low-viscosity epoxy is usually selected for strengthening in negative moment regions since the epoxy can be poured into the upward facing grooves. For other cases, a high-viscosity epoxy is needed to avoid dripping or flowing-away from downward facing grooves.

Epoxy is used as a groove filler in the experimental program conducted in this thesis (Chapter 2). Therefore, the remainder of this Chapter focuses on research conducted using epoxy as a groove filler.

1.2.3 Groove dimensions

The groove width, the groove depth, the net distance between two adjacent grooves, and the net distance between a groove and the beam edge all can influence the bond performance and hence the structural behaviour.

Based on results of bond tests for round rods within square grooves, De Lorenzis (2002) proposed a minimum value of 1.5 for the ratio between groove width to depth for smooth or lightly sand coated rods and a minimum value of 2.0 for deformed rods. Parretti and Nanni (2004) suggested that both the width and the depth should be no less than 1.5 times the rod diameter. Kalayci et al. (2010) studied the construction threshold for groove size tolerance. They tested 6 beams reinforced with 9 mm NSM FRP rods. Three groove sizes were used; (11× 11), (14×14) and (17 ×17) mm. They reported that the groove size tolerance within the studied range did not affect the response of the strengthened beams.

ACI (440.2R-08) recommends a minimum value of 1.5 times the rod diameter for both groove width and depth.

1.3 Bond of non-prestressed NSM FRP strengthened beams under monotonic loading

Several tests have been used to assess the bond strength of round NSM FRP rods. Most tests were either direct pull-out tests or beam pull-out tests. A major concern with the use of direct pull-out tests to determine the bond strength is that this test does not represent the bond forces in a reinforced concrete member. It has been suggested that bond strengths found by pull-out testing are higher than those in beams. In a pull-out test, tension is applied in an axial direction to the reinforcing rod and the surrounding concrete is restrained against the pull resulting in compressive stresses parallel to the rods which would not occur under flexural loading of a beam. (ACI 440.3)

Beam end testing or beam pull-out tests better represent the forces involved in the bond of FRP to concrete under flexural loading. This test differs than the direct pull-out test in that it does not rely on a pure axial pull-out force. Although, more complicated than direct pull-out tests, a beam pull-out test produces realistic bond strength values for flexural members. A number of practical disadvantages of beam pull-out tests have been pointed out by De Lorenzis and Teng (2007). The specimen size is large, especially if long bond lengths are tested and it is difficult to conduct the test in slip-control mode. It is also difficult to visually inspect the behaviour of the joint during loading to observe the initiation and propagation of cracks.

A number of researchers have studied the bond behaviour of NSM FRP reinforcements. Some experiments were concerned only with bond, while others investigated the embedment length for FRP reinforcement in NSM flexural strengthening. The latter experiments while not pure bond problems nevertheless addressed bond related phenomena. A summary of the work done to date and the major findings is presented below.

1.3.1 Pull out bond tests

Warren (1998) performed direct pull-out tests using a 9.5 mm diameter CFRP rod embedded concentrically in an epoxy filled plastic pipe. The groove filler was either epoxy or epoxy and sand. The observed mode of failure was interfacial failure between the rod and epoxy. De Lorenzis and Nanni (2002) and De Lorenzis et al. (2004) conducted large scale direct pull-out tests on a C- Shaped specimen, with one NSM rod in the middle of the specimen in order to evaluate the local bond strength of the NSM system. They concluded that ribbed and spirally wound CFRP shapes were the most suitable of those tested NSM systems. Also, they found a groove size to rod diameter ratio equal to 2 to be optimal.

De Lorenzis and Nanni (2002) conducted beam pull-out tests on un reinforced inverted T- beams strengthened with a single NSM FRP rod. They concluded that the surface configuration of the FRP rod influences the bond strength. Also, they concluded that increasing the groove size and thus the cover thickness leads to a higher bond strength

when failure is controlled by splitting of the epoxy cover. Yet it has no effect when a pullout failure occurs by slip of the FRP rod.

Al Mahmoud et al. (2010) conducted pull out tests on plain concrete blocks strengthened with NSM CFRP rods. The rods used were sand coated CFRP rods with a 12 mm diameter. They used epoxy or ready mixed mortar as a filler. The grooves were either (20× 20) or (30× 30) mm. For the epoxy filling, they reported that failure occurred by de-bonding at the CFRP-epoxy interface and that the ultimate load was always higher than the ultimate load obtained with the mortar filling.

Novidis and Pantazopoulou (2008) reported bond tests of short NSM FRP rods. They performed a modified pull out test on 12 mm sand coated CFRP rods embedded in a groove in a 240mm square by a 210mm long concrete block with the test rod located in a plane of symmetry of the block near the free surface. The test variables were the bonded length, the size and the surface roughness of the groove. The bonded length was 3, 5 or 10 times the rod diameter. The groove width was fixed at 20mm and the depth was either 20 or 40 mm. All the specimens failed by pull-out at the interface between the epoxy paste and the concrete. It was found that for a given groove size, the bond capacity increases with the bonded length, whereas the average bond strength decreases after a critical bonded length value, due to the non uniform distribution of bond stresses.

Failure modes in pull out tests

The following different modes of failure were reported in the literature and are shown in Figure 1.1.

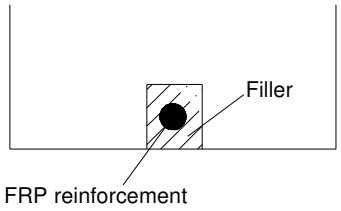

a- Cross section of the beam

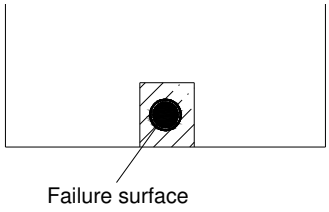

b- Failure at the FRP-filler interface

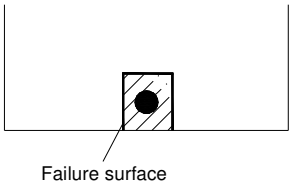

c- Failure at the filler-concrete interface

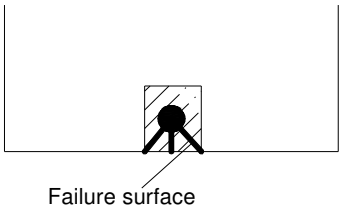

d- Splitting of the cover without cracking of the concrete

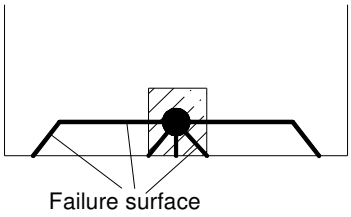

e-Cracking of the epoxy cover and fracture in the concrete

Figure 1.1: Schematic of bond failure modes of NSM system

a- Bond failure at the FRP-filler interface

Failure may occur as a pure interfacial failure at the rod to epoxy interface as shown in Figure 1.1-b. The failure mode occurs for rods with a smooth or lightly sand coated surface, where the degree of surface deformation is insufficient to provide a significant degree of mechanical interlocking between the rod and the groove epoxy and the bond resistance is primarily due to failure of the adhesion between the rod and the epoxy. For round rods, this mode tends to occur when the groove size is large (De Lorenzis and Teng

2007). Novidis et al. (2006) reported this mode of failure for sand coated CFRP rods (12mm diameter) embedded for 5 times the rod diameter in a (25 ×25) mm groove. Teng et al. (2006) performed a pull out test on a NSM CFRP strip placed in a concrete block (150 ×150 × 350mm). Epoxy was used as a groove filler. The strip dimension was 5 mm thick by 16 mm wide. The groove dimension was 9 mm wide by 22 mm deep. Failure was by pull out at the strip/epoxy interface.

Galati and De Lorenzis (2009) studied the effect of construction details on the bond performance of NSM FRP rods in concrete using direct pull-out tests to investigate the bond performance of NSM round CFRP rods in concrete. They reported that regardless of the joint length, for small grooves, bond failure was at the rod-epoxy interface accompanied by concrete cracks adjacent to the groove. For large grooves, failure was at the rod epoxy interface with no visible cracks in the concrete. They suggested using a square groove with a width to depth ratio of 2 and a development length ranging from 30 to 55 times the rod diameter depending on the type of epoxy used.

b-Bond failure at the filler–concrete interface

Bond failure at the epoxy–concrete interface may occur as a pure interfacial failure shown in Figure 1.1-c, or as a cohesive shear failure in the concrete. De Lorenzis et al. (2002) found that this mode was critical for spirally wound rods or ribbed rods with low rib protrusions, whenever the groove was pre-formed, independent of the ratio of the groove size to the rod diameter. For ribbed rods with high rib protrusions, this mode was found to be critical only for ratios of groove size to rod diameter larger than 2.0 while for

lower ratios, splitting failure of the epoxy cover dominated. Novidis et al. (2006) reported this mode of failure for sand coated 12mm CFRP rods embedded for 3, 7.5 or 10 times the rod diameter in a (25 ×25) mm groove. The cohesive shear failure mode was not observed in bond tests, but it was observed in bending tests for beams strengthened with NSM CFRP strips within the strengthened region or at the rod cut-off point (Hassan and Rizkalla 2003, Teng et al. 2006).

c- Splitting of the filler cover

Longitudinal cracking of the groove filler and/or fracture of the surrounding concrete along inclined planes is herein referred to as cover splitting as shown in Figures 1.1-d and e. This was observed to be the critical failure mode for deformed (ribbed and spirally wound) round rods. For an NSM FRP rod, the radial component of the bond stresses is balanced by circumferential tensile stresses in the epoxy cover which may lead to the formation of longitudinal splitting cracks of the cover. The concrete surrounding the groove is also subjected to tensile stresses and may eventually fail when its tensile strength is reached, causing fracture along inclined planes. Whether fracture in the concrete occurs before or after the appearance of splitting cracks in the cover or even after the complete fracture of the cover, depends on the groove size and the tensile strength of the two materials. The tensile strength of epoxy is one order of magnitude larger than that of concrete, but the epoxy cover thickness for NSM FRP reinforcement is one order of magnitude smaller than the thickness of concrete cover to internal steel reinforcement in an ordinary RC member. Moreover, longitudinal steel reinforcement in RC beams benefits from the restraint of shear stirrups, but this restraint is not available

for NSM longitudinal reinforcement. These factors explain why cover splitting is a likely bond failure mode for an NSM system (De Lorenzis and Teng 2007). Figure 1.2 illustrates how the bond mechanism of an NSM system in a pull-out test can be modelled.

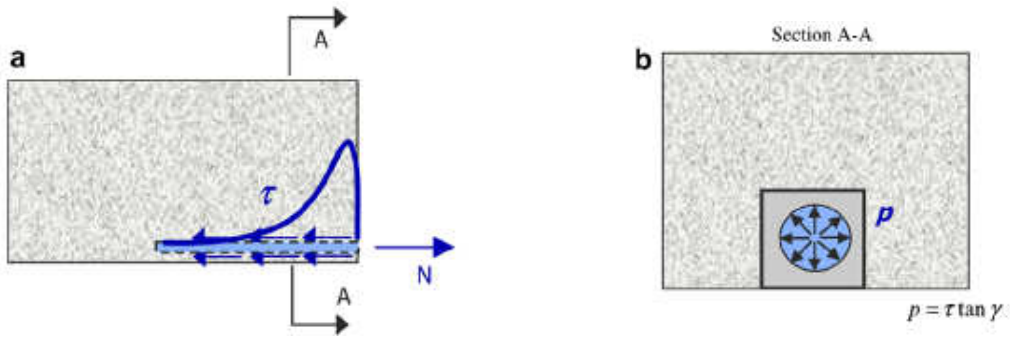

Figure 1.2: Schematic of the bond behaviour of NSM FRP reinforcement in a pullout test: (a) bond stresses in the longitudinal plane; (b) normal stresses in the transverse plane generated by a round rod (De Lorenzis and Teng 2007)

Different patterns of cover splitting failure of NSM systems occur for different ratios of groove size to rod dimension. When the ratio is very low (1.12-1.18), failure is limited to the epoxy cover and involves little damage in the surrounding concrete. For higher ratios, failure involves a combination of longitudinal cracking in the epoxy cover and fracture of the surrounding concrete along inclined planes. Concrete fracture starts as soon as the epoxy cover cracks and the tensile stresses are redistributed (De Lorenzis et al. 2004).

When an NSM rod is close to the edge of a concrete member, failure can involve the splitting of the edge concrete. This failure mode was found to occur when the edge distance is smaller than 20 mm (De Lorenzis and Teng 2007).

1.3.2 Flexural strengthening

Studies investigating the embedment length of the FRP reinforcement needed for NSM flexural strengthening examined the bond failure mechanisms. Yet, the testing was not a ‘‘pure’’ bond test as the bond performance is affected by flexural cracking. In these tests, the rod extends over the maximum moment region and is embedded for a limited length in the shear span.

Hassan and Rizkalla (2003) conducted three point bending tests on T-beams strengthened with NSM CFRP strip. The beam dimensions were as follows; total height 300mm, web width 150mm, web height 250mm and flange width 300mm.The beams were strengthened with CFRP strips (1.2 mm thick by 25 mm wide) with various embedment lengths. The strip was placed in a groove 5 mm wide by 25 mm deep. Epoxy was used as a groove filler. Eight different embedment lengths of 150, 250, 500, 750, 850, 950, 1,050, and 1,200 mm were investigated to evaluate the minimum embedment length required to develop the ultimate force of the strip. Failure of the beams strengthened with NSM CFRP strips embedded for lengths less than 850mm was by debonding at the epoxy concrete interface at the cut off sections. Beams strengthened with NSM CFRP strip embedded for lengths greater than 850mm failed by rupture of the CFRP strip.

De Lorenzis (2002) and Taljsten et al. (2003) extended the NSM FRP reinforcement over the beam supports to simulate anchorage in adjacent members. The failure was then changed to rupture of the NSM FRP rods. Yet for the beams strengthened with rods terminated away from the support they experienced an anchorage failure in the form of

slippage between the rod and the concrete in the groove. Despite this anchorage failure, De Lorenzis (2002) reported that debonding failures can still occur.

Hassan and Rizkalla (2004) conducted flexural tests on RC beams with NSM CFRP round ribbed rods of varying embedment length. Failure of the beams with NSM round ribbed rods occurred by splitting of the concrete cover at the concrete to epoxy interface followed by a complete debonding of the rods in all cases. They recommended that the development length of the kind of NSM CFRP rods tested in their investigation should not be less than 80 times the diameter of the rod.

Teng et al. (2006) tested beams strengthened with NSM CFRP strip in four point bending test with a constant moment zone of 600mm. The groove was 8mm wide by 22 mm deep cut on the tension side of the beam. The CFRP strip was 4 mm thick by 16 mm wide, embedded for various embedment lengths. The strip total length was varied as follows; 500 mm, 1200 mm, 1800 mm and 2900 mm. The beams strengthened with strips of total length of 500, 1200 and 1800 mm failed by concrete cover separation starting from the cut off section. Failure for the beams strengthened with strips of total length 1800 mm was also accompanied by debonding at the epoxy-concrete interface. The beams strengthened with strips of total length of 2900 mm failed by concrete crushing after steel yielding.

Castro et al. (2007) studied the flexural strengthening of RC 'T' beams with near surface mounted strips and rods. In their study, two reinforced concrete simply supported T-

beams, with an overall length of 4400 mm and a clear span of 4000 mm were tested. The width of the web and the flange thickness were 150 and 100 mm, respectively. The overall height of the cross section was 400 mm. The beams were internally reinforced with 2 steel rebars No. 20. The beams were tested in four point bending with a shear span of 1500 mm under monotonic loading. Each beam was strengthened with one NSM CFRP rod (10mm diameter). They reported that the beams failed by slipping of the CFRP rod followed by rupture of the CFRP rod. This was accompanied by cracking in the concrete along the rod, but there was no peeling off the concrete cover.

Kalayci et al. (2010) tested 6 reinforced concrete beams. The beams had a T-shaped cross section with a total length of 2100 mm and a clear span of 2000 mm. Grooves were cut into the soffit of the beams. Three groove sizes were investigated; (11× 11), (14×14) and (17 ×17) mm. The beams were strengthened with 9 mm CFRP rods that were 1715 mm long. All the beams were tested in three point bending. Two different modes of failure were observed: epoxy splitting and concrete splitting. The predominant failure mode in specimens with a small grove was epoxy splitting, whereas concrete splitting was observed in specimens with larger grooves.

Failure modes of flexurally-strengthened beams

Based on the available experimental evidence, the possible failure modes of beams flexurally strengthened with NSM FRP reinforcement are described in the following:

a- FRP-filler interfacial debonding

This mode involves interfacial debonding between a rod and the epoxy and has been observed for sand coated round rods (De Lorenzis et al. 2000). This mode is similar to the failure mode observed in bond pull-out tests on the same type of rods by De Lorenzis and Nanni (2002).

b- Concrete cover separation

De Lorenzis (2002) and Teng et al. (2006) observed bond cracks on the soffit of the beams in their tests. Teng et al. (2006) reported that these bond cracks are inclined at approximately 45^0 to the beam axis. Upon reaching the edges of the beam soffit, these cracks may propagate upwards on the beam sides maintaining a 45^0 inclination within the cover thickness, and then propagate horizontally at the level of the steel tension bars. The subsequent evolution of the debonding crack pattern may then occur in various forms described below:

(i) FRP end cover separation

If the beams are strengthened with NSM FRP reinforcement with a limited bonded length in the shear span, separation of the concrete cover typically starts from the cut-off section and propagates inwards (Teng et al., 2006 and Soliman et al., 2010). Soliman et al. (2010) tested beams strengthened with NSM CFRP rods with a limited bonded length in the shear span. They reported that failure was by debonding in the form of concrete cover splitting at the level of the steel reinforcement where the debonding process started at the cut-off point of the NSM-FRP rod.

(ii) Localized cover separation

Bond cracks within or close to the maximum moment region, together with the pre-existing flexural and flexural-shear cracks, may isolate triangular or trapezoidal concrete wedges, of which one or more are eventually split off. (De Lorenzis, 2002, and Teng et al., 2006)

(iii) Flexural crack-induced cover separation

It involves separation of the concrete cover simultaneously over a long portion of the NSM reinforcement, often involving one of the shear spans and the maximum moment region. This mode was observed by De Lorenzis et al. (2000) to start from the maximum moment region. This mode is similar to the intermediate crack-induced debonding failure mode observed in RC beams with an externally bonded FRP laminate.

(iv) Beam edge cover separation

NSM rods located near the edges may generate detachment of the concrete cover along the edges.

c- Filler–concrete interfacial debonding

This mode was reported by Hassan and Rizkalla (2003 and 2004) for beams with NSM rods and strips of a limited embedment length. In their study, all beams strengthened with CFRP rods failed by splitting of the concrete surface at the concrete epoxy interface.

Debonding occurred at the location where the secondary steel reinforcement was terminated.

d-Other debonding failure mechanisms

Teng et al. (2006) observed that upon the formation of bond cracks, the opening-up of these inclined bond cracks was restrained by the dowel action of NSM strips (placed vertically in the NSM grooves) which in turn tended to cause the detachment of the NSM FRP reinforcement from the soffit of the beam.

1.4 Bond of prestressed NSM FRP strengthened beams under monotonic loading

Prestressing of the strengthening FRP reinforcement has many advantages. It provides a better utilization of the FRP reinforcement, reduces the stress in the internal steel reinforcement and increases the load at which the internal steel yields. It also decreases the crack width size and the mean crack spacing resulting in more durable structures. It also reduces the deflection at service loads.

In a prestressed NSM application, the FRP reinforcement is prestressed, and then the epoxy is applied and allowed to cure before a gradual release of the prestressing force (Nordin and Taljsten, 2006, Taljsten et al., 2003, and Badawi, 2007). The release of the force in the prestressing rod creates shear stresses in the surrounding epoxy. A weak bond between the FRP reinforcement and the epoxy results in a long transfer length. Also, if

the bond is weak, the prestressing force may be lost as the member is loaded due to slipping of the rod.

Nordin and Taljsten (2006), Taljsten et al. (2003) and Badawi (2007) investigated the flexural strengthening of reinforced concrete beams using prestressed FRP rods under monotonic loading. They all concluded that prestressing increases the flexural capacity and service performance of the strengthened beams.

According to the author's knowledge, the bond of prestressed FRP reinforcement used in NSM strengthening technique has not yet been investigated.

1.5 Fatigue behaviour of NSM strengthening system

Repeated or cyclic loading produces a progressive deterioration of bond that may lead to failure at a cyclic bond stress considerably lower than the ultimate bond stress under monotonic loading. An accumulation of bond damage is thought to be caused by the propagation of micro cracks. Slip provides a measure of the deterioration of bond strength under repeated loading (Fib 2000). In the following sub section, the effect of fatigue will be introduced on the components of the NSM system:

1.5.1 Plain concrete

The fatigue strength of concrete is often defined as fraction of its monotonic strength that can be supported for a given number of cycles (ACI 215R-97). The fatigue strength is influenced by the range of loading, the rate of loading, the load history and the material

properties. Fatigue fracture of concrete is characterized by considerably larger strains and micro cracks than those found in the fracture of concrete under monotonic loading. The strain of concrete during repeated loading increases substantially beyond the value observed after the first load application which is similar to the behaviour of concrete under high sustained loads.

The design of concrete for fatigue loads may be facilitated by the use of a modified Goodman diagram as shown in Figure 1.3. This diagram is based on the observation that the fatigue strength of plain concrete is essentially the same fraction of the ultimate strength whether the mode of loading is tension or compression. The chart shows a relationship between the minimum and maximum stresses applied to concrete for a fatigue life of one million cycles. For a given minimum stress, the chart can be used to get the corresponding maximum stress for concrete to withstand one million cycles.

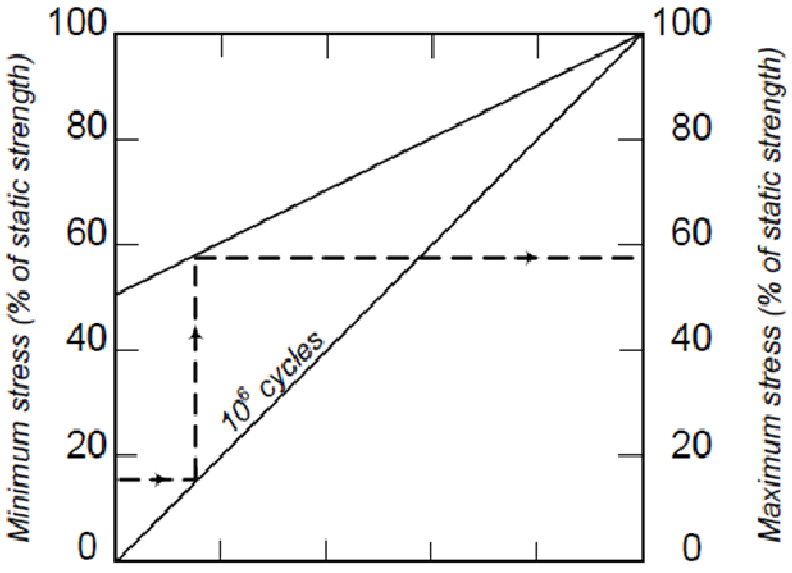

Figure 1.3: Modified Goodman Diagram (ACI 215R-97)

1.5.2 Steel bars

The fatigue life of steel bars depends on the stress range, minimum stress, bar size and geometry of deformations. Most of the stress range versus fatigue life (S-N) curves tend to show a transition from a steeper to flatter slope in the vicinity of one million cycles indicating that the reinforcing bars exhibit a practical fatigue limit. Deformed lugs on the surface of the reinforcing bars provide a good bond between the steel and the concrete. However these deformations produce a stress concentration at their base. These points of stress concentrations are where the fatigue fractures are observed to initiate. Yet, failure by fatigue of steel reinforcing bars in their application as reinforcement in concrete structures is not common (ACI 215 R-97).

1.5.3 Fibre reinforced polymer rods

Of all the types of FRP composites used for infrastructure applications, CFRP is the least prone to fatigue failure. An endurance limit equal to 60 to 70% of the initial monotonic ultimate strength of CFRP is typical. On a plot of stress versus the logarithm of the number of cycles at failure (S-N curve), the downward slope of CFRP is usually about 5% of the initial monotonic ultimate strength per decade of logarithmic life. At one million cycles, the fatigue strength is generally between 60 and 70% of the initial monotonic ultimate strength (ACI 440.2R-08).

1.6 Bond of non-prestressed NSM FRP strengthened beams under fatigue loading

Aidoo et al. (2004) and Quattlebaum et al. (2004) investigated the flexural behaviour of members strengthened with non-prestressed CFRP strips in a NSM technique under fatigue loading. They concluded that strengthening with CFRP strips increased the strength over that of control beam. Aidoo et al. (2006) tested two beams strengthened with NSM CFRP strips in three point bending. One beam was tested monotonically. The other beam was tested under fatigue loading at a load range equal to the application of an AASHTO HS25 vehicle service load for 2 million cycles, and then loaded monotonically to failure. The beam tested monotonically failed by crushing of the concrete followed by propagation of a shear crack to the level of the bottommost reinforcing steel and a splitting failure detaching the concrete cover from midspan towards one of the supports. The failure was not associated with debonding of the CFRP strip. For the fatigue test, they concluded that the application of two-million cycles of HS25 service load resulted in little significant damage accumulation and did not affect the ultimate load-carrying capacity of the girders.

Rosenboom and Rizkalla (2006) investigated the flexural behaviour of prestressed concrete beams strengthened with non -prestressed CFRP laminates in a NSM technique under fatigue loading. They found that the deterioration of the bond between the CFRP laminates and concrete during fatigue loading was a concern, and that it needed further research.

Badawi (2007) investigated the flexural behaviour of beams strengthened with non-prestressed CFRP rods in a NSM technique under fatigue loading. The mode of failure was rupture of the steel reinforcing bar. Yost et al. (2007) investigated the effect of the service level fatigue loading for 2,000,000 cycles on the monotonic strength of simply supported steel reinforced beams strengthened in flexure with NSM CFRP rods and strips. Beams strengthened with NSM CFRP rods were fatigue loaded between 3.1 kN and 20 kN (5.2% and 33.5% of the monotonic capacity) for 2,000,000 cycles, then loaded monotonically to failure. They commented that all beams survived the 2,000,000 cycles without loss in bond or force transfer.

Yun et al. (2008) investigated the response of the NSM GFRP reinforcement under fatigue loading. Three specimens were tested. The specimens consisted of two concrete prisms 200 ×200 in cross section and 400mm long joined by four steel rods embedded in each prism. Two 16 mm GFRP rods were bonded into opposite prisms with one rod on one face. The FRP rods had bonded lengths of 100 mm and 25×25 mm bonded grooves. The double-face shear specimens were tested with a vertical pulling load. One specimen was tested monotonically and two specimens were tested under fatigue load at 50% and 66% of their monotonic capacity. The specimens tested under fatigue load sustained two million cycles without failure. Then, they were loaded monotonically to failure. All specimens failed by de-bonding. The monotonic post-fatigue tests showed that the peak load was not influenced by the fatigue load amplitude.

The bond of the NSM CFRP rods under fatigue loading using full scale beam testing needs more investigation.

1.7 Bond of prestressed NSM FRP strengthened beams under fatigue loading

Badawi (2007) investigated the fatigue behaviour of the prestressed NSM CFRP strengthened RC. He reported a bond failure under cyclic loading for a beam prestressed to 40% of the ultimate strength of the rod. He commented that under cyclic loading, shear / flexural cracks started to develop leading to a redistribution of the interfacial shear stresses between the CFRP rod and the concrete. The shear stress remains a maximum at the end of the bonded length, but drops to zero at crack locations. He observed local de-bonding accompanied by a continuous increase in the slip between the prestressed CFRP rod and the epoxy with an increasing number of cycles. In a subsequent test, the ends of the beams were wrapped with transverse FRP reinforcement (300mm wide CFRP sheet that was bonded at 100 mm from the location of the support) and concluded that a bond fatigue failure was more likely for unwrapped than wrapped beams.

No other study has been undertaken to examine the bond of prestressed NSM FRP reinforcement in concrete under fatigue loads.

1.8 Bond failure for externally bonded plates

Some bond failures for beams strengthened with externally bonded plates can occur for those with near surface mounted reinforcement. In externally bonded systems, the FRP

plate is bonded to the tension side of the beam. The interface between the FRP plate and the beam is subjected to both shear stresses at the interface and stresses normal to the interface. When a flexural or flexural/shear crack intercepts a plate as in Figure 1.4, infinite strains need to be induced in the plate to accommodate the crack which cannot occur. Hence, the stress concentrations induced by the crack intercepting the plate cause the intermediate crack (IC) interface cracking in the concrete adjacent to the interface. The flexural cracks first form and then between these cracks the plate gradually debonds. Debonding starts from the flexural cracks and from where the strains are at their maximum and spread outwards towards the supports (Ohelers, 2006, Harries and Aidoo, 2006, Harries et al. 2006 and 2007).

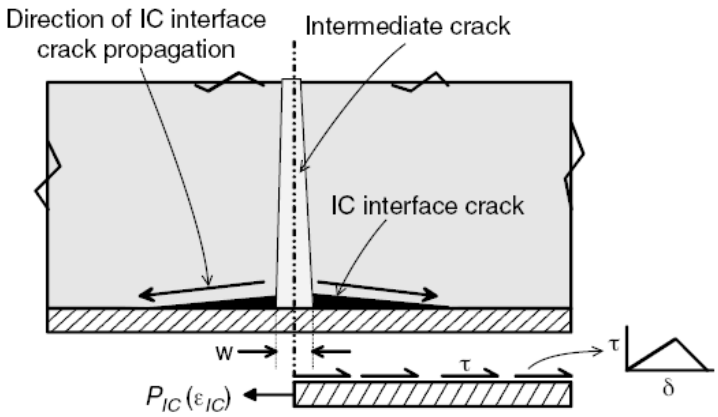

Figure 1.4: Intermediate crack debonding mechanism (Ohelers, 2006)

1.9 Summary

In the near surface mounted (NSM) method, grooves are first cut into the concrete cover of an RC element and the FRP reinforcement is bonded inside the groove with an appropriate filler. The components of NSM FRP system are: FRP reinforcement, groove filler and groove dimensions. The FRP reinforcement can be GFRP, CFRP or AFRP.

The tensile strength and elastic modulus of CFRP are higher than those of GFRP. Also, the reinforcement could be round rods, square bars or strips. The groove filler could be cement paste (mortar) or epoxy. The cement paste has a lower tensile strength than the epoxy paste. ACI (440.2R-08) recommends a minimum groove dimension of 1.5 times the rod diameter for both groove width and depth.

For non-prestressed NSM FRP under monotonic loading, most tests were direct pull-out tests or beam pull-out tests or flexural tests conducted on beams strengthened with limited length FRP reinforcement. The latter experiments while not pure bond problems nevertheless addressed bond related phenomena. The bond failure modes are mainly failure at the FRP-filler interface, failure at the filler–concrete interface or splitting of the filler cover. In addition to these modes, the flexurally strengthened beams showed concrete cover separation in the form of FRP end cover separation, localized cover separation, flexural crack-induced cover separation or beam edge cover separation.

Most of the research conducted under fatigue loading investigated the flexural capacity for beams strengthened with non-prestressed NSM FRP reinforcement. Strips were more commonly used for strengthening than rods and were found to have good bond strength. Deterioration of the bond between the CFRP laminates and concrete during fatigue loading is a concern.

Strengthening beams with NSM prestressed CFRP rods increased the flexural capacity under monotonic load. No tests were reported in the literature on the bond behaviour of NSM prestressed CFRP rods under fatigue load.

1.10 Research Needs

The repair of reinforced concrete beams using NSM CFRP rods is a relatively new technique. It is clear, from the literature review, that the majority of the research on strengthening RC beams with NSM CFRP rods has been concerned with their flexural behaviour under monotonic loading. A limited amount of research examined the bond of the NSM CFRP reinforcement to concrete mainly by pull out tests. The disadvantage of the pull out test is that it gives a higher bond stress than the real one typically expected in beam specimens. ACI (440.2R-08) recommends a design bond strength that varies between 3.5 MPa and 20.7 MPa which is a wide design range.

Prestressing the CFRP rod in NSM strengthening is a recent application. It provides a better utilization of the CFRP rod and decreases deflection and crack widths resulting in a more durable structure. The research to date focused on investigating the flexural strengthening of reinforced concrete beams with a prestressed CFRP NSM system. To the author's knowledge, no one has investigated the bond of a prestressed CFRP rod in a NSM strengthening application.

Most of the research in the literature investigated monotonic behaviour of NSM CFRP strengthened beams. A limited amount of research investigated the effects of fatigue

loading on the flexural behaviour of the NSM CFRP rods. The bond of the NSM CFRP rods under fatigue loading using full scale beam testing needs more investigation. In addition, a model that describes failure of the beams tested under fatigue load is needed.

1.11 Research Objectives

The main objectives of the research can be summarized as follow:

1- The bond between a non-prestressed CFRP rod and the surrounding concrete and the mode of failure will be investigated for beams tested under monotonic and fatigue loading in four point bending.

2- The bond between a prestressed CFRP rod and the concrete as well as the mode of failure will be investigated for beams tested under monotonic and fatigue loading in four point bending.

3- The effect of tension steel reinforcement on the mode of bond failure and bond stress distribution will be studied. This will be done by testing beams having internal tension steel reinforcement and beams without internal steel reinforcement.

4- The research will also examine the transfer length (defined as the distance from the end of the beam over which the force in the rod increases gradually from zero to the desired prestressing level) for spirally wound and sand coated CFRP rods.

5- A model that describes the process of failure including the life and the forces at failure in the shear span will be developed.

1.12 Scope

The present research work investigates, experimentally and analytically, the bond of prestressed and non-prestressed near surface mounted CFRP rods used in strengthening concrete beams under monotonic and fatigue loading.

Chapter 1 provides the background and literature review on the bond of near surface mounted FRP reinforcement. The chapter concludes with the research needs and the main objectives of the current work.

Chapter 2 presents the test program for the concrete beams strengthened with prestressed and non-prestressed near surface mounted (NSM) CFRP rods. The test matrix including information on the test specimens, fabrication and material properties is presented. It also describes the instrumentations used, the strengthening procedure and the test procedure.

Chapter 3 discusses the experimental test results for the beams strengthened with non-prestressed CFRP rods. The beams were tested under monotonic and fatigue loading. Cracking, test observations, failure mechanism, load, steel and CFRP strains for the specimens strengthened with non-prestressed CFRP rods are discussed in this chapter.

Chapter 4 discusses the experimental results for the beams strengthened with prestressed CFRP rods. The beams were tested under monotonic and fatigue loading. The strain

distributions due to prestressing and testing are presented. The transfer length results, cracking behaviour and failure mechanism of the beams are presented.

Chapter 5 discusses modelling of the experimental test results. A model was developed to simulate the bond failure of the beams. The assumptions of the model for prestressed and non-prestressed CFRP rods and steps in the calculations are given. Then, a comparison between the calculated and experimental lives and forces is carried out. Chapter 6 summarizes the main findings and conclusions of the current study.

Chapter 2: Experimental Program

2.1 Overview

This chapter presents the test program for the concrete beams strengthened with prestressed and non-prestressed near surface mounted (NSM) CFRP rods. Section 2.2 describes the test matrix including information on the test specimen, fabrication and material properties. Section 2.3 describes the instrumentation used and Section 2.4 explains the strengthening procedure. Finally, Section 2.5 describes the test procedure.

2.2 Test program

Forty reinforced concrete beams were cast and tested in seven groups as given in Table 2.1. The test variables considered in this study were: presence of internal steel reinforcement or not, type of CFRP rod (sand coated or spirally wound) and prestressing force (non-prestressed or prestressed) as shown in Figure 2.1 and Table 2.1.

Twenty eight beams were strengthened with non-prestressed CFRP rods. Of these, seven beams had no internal steel reinforcement and were strengthened with non-prestressed spirally wound CFRP rods. Eight beams had no internal steel reinforcement and were strengthened with non-prestressed sand coated CFRP rods. For handling the beams with no internal steel, steel hooks were placed on the compression side such that the beam would act as a double cantilever during handling to avoid cracking. Eight beams had internal steel reinforcement and were strengthened with non-prestressed spirally wound CFRP rods. Five beams had internal steel reinforcement and were strengthened with non-prestressed sand coated CFRP rods.

Twelve beams were strengthened with prestressed CFRP rods. Of these, two beams had no internal steel reinforcement and were strengthened with prestressed spirally wound CFRP rods. Five beams had internal steel reinforcement and were strengthened with prestressed spirally wound CFRP rods. Five beams had internal steel reinforcement and were strengthened with prestressed sand coated CFRP rods.

In each group, one beam was loaded monotonically. The remaining beams were loaded under different fatigue load levels. The minimum load was kept constant for all beams at 10% of their monotonic capacity and the peak load was varied from one beam to another as a percentage of the monotonic capacity as explained in Section 2.5. Table 2.2 gives the beam notations, the test matrix and the loading level. The first letter (S, NS) represents whether the beam did or did not have internal steel. The type of CFRP reinforcement is represented by (SW) or (SC), which stands for spirally wound or sand coated, respectively. The third number in percentage represents the level of prestressing in the CFRP rod. Thus, 0% represents non-prestressed CFRP rods and 45% represents prestressed CFRP rods to 45% of their ultimate capacity. The last number represents the peak load level as a percentage of the monotonic capacity of the beam. Thus, NS-SC-0%-65% is a beam with no internal steel, strengthened with non-prestressed sand coated CFRP and is loaded to a peak load of 65% of the beam's monotonic capacity.

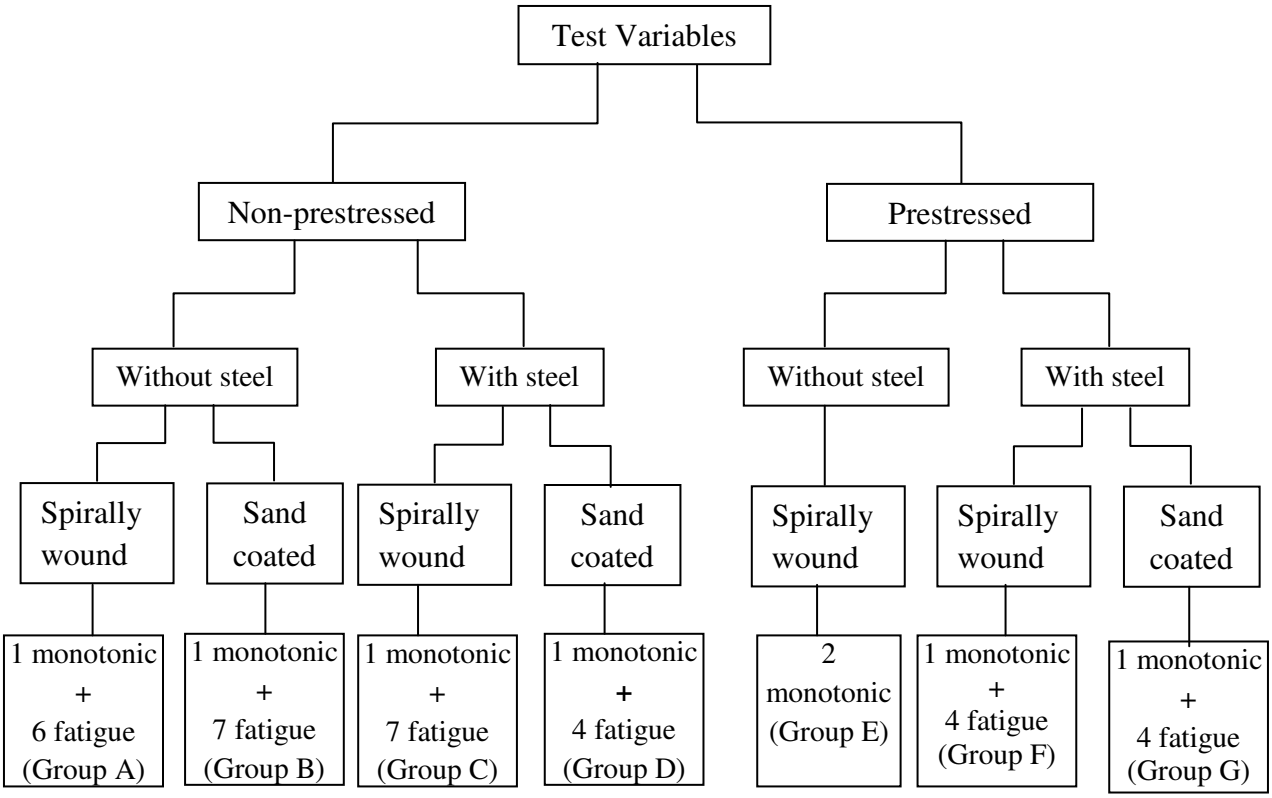

Figure 2.1: Test variables

Table 2.1: Test matrix

Group	Notation	Tensile reinforcement	CFRP rod	CFRP Prestressing Level	Number of beams
A	NS-SW-0%	No internal steel	Spirally wound	0%	7
B	NS-SC-0%	No internal steel	Sand coated	0%	8
C	S-SW-0%	2 No. 10	Spirally wound	0%	8
D	S-SC-0%	2 No. 10	Sand coated	0%	5
E	NS-SW-45%	No internal steel	Spirally wound	45% of ultimate capacity of the rod	2
F	S-SW-45%	2 No. 10	Spirally wound	45% of ultimate capacity of the rod	5
G	S-SC-40%	2 No. 10	Sand coated	40% of ultimate capacity of the rod	5

Table 2.2: Detailed test matrix

Group	Specimen notation	Min Load	Max. Load
A	NS-SW-0%-M	Monotonic (M)	
	NS-SW-0%-65%	10%	65%
	NS-SW-0%-60%(a)	10%	60%
	NS-SW-0%-60%(b)	10%	60%
	NS-SW-0%-54%	10%	54%
	NS-SW-0%-47%	10%	47.65%
	NS-SW-0%-44%	10%	44.3%
B	NS-SC-0%-M	Monotonic (M)	
	NS-SC-0%-70%	10%	70%
	NS-SC-0%-62.5%(a)	10%	62.5%
	NS-SC-0%-60%	10%	60%
	NS-SC-0%-57.5%	10%	57.5%
	NS-SC-0%-50%	10%	50%
		10%	65%
	NS-SC-0%-65%	10%	65%
	NS-SC-0%-62.5%(b)	10%	62.5%
C	S-SW-0%-M	Monotonic (M)	
	S-SW-0%-81.6%	10%	81.6%
	S-SW-0%-75.1%	10%	75.1%
	S-SW-0%-71.4%	10%	71.4%
	S-SW-0%-68.75%	10%	68.75%
	S-SW-0%-50%	10%	50%
	S-SW-0%-55%	10%	55%
	S-SW-0%-40%	10%	40%
D	S-SC-0%-M	Monotonic (M)	
	S-SC-0%-85%	10%	85%
	S-SC-0%-81.3%	10%	81.3%
	S-SC-0%-78%	10%	78%
	S-SC-0%-76%	10%	76%
E	NS-SW-45%-M(a)	Monotonic (M)	
	NS-SW-45%-M(b)	Monotonic (M)	
F	S-SW-45%-M	Monotonic (M)	
	S-SW-45%-70%	10%	70%
	S-SW-45%-65%	10%	65%
	S-SW-45%-60%	10%	60%
		10%	62.5%
	S-SW-45%-63%	10%	63%
G	S-SC-40%-M	Monotonic (M)	
	S-SC-40%-63%	10%	63%
	S-SC-40%-58%	10%	58%
	S-SC-40%-53%	10%	53%
		10%	56%
	S-SC-40%-60%	10%	60%

2.2.1 Test specimen

The beams were 150 mm wide × 250 mm deep × 2200 mm long. Twenty three beams had 2 No. 10 deformed bars as tension steel reinforcement and seventeen beams had no tensile steel reinforcement. The beams without tension steel reinforcement had Acrylic bars (12.5mm diameter) as tensile reinforcement to help in caging. All beams had 8mm diameter smooth bars as compression steel reinforcement. All beams were reinforced in shear with deformed bars No. 10 (11.3 mm diameter) closed stirrups spaced at 100 mm centerline to centerline except above the support where the stirrup spacing was reduced to 50 mm to avoid any crushing of the concrete due to high bearing stresses. The concrete clear cover (measured from the stirrup to the concrete surface) for the tension and compression steel reinforcement was 40 and 20 mm, respectively. Figure 2.2 shows a schematic of the beam dimensions and reinforcement details.

The specimens were fabricated using three concrete batches. The beams were first cured for 28 days after concrete placement and then grooves were cut into the tension soffit of the beam. The grooves were 15 mm wide × 25 mm deep × 2200 mm long as recommended by ACI 440.2R-08. Then, the beams were strengthened with either a spirally wound or sand coated CFRP rod that was inserted into the groove.

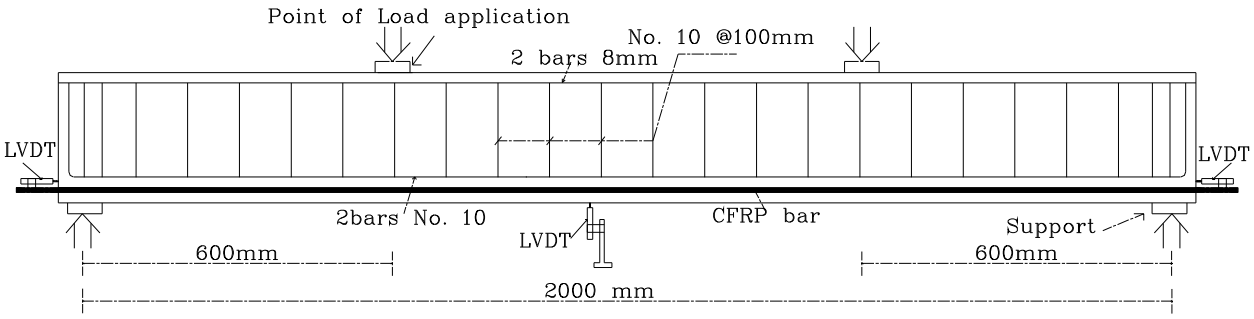

a- Beam elevation

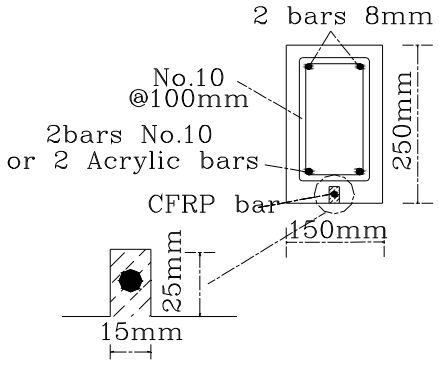

b- Cross section of the beam and groove dimensions

Figure 2.2: Schematic showing the beam dimensions and test setup

2.2.2 Specimen fabrication

Reinforcing steel cages were assembled and re-usable wood forms were oiled. The cages were then placed in the forms on plastic chairs with the tensile steel at the bottom. Ready-mixed concrete was delivered by truck and poured into the form and vibrated with vibrators as shown in Figure 2.3. The surface was finished by trowelling. Four hours after finishing the surface, the beams were covered with wet burlap and plastic sheets. The beams were sprayed with water twice a day for a whole week then they were removed from the forms and were covered with wet burlap and polyethylene sheets for another week. Then for the following two weeks they were left to dry in the air.

a-Steel cages inside the wooden forms

b- Concrete pouring

c- Concrete vibration

d- Concrete beams after finishing

Figure 2.3: Casting concrete into the forms

2.2.3 Material properties

Concrete

Three concrete pours were used to fabricate the specimens. The aggregate used was 20mm diameter (maximum). Twenty one standard cylinders, 100mm diameter ×200mm long, were cast from each pour. Six cylinders were tested at each of the ages of 7, 21 and 28 days. The average concrete compressive strength at 28 day was approximately 60 MPa. Table 2.3 shows the compressive strength at 28 days for different concrete pours. The third column shows the specimens fabricated from each batch.

Table 2.3: Average cylinder strength at 28 days for different concrete mixes

Mix #	Compressive strength (MPa)	Specimens
1	60.4MPa ± 6MPa	All the beams tested monotonically Beams without internal steel and strengthened with non-prestressed spirally wound rods and tested under fatigue load.
2	60MPa ± 2.6MPa	Beams with internal steel and strengthened with prestressed or non-prestressed rods and tested under fatigue load.
3	60.3MPa± 1MPa	Beams without steel and strengthened with sand coated CFRP rods and tested under fatigue load in addition to four extra beams with internal steel.

Reinforcing steel

Deformed No. 10 reinforcing steel bars (diameter of 11.3mm) were used as tensile and shear reinforcement. The steel had a nominal yield strength of 510 MPa and a nominal ultimate strength of 630 MPa according to the manufacturer's data sheet.

CFRP rods

The mechanical properties for the carbon fibre reinforced polymer (CFRP) rods were provided by the manufacturer. The rods were supplied by Hughes Brothers. Two different types of CFRP rods were used: sand coated rods and spirally wound rods as shown in Figure 2.4. The spirally wound and the sand coated rods had a nominal diameter of 9 mm and 9.5 mm, respectively. The mechanical properties of the CFRP rods as provided by the manufacturer were: tensile strength of 1970 MPa (spirally wound) or 2166 MPa (sand coated), modulus of elasticity of 136 GPa (spirally wound) or 130 GPa (sand coated) and average ultimate strain of 1.45% strain (spirally wound) or 1.67% (sand coated). Table 2.4 shows the properties for the used CFRP rods.

a- Spirally wound (SW) CFRP rod

b- Sand coated (SC) CFRP rod

Figure 2.4: Different CFRP rod types

Table 2.4: Properties of CFRP rods

	Spirally wound	Sand coated
Nominal diameter(mm)	9	9.5
Tensile strength (MPa)	1970	2166
Modulus of elasticity (GPa)	136	130
Ultimate strain (%)	1.45	1.67
Area (mm^2)	70*	71.3

*: calculated

Epoxy

Sikadur® 30 was used for bonding the CFRP rods inside the groove. The mechanical properties of the epoxy used as provided by the manufacturer were: tensile strength at seven days is 24.8 MPa, shear strength at 14 days is 24.8 MPa, an elongation at failure of 1% and a modulus of elasticity of 4.48 GPa.

Acrylic bars

The acrylic bars were used to hold the cage in the plain concrete beams. They were 12.5 mm (0.5 inch) in diameter. They had an ultimate tensile strength of 54MPa, an elongation at break of 2.4%, a modulus of elasticity of 2.8 GPa and a flexural yield strength of 81 MPa.

2.3 Instrumentation

Strain gauges were mounted on the tension steel reinforcement, the concrete and the CFRP rod to monitor their behaviour during prestressing and loading. The strain gauges were supplied by Tokyo Sokki Kenkyujo Co., Ltd. Five (5) mm long gauges were used for the steel reinforcement

and the CFRP rod. Sixty (60) mm long gauges were used for the concrete. The strain gauges had a resistance of 120±0.3 ohms with a thermal expansion of 11 PPM/ºC.

Seven strain gauges were mounted on the tension steel; 3 gauges at each beam end at 125mm, 250mm and 375mm measured from centerline of the support and one gauge at midspan. The ribs were first ground flat, then the surface was cleaned before placing the strain gauge. Four strain gauges were mounted on the CFRP rod at each end at 125mm, 250mm, 375mm and 500mm measured from the centerline of the support in addition to one gauge at midspan as shown in Figure 2.5. For the sand coated rods, the coating was removed over a small distance just enough to glue the strain gauge. After placing the strain gauge on either the steel rebar or the CFRP rod, the strain gauge was waxed and coated with V-M tape (3mm thick). This local protection was used to minimize the disturbance to the bond (between the reinforcement and the concrete or the epoxy) by the strain gauges as much as possible. Five strain gauges were mounted on the concrete; 2 gauges on each side at 125mm and 375mm measured from centerline of the support and one gauge at midspan.

a- Strain gauge on CFRP rod

b- Strain gauge on steel rebar

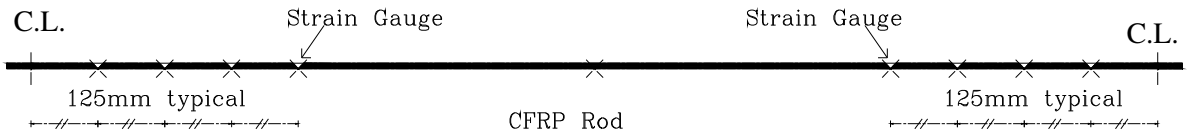

c- Strain gauge location on CFRP rod

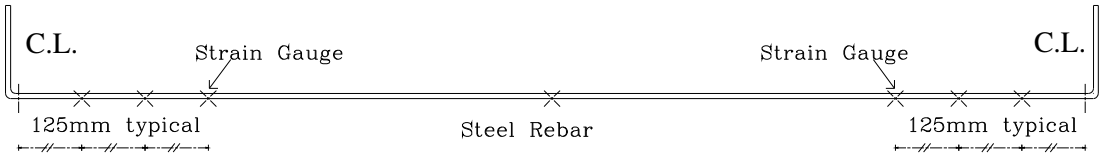

d- Strain gauge location on steel rebar

Figure 2.5: Strain gauges and their location on CFRP rod and steel rebar

Two linear variable differential transformers (LVDTs) were attached to the CFRP rod at each end of the beam to measure the slip between the rod and the concrete as shown in Figure 2.6. The vertical deflection of the beam was measured using an internal LVDT on the loading ram and an external LVDT at midspan.

Figure 2.6: LVDTs attached to the CFRP rod to measure end slip

2.4 Specimen strengthening

2.4.1 Groove cutting

For this stage, the beams were turned upside down such that the tension steel was at the top. Grooves were cut along the centerline of the beam in the longitudinal direction. The tension side of the beams was centered and chalk marked with 2 lines 15mm apart. Then, using a diamond concrete saw, the 2 marked lines were cut into the concrete and the remaining pieces were chipped as shown in Figure 2.7. The grooves were 15 mm wide × 25 mm deep × 2200 mm long as recommended by ACI 440.2R-08.

a- Beams before cutting the groove

b-Grooves being cut in the concrete

c-Chipping concrete pieces from the groove

d-The final Groove

Figure 2.7: Cutting the grooves in the beams

2.4.2 Application of non-prestressed NSM CFRP rods

The beams strengthened with non-prestressed CFRP rods were prepared as follows. The grooves were cleaned with compressed air. Then, the grooves were half filled with epoxy, and the CFRP rod was placed in the groove and pressed into the epoxy. Then, the remainder of the groove was filled with epoxy as shown in Figure 2.8. The epoxy was left to cure for 7 days.

a- Groove half filled with epoxy

b- Rod placed and pressed into the epoxy

c- Groove completely filled with epoxy

Figure 2.8: Beams strengthened with non-prestressed CFRP rods

2.4.3 Application of prestressed NSM CFRP rods

The procedure for strengthening beams with prestressed NSM CFRP rods is described in the following.

Prestressing set up, monitoring and release

Prestressing was carried out according to the procedure described by Al Mayah (2004) and Badawi (2007). The CFRP rod was prestressed to a force of 62 kN which corresponds to 45% of

the monotonic capacity of the spirally wounded rods and to 40% of the monotonic capacity of the sand coated rods. The prestressing set up is shown in Figure 2.9. It consists of 2 prestressing chairs, 3 clamps, 2 load cells, a hydraulic jack and spacers. The clamp was used to grip the CFRP rod during the prestressing operation. The clamp consists of two steel blocks with a half circular groove along each block to form a circular hole with the same diameter as the outer diameter of the sleeve. An annealed aluminium sleeve was used to encase the rod and avoid the crushing of the fibres under high confinement pressure. The two blocks were fastened to each other by six prestressed bolts, three bolts on each side of the rod.

Before starting the prestressing, the 3 clamps were tightened. All the strain gauges were connected to the data acquisition system to monitor the prestressing strain. The prestressing force was applied using the hydraulic jack and thus the piston would push against clamp 1. The force in the rod was monitored through the load cell readings at both the dead and live end. Once the desired force was reached in the rod the screw adjustor was tightened. Thus, the force would be locked between clamps 2 and 3. Then the piston was released and clamp 1 would be free. The groove was then completely filled with epoxy that was allowed to cure for at least six days before the prestressing force was released. During the six days, the load cell and the strain gauge readings were monitored. On the 7^{th} day, the force was released gradually. This was carried out by loosening the bolts of the clamps at the free end and re-tightening them to a lower clamping force. The same process was done for the middle bolts and for the two bolts nearest to the beam side. The load in the CFRP rod at the free end drops gradually in each full rotation of the nut. This process was repeated several times until the load dropped to zero. Thus, using this procedure the prestressing force was transmitted gradually to the beam.

Transfer length measurements

During prestressing, the CFRP gauges were connected to a data acquisition system to monitor the strain behaviour along the rod. Once the rod was fully prestressed the strain gauge readings at all locations were equal to the prestressing strain (0.65% for the spirally wound rod and 0.69% for the sand coated rod). During release of the prestressing force, the strain gauge measurement indicated the remaining strain in the CFRP rod. When a rod was released, the strain in the rod at the free end dropped to zero. The free end is considered to start from the point where the epoxy was terminated (the centerline of the support). During release, some slip occurred between the CFRP rod and the epoxy and the crack front shifted inward for a distance (s_i). The CFRP rod slip from the epoxy could be represented by a crack at the interface of the CFRP rod and the epoxy with the tip of the crack (location of maximum shear stress due to prestressing as discussed in Chapter 4) referred to as the crack front. The distance (s_i) for the two types of rods will be discussed in Chapter 4. Beyond this point, the strains in the rod increased with distance along the rod until it reached the prestressing strain. The distance from the crack front until the strains in the rod reach the prestressing strain is called the transfer length and is typically as shown in Figure 2.10. The experimental transfer lengths and the predicted ones will be presented in Chapter 4.

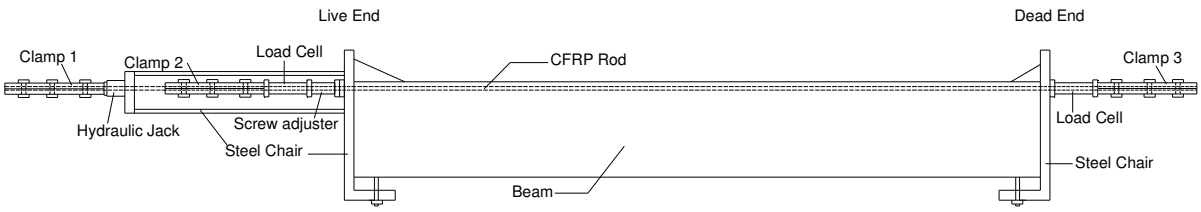

a- Schematic showing the prestressing set up

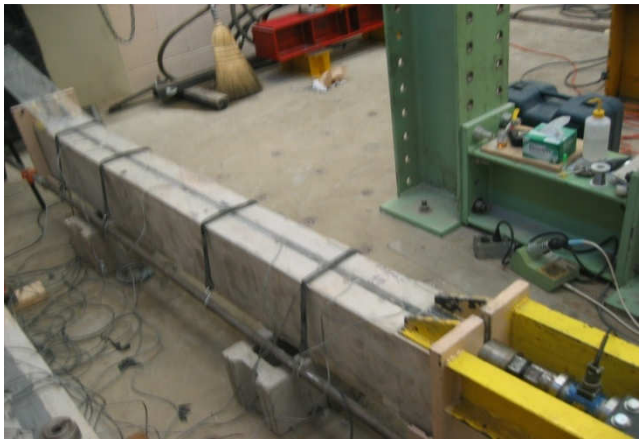

b- Prestressing the CFRP rod

c-Set up at live end

d-Set up at dead end

Figure 2.9: Strengthening the beam with a prestressed CFRP rod

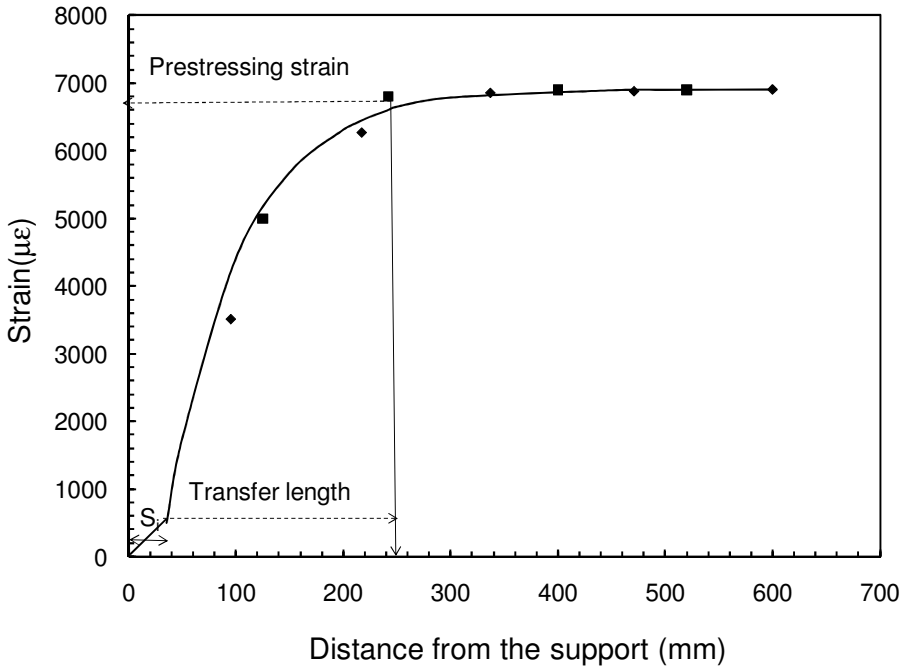

Figure 2.10: Transfer length for a typical CFRP rod

2.5 Test procedure

The beams were tested in four-point bending with a shear span of 600mm using a servo-hydraulic actuator controlled by a MTS 407 controller. The test set up is shown in Figure 2.11. The beam had a hinge support at one end and a roller support at the other. The hinge support was a half cylinder resting on a curved plate. The roller support was a steel cylinder between two curved plates. Two steel plates, each 42mm wide x 112 mm long, were used at each side underneath the beam. The plates were centered in the cross section. At each end, the beam was resting on 2 plates that were resting on the support as shown in Figure 2.12. The reactions at the supports would produce compressive forces at the bottom face of the beam. When the beam rests directly on a bearing plate, these compressive forces increase the frictional force on the CFRP rod and increase the shear stress between the rod and the epoxy. Thus, the support shown in Figure 2.12 was aimed at minimizing the compressive forces transmitted from the supports to the CFRP rod.

Figure 2.11: Test set up

a- Hinge support

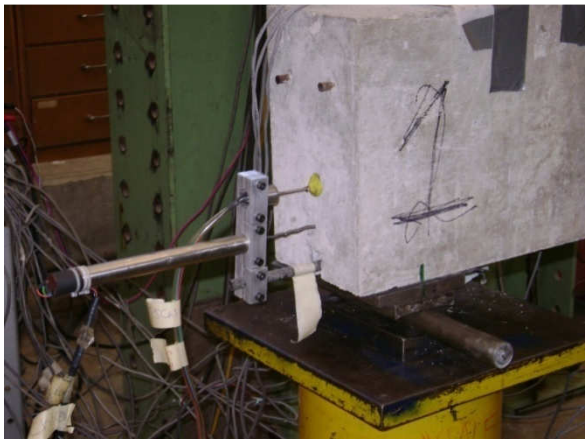

b- Roller support

Figure 2.12: Support system for the test set up

Load was measured using a 222kN (50kip) load cell mounted on the actuator. The monotonic loading was applied in displacement control at a rate of 1mm/min. The monotonic load was increased from zero load until failure occurs in the test specimen. The fatigue loading was load-controlled at a frequency of 1 or 1.5 Hz depending on the expected fatigue life of the beam. For longer expected lives (lower load levels), the frequency was 1.5 Hz. For shorter expected lives (higher load levels), the frequency was 1 Hz. In the fatigue tests, the beam was loaded manually

to the peak load, where the strains and deflection were recorded, and then the load was dropped to the mean value. The controller was then used to automatically increase and decrease the load to the maximum and minimum value using a sine curve as shown in Figure 2.13. A displacement limit equal to the deflection recorded in the first cycle plus 15 mm was input to the controller. The deflection limit ensures that the test stops when extra deflection occurs as the specimen fails (to guard against collapse). The minimum load was kept constant for all beams at 10% of their monotonic capacity. The maximum load was varied to achieve a fatigue life within a reasonable number of cycles. The beam loaded to the highest load level (shortest life) was tested first followed by beams loaded to lower load levels (longer life). When a beam sustained one million cycles without failure, it was considered to be a run out (the run out load is the load that could be safely applied to the beam for one million cycles). If a beam experienced a run out, the load was reported and then increased to a higher level. Fatigue failures occurred in the form of steel rebar rupture, shear failure in the concrete, or bond failure at the CFRP rod – epoxy interface. Fatigue failures were accompanied by excessive deflection at midspan at which time the controller interlocked and the test was terminated.

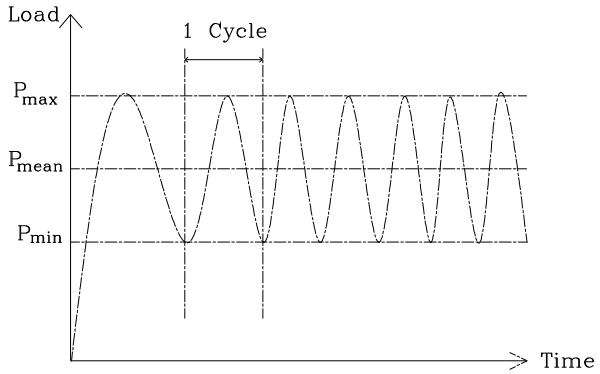

Figure 2.13: Fatigue loading

Chapter 3: Experimental Results for Non-Prestressed Beams

3.1 General

This chapter discusses the experimental test results for the beams strengthened with non-prestressed CFRP rods. The monotonic test results are discussed first followed by the cracking and the failure mechanism for the beams tested monotonically. Then, the fatigue test results are discussed followed by a discussion of the strain distribution along the CFRP rod at failure.

3.2 Monotonic test results

3.2.1 General

Four beams were tested under monotonic load. Table 3.1 summarizes the peak loads and modes of failure of the monotonic beams. All the beams failed by debonding between the CFRP rod and the epoxy that started at the loading point and propagated towards the support. The specimen nomenclature was explained earlier in Chapter 2 (Section 2.2).

Table 3.1: Peak loads and mode of failure for all monotonic beams

Group	Specimen notation	Max. Capacity (kN)	Failure mode
A	NS-SW-0%-M	87.6 kN	Bond
B	NS-SC-0%-M	92.5 kN	Bond
C	S-SW-0%-M	161.34 kN	Bond
D	S-SC-0%-M	147.8 kN	Bond

3.2.2 Load –deflection behaviour

Figure 3.1 shows a typical load versus midspan deflection curve for beams strengthened with non-prestressed CFRP rods and tested under monotonic load. Figures for each beam are provided in the appendix. As the load increases, the midspan deflection increases until concrete cracks at midspan (at about 30 kN in Figure 3.1). Past midspan cracking, load versus deflection slope decreases and midspan deflection continues to increase as the load increases until peak load is reached.

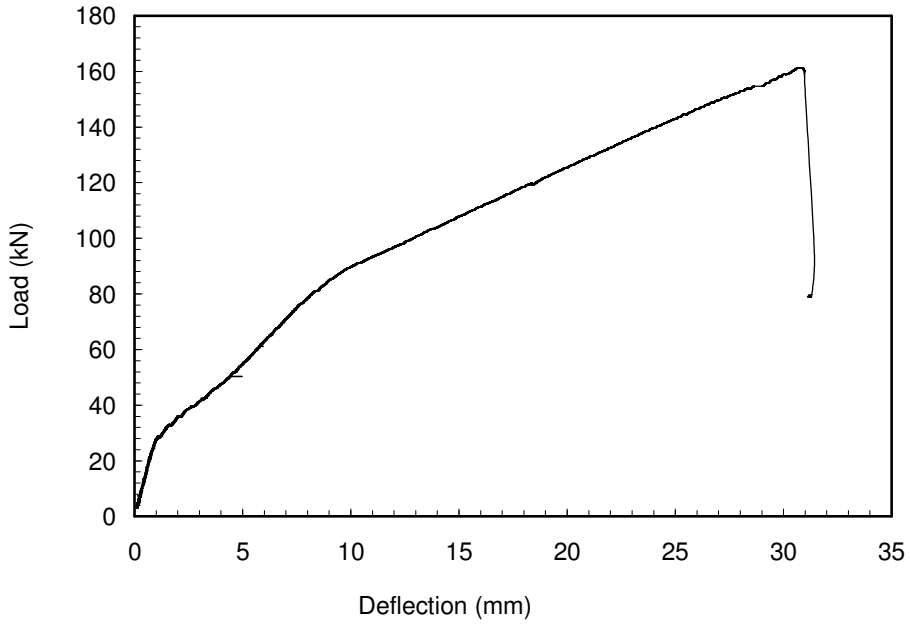

Figure 3.1: Load versus midspan deflection for beam S-SW-0%-M

3.2.3 Beam with no internal steel and strengthened with spirally wound CFRP rod

Cracking behaviour

Beam NS-SW-0%-M had no internal steel and was strengthened with spirally wound CFRP rod. Figure 3.2-a shows the load versus CFRP strain gauge measurements and Figure 3.2-b shows the load versus the end slip between the CFRP rod and the concrete. The CFRP strain

increases at a low rate with increasing load until the load reaches a level at which the concrete at midspan cracks. Then the reading of the strain gauge located at midspan increased as the tensile forces in the cross section were suddenly transferred to the CFRP rod. There was also a change in the slope of the load- strain curve at midspan. As the load increased further, cracks were observed in the shear span close to the location of the load application location and progressed towards the supports. The first cracks that appeared in the shear span were underneath the loading point and at 100mm from the loading point. Then a crack appeared at about 170 mm from the loading point. As each crack occurred, the reading of the strain gauge located nearest to the crack increased suddenly as the tensile forces were transferred from the concrete to the CFRP rod. As the test proceeded, the crack at 170 mm from the loading point was at all times noticeably wider than any of the other cracks. As the load approached its peak value, the inclined cracks close to the loading point widened and propagated through the depth of the beam. These cracks connected with the large vertical crack at 100mm from the loading point, isolating a prism of concrete as shown in Figure 3.3-a. At the peak load, debonding occurred between the CFRP rod and the epoxy and an isolated prism of epoxy covered with concrete separated from the CFRP rod and the beam as shown in Figure 3.3-b. At the same time, longitudinal cracks occurred in the concrete surrounding the groove in the shear span and chunks of epoxy covered with concrete separated from the bottom of the beam as shown in Figure 3.3-c. Closer to the support, the longitudinal cracks in the concrete were visible, but the epoxy and the concrete did not separate from the rod (Figure 3.3-d). At failure, the slip between the CFRP rod and the beam end was 13 mm and coincided with an abrupt drop in load (Figure 3.2-b).

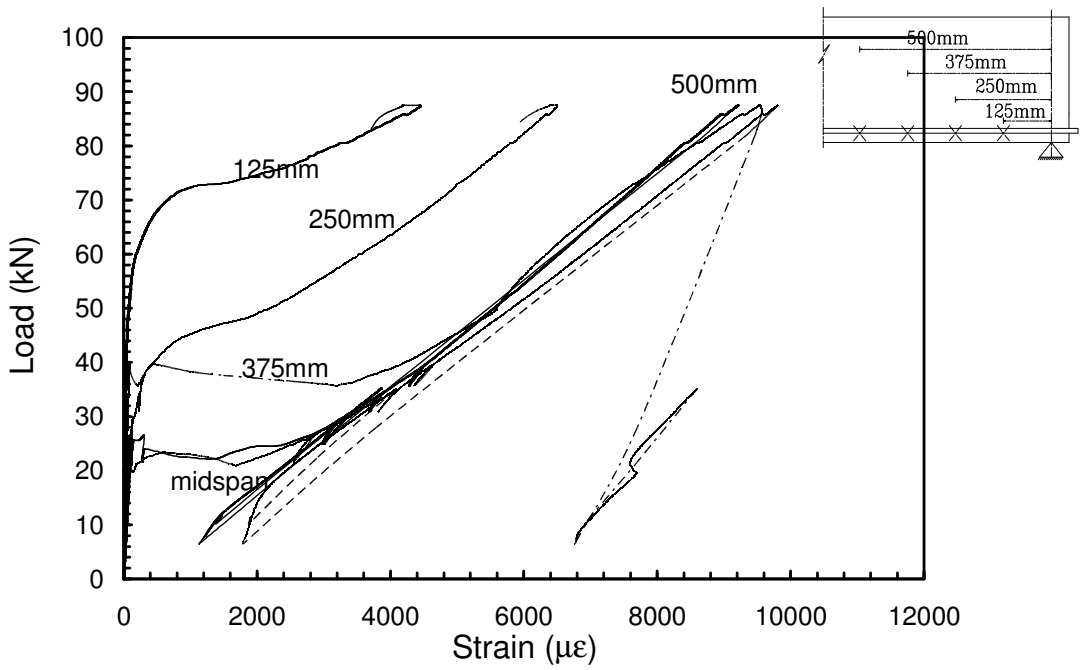

a-Load versus CFRP rod strain

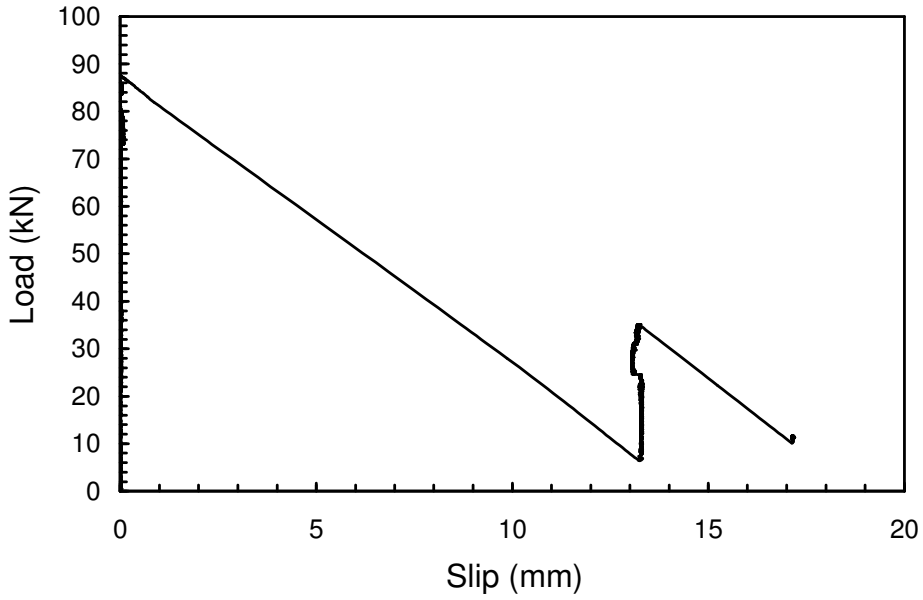

b-Load versus slip

Figure 3.2: Test results for beam NS-SW-0%-M

a-Crack in the shear span

b-The same crack after complete failure with chunk of concrete separated

c-Bottom view of the beam after failure

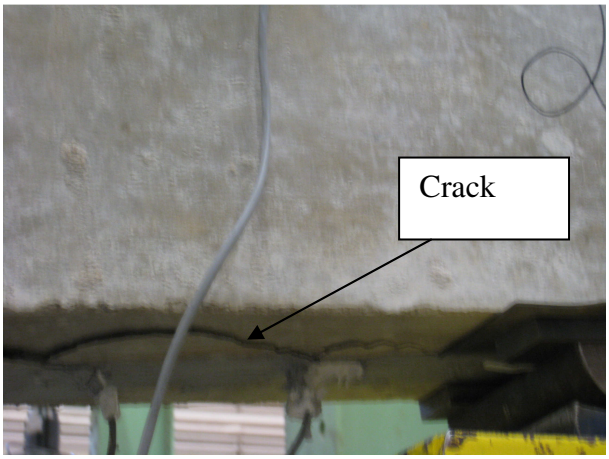

d-Cracks in concrete close to the support

Figure 3.3: Beam after failure for beam NS-SW-0%-M

Strain distribution along the CFRP rod

Figure 3.4 shows the strain distribution along the CFRP rod at different load levels (as indicated in the legend). At a load of 20 kN, the strain gauge reading at all location was too low (less than 50 με). As the load increased to 26 kN, the concrete at midspan section cracked

and the strain gauge reading at midspan increased. As the load increased further to 31kN, the reading at 500mm increased and was almost equal to the reading at midspan indicating de-bonding between these two locations. At a load of 60 kN, the readings at 375, 500 mm and midspan were equal. That indicates that the CFRP rod is debonded from the epoxy in this region and that the stress raiser along the rod is moving towards the support. As the load increased further, the gauge readings at 375, 500 mm and midspan increased and remained equal and at the same time the readings at 125 and 250 mm increased until reaching a peak load of 88 kN. At a peak load of 88 kN, the strain gauge reading at 125mm was equal to 4185 με.

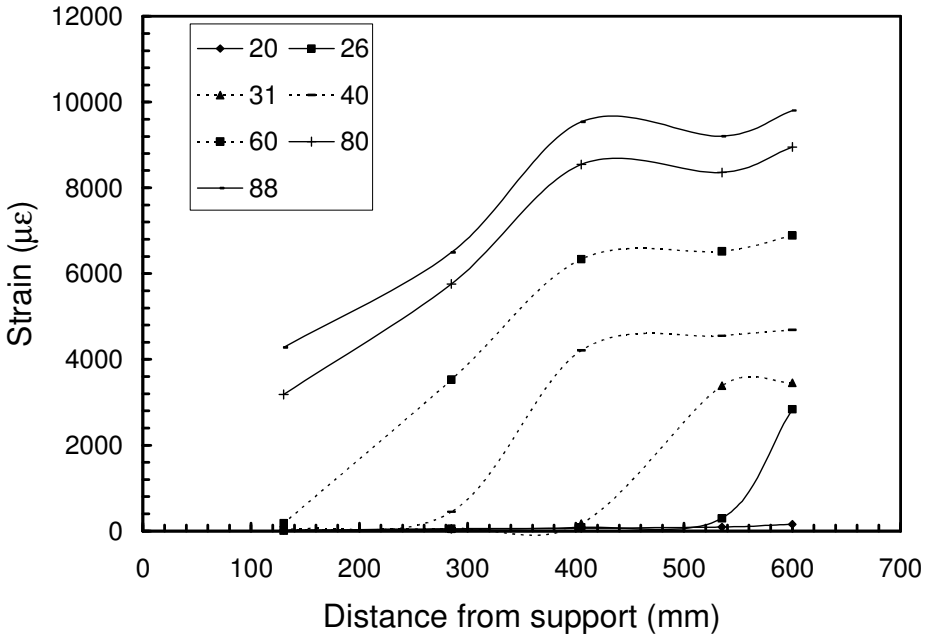

Figure 3.4: Strain distribution along the CFRP rod for beam NS-SW-0%-M

3.2.4 Beam with no internal steel and strengthened with sand coated CFRP rod

Cracking behaviour

Beam NS-SC-0%-M had no internal steel and was strengthened with non-prestressed sand coated CFRP rods. The load-strain and load-slip behaviour were similar to beam NS-SC-0%-M. Figure 3.5-a shows the load versus CFRP strain gauge measurements and Figure 3.5-b shows the load versus the end slip between the CFRP rod and the concrete. The strain gauge reading located at midspan increased as the tensile forces in the cross section were suddenly transferred to the CFRP rod. Similar to NS-SW-0%-M, as the load increased further, cracks were observed in the shear span starting close to the load application and progressed towards the supports. The first crack that appeared in the shear span was underneath the loading point and at 10 mm from the loading point. As the test proceeded, the crack at 10mm from the loading point was at all times noticeably wider than any of the other cracks. As the load approached its peak value, the crack underneath the loading point widened and propagated through the depth of the beam. Then, it connected with the large vertical crack at 10mm from the loading point, isolating a prism of epoxy and concrete. At the peak load, debonding occurred between the CFRP rod and the epoxy and an isolated prism of epoxy covered with concrete separated from the CFRP rod and the beam as shown in Figure 3.6-a. At the same time, longitudinal cracks occurred in the concrete surrounding the groove in the shear span and chunks of epoxy covered with concrete separated from the bottom of the beam as shown in Figure 3.6-b. However, closer to the support longitudinal cracks in the concrete occurred, but the epoxy and the concrete did not separate from the rod (Figure 3.6-c). These cracks were wider than the cracks that occurred for NS-SW-0%-M. At failure, the slip between the CFRP rod and the beam increased to 11mm with a sharp drop in load (Figure 3.5-b).

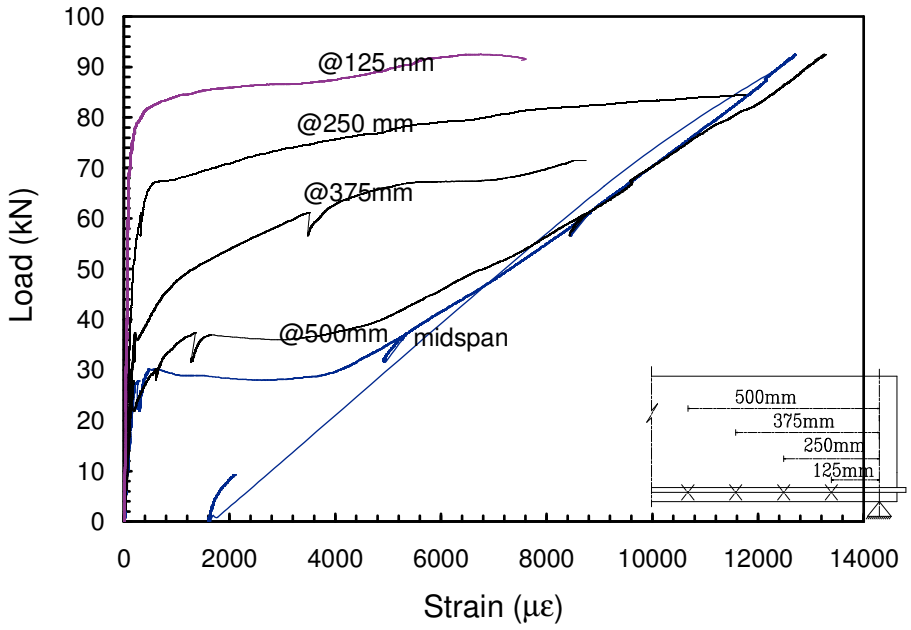

a-Load versus CFRP rod strain

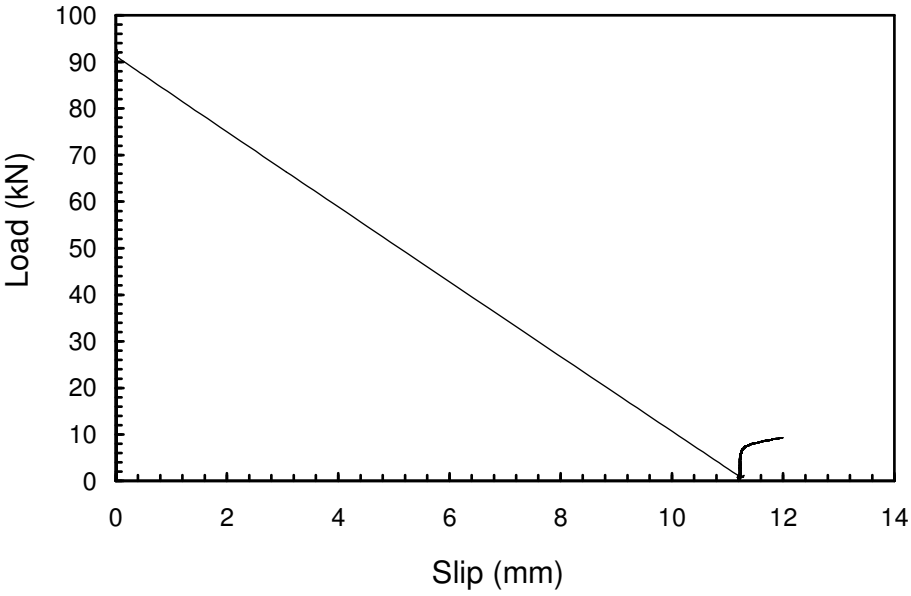

b-Load versus slip between the CFRP rod and the concrete

Figure 3.5: Test results for beam NS-SC-0%-M

a-Beam just after failure

b-Bottom view of the beam

c- Longituidnal cracks in the epoxy and the

Figure 3.6: Beam NS-SC-0%-M at failure

Strain distribution along the CFRP rod

Figure 3.7 shows the strain distribution along the CFRP rod for beam NS-SC-0%-M. At a load of 40 kN, the strain at 500mm was almost equal to that at midspan indicating de-bonding between these two locations. As the load increased further, the strain at 375mm started increasing until a load level of 70 kN. The strain reading at 375mm increased significantly between 60 and 70 kN but it was still less than the strain at midspan indicating partial debonding between 375 and 500 mm. Above a load of 70 kN, the strain readings at 125 and 250 mm start increasing, indicating that the partial de-bonding is moving towards the support. At peak load of 92.5 kN, the strain gauge at 125mm was equal to 6757 με.

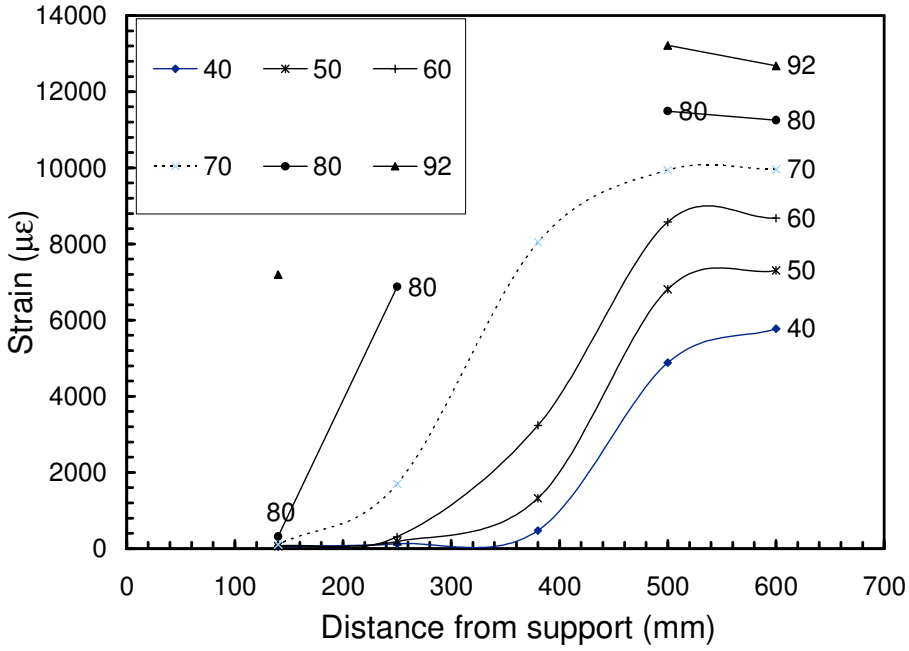

Figure 3.7: Strain distribution along the CFRP rod for beam NS-SC-0%-M

3.2.5 Beam with internal steel and strengthened with spirally wound CFRP rod

Cracking behaviour

Beam S-SW-0%-M had 2 No. 10 bars (10mm) as internal steel reinforcement. It was strengthened with non-prestressed spirally wound CFRP rod. Figures 3.8-a and 3.8-b show the load versus strains on the CFRP rod and the steel rebar, respectively. Figure 3.9 shows the load versus end slip.

Figures 3.8-a and 3.8-b show that both the CFRP strain and the steel strain increase slowly with load until concrete cracking at midspan. Once the concrete at midspan cracked, the tensile forces carried by the concrete were transferred to the steel and the CFRP rod causing a sudden increase in both the steel and the CFRP strain gauges at midspan. There was also a change in the slope of the load-strain curve. As the load increased further, cracks occurred at locations

successively further from the loading point. First cracking occurred in the shear span at the loading points and at 100mm from the loading point. Then, cracks appeared successively at the 225 mm and 350mm from the loading point. Cracks also appeared between these locations. Each new crack was accompanied by a sudden increase in the readings of the nearby steel and CFRP strain gauges. The cracks were more uniformly and closely spaced in the shear span than in the previous beam. For beam S-SW-0%-M, as the load increased, cracks on both faces of the beam increased in width and were connected to one another through cracks at the soffit of the beam as the loading progressed. At a load of 88kN, there was a sudden change in the slope of the load versus CFRP strain gauge at midspan. This was coincident with the steel reaching its yield strain as seen from Figure 3.8-b. Beyond this load, the tensile forces carried by the steel rebar remain nearly constant and the CFRP rod resists all the subsequent increase of the flexural tensile forces. At the peak load, beam failure occurred by debonding between the CFRP rod and the epoxy. Horizontal cracks propagated between the vertical cracks along the steel rebar to concrete interface and the slip between the CFRP rod and the epoxy increased to 6 mm as shown in Figure 3.9.

Figure 3.10 shows the beam after failure. In some regions, longitudinal cracks occurred in the concrete surrounding the epoxy and chunks of epoxy covered with concrete separated from the beam. In other regions, a combination of vertical cracks running along the bottom of the beam through the epoxy and the rod followed by inclined cracks from the rod to the base of the beam led to triangular chunks of epoxy and concrete separating from the base of the beam as shown in Figure 3.10.

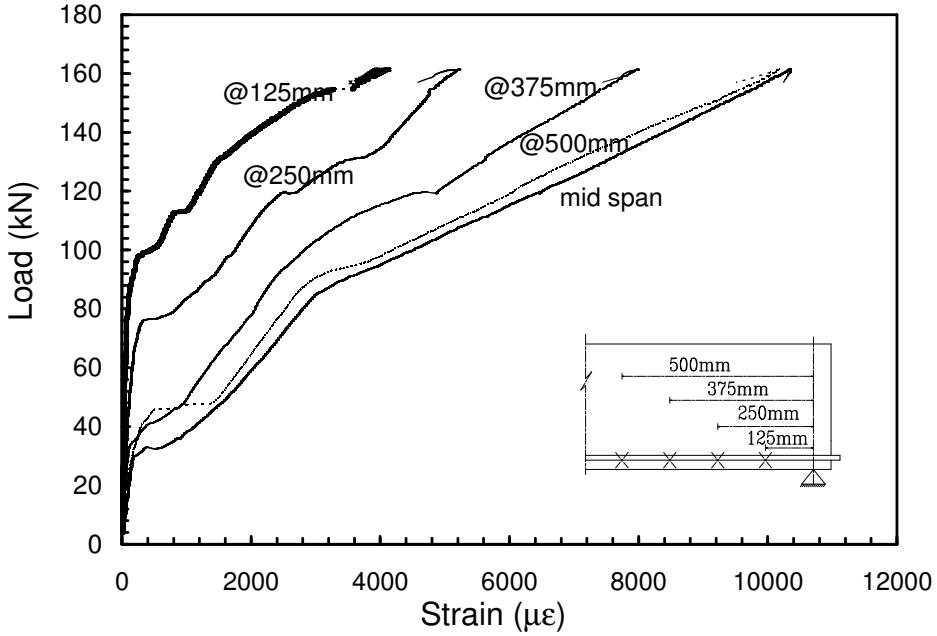

a- CFRP strain

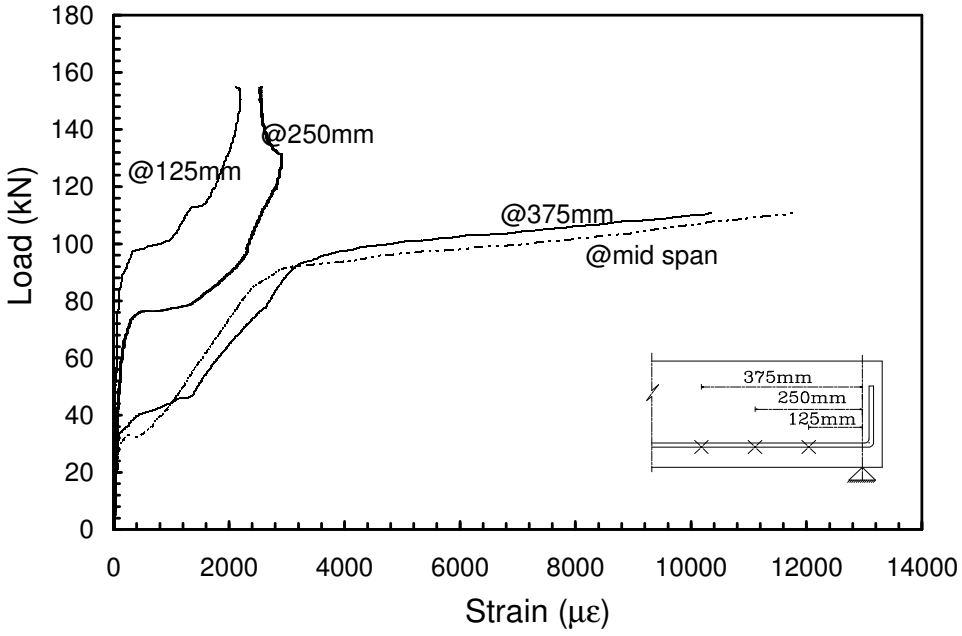

b- Steel strain

Figure 3.8: Load versus strain response for beam S-SW-0%-M

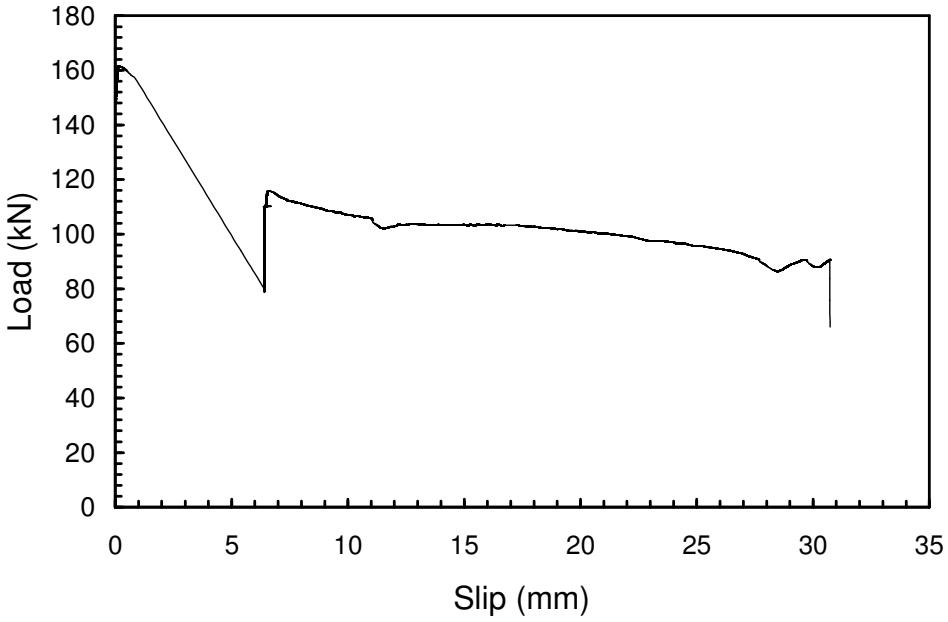

Figure 3.9: Load versus end slip for beam S-SW-0%-M

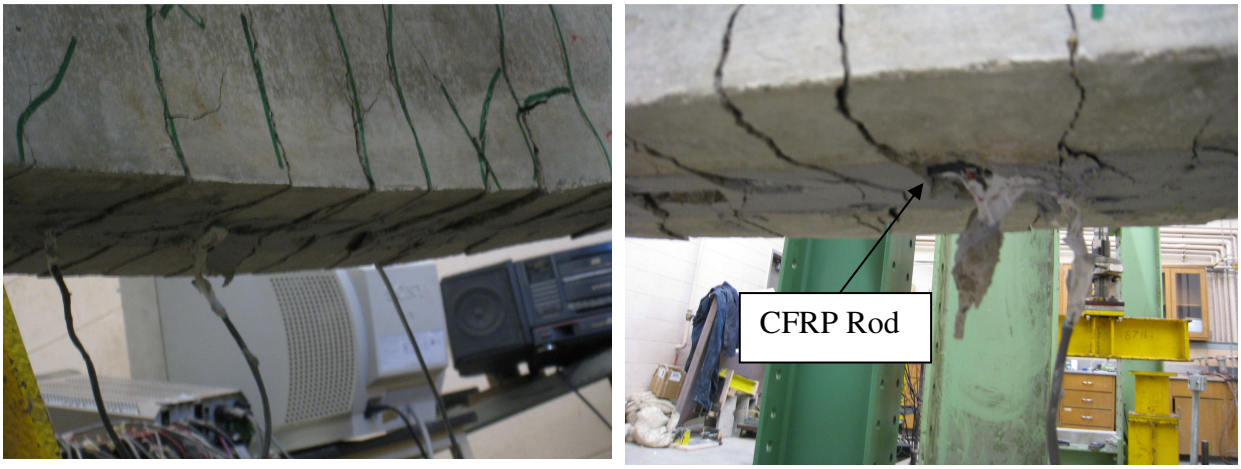

a-Bottom view showing the uniform spaced crack inter- connected

b-Concrete cover with epoxy separated from the CFRP rod

Figure 3.10: Beam S-SW-0%-M after failure

Strain distribution along the CFRP rod

Figure 3.11 shows the strain distribution along the CFRP rod. This beam behaved similar to the previous beams. At a load of 40 kN, the concrete at midspan section cracks and the strain gauge reading at midspan increases. As the load increases further to 100 kN, full debonding between 600 mm and 500 mm is clear where the strain gauges readings at both locations are equal. At 120 kN, the strain gauges readings indicate partial debonding between 375mm and 500mm. The readings at all locations increase until a peak load of 160 kN is reached. At 160kN, the strain gauge reading at 125 mm was equal to 4103 με.

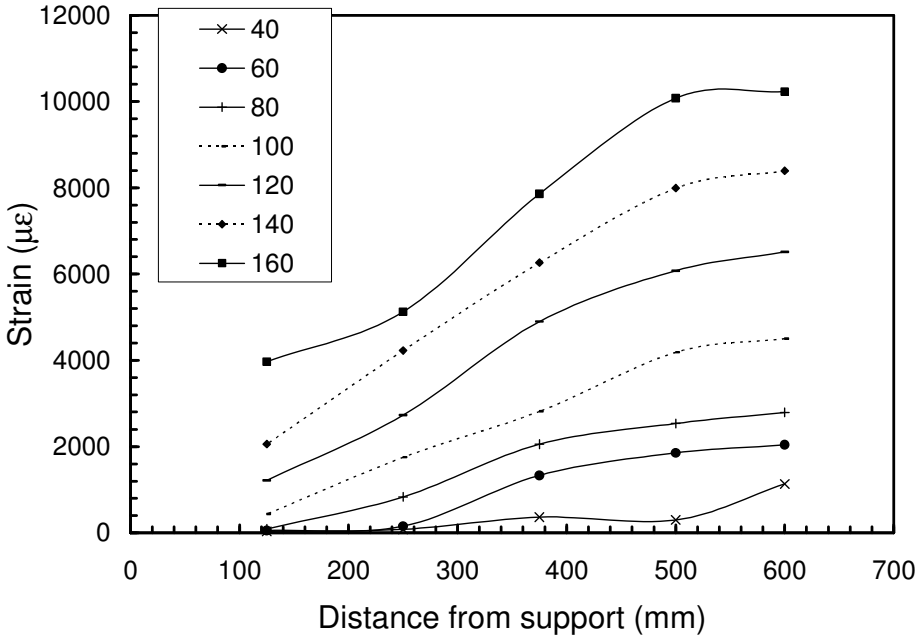

Figure 3.11: Strain distribution along the CFRP rod for beam S-SW-0%-M

3.2.6 Beam with internal steel and strengthened with sand coated CFRP rod

Beam S-SC-0%-M had 2 No. 10 bars (10mm) as internal steel reinforcement. It was strengthened with non-prestressed sand coated CFRP rod. The beam exhibited similar behaviour of CFRP and steel strains with load to beam S-SW-0%-M. Figures 3.12-a and 3.12-

b show load versus strains on the CFRP rod and the steel rebar, respectively. Figure 3.13 shows the load versus the end slip between the CFRP rod and the epoxy.

Cracking behaviour

The beam cracked similar to beam S-SW-0%-M, with cracking occurring initially within the midspan followed by cracking underneath the loading point. As the load increased further, cracks spread in the shear span. Cracking first occurred at the loading points and at 100mm from loading point. Then, cracks appeared successively at the 225 mm and 350 mm from the loading point. Yet, these cracks were not as wide as the cracks in beam S-SW-0%-M. At a load of 90 kN, there was a sudden change in the slope of the load versus CFRP strain at midspan due to yielding of steel rebar as seen from Figures 3.12-a and 3.12-b. Beyond this load, the tensile forces carried by the steel rebar remain nearly constant and the CFRP rod resists all the subsequent increase of flexural tensile forces. The crack closest to the support was at 140mm from centerline of the support and occurred at the peak load. At the peak load of 147 kN, the crack at 140mm from the centerline of the support propagated horizontally towards the midspan and debonding occurred between the CFRP rod and the epoxy as shown in Figure 3.14. The slip between the CFRP rod and the beam end increased to 16 mm and the load dropped as shown in Figure 3.13. Epoxy covered with concrete separated from the bottom of the beam and the rod separated from the remaining epoxy in the region which starts at the centerline of the support and continued to 160mm from the centerline of the support (Figure 3.14). In the region between 160mm and 520mm from the centerline of the support, chunks of epoxy covered with concrete separated from the CFRP rod and the internal steel. In the region furthest from the support, starting at 520mm from the centerline of the support and continuing

up to the loading point, the crack that propagated horizontally caused the rod to separate from the beam. The separated rod had chunks of epoxy covered with concrete adhering to it (Figure 3.14).

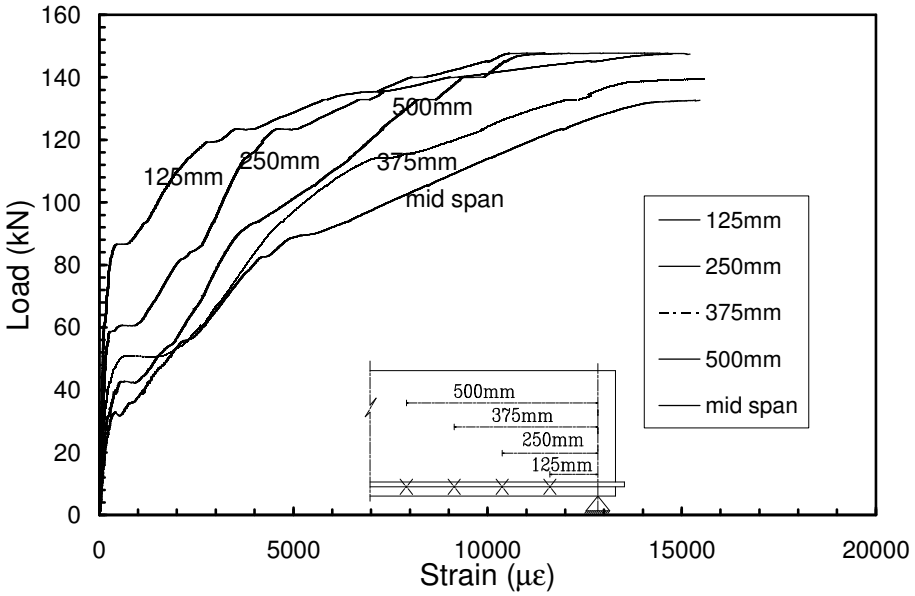

a-CFRP rod strain

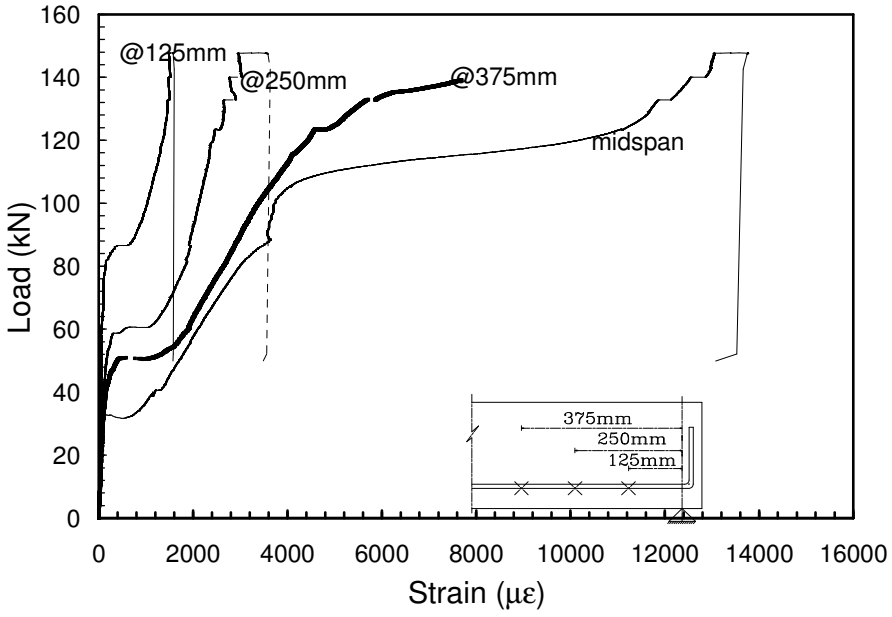

b- Steel rebar strain

Figure 3.12: Load versus strain behaviour for beam S-SC-0%-M

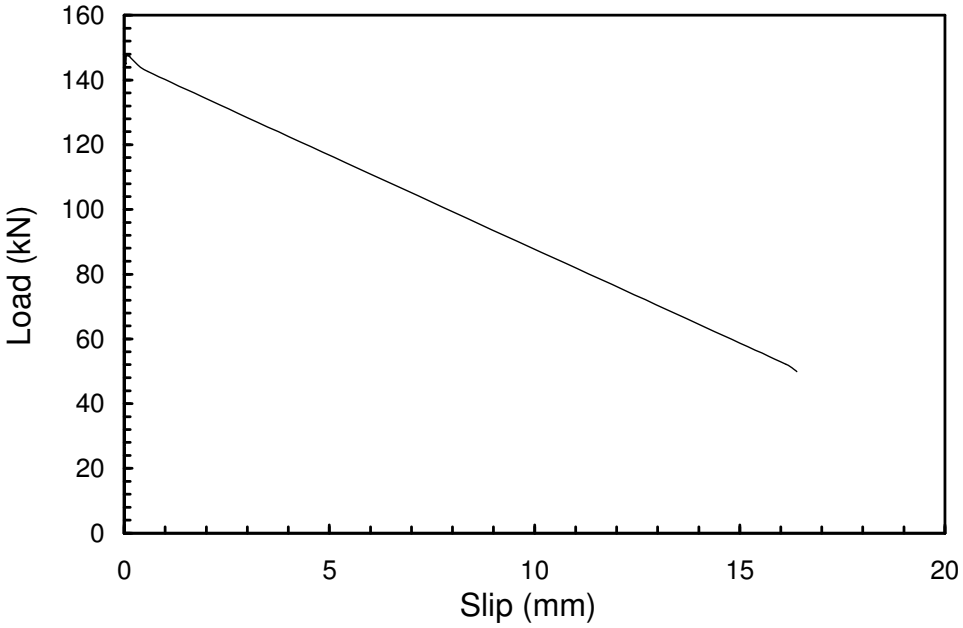

Figure 3.13: Load versus slip for beam S-SC-0%-M

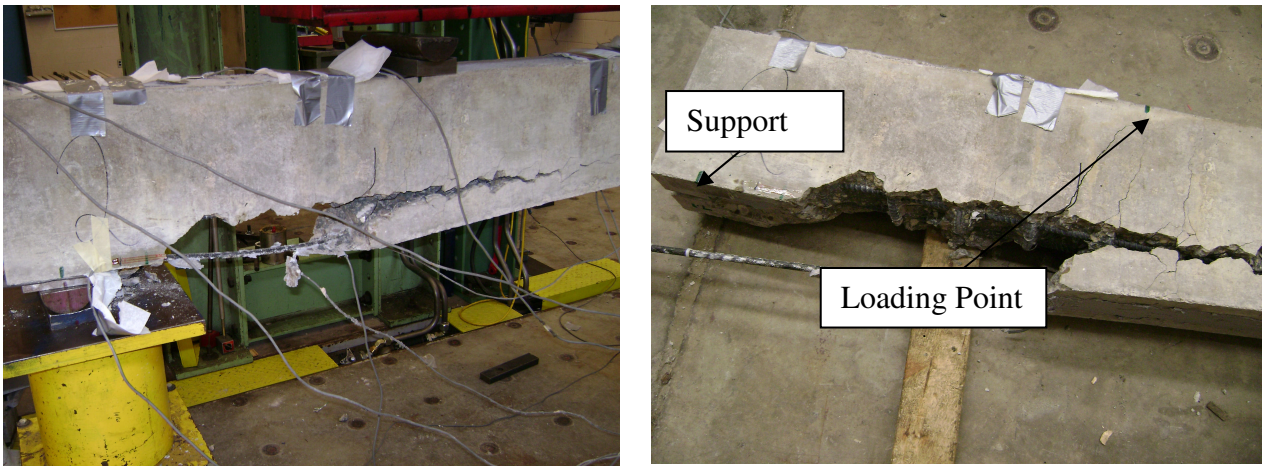

Figure 3.14: Beam S-SC-0%-M after failure

Strain along the CFRP rod

Figure 3.15 shows the strain distribution along the CFRP rod for beam S-SC-0%-M. At a load of 20 kN, all strain readings were very low (less than 100με) and there was no sign of cracking. At a load of 40 kN, there was cracking at midspan and the strain gauge reading at midspan increased to 1150με. It is noteworthy, that the gauge at 500mm was in uncracked zone and the measured readings were lower than expected by beam theory. At a load of 131kN, the strain at 375mm was slightly less than that at midspan. This indicates partial debonding between these two locations. Also, the strain at 125mm was almost equal to that at 250mm indicating partial debonding between these two locations. At the peak load, strain gauges at 125mm, 375mm and midspan were already malfunctioning.

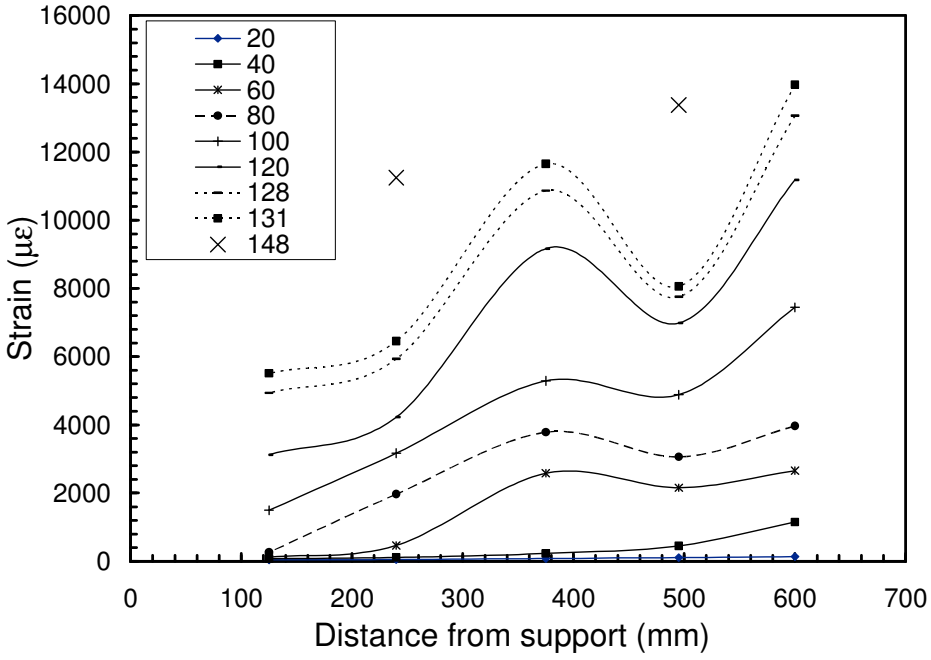

Figure 3.15: Strain along the CFRP rod for beam S-SC-0%-M

3.3 Discussion of monotonic test results

3.3.1 Cracking mechanism

Initially as the concrete beam was loaded, most of the tensile forces were carried by the concrete. When the concrete cracked, these tensile forces were transferred to the CFRP rod and the steel rebar at the crack location. Then, once the steel reinforcement yielded, all of the additional tensile forces were carried by the CFRP rod. If a strain gauge location coincides with or near the crack location, the transfer of tensile stresses from the concrete to the steel will result in a sudden increase in the strain gauge reading. If the strain gauge is far from the crack in an uncracked region, its reading will exhibit little change. Moving away from a crack into an uncracked region, the tensile stresses in the concrete rapidly increase and the stresses in the steel rebar and the CFRP rods rapidly drop to a low level. This abrupt variation of the stress distribution along the rod creates high local shear stresses at crack locations that decrease with distance into the uncracked region of the beam.

The distribution of the shear (bond) stress on the CFRP rod is illustrated for various crack spacings in Figure 3.16. If the cracks are widely spaced, the high shear stresses created at the crack location will decrease to a low value (the uncracked shear stress) between two adjacent cracks. However, if the cracks are closely spaced then the distributions of the shear stresses due to cracking will overlap resulting in a continuous high shear stress between the two cracks. When the shear stresses at a crack are high enough the rod will slip and eventually de-bond from the surrounding media and the stress raiser will move to the still bonded region. Once complete debonding has occurred there will be no shear stresses acting along the perimeter of the rod and the stress and strain in the CFRP rod in the debonded region will be equal to the

stress and strain at midspan. Thus, along the CFRP rod there will be 2 regions; one region where the CFRP rod is fully or partially debonded from the epoxy and a second region where the CFRP rod is fully bonded to the epoxy. The de-bonding mechanism can be represented by a crack growing at the interface between the CFRP rod and the epoxy as shown in Figure (3.17). This will be discusses again in Chapter 5. In the bonded region, the strains and shear stress will decay rapidly with distance from the crack front. The integration of the shear stress along the perimeter of the rod in the bonded region is equal to the force at the crack front.

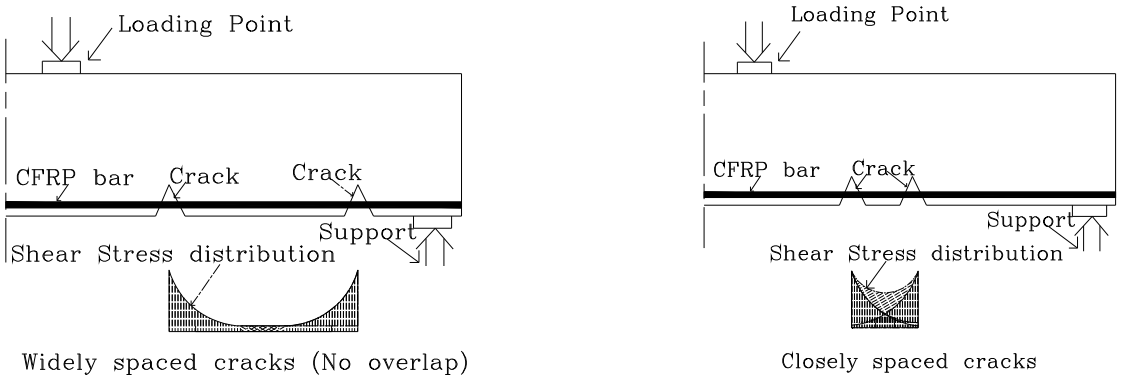

Figure 3.16: Shear stress distribution along the CFRP rod at the crack location

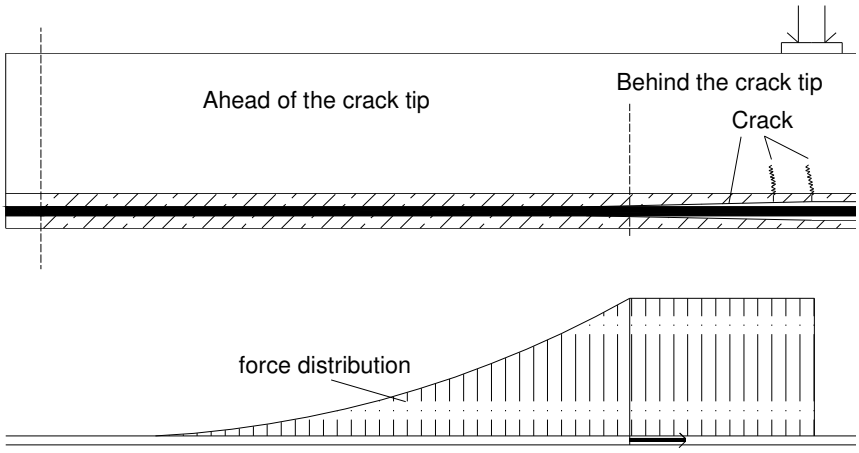

Figure 3.17: Schematic showing crack at the interface between the CFRP rod and the epoxy

3.3.2 Failure mechanism

Minimal slip between the CFRP rod and the beam end was recorded until the peak load was reached. At the peak load, once failure occurred, the CFRP rod started slipping from the epoxy. Thus, the maximum strain at all locations will be at the peak load at onset of excessive slip. Figure 3.18 shows the strain distribution at failure (onset of excessive slip) for all the beams. In this figure, the x-axis represents the location of the strain gauges along the rod and the y-axis represents the strain gauge readings in micro strain. The strain distribution for all beams was at their peak load. Once the rod started slipping, the readings of the strain gauges at 125 mm and 250 mm from centerline of the support decreased. Thus, the CFRP rod starts to unload and failure occurs.

From Figure 3.18, it is clear that at failure the strain profile is almost the same for each rod type. The gauges closer to the midspan sections, at 500 mm and 375 mm from the support, recorded almost the same strain as the strain gauge at midspan. This indicates as discussed in the previous section that the CFRP rod was fully debonded in this region. The gauges that are closer to the support, at 125 mm and 250 mm from the support, recorded strain values higher than the value expected based on strain compatibility analysis for a bonded cross section but lower than the strain value at midspan. This indicates that they are in the fully bonded region but the crack at the CFRP-epoxy interface has progressed towards the support.

At failure, the CFRP strain recorded in the fully bonded region had the same value and distribution for all beams strengthened with a given rod type. This indicates that the force in

the CFRP rod and the shear stress in the fully bonded region (ahead of the crack) at failure was the same for all beams strengthened with a given rod type.

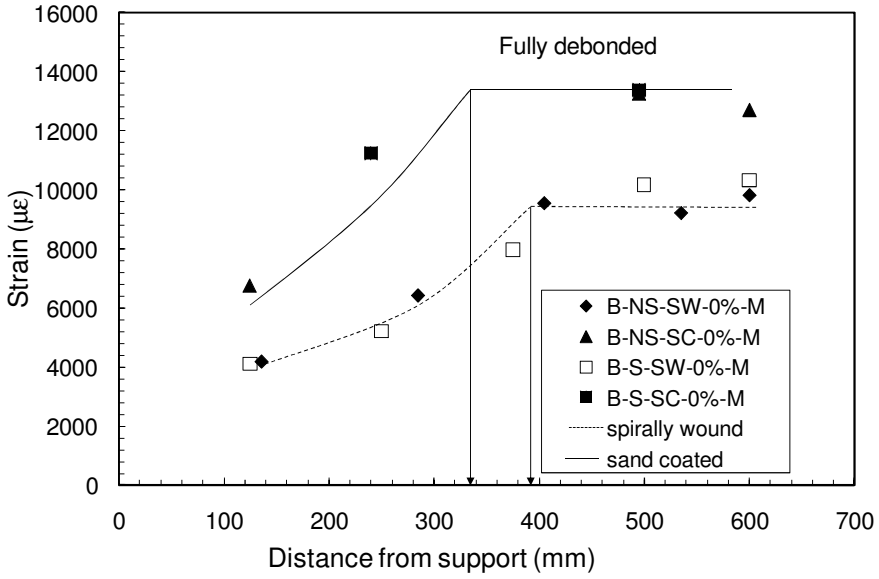

Figure 3.18: CFRP Strain distribution at failure for monotonic beams

3.4 Fatigue test results

3.4.1 Fatigue life

Figure 3.19 shows the fatigue life in cycles for different beams tested at different load levels (%). The vertical axis represents the load range in percentages which is the difference between the upper and lower load levels divided by the beam's monotonic capacity. The horizontal axis represents the life in cycles. The lower load level was kept at 10% of the monotonic capacity of the beam and the upper load level was varied. The beams that sustained one million cycles without failure (run out) are indicated by an arrow. Table 3.2 summarizes the fatigue test results for all groups. The specimen nomenclature was explained in Chapter 2 (Section 2.2).

Three modes of failure occurred in fatigue, namely; bond failure (at the CFRP epoxy-interface), steel rupture and shear failure in concrete. Bond failures, regardless of the presence of the internal steel rebar or the CFRP rod type, occurred by debonding between the CFRP rod and the epoxy that started at the loading point and propagated towards the support. This is the same failure mechanism as observed for the monotonic beams.

The fatigue life curve for the beams that failed in bond was flat especially when compared to that for the beams that failed by rupture of the internal steel rebar. Thus, a minor change in the applied load will result in a major increase in life if beam were to fail in bond as opposed to rupture of the steel rebar. Also, the beams that were strengthened with sand coated rods exhibited a longer life for the same percentage of load range in comparison to the beams strengthened with spirally wound rods as shown in Figure 3.19.

Steel reinforced beams that were strengthened with spirally wound rods showed 2 different modes of failure; rupture of steel and bond failure as shown in Figure 3.19. Beams loaded to a load range of 45%, 40% and 30% of the monotonic capacity of the beam and thus experiencing longer life failed by steel rupture. In other words, the load level is not enough to cause bond failure. Based on these results, the upper load level for the beams strengthened with spirally wound rods was increased to 81.6%, 75.1%, 71.4% and 68.75% of the monotonic capacity of the beam to investigate bond failure. Similarly, the upper load level for the beams strengthened with sand coated rods varied from 85% to 76% of the monotonic capacity of the beam to avoid steel rupture.

Some of the concrete beams (with no internal steel) that were strengthened with sand coated rods failed in shear. The trend line for the fatigue life of those beams is parallel and very close to that for the beams failing in bond. In fact, those beams cracked in the same way as the ones that failed in bond. Yet, they showed a higher resistance causing them to fail in shear instead of bond.

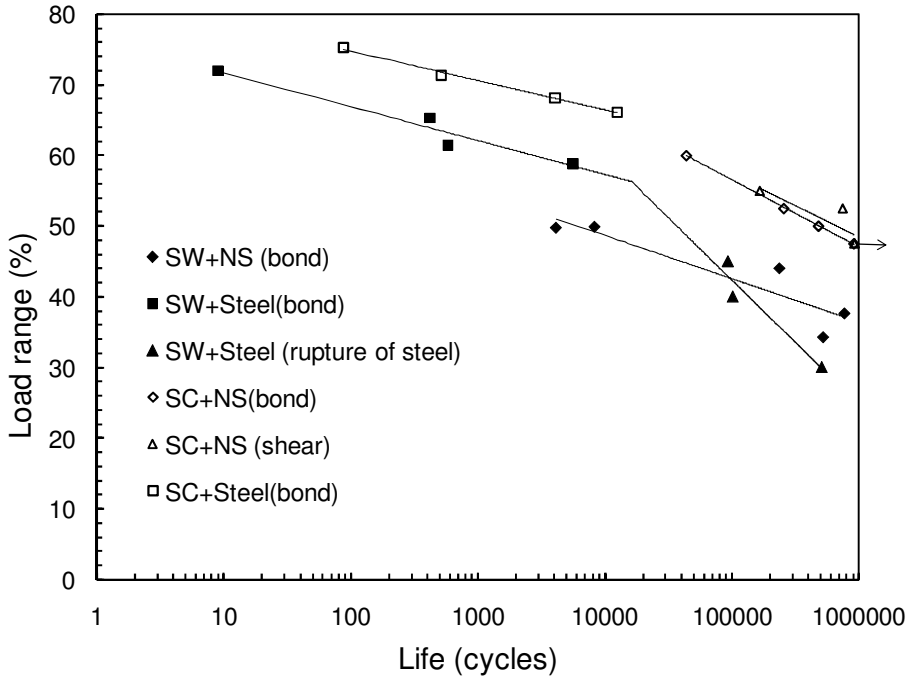

Figure 3.19: Life in cycles versus load range (%) for all tested beams

Table 3.2: Test results for non-prestressed beams

Group	Specimen notation	Min. Load	Max. Load	Measured strain range at midspan (με)		Max. Capacity (kN) or Life (cycles)	Failure mode
				CFRP	Steel		
A	NS-SW-0%-M	monotonic		NA	NA	87.6 kN	Bond
	NS-SW-0%-65%	10%	65%	4024	NA	15,038	Bond
	NS-SW-0%-60%(a)	10%	60%	4189	NA	8,306	Bond
	NS-SW-0%-60%(b)	10%	60%	---*	NA	4,138	Bond
	NS-SW-0%-54%	10%	54%	2094	NA	236,440	Bond
	NS-SW-0%-47%	10%	47.65%	2623	NA	767,125	Bond
	NS-SW-0%-44%	10%	44.3%	2512	NA	521,499	Bond
B	NS-SC-0%-M	monotonic		NA	NA	92.5 kN	Bond
	NS-SC-0%-70%	10%	70%	6093	NA	43,912	Bond
	NS-SC-0%-62.5%(a)	10%	62.5%	5000	NA	256,896	Bond
	NS-SC-0%-60%	10%	60%	3858	NA	482,472	Bond
	NS-SC-0%-57.5%	10%	57.5%	4156	NA	915,000	Shear
	NS-SC-0%-50%	10%	50%	4093	NA	1,000,000	Run out
		10%	65%	---*	NA	9,601	Bond
	NS-SC-0%-65%	10%	65%	5906	NA	165,351	Shear
	NS-SC-0%-62.5%(b)	10%	62.5%	4990	NA	740,297	Shear
C	S-SW-0%-M	monotonic		NA	NA	161.34kN	Bond
	S-SW-0%-81.6%	10%	81.6%	4415	3492	9	Bond
	S-SW-0%-75.1%	10%	75.1%	3815	3058	418	Bond
	S-SW-0%-71.4%	10%	71.4%	3589	2761	580	Bond
	S-SW-0%-68.75%	10%	68.75%	3460	2650	5,593	Bond
	S-SW-0%-50%	10%	50%	2486	1726	101,357	Steel rupture followed by bond failure
	S-SW-0%-55%	10%	55%	2378	2124	92,838	Steel rupture
	S-SW-0%-40%	10%	40%	1540	1119	507,964	Steel rupture
D	S-SC-0%-M	monotonic		NA	NA	147.8 kN	Bond
	S-SC-0%-85%	10%	85%	---*	3880	87	Bond
	S-SC-0%-81.3%	10%	81.3%	4362	3196	512	Bond
	S-SC-0%-78%	10%	78%	4640	3504	4,042	Bond
	S-SC-0%-76%	10%	76%	4117	3383	12,562	Bond

*: midspan gauge was damaged

3.4.2 Load-deflection behaviour

Figure 3.20 shows a typical load versus midspan deflection curve for beams strengthened with non-prestressed CFRP rods and tested under fatigue load. Figures for each beam are provided in the appendix. A major increase in midspan deflection usually occurs within 10% of the life. Past 10% of the life, midspan deflection increases slowly as life increases where the de-bonding is progressing towards the support. Once excessive end slip between the CFRP rod and the epoxy occurs (at 70% life in Figure 3.20), midspan deflection increases at a high rate as the beam is cycled until complete failure occurs.

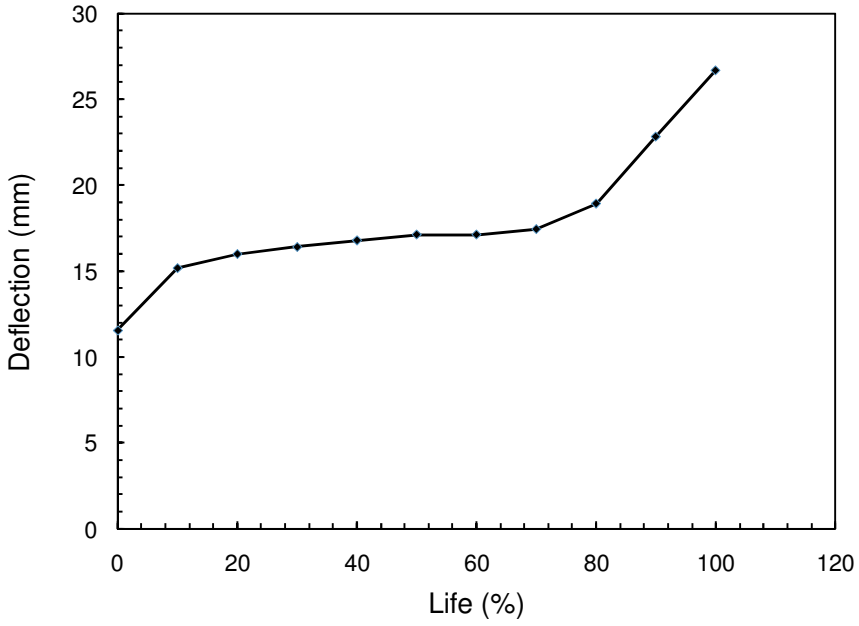

Figure 3.20: Midspan deflection versus fraction of life (%) for Beam NS-SW-0%-65%

3.4.3 Group A: Beams without internal steel and strengthened with non-prestressed spirally wound CFRP rod

All the beams in this group cracked and failed in a similar fashion. Also, they failed in the same way as the monotonic beams.

Cracking behaviour

As the beam was loaded monotonically in the first cycle, the first crack occurred at midspan. As the load increased, cracks occurred underneath the loading points. As the load was increased to the peak load a major (flexural-shear) crack occurred in the shear span. This major crack location ranged from 400 to 570 mm and it was deeper than other cracks. As the load was cycled, the major crack in the shear span grew deeper. It was clear that the CFRP rod at the major crack location is separated from the epoxy and that the debonding between the CFRP rod and the epoxy is spreading towards the supports as the beam was cycled further. At failure, concrete prisms separated from the sides of the beam at the major crack location and the CFRP rod separated from the surrounding epoxy. These concrete prisms were with or without epoxy attached to it. Also, the epoxy cover with concrete attached to it separated from the soffit of the beam at the major crack location as shown in Figure 3.21.

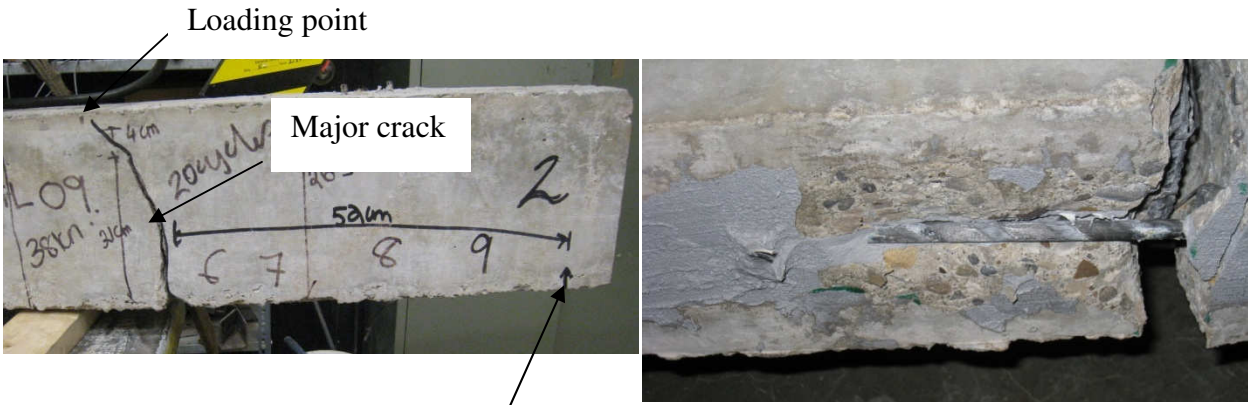

a-Beam after failure showing the major crack

b-Bottom view at major crack location showing CFRP rod separation

c-Epoxy with concrete separated from the bottom of the beam

Figure 3.21: Beam after failure NS-SW-0%-44%

Strain distribution along the CFRP rod

Figure 3.22 shows a typical strain distribution along the CFRP rod at upper load level for beam NS-SW-0%-44%. In the first cycle, the strain gauges located at 125, 250 and 375mm record a low strain reading. At 10% life, the gauge readings at 250 and 375 mm jumps to high strains and the reading at 500mm slightly increases. The strain profile at 10% life indicates partial debonding between midspan and the gauge located at 500mm. At 30 % life, the strain gauge reading at 500 and 600 mm are equal as well as the strain reading at 250and 375mm are equal.

Thus, there is full debonding between 500 and 600 mm and between 250and 375mm. As the life increases, the reading of the strain gauge located at 125mm increases and reaches its peak at 70% life. Past 70% life, the CFRP rod started slipping from the epoxy as shown in Figure 3.23. This is accompanied by a reduction in the strain gauge reading at 125mm as shown in Figure 3.22.

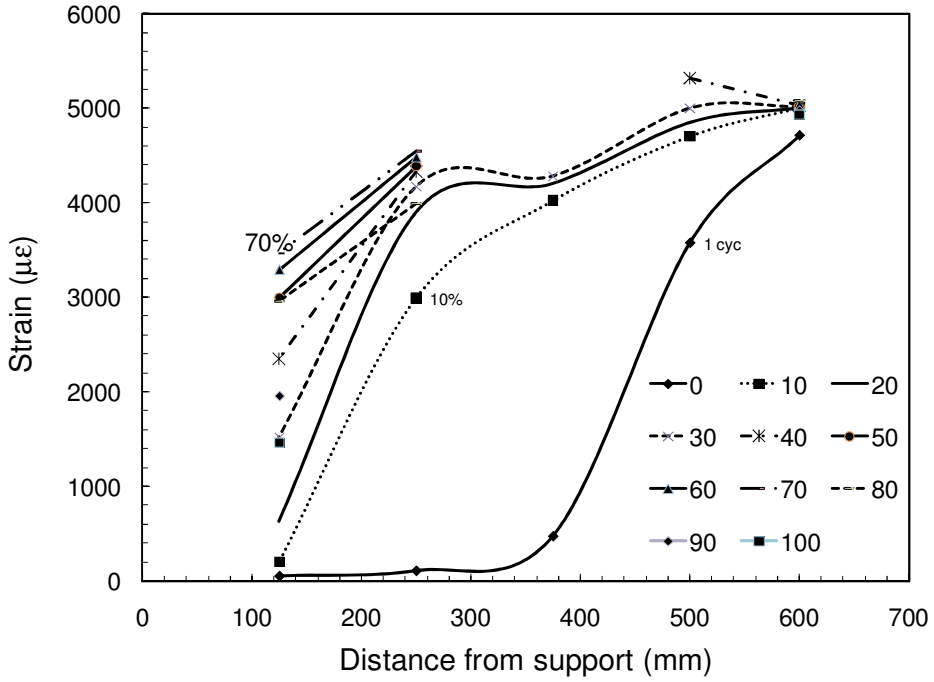

Figure 3.22: Strain distribution along the CFRP rod for beam NS-SW-0%-44%

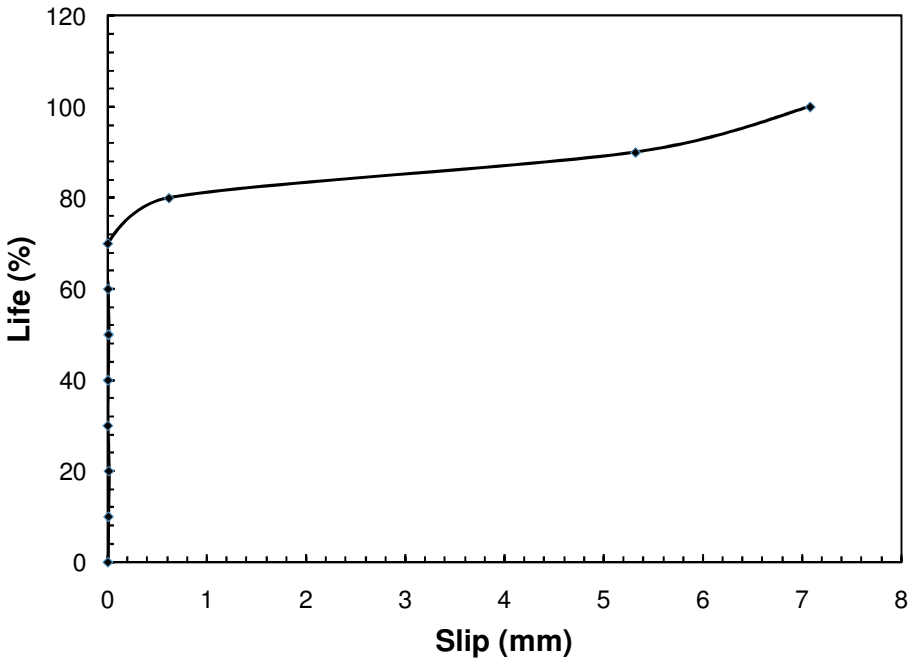

Figure 3.23: Slip (mm) versus life (%) for beam NS-SW-0%-44%

3.4.4 Group B: Beams without internal steel and strengthened with non-prestressed sand coated CFRP rod

Beams in this group showed two different modes of failure: shear and bond failures as shown in Figure 3.19. The upper scatter bound (stronger beams) showed shear failure. Meanwhile, the lower scatter bound showed bond failure. Yet, all the beams that experienced bond failure cracked and failed in the same way. The beams failed by debonding between the CFRP rod and the epoxy that started at the loading point and spread towards the support.

Cracking behaviour

Similar to group A, the beams in this group were loaded monotonically in the first cycle and cracking occurred first at midspan. As the load was increased further, cracks occurred

underneath the loading points followed by a major crack in the shear span. The major crack location ranged from 300 to 515 mm from the support. As the load was cycled, the major crack in the shear span grew deeper. At failure, the cracks occurred in the concrete surrounding the epoxy at the soffit of the beam as shown in Figure 3.24. Epoxy cover with concrete attached to it separated from either the bottom or side of the beam at the major crack location and the CFRP rod separated from the surrounding epoxy. In some cases, the epoxy cover together with concrete separated form the bottom of the beam in the shear span, starting from 50mm from the support until the location of the major crack. Also, in the cross section of the beam, at the support (free end) the epoxy around the CFRP rod was cracked as shown in Figure 3.24. It is noteworthy that the beams that failed in shear cracked in a similar way as the beams that failed in bond, yet the final failure was shear failure.

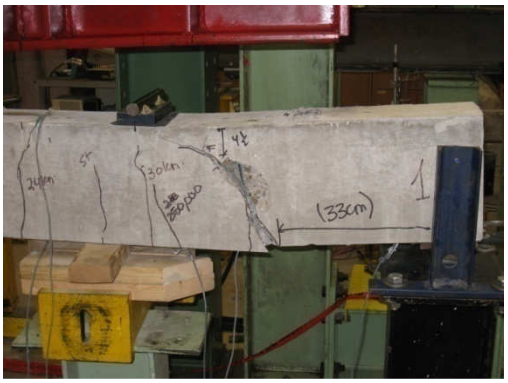

a-Major crack in shear span after failure

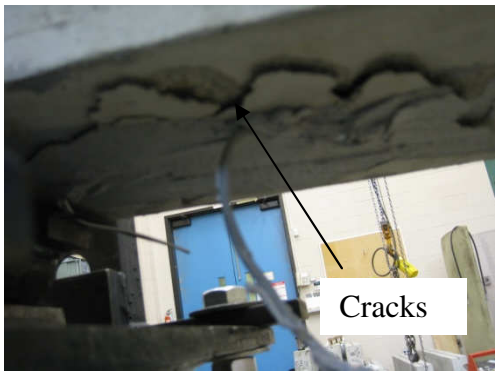

b-Cracks in concrete surrounding the epoxy

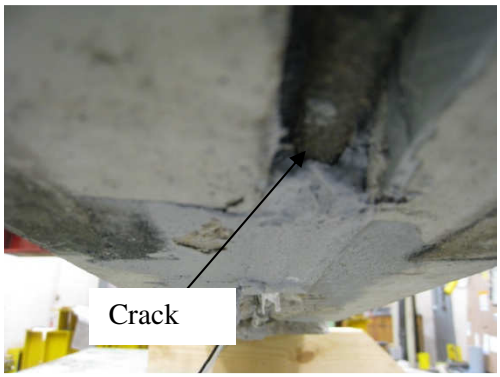

c-Cracks in epoxy at the free end

Figure 3.24: Beams after failure

Strain distribution along the CFRP rod

Figure 3.25 shows a typical strain distribution at the upper load level along the CFRP rod for beam NS-SC-0%-70%. In the first cycle, the strain gauges located at 125 and 250 recorded a low strain reading. At 10% life, the gauge readings at 250 and 375 mm jump to a higher value and the reading at 500mm slightly increases. The strain profile at 10% life indicates partial debonding between the gauges located at 250 mm and 375mm. The midspan strain gauge stopped working at 10% life. Yet, since there are no shear stresses at midspan, the strain reading is expected to stay the same until failure. At 40 % life, the strain gauge reading at 250 and 375mm is equal. Thus, there is full debonding between 250 and 375mm. As the life increases, the reading of the strain gauge located at 250 and 125mm increases. At 90% life, the reading at 250mm is almost equal to the midspan reading indicating a full debonding between the two locations. At 90% life, the gauge reading at 125mm reaches its peak value of 5510 με before slip starts as shown in Figure 3.26. As the rod slips from the epoxy, the strain readings decreases and the slip increases to 5.7 mm.

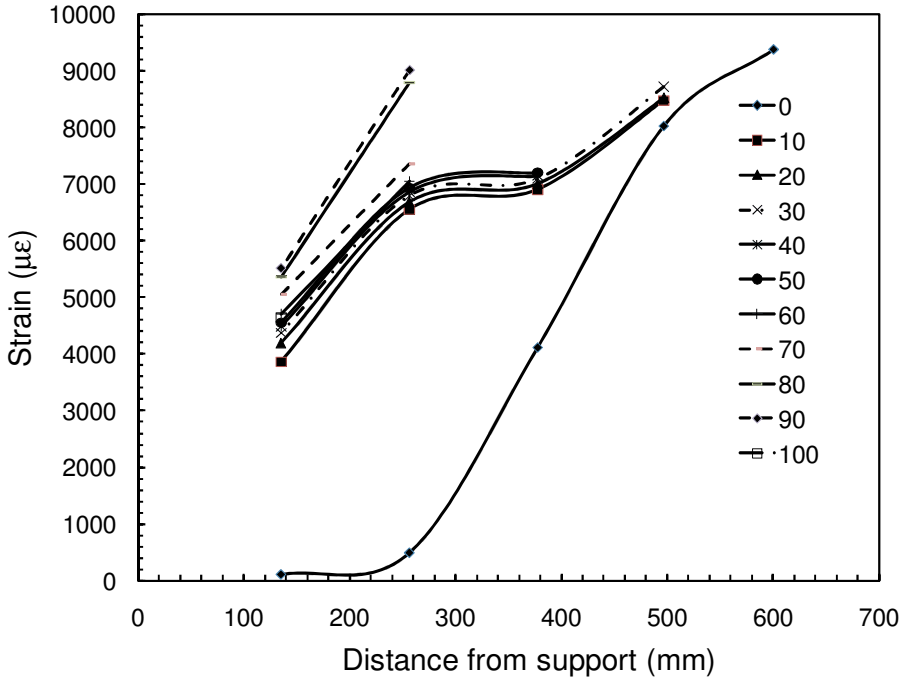

Figure 3.25: Strain distribution along the CFRP rod for beam NS-SC-0%-70%.

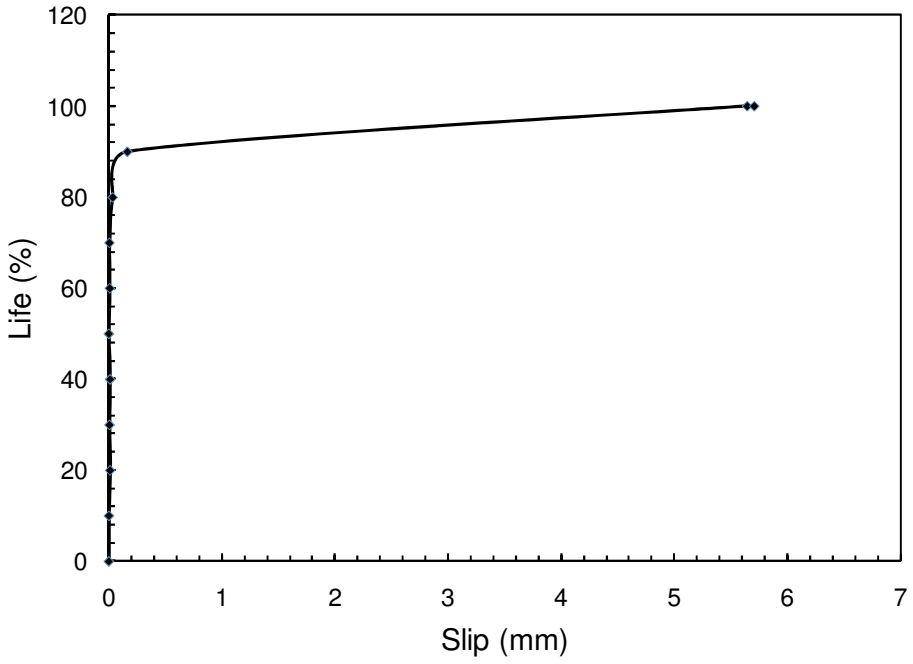

Figure 3.26: Slip (mm) versus life (%) for beam NS-SC-0%-70%

3.4.5 Group C: Beams with internal steel and strengthened with non-prestressed spirally wound CFRP rod

Beams in this group showed two different modes of failure; rupture of steel and bond failures as shown in Figure 3.19. All of the beams that experienced bond failure cracked and failed in the same way. Similar to the beams in Group A, beams in this group failed by debonding between the CFRP rod and the epoxy that started at the loading point and spread towards the support.

Cracking behaviour

Cracks occurred at midspan and underneath the loading points as the beam was loaded monotonically to peak load and as the load was cycled. Yet, due to presence of internal steel, cracks were more uniformly spread in the shear span. The crack closest to the support was located between 180mm to 200 mm. At complete failure, the vertical cracks that formed during cycling and loading propagated horizontally and joined one another at the steel-concrete interface.

After failure, the cracking pattern in the shear span could be divided into two regions: a region from center line of the support to the crack closest to the support and a region from the crack closest to the support to the loading point. In the first region; from center line of the support to the closest crack, longitudinal cracks formed in the concrete parallel to the CFRP rod. In some cases, they were accompanied with longitudinal cracks in the epoxy. In other cases, they were accompanied with cracks in the epoxy that separated the bottom epoxy cover and could be seen in the cross section of the beam at the support (free end) as shown in Figure 3.27.

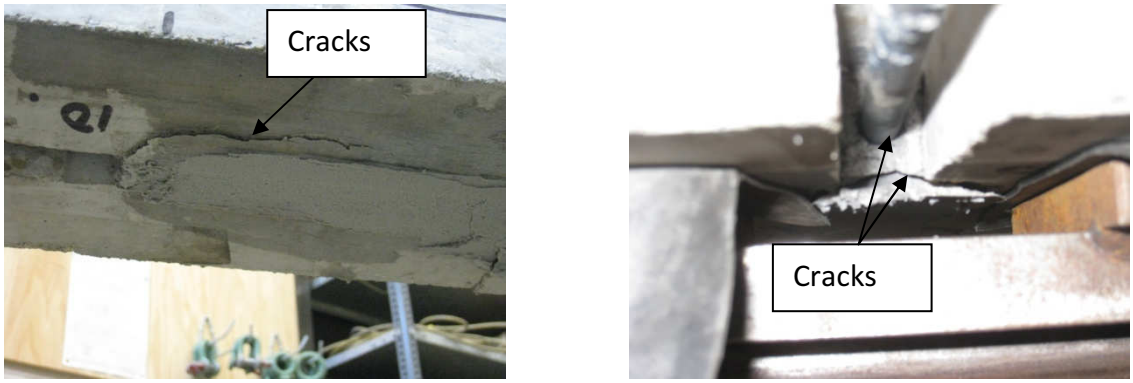

a-Cracks in the concrete surrounding the epoxy

b-Cracks in the cross section of the beam

Figure 3.27: Cracking in the region close to the support

In the second region; from the closest crack to the support to the loading point, the vertical cracks that formed during cycling and loading propagated horizontally and joined one another at the steel- concrete interface. Chunks of concrete and epoxy separated from the beam leaving the CFRP rod. Figure 3.28 illustrates the possible chunks that could separate from the cross section. As shown in the figure, the chunks of concrete and epoxy separate as either the bottom cover of the CFRP rod (chunk 3) or at the steel interface (chunk 1 or 2). Figure 3.29 shows a beam after failure.

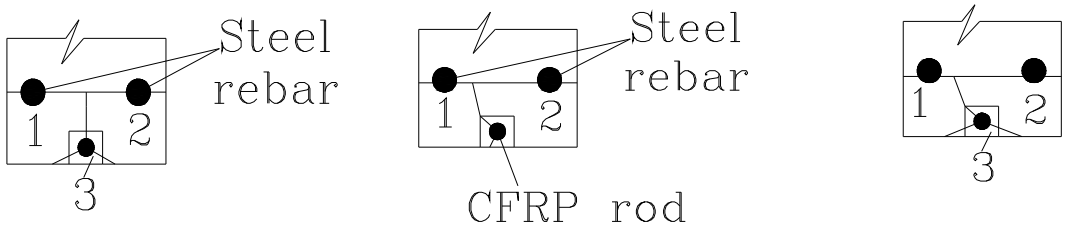

Figure 3.28: Illustrative drawing showing the possible failing chunks

a-Cracking in shear span before chunk separation

b-Beam after complete failure

c-Samples of separated blocks from the beam

Figure 3.29: Beams after failure

Strain along the CFRP rod

Beams in this group behaved in a similar way to beams in group A. Yet, due to the presence of internal steel that yields and the variation of its properties from one beam to the other, some scatter occurred. Figure 3.30-a and Figure 3.30-b show the strain distribution at upper load level along the CFRP rod and steel rebar at different percentages of life for beam S-SW-0%-

71.4%, respectively. At 10 % life, strain gauge reading of the CFRP rod at 375 mm slightly increased. As life increased further, strain gauge readings of the CFRP rod at 125 and 250mm increased. At 80% life, the strain reading at 125 mm reached its peak value of 2500 με. Past 80% life, slip started as shown in Figure 3.31 and the CFRP rod strain reading at 125 and 250 mm dropped. Figure 3.30-b shows the strain distribution along the steel rebar at different percentages of life. It is clear that the steel rebar yielded during the 1st cycle between 375mm and midspan. At 10 % life, the strain gauge reading at midspan and 375mm increased and remained almost the same until 80% of the life. At 80% life, once the CFRP rod started slipping, the reading of the strain gauge at 125mm increased to account for the tensile force lost by the slipping CFRP rod. The reading of the strain gauge at 125mm increased from 1584 με at 80 % life to 2134 με at 100% life and thus corresponded to a slip of 5.6mm.

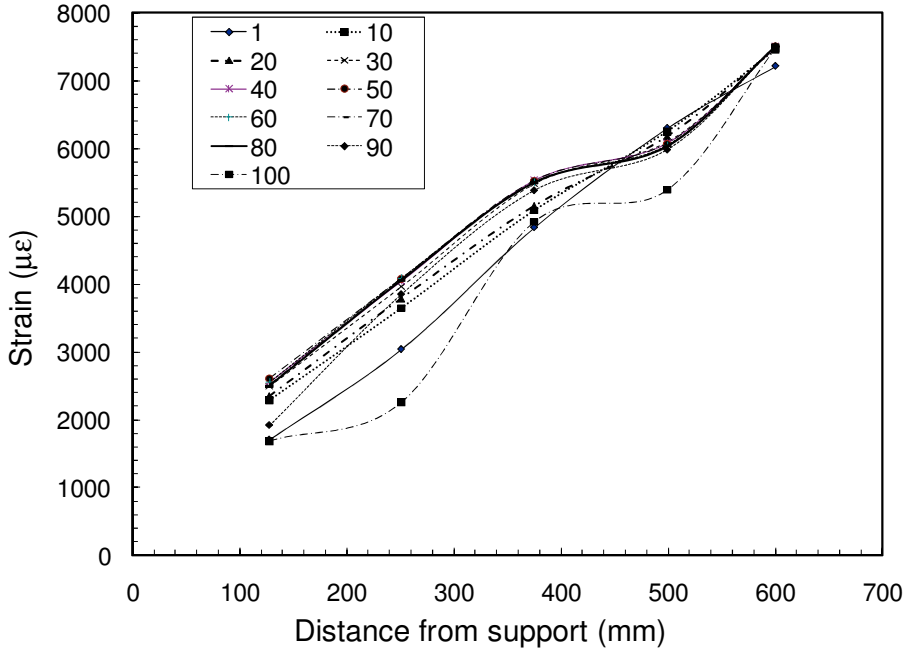

a-Strain distribution along CFRP rod at different life

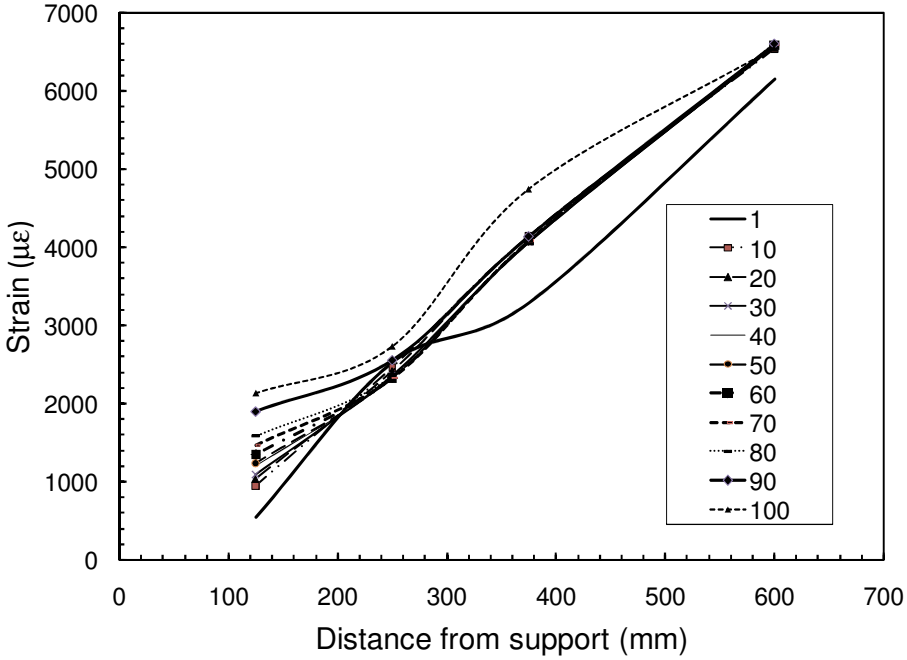

b-Strain distribution along steel rebar at different life

Figure 3.30: Strain distributions for beam S-SW-0%-71.4%

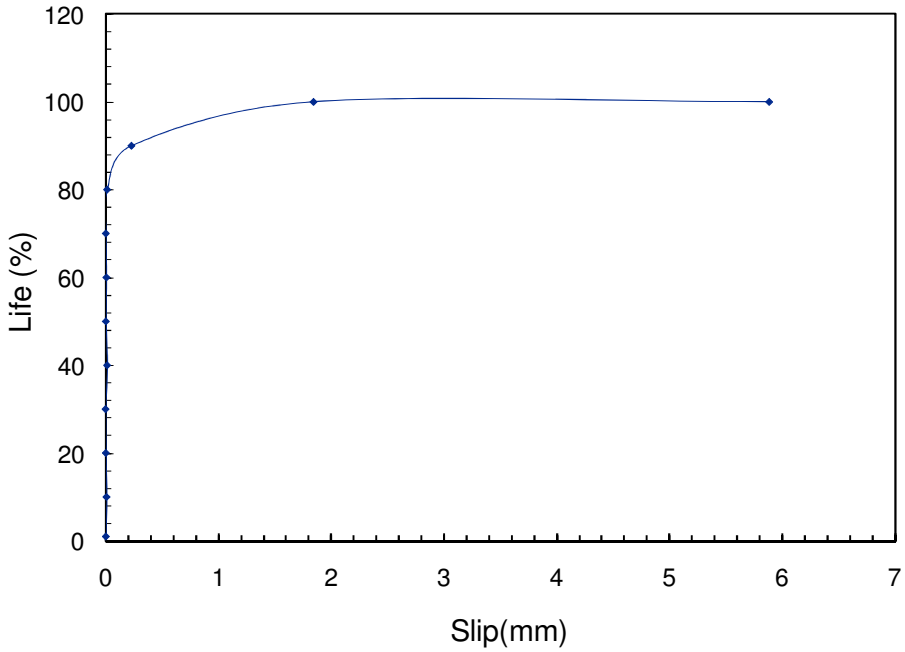

Figure 3.31: Life versus CFRP rod end slip from epoxy for beam S-SW-0%-71.4%

3.4.6 Group D: Beams with internal steel and strengthened with non-prestressed sand coated CFRP rod

Four beams were tested in this group. The upper load levels were chosen to avoid steel rupture based on the load levels in group C. All the beams cracked and failed in bond in the same way. Similar to the previous groups, beams in this group failed by debonding between the CFRP rod and the epoxy that started at the loading point and spread towards the support.

Cracking behaviour

Beams of this group cracked similarly to beams in group C. The cracks were uniformly spread in the shear span due to the internal steel rebars. The closest crack to the support ranged from 80mm to 190mm. In 3 beams, the closest crack was seen during cycling close to failure. Only

in one beam, a monotonic crack formed in the first cycle. At complete failure, the vertical cracks that formed during cyclic loading propagated horizontally and joined one another at the steel- concrete interface. After failure, the shear span of the beam could be divided into 2 regions. Region1 extends from center line of the support to the closest crack to the support. Region 2 extends from the closest crack to the support to the loading point.

In region1, bounded between the support and the first crack, there were cracks in the concrete parallel to the CFRP rod or fanning from the CFRP rod as shown in Figure 3.32. Also, some of the beams showed debonding between the CFRP rod and the epoxy in the cross section at the free end. The debonding might be accompanied by the epoxy cracking in the cross section as shown in Figure 3.32.

Region 2 is bounded by the closest crack to the support and the loading point. At the beginning of this zone (from the support side), the cracks that occurred at both sides of the beam connected together through cracks at the soffit of the beam. Some of the side cracks might have interconnected with one another or propagated horizontally at the steel to concrete interface. Yet, in all cases the chunks of concrete and epoxy would still be intact with the beam and the CFRP rod and if any separation happened it would be the bottom cover of the epoxy and concrete (chunk 3 in Figure 3.28). Close to the loading point, chunks of epoxy and concrete separated from the side of the beam as shown in Figure 3.33 leaving the CFRP rod and the beam.

Past the loading point, the horizontal crack would propagate at the steel concrete interface separating the CFRP rod with the epoxy and the concrete as one unit from the rest of the beam as shown in Figure 3.33.

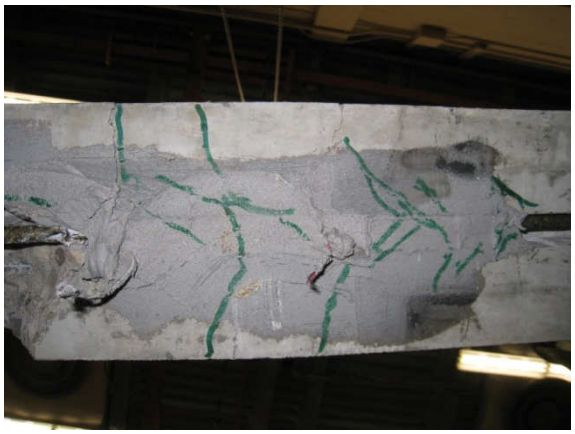

a-Cracks fanning from the CFRP rod

b-Cracks parallel to the CFRP rod

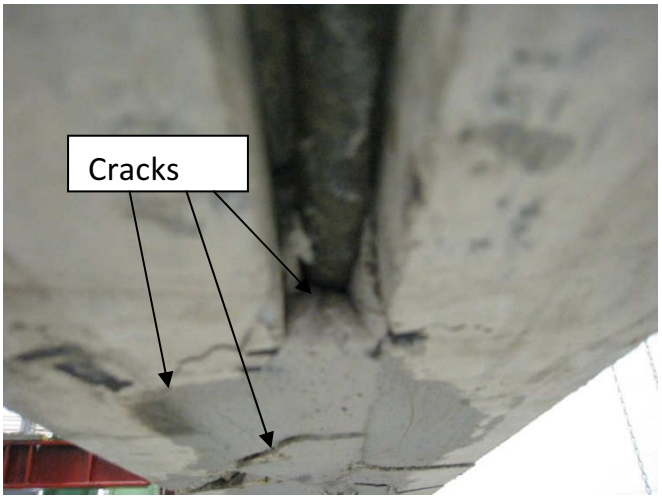

c-Cracks at the free end

(Show debonding)

Figure 3.32: Beams after failure (zone 1)

a-Beams after failure

b-Separated chunks from the CFRP rod

Figure 3.33: Beams after failure (zone 2)

Strain distribution along the CFRP rod

Beams in this group behaved in a similar way to beams in groups B and C. Figure 3.34-a and Figure 3.34-b show the strain distribution at the upper load level for beam S-SC-0%-78% along the CFRP rod and steel rebar, respectively. At 10 % life, strain gauge reading of the CFRP rod at 250, 375 mm and 500mm increased. The readings at 375 and 500mm indicate partial debonding between these two locations. As life increased further, strain gauge reading

at 250 mm increased. It is clear that there is almost full debonding between the strain gauges at 250 and 375mm. At 70% life, the strain reading at 125 mm reaches its peak value of 3160 με and the reading was almost constant until reaching 90% of the life.

Figure 3.34-b shows the strain distribution along the steel rebar at different percentages of life. It is clear that at 1st cycle the steel rebar had yielded at midspan. As the load was cycled, the gauge readings remained almost constant until reaching 90% life. After 90% life, as slip increased, the strain gauge readings at 125, 250 and 375mm increased to take up the forces from the slipping CFRP rod. Past 90 % of the life, the CFRP rod started slipping from the epoxy as shown in Figure 3.35 and the CFRP strain readings at 125 and 250 mm dropped.

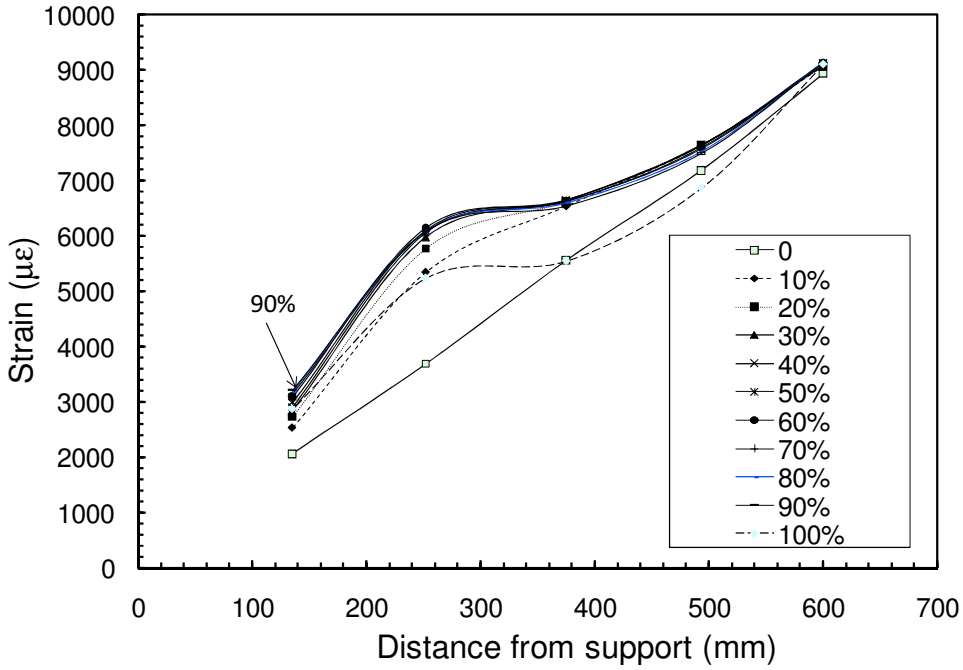

a-Strain distribution along CFRP rod at different life

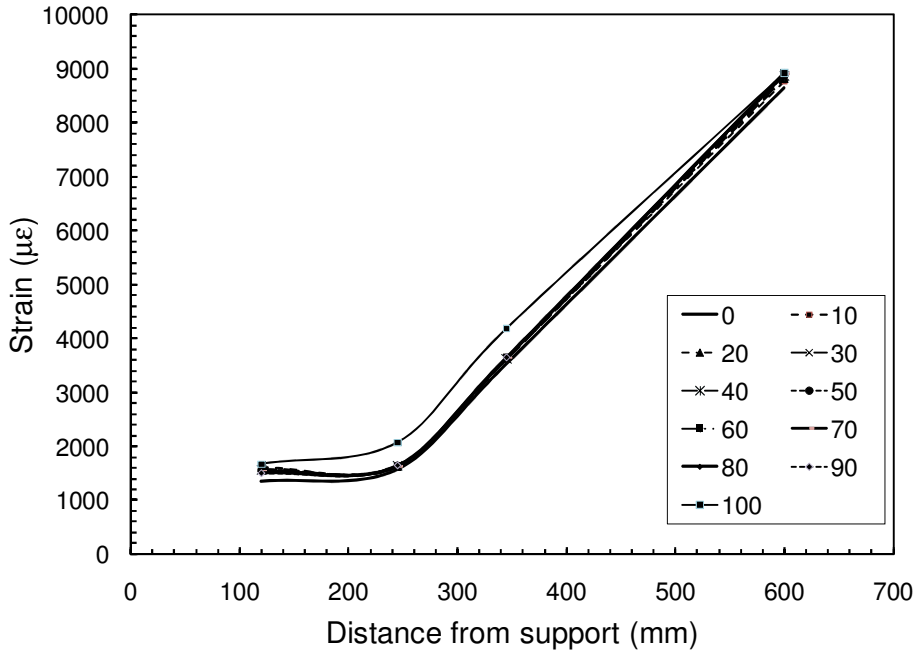

b-Strain distribution along steel rebar at different life

Figure 3.34: Strain distributions for beam S-SC-0%-78%

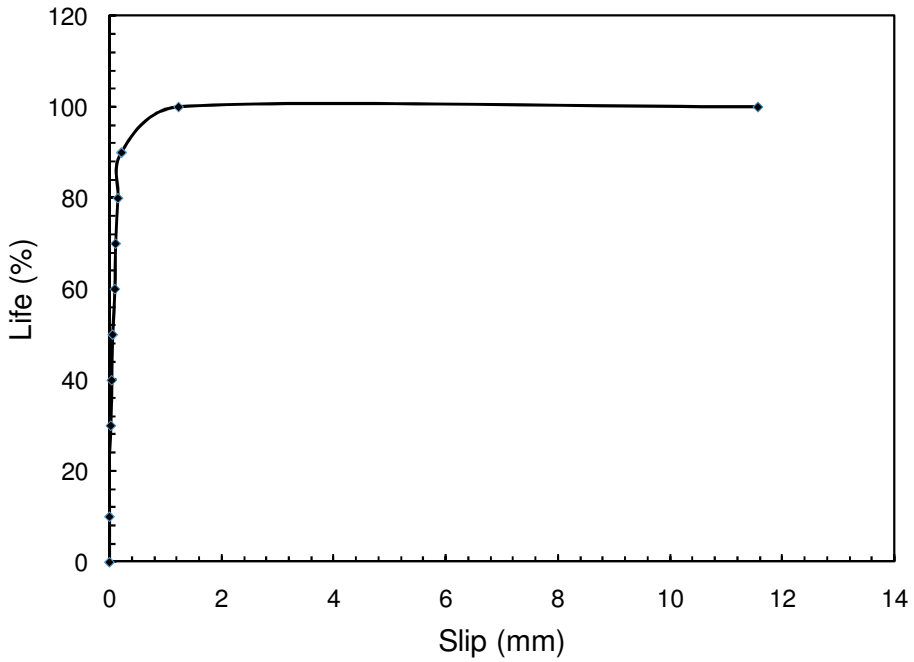

Figure 3.35: Life versus CFRP rod end slip from epoxy for beam S-SC-0%-78%

3.5 Strain distribution at onset of slip

Figure 3.36 shows the strain distribution plotted at the first cycle and at onset of excessive slip for beams tested at different load levels. For example, for the beams with no internal steel and strengthened with spirally wound rods the notation 60%- 1cycle is the strain distribution along the CFRP rod at 1st cycle for the beam with a peak load of 60% of its monotonic capacity. The notation the notation 60%- 60% for the same beam, means the strain distribution along the CFRP rod at 60% of the life (onset of slip). Since slip is the failure criteria, then the strain readings at onset of excessive slip represent the maximum value for the readings at any given location for any beam. It is clear that for all the beams strengthened with the same CFRP rod, regardless of the load level, the strain distribution had the same shape. At the onset of slip, sections close to midspan showed full debonding where the strain reading is equal to the strain at midspan. Sections closer to support show strain readings higher than the first cycle but not

equal to the strain at midspan. This indicates that the crack at the CFRP-epoxy interface has progressed towards the support. Also, the strains recorded by the strain gauges closest to the support were almost the same for the same set of beams strengthened with the same CFRP rod type. This implies the same maximum shear stress for a given rod type prior to excessive slip. Spirally wound rods showed an average peak strain of 3560 and 2684 με (85% and 64% of the monotonic value) before failure, for the beams that had no steel and with steel, respectively. Sand coated rods showed an average peak strain of 5140 and 3623 με (76% and 54% of the monotonic value) before failure, for the beams that had no steel and reinforced with steel, respectively. From Figure 3.36, it is clear that, regardless of the applied load, the spirally wound rod starts slipping somewhere between 60% and 80% of the life. Meanwhile, the sand coated rod starts slipping somewhere between 80% and 90% of the life. This implies that beams strengthened with sand coated rods are better under fatigue loading as concluded earlier (Figure 3.19).

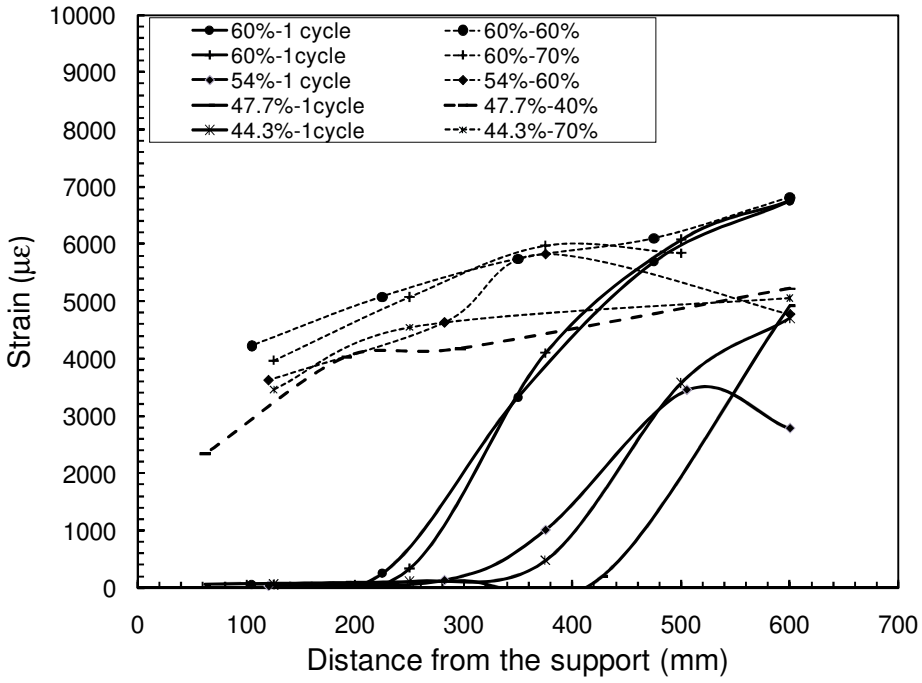

a-Beams with no internal steel rebars and strengthened with spirally wound rods

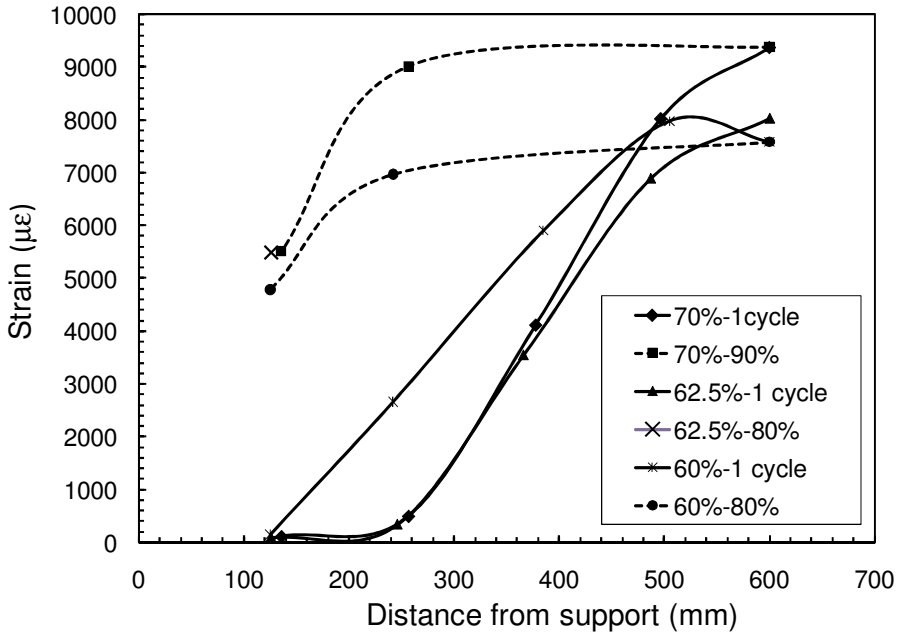

b-Beams with no internal steel rebars and strengthened with sand coated rods

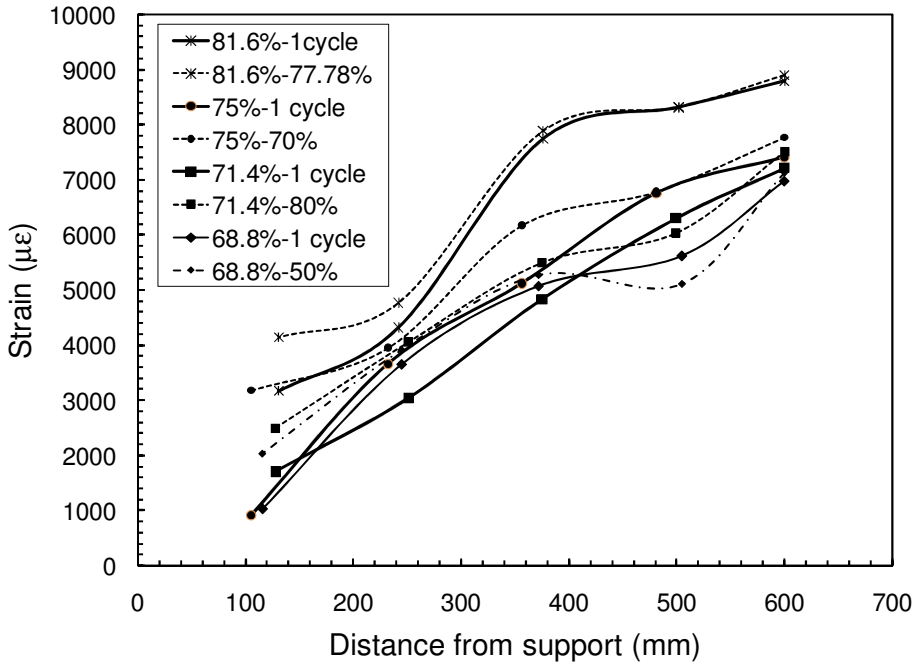

c-Beams with internal steel rebars and strengthened with spirally wound rods

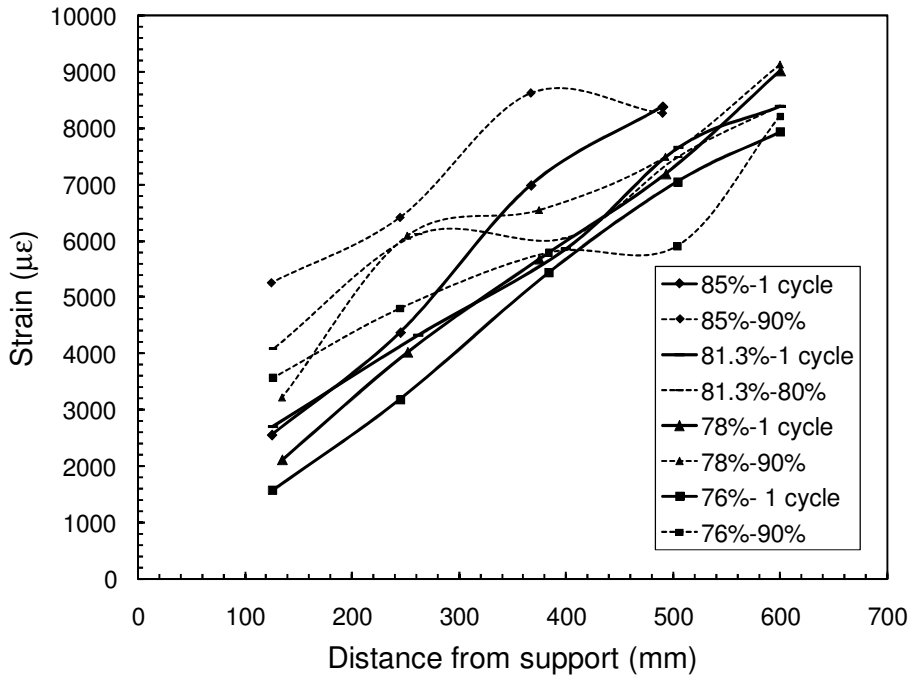

d-Beams with internal steel rebars and strengthened with sand coated rods

Figure 3.36: Strain distribution along the shear span at first cycle and at peak value

Chapter 4: Experimental Results for Prestressed Beams

4.1 Overview

Twelve beams were prestressed with NSM CFRP rods and tested. Two beams had no internal steel reinforcement. Ten beams were internally reinforced with 2 No.10 steel reinforcing bars. Seven beams were strengthened with spirally wound CFRP rods and five beams were strengthened with sand coated CFRP rods. The CFRP rods were prestressed to a tensile force of 62 kN which corresponds to 45% of the monotonic capacity of the spirally wounded rods and to 40% of the monotonic capacity of the sand coated rods. Four beams were tested monotonically and eight beams were tested under different fatigue load levels. The beams failed by either rupture of the CFRP rod or by bond failure.

4.2 Strain distribution and modes of failure

The axial strain (and stress) distribution along the CFRP rod is a combination of strain due to prestressing and strain due to loading.

4.2.1 Strain distribution due to prestressing

As mentioned earlier, during prestressing the strain in the CFRP rod was constant along the length of the rod and was equal to the prestressing strain. When the prestressing force was released, the strain in the rod at the free end dropped to zero. The free end is considered to start from the centerline of the support (where the epoxy was terminated). During release, some slip occurs between the CFRP rod and the epoxy at the end of the CFRP rod. When the CFRP rod slipped inside the epoxy, the crack front will be located at a distance from the centerline of the

support. That distance will be discussed in Section 4.3. Figure 4.1 shows the transfer length. Transfer length is the distance from the crack front until the strains in the CFRP rod reach the prestressing strain.

The shear stress distribution along the length of the rod is also shown in Figure 4.1. The shear stresses between the CFRP rod and the epoxy are the highest at the crack front and then decrease until they reach zero at the end of the transfer length. From equilibrium, there is a residual shear stress between the maximum shear stress and the free end as shown in Figure 4.1. The residual shear stress drops the value of the shear stress between the CFRP rod and the epoxy from a high shear stress at the beam end to the maximum shear stress that could occur at the rod-epoxy interface. However, since the distance from the free end to the point of zero strain is small (25-50 mm as will be explained in Section 4.3), the residual shear stress in this region will be ignored in the calculations.

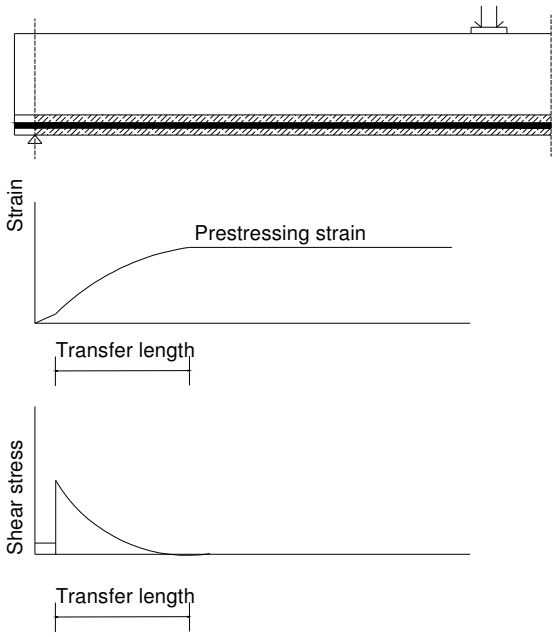

Figure 4.1: Strain distribution in the CFRP rod due to prestressing

4.2.2 Strain distribution due to applied load

The beam is loaded in four point bending. The strain due to external applied load will increase from zero at the support to a maximum strain underneath the loading point and remain constant at midspan.

The total strain in the CFRP rod is the summation of strain due to prestressing and strain due to the applied load. The peak strain/stress (shear) due to prestressing is at the support and the peak strain/stress (shear) due to the applied load is at the loading point. When both cases are superimposed, the section with the peak stress will be the critical section. The mode of failure will depend on the location of the critical section. The expected modes of failure are:

1-Bond failure:

a- Debonding that starts at the loading point and spreads towards the support

Debonding between the epoxy and the CFRP rod that starts at the loading point and spreads towards the support will occur if the critical section with the highest shear stresses is at the loading point. This mode of failure was discussed in Chapter 3 for the case of the beams strengthened with non-prestressed NSM CFRP rods.

b- Slipping between the CFRP rod and the epoxy that starts at the support and travels to the loading point

This mode of failure will occur if the critical section with the highest stresses between the rod and the epoxy is the one close to the support. In this case, slipping between the CFRP rod and the

epoxy at the support will occur before debonding at sections close to the loading point. This mode of failure could occur only for beams strengthened with prestressed CFRP rods.

2-Rupture of the CFRP rod:

This mode of failure will occur if the normal stress in the CFRP rod is high and the bond failure is expected to occur by slipping between the CFRP rod and the epoxy that starts at the support and travels to the loading point. In this case, rupture of the CFRP rod occurs prior to bond failure.

4.3 Transfer length

4.3.1 Measured data

As discussed earlier in Chapter 2, the CFRP rods were prestressed to the desired strain (0.65% for the spirally wound rod and 0.69% for the sand coated rod). The epoxy was cured for 7 days then the prestressing force was released. During the release of the prestressing force, the strain gauges recorded the remaining strain in the CFRP rod. The transfer length of the prestressed NSM CFRP rod in the epoxied groove inside the reinforced concrete beams was determined from the distribution of the strain along the length of the rod. During release, some slip occurs between the CFRP rod and the epoxy at the end of the CFRP rod. Between the free end and the crack front, there is linear strain as indicated by the dotted circle in Figure 4.2 and therefore, the residual shear stress in this region is uniform. The end slip was measured for some beams. It ranged from 0.2-0.4 mm. The distance (s_i) from the end of the bonded length (free end) to the crack front is taken to be the measured end slip divided by the difference between the prestressing strain and the residual strain (remaining strain in the rod) and gave a value of 25mm

for the sand coated rod and 50mm for the spirally wound rod. Figure 4.2 shows a typical strain distribution along the transfer length for Beam S-SC-40%-63%.

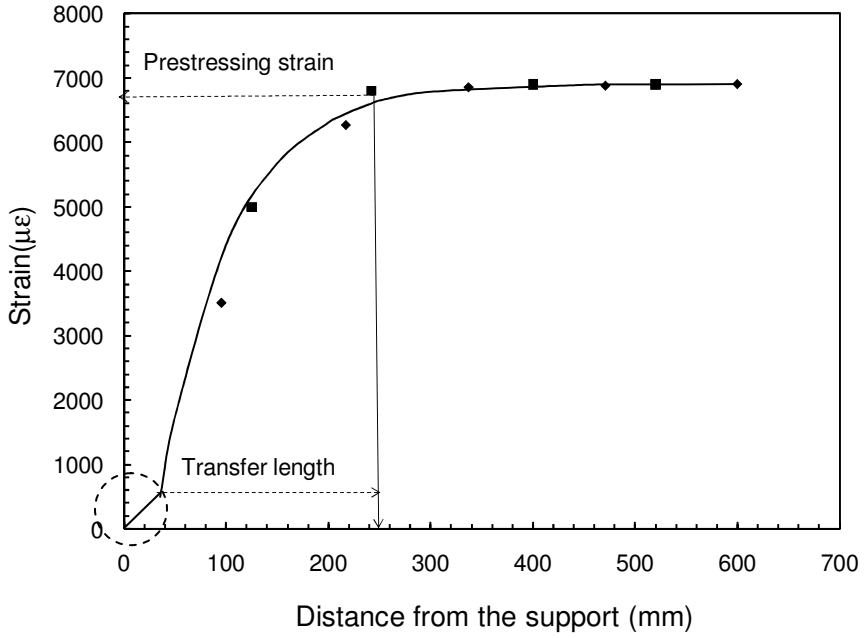

Figure 4.2: Transfer length for beam S-SC-40%-63%

The final strain readings after the prestress force release for all gauges along the length of the CFRP rod were normalized to the initial prestressing strain. The normalized stress values are equal to the normalized strain values since the CFRP rod is a linear elastic material. Thus, the normalized stress was plotted versus the beam length as shown in Figure 4.3. The normalized readings were combined from both sides in addition to the reading at midspan. Thus each beam provided 9 data points. Based on the experimental data, the transfer length for the 45% prestressed spirally wound CFRP rods ranged between 150 and 210 mm measured from the end of bonded length (free end) while the transfer length for the 40% prestressed sand coated CFRP rods varied from 140 to 185 mm measured from the end of bonded length (free end). Thus, the transfer length for the 45% prestressed spirally wound CFRP rods ranged between 100 and 160

mm measured from the crack front (located at distance s_i), while the transfer length for the 40% prestressed sand coated CFRP rods varied from 115 to 160 mm measured from the crack front.

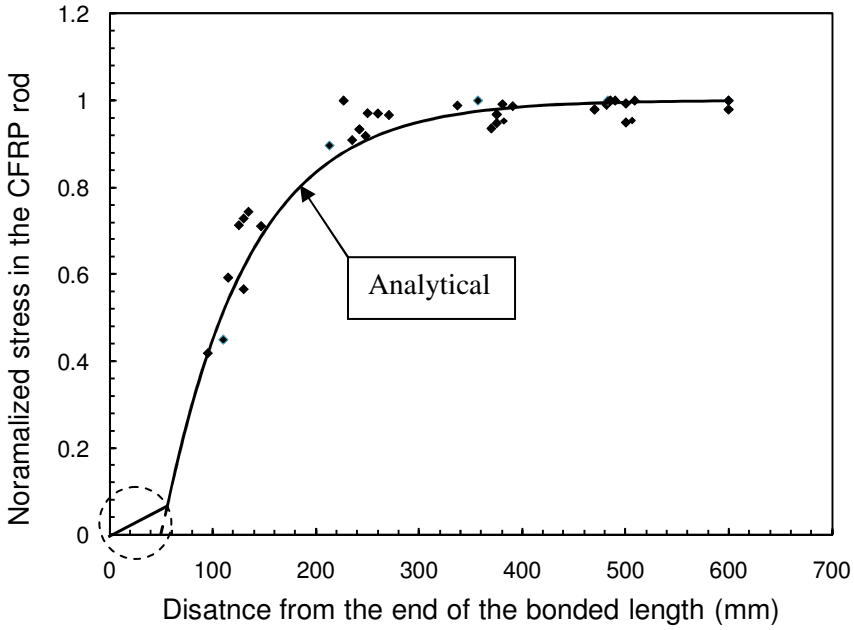

a- Spirally wound CFRP rods

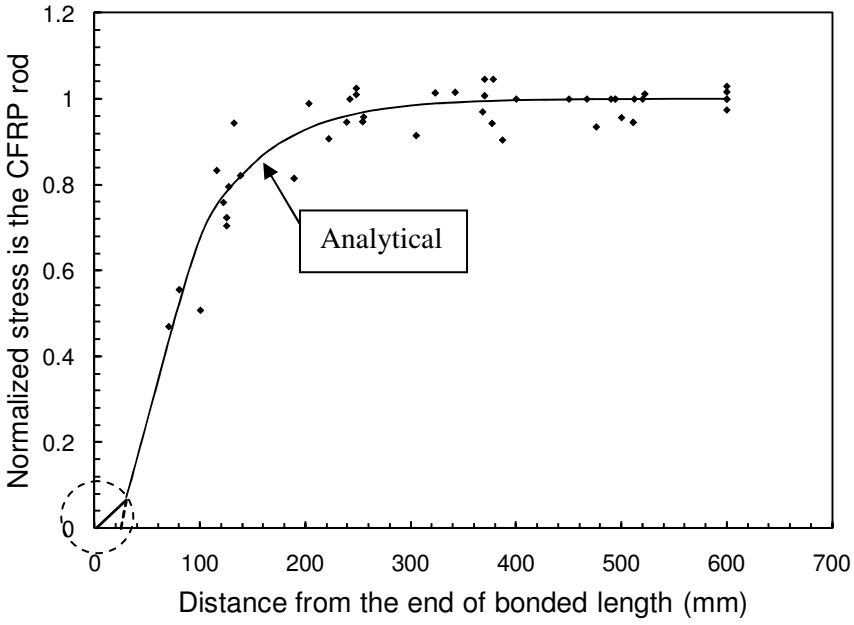

b- Sand coated CFRP rods

Figure 4.3: Strain distribution of prestressed beams: experimental data vs. analytical predictions

In comparison, Badawi (2007) prestressed spirally wound CFRP rods to 40% and 60 % of their ultimate capacity. He reported a range for the transfer length of 200 to 300mm and 230 to 400mm for the 40% and 60% prestressing levels, respectively. Wahab et al. (2008) reported a range for the transfer length of 250 to 300mm for a 50% prestressing level for spirally wound rods. Both studies considered the free end to be the point where the strain drops to zero. No prestressing data for sand coated rods were found in the literature. Therefore, the transfer length results presented in this chapter for the spirally wound rods were in the same order of magnitude as these reported in previous studies.

4.3.2 Empirical expression

A semi-empirical equation was proposed by Badawi (2007) to predict the variation of the prestressing stress in the spirally wound CFRP rod along the beam at transfer. It was found that an exponential equation provides the best fit of the measured data, as follows:

$$f_s = f_{pre}(1-\exp^{-\mu \cdot x}) \qquad \text{E.q.(4.1)}$$

where,

f_s :Prestressing stress in CFRP rod for a given distance (x) from the end of the bonded length

f_{pre}: Upper limit of the stress in the CFRP rod or the maximum prestressing stress

x: Distance from the end of the bonded length minus the distance (s_i)

s_i: Distance ranges from 25-50mm. It is 25mm for sand coated rods and 50mm for spirally wound rods.

μ: Factor to account for the rod type, epoxy type, epoxy thickness, and method of release. Based on the current study, it was taken equal to the exponent of the monotonic shear stress distribution

due to loading in the non-prestressed beams. It is equal to 0.015 or 0.012 for the sand coated and spirally wound rods, respectively as will be explained in Chapter 5.

Figure 4.3 also shows the transfer length prediction using Equation 4.1 with the experimental results for the spirally wound and sand coated rods prestressed to 45% and 40% of their monotonic capacity, respectively. The predicted curves using the exponential expression are a good fit to the experimental data.

4.4 Monotonic test results

Four beams were tested under monotonic load. Three beams were strengthened with prestressed spirally wound CFRP rod and the other was strengthened with prestressed sand coated CFRP rod. Two beams were strengthened with prestressed spirally wound CFRP rods and had no internal steel reinforcement. These beams failed by rupture of CFRP rod. One beam was strengthened with prestressed spirally wound CFRP rods and had internal steel reinforcement. The beam failed by slipping between the CFRP rod and the epoxy that started at the support and propagated towards the loading point. One beam was strengthened with the sand coated CFRP rod and had internal steel reinforcement. It failed by debonding between the rod and the epoxy that started at the loading point and propagated towards the support. The test results and observations for the monotonic beams are presented in the following sections. Table 4.1 summarizes the monotonic test results.

Table 4.1: Monotonic test results for prestressed beams

Group	Specimen notation	Minimum Load	Maximum Load	Max. Capacity (kN) or Life (cycles)	Failure mode
E	NS-SW-45%-M(a)	monotonic		103.5 kN	CFRP Rupture
	NS-SW-45%-M(b)	monotonic		107 kN	
F	S-SW-45%-M	monotonic		130.16 KN	Bond
G	S-SC-40%-M	monotonic		174.63 kN	Bond

4.4.1 Load-deflection behaviour

Figure 4.4 shows a typical load versus midspan deflection for beams with internal steel, strengthened with prestressed CFRP rod and tested under monotonic load. As the load increases, the midspan deflection increases until concrete cracks at midspan (at about 68 kN in Figure 4.4). Past midspan cracking, load versus deflection slope decreases. Midspan deflection continues to increase as the load increases until complete failure.

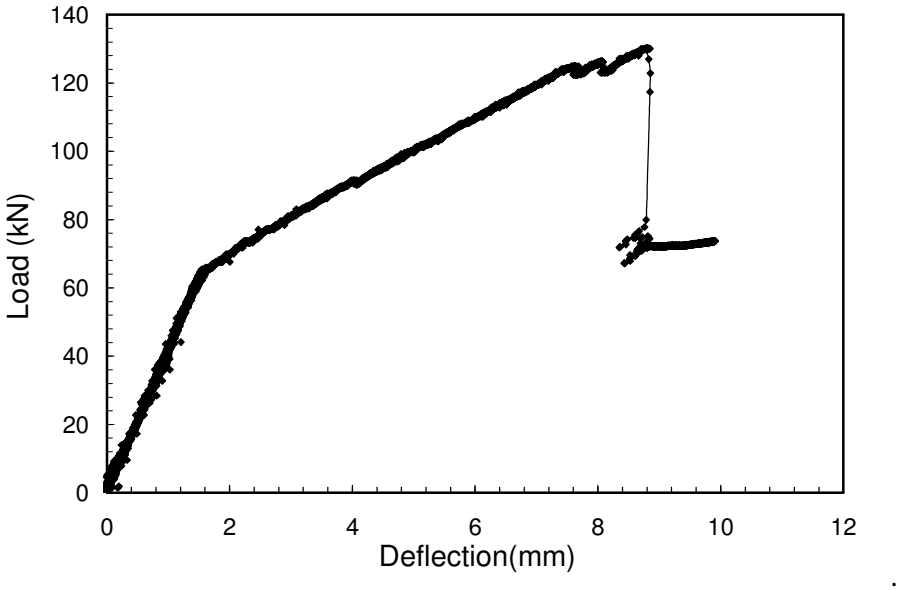

Figure 4.4: Load versus midspan deflection for beam S-SW-45%-M

4.4.2 Beam with no internal steel and strengthened with prestressed spirally wound CFRP rod

These beam failed by rupture of the CFRP rod at midspan. Figure 4.5 shows the load versus CFRP total strain at midspan for beam NS-SW-45%-M (a). The concrete cracked at midspan at about 70 kN. As the load increased, the CFRP strain at midspan increased until reaching a peak load of 103.5 kN at a strain of 12700 με. The CFRP rod ruptured at this load level and there were no signs of bond failure.

Other groups (beam with steel and strengthened with prestressed CFRP rods) were then tested and sufficient information on bond failure of prestressed NSM CFRP rods was obtained. Thus, this group was discontinued and was not tested under fatigue loading.

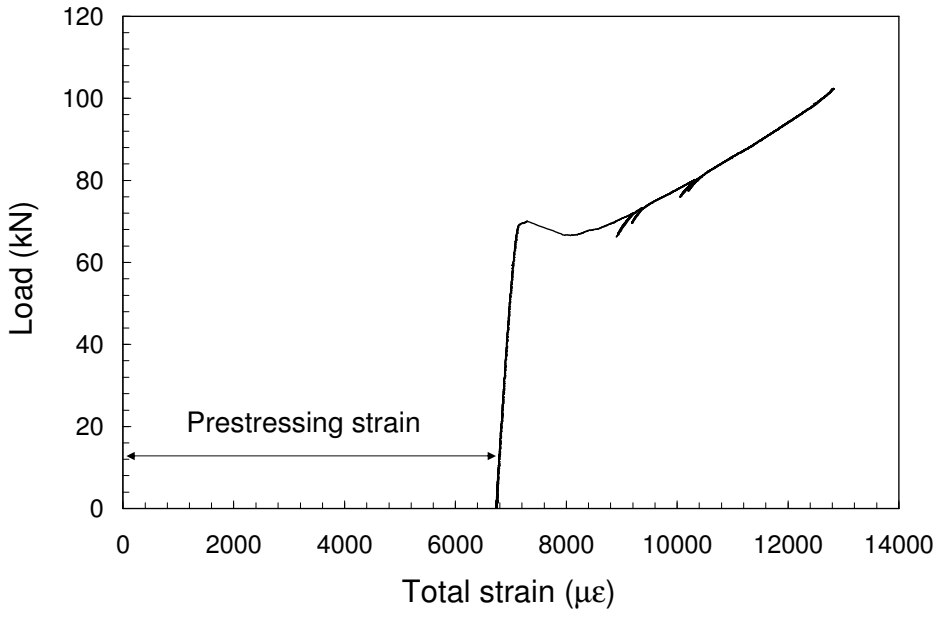

Figure 4.5: Load versus total strain in the CFRP rod for Beam NS-SW-45%-M (a)

4.4.3 Beam with internal steel and strengthened with prestressed spirally wound CFRP rod

Cracking behaviour

Figures 4.6 and 4.7 show the load versus CFRP strain and the load versus steel strain for beam S-SW-45%-M. As the load increased, the steel and CFRP strains increased at all locations along the beam length until the load reached 68 kN at which point the beam cracked at midspan. The tensile stresses were transferred from the concrete to the CFRP rod and the steel rebar and there was a sudden increase in the readings of the strain gauges mounted on the CFRP rod and the steel rebar. When the load reached 124kN, the first evidence of slip between the CFRP rod and the epoxy was recorded. At the same time a crack was observed at 140 mm from centerline of the support. At this stage, the internal steel which was still in the elastic range (has not yielded) took up the tensile forces released by the slipping CFRP rod. When the load was increased to 126kN, slip between the CFRP rod and the epoxy increased to 0.4mm, the CFRP strains at 125mm and 250 mm from centerline of the support decreased and the steel strains at 125mm and 250mm from centerline of the support increased. Then, the load decreased to 123kN as the slip between the CFRP rod and the epoxy continued to increase. The load increased to 130kN and the slip was 0.65 mm at which time the crack at 140mm from centerline of the support was joined by a crack that propagated horizontally towards the midspan at the epoxy concrete interface. The slip between the CFRP rod and the epoxy increased to 6 mm and the load dropped to 73 kN (Figure 4.8). The cracked concrete cover is shown in Figure 4.9. In a region close to the support (140mm from the centerline of the support) epoxy covered with the concrete separated from the bottom of the beam and the rod separated from the remaining epoxy.

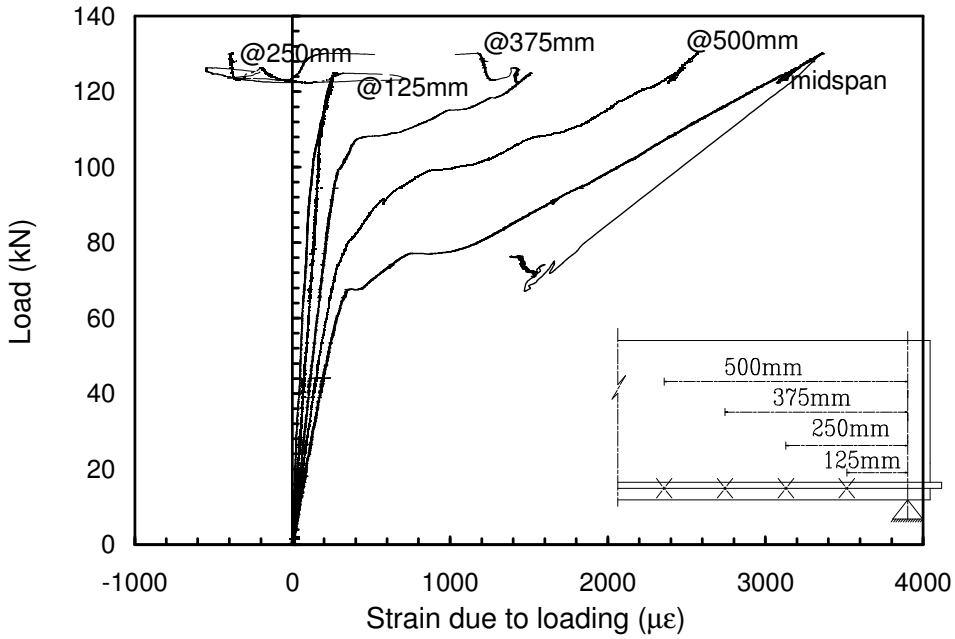

a- CFRP strain due to loading

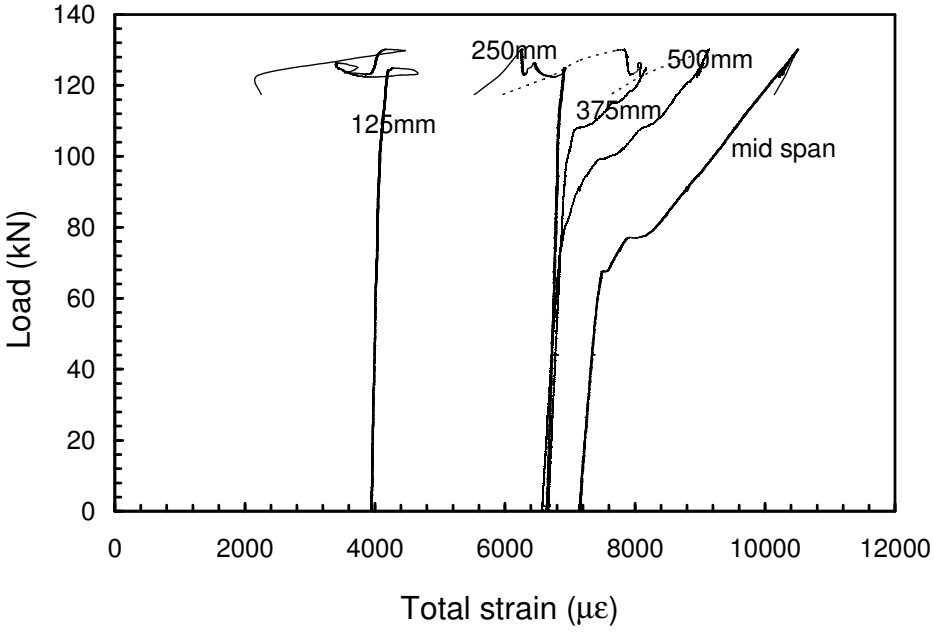

b-Total CFRP strain

Figure 4.6: Load versus CFRP strain for beam S-SW-45%-M

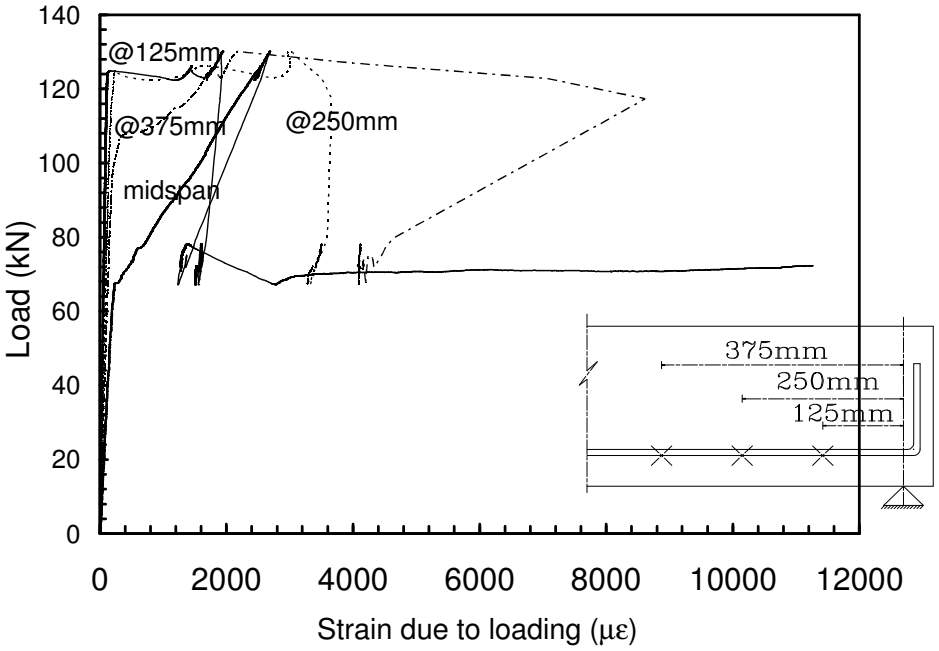

Figure 4.7: Load versus strain for steel rebar for beam S-SW-45%-M

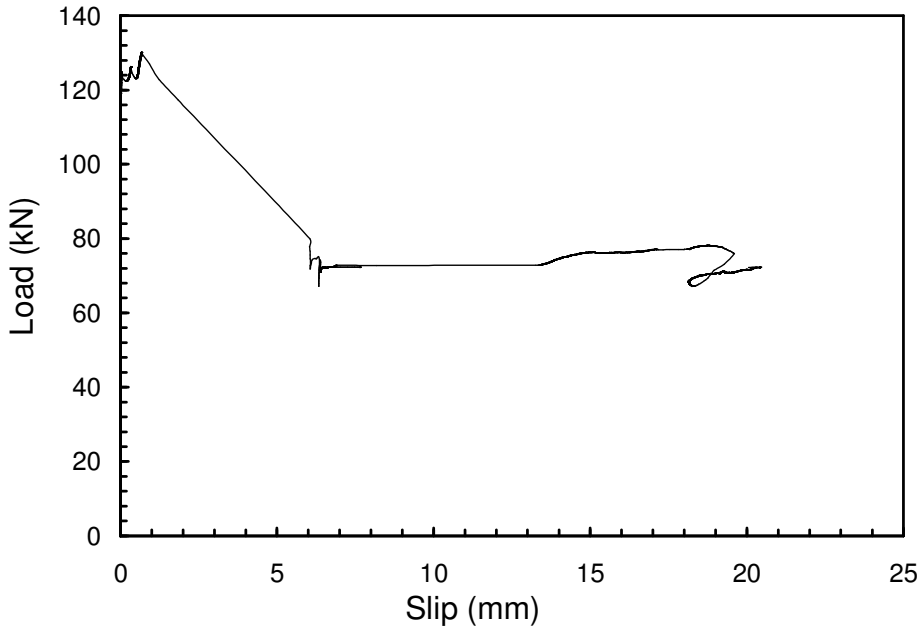

Figure 4.8:Load versus end slip for beam S-SW-45%-M

a-Beam after failure b-Soffit of the beam after failure

Figure 4.9: Beam S-SW-45%-M after failure

Strain distribution in the shear span

Figures 4.10-a and 4.10-b show the strain profile due to applied load and the total strain profile (the strain due to prestressing plus the strain due to the applied loading) at different locations along the CFRP rod at various load levels for beam S-SW-45%-M. Figure 4.11 shows the strain distribution along the steel rebar at various load levels. As the load increased, the strain at all locations increased. The increase in strain at midspan, 500 and 375mm was greater than the strain increase at 125 and 250mm until a load of 125kN. The strain distribution in the CFRP rod remained linear in the shear span with no signs of debonding at all. At a load of 125kN, the CFRP rod started slipping from the epoxy as shown in Figure 4.8. This was accompanied by a decrease in the CFRP strain readings at 125 and 250mm and an increase in the steel strain readings at 125 and 250 mm as shown in Figure 4.10-a and 4.11. At peak load of 130kN, the CFRP strain decreased further and the steel strain increased to compensate for the loss in tensile force in the CFRP rod due to slip.

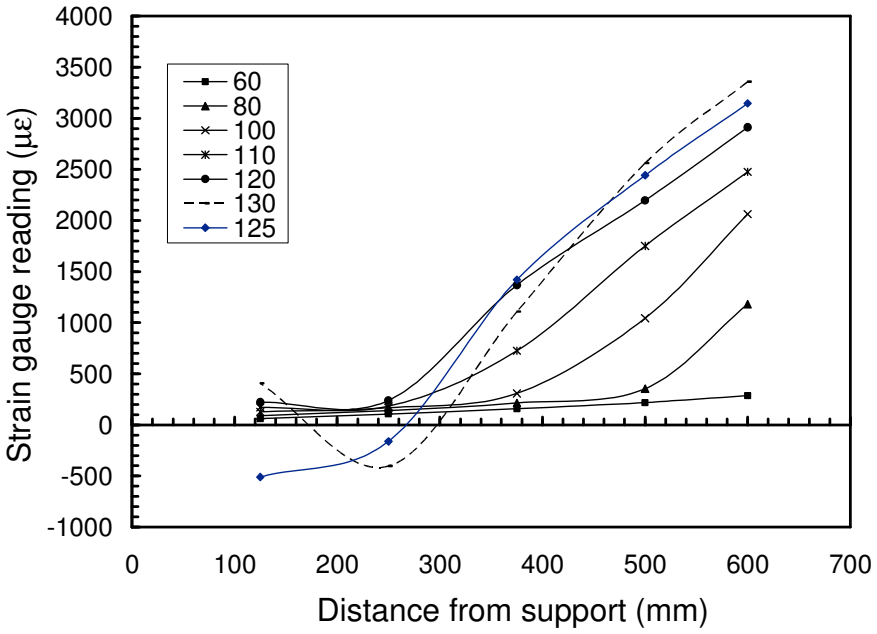

a-Strain due to applied load along the CFRP rod at different load levels

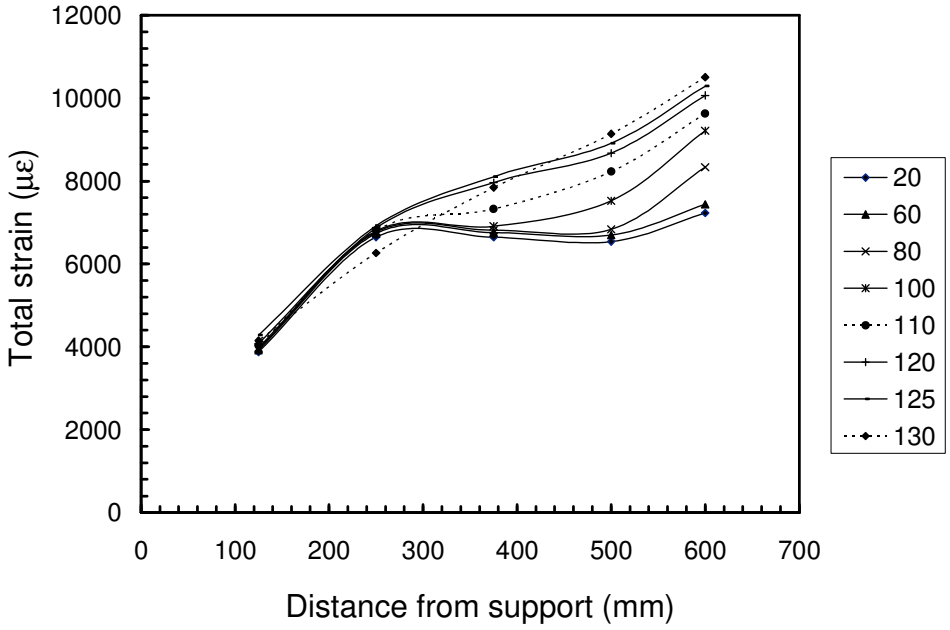

b-Total Strain in the CFRP rod at different load levels

Figure 4.10: CFRP strain distribution along the shear span for Beam S-SW-45%-M

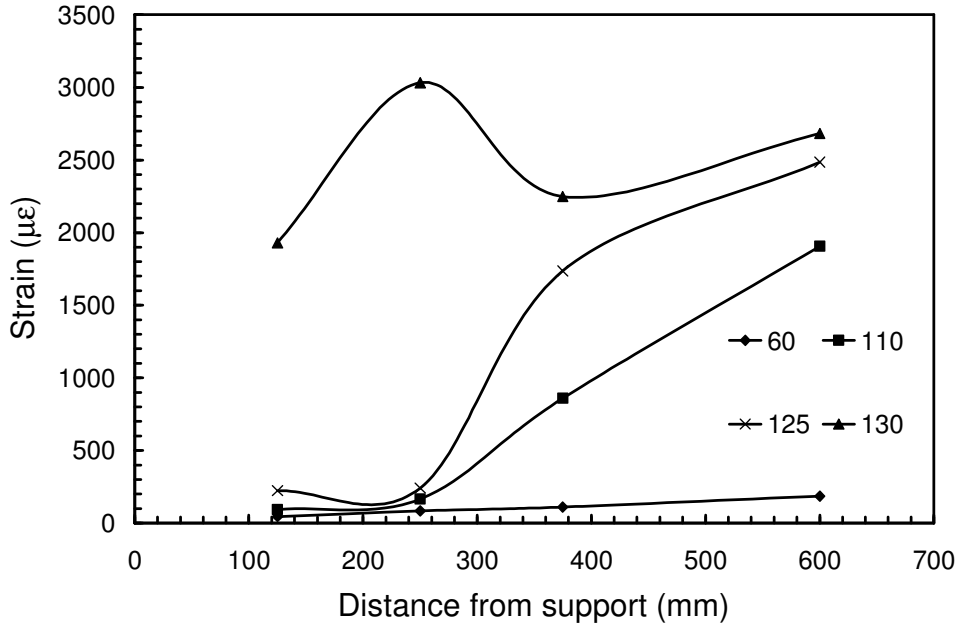

Figure 4.11: Steel strain distribution along the shear span for Beam S-SW-45%-M

4.4.4 Beam with internal steel and strengthened with prestressed sand coated CFRP rods

Cracking behaviour

The beam strengthened with prestressed sand coated CFRP rod behaved in a similar way to the beam strengthened with prestressed spirally wound CFRP rod. Figures 4.12 and 4.13 show the load versus CFRP strain and the load versus steel strain, respectively. The strain gauge readings of both the steel reinforcing bar and the CFRP rod increased slowly with the load until the load reached 77kN when the beam cracked at midspan. At this stage, the strain readings of both the steel and the CFRP gauges increased suddenly as the flexural tensile forces were transferred from the concrete to the steel reinforcing bars and the CFRP rod. As the test progressed, cracks were observed at locations away from the loading point. At a load of 140 kN, the steel strain at

midspan indicated yielding of the rebar at this section and there was an increase in the slope of the load versus CFRP strain. As the load increased further, the cracks on both beam faces connected with one another through the cross section of the beam. At the peak load of 174.4kN, debonding occurred between the CFRP rod and the epoxy. At failure, the end slip between the CFRP rod and the beam end was 21mm and the load dropped abruptly (Figure 4.14).

A horizontal failure plane occurred at the concrete steel interface on the sides of the beam and at the epoxy-concrete interface at the center of the beam where the beam was seen to split vertically and a crack close to the support propagated horizontally. After the crack propagated horizontally, the CFRP rod together with epoxy and concrete cover separated from the beam. At sections close to the loading point, the epoxy and the concrete did not separate from the rod. Further away from the loading point into the shear span and close to the supports, epoxy covered with concrete separated from the rod and the beam. However, for a zone of 100mm from the support, the epoxy covered with concrete separated from the bottom of the beam and the rod separated from the remaining epoxy as shown in Figure 4.15.

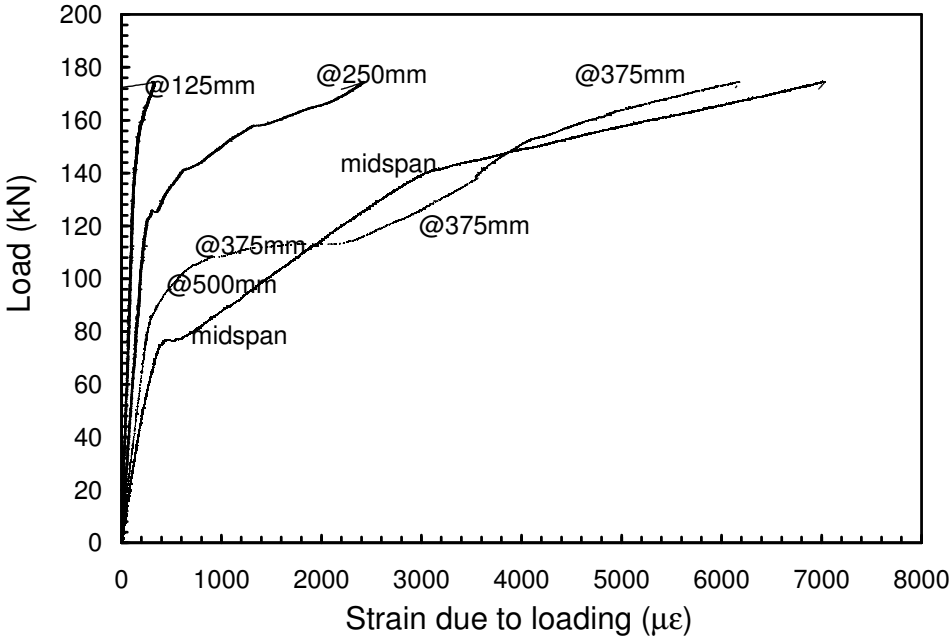

a- CFRP strain due to loading

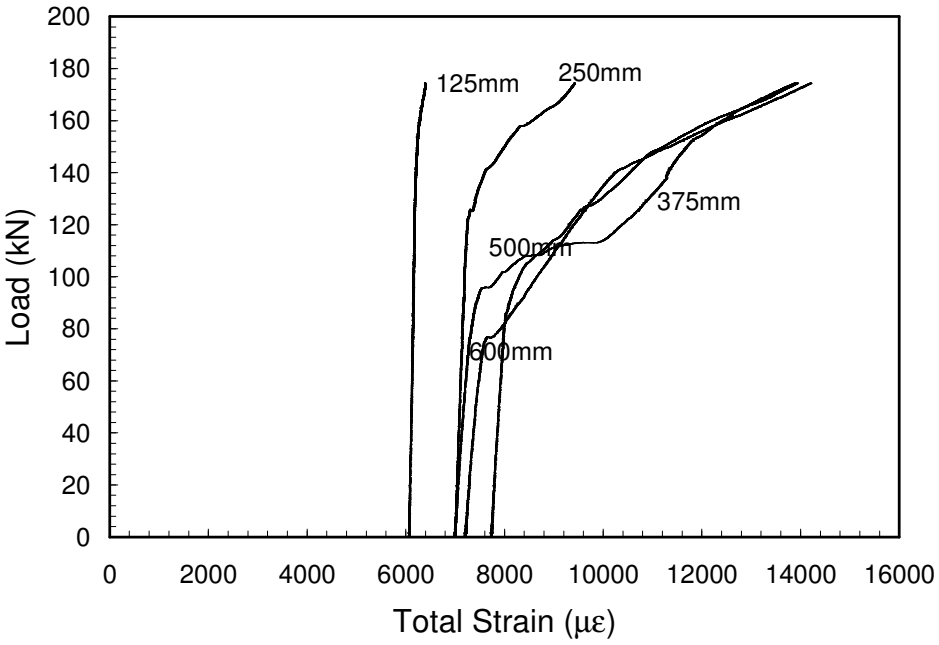

b-Total CFRP strain

Figure 4.12: load versus CFRP strain for Beam S-SC-40%-M

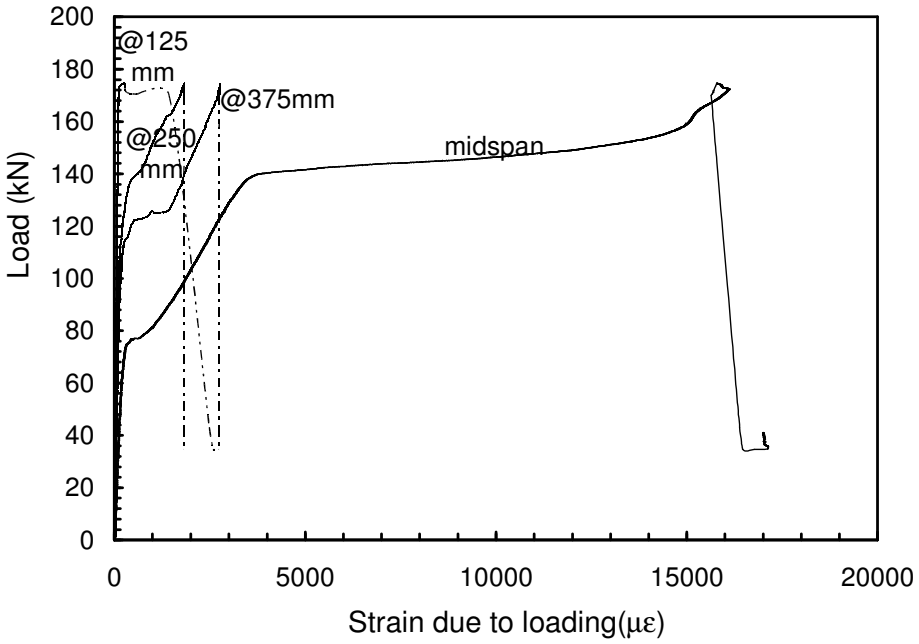

Figure 4.13: Load versus strain for steel rebar for Beam S-SC-40%-M

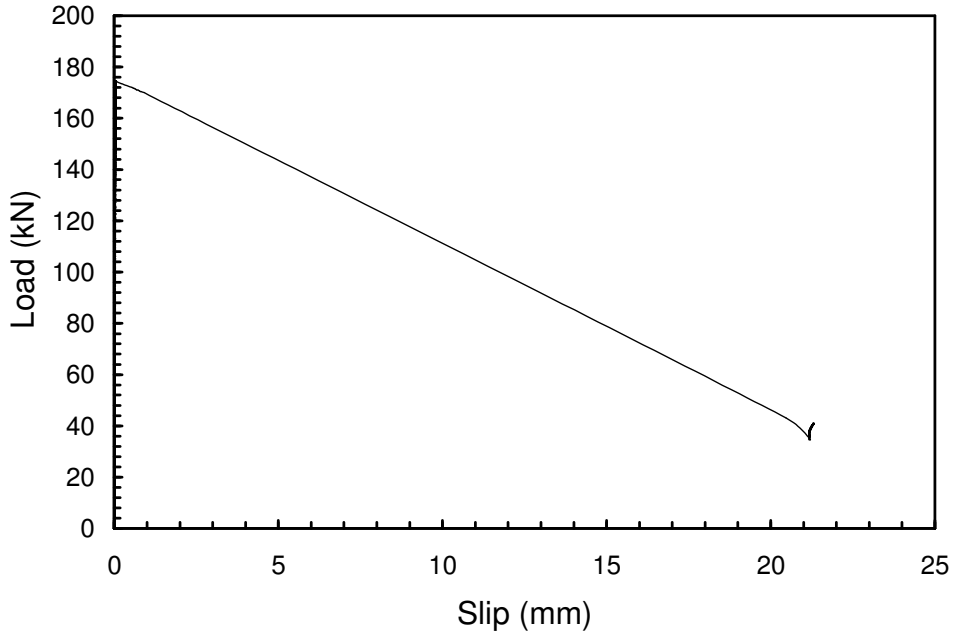

Figure 4.14: Load versus end slip for Beam S-SC-40%-M

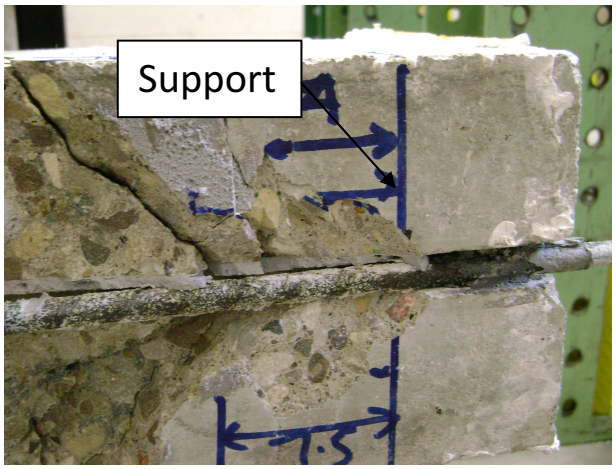

a-Shear span showing the plane of failure b-Soffit of the beam at the support

Figure 4.15: Beam S-SC-40%-M after failure

Strain distribution in the shear span

Figures 4.16-a and 4.16-b show the strain profile due to applied load and total strain profile (prestressing strain plus strain due to the applied loading) in the CFRP rod at various load levels for beam S-SC-40%-M. At a load of 100kN, the total CFRP strain at midspan was the highest (8647με) and close to the support it was almost equal to the prestressing strain. At a load of 110kN, strain due to loading at 500m and midspan was the same indicating debonding between these two locations. As the load increased to 120kN, debonding progressed to the gauge located at 375mm. Beyond a load of 120kN, the CFRP strain at 250mm increased until reaching its peak value at 174 kN. At this load level (174kN), there was full debonding between the CFRP rod and the epoxy at 375mm and midspan. At 174kN, the CFRP rod slipped from the epoxy. Figure 4.17 shows the distribution of strain along the steel rebar at different load levels. It is clear from this figure that before failure the strain readings at 125mm and 250mm were low. After the CFRP rod slips (at a load of 174kN), the CFRP strains at 125mm and 250mm increased as the force was transferred from the slipping CFRP rod to the steel reinforcing bar.

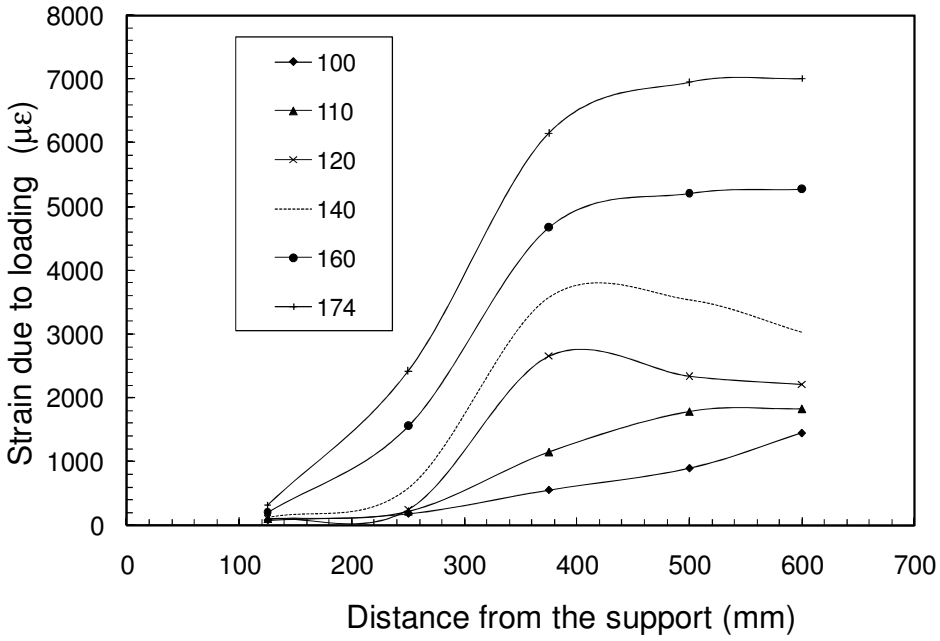

a-Strain distribution due to applied load along the CFRP rod at different load levels

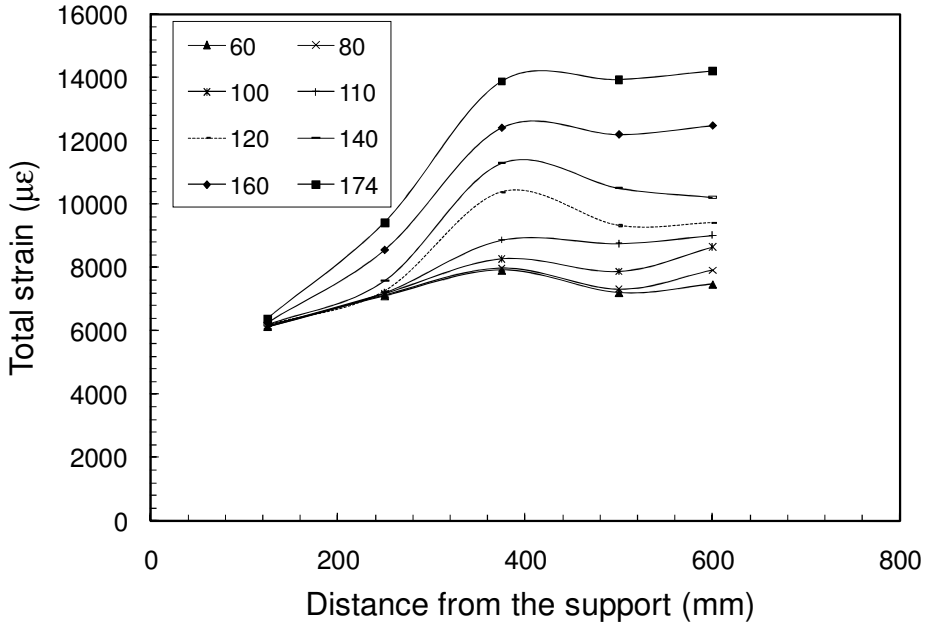

b-Total strain distribution along the CFRP rod at different load levels

Figure 4.16: CFRP strain distribution along the shear span for Beam S-SC-40%-M

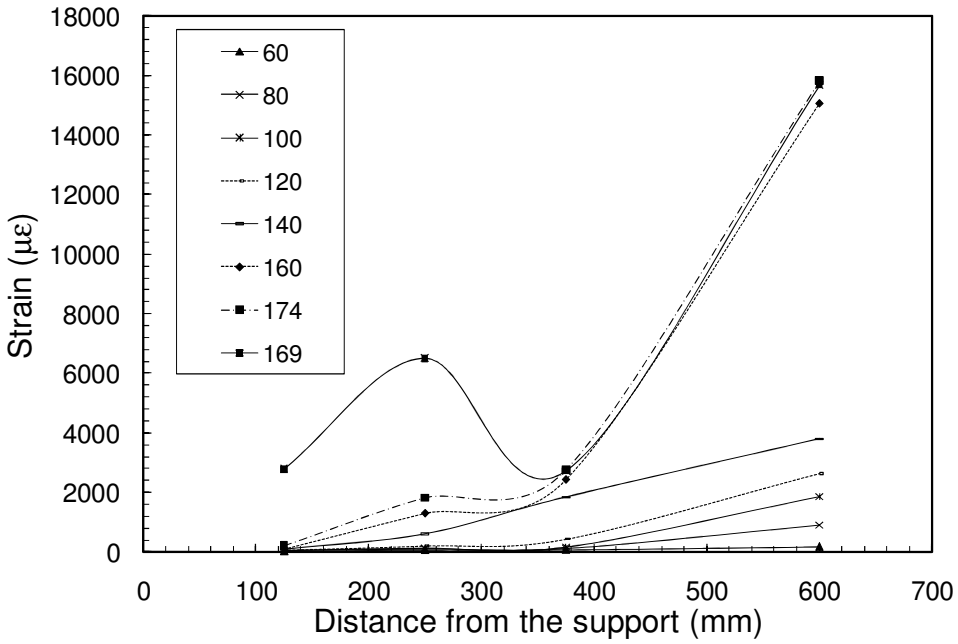

Figure 4.17: Strain distribution along steel rebar at different load levels for Beam S-SC-40%-M

4.5 Fatigue test results

4.5.1 Fatigue life

Table 4.2 summarizes the fatigue test results for all groups. Eight beams were tested under different fatigue load levels. All the beams had internal steel reinforcement. Four beams were strengthened with a prestressed spirally wound CFRP rod and the remaining four were strengthened with a prestressed sand coated CFRP rod. The measured strain range in Table 4.2 is calculated as the difference between the recorded readings of the strain gauge at midspan in the first cycle at upper and lower load levels. Some gauges were already damaged in the first cycle. Figure 4.18 shows the fatigue lives at different load ranges (kN) for beams with internal steel bars and strengthened with a prestressed CFRP rod. Figure 4.19 shows the fatigue lives at different load ranges (kN) for beams with internal steel strengthened with prestressed and non-

prestressed CFRP rods. For comparison purposes, the load range used for the prestressed beams is the difference between the maximum and minimum applied load (kN). The load range is not used as a percentage of the monotonic capacity because the beam S-SC-40%-M failed by debonding between the CFRP rod and the epoxy that started at the loading point and spread towards the supports. Meanwhile, all the beams with internal steel, strengthened with prestressed CFRP rod and tested under fatigue load in addition to the beam S-SW-45%-M failed by slipping between the CFRP rod and the epoxy that started at the support and propagated towards the loading point (as will be explained latter). Therefore, to compare the behaviour of the prestressed sand coated and spirally wound rods, by expressing the load ranges for group (G) as a percentage of the beam's monotonic capacity will give misleading results.

During testing, the lower load level was 10% of the monotonic capacity of the beam and the upper load level was varied to achieve failure between 1,000 cycles and 1,000,000 cycles. The beam loaded to the highest load level (65% or 70% of the monotonic capacity) and thus the shortest life was achieved first. Then, the beams with lower load levels were tested. This sequence was used to avoid having a run out in the first test. When a beam sustained one million cycles without failure, it was considered to be a run out. If a beam experienced a run out, the load was reported (indicated by an arrow in Figure 4.18 and 4.19) and then increased to a higher level.

Table 4.2: Fatigue test results for prestressed beams

Group	Specimen notation	Min. Load	Max. Load	Measured strain range at midspan (με)		Max. Capacity (kN) or Life (cycles)	Failure mode
				CFRP	Steel		
F	S-SW-45%-M	monotonic		NA	NA	130.16 kN	Bond
	S-SW-45%-70%	10%	70%	1860	1639	65,625	Bond
	S-SW-45%-65%	10%	65%	1738	1318	153,771	Bond followed by steel rupture
	S-SW-45%-60%	10%	60%	1649	1339	1,000,000	Run-out
		10%	62.5%	1282	673	386,155	Steel rupture
	S-SW-45%-63%	10%	63%	---*	1201	996,257	Steel rupture
G	S-SC-40%-M	monotonic		NA	NA	174.63 kN	Bond
	S-SC-40%-63%	10%	63%	3441	2118	1,000	Bond
	S-SC-40%-58%	10%	58%	1766	1680	24,000	Bond
	S-SC-40%-53%	10%	53%	2336	1316	1,000,000	Run out
		10%	60%	---*	---*	40,000	Steel rupture
	S-SC-40%-56%	10%	56%	1338	1521	375,000	Steel rupture followed by bond failure

*: midspan gauge was damaged

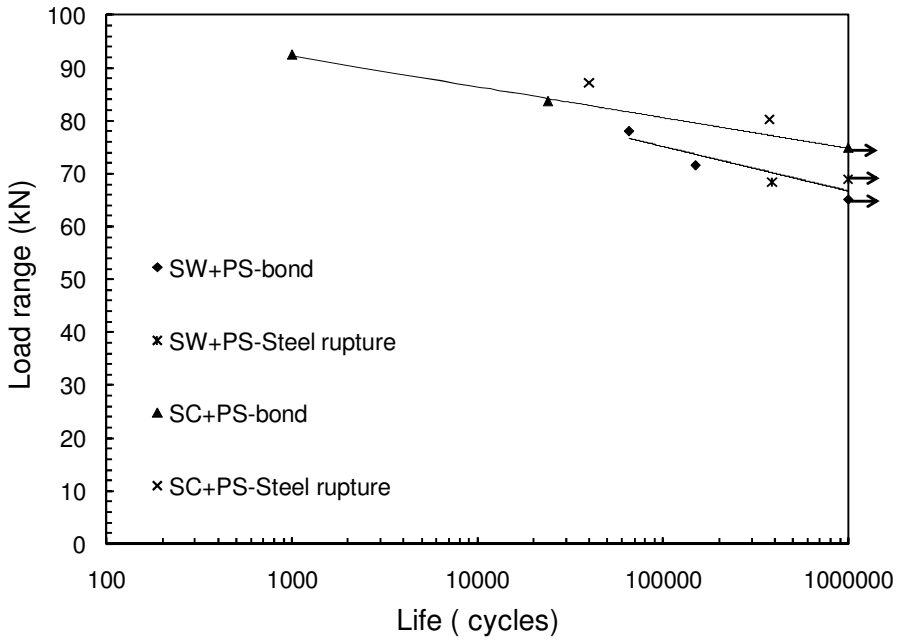

Figure 4.18: Load range (kN) versus life for the prestressed beams

From Figure 4.18, it is clear that the bond fatigue failure curve is flat. For the sand coated rods, varying the load range from 92.5 kN to 75 kN changes the life from 1,000 cycles to 1,000,000 cycles. For the spirally wound rods, varying the load range from 78 kN to 69 kN changes the life from 65,000 cycles to 1,000,000 cycles. Bond failures for beams tested under fatigue load in these groups were by slipping of the CFRP rod from the epoxy that started at the support followed by CFRP rod separation from the beam in the shear span.

Figure 4.19 compares the life of the prestressed and the non-prestressed beams. It is noteworthy that all the beams strengthened with non-prestressed CFRP rods failed by debonding between the CFRP rod and the epoxy that started at the loading point and propagated towards the support. In Figure 4.19 a, the trend line was extended as a dotted line for comparison purposes. Prestressing the CFRP rod prevented the rupture of the steel reinforcement from occurring at low load ranges.

For high load ranges, prestressing the CFRP rod decreased the life at a given load range (kN). For a given number of cycles, the beam strengthened with prestressed CFRP rods failed in bond at a lower applied load range (kN) than the beam strengthened with non-prestressed CFRP rod.

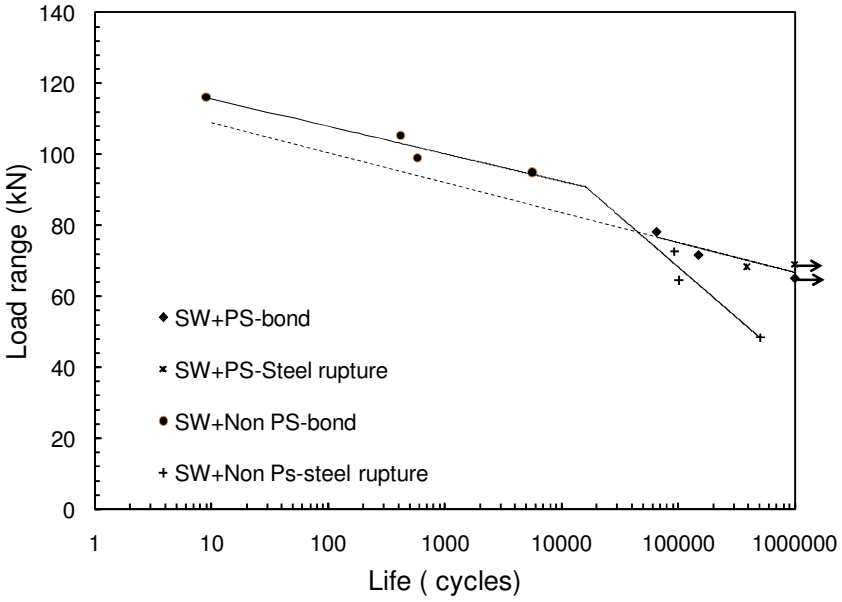

a- Spirally wound rods

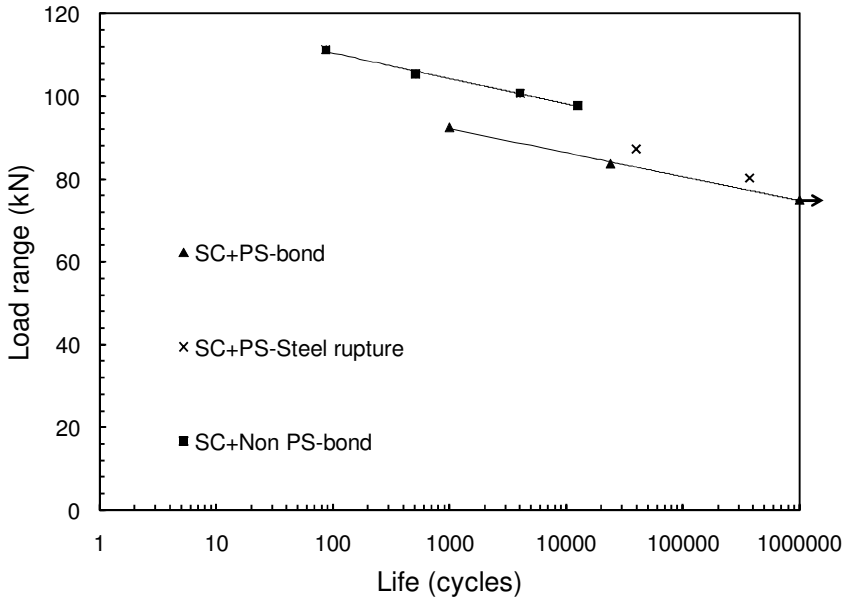

b- Sand coated rods

Figure 4.19: Load range (kN) versus life for all beams (prestressed versus non-prestressed)

4.5.2 Load-deflection behaviour

Figure 4.20 shows a typical load versus midspan deflection curve for beams with internal steel, strengthened with prestressed CFRP rod and tested under fatigue load. Figures for each beam are provided in the appendix. The midspan experiences some increase within 10% of the life then remains almost constant until excessive end slip between the CFRP rod and the epoxy occurs (at 90% of the life in Figure 4.20). Once excessive end slip occurs, midspan deflection increases until complete failure is attained.

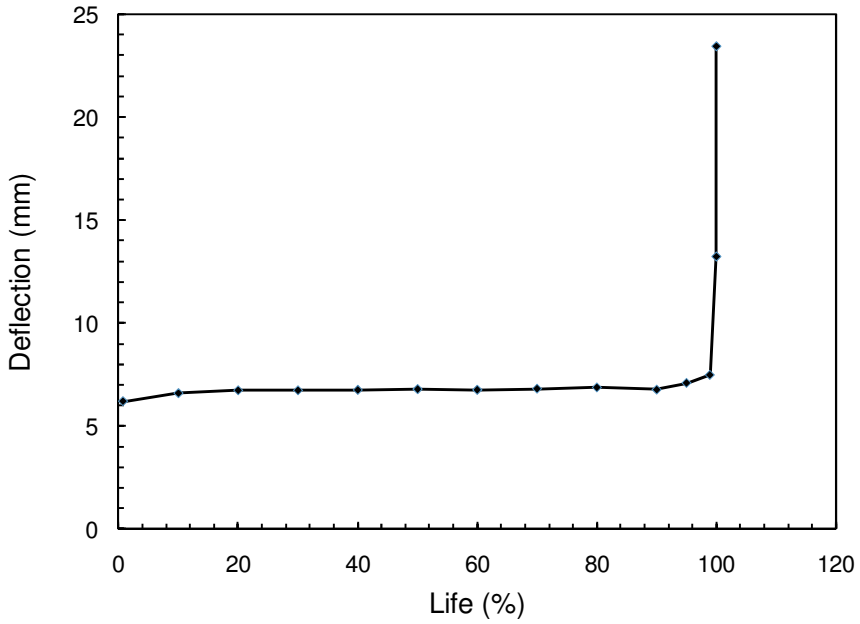

Figure 4.20: Midspan deflection for beam S-SW-45%-70%at different percentages of life

4.5.3 Beams with internal steel and strengthened with prestressed spirally wound CFRP rod

This group consists of 5 beams with internal steel that were strengthened with prestressed spirally wound CFRP rods. One beam was tested monotonically and four beams were tested in fatigue. This section discusses the fatigue test results.

Cracking behaviour

As a beam was loaded monotonically in the first cycle, cracks occurred at midspan and underneath the loading point. Since the CFRP rod was prestressed, these cracks were fine. As the load was cycled, cracks occurred at about 100mm past the loading point (outside the constant moment region). No further cracks were observed until failure, when the CFRP rod slipped from the epoxy at the support. Once the rod slipped from the epoxy, the strain in the CFRP rod decreased and cracks occurred in the shear span. The shear span could be divided into 3 main regions; region 1 from the support to the first crack, region 2 from the first crack to the crack that was noticed under fatigue loading (100mm past the loading point) and region 3 which extends from region 2 to midspan.

In region 1, which extends from the support to the first crack, there were no vertical cracks in the cross section and the epoxy cover remained intact with the CFRP rod. Yet, there were longitudinal cracks in the concrete surrounding the epoxy parallel to the CFRP rods as shown in Figure 4.21-a.

In region 2, which extends from 150mm to 500 mm from the support, cracks that occurred on both sides of the cross section after the CFRP rod slipped, connected through the bottom of the beam and connected horizontally with one another though a horizontal crack at the steel concrete interface as shown in Figure 4.21-b. At the beginning of this region (at 150mm), separated chunks of concrete remain intact with the rod and the beam. In the middle and end of this region, chunks of concrete separated from the beam and the rod as shown in Figure 4.21-c. In region 3, which extends from 500 mm from the support to midspan, chunks of concrete separated from the

beam at the steel interface and from the rod at the epoxy interface as shown in Figure 4.21-d. At the same time, the CFRP rod together with epoxy separated from the beam. The separated concrete and epoxy chunks had various forms as shown schematically in Figure 4.22.

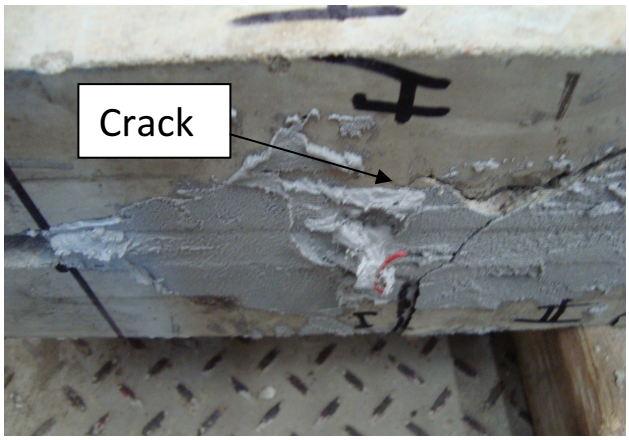

a-Regions 1 with cracks in the concrete

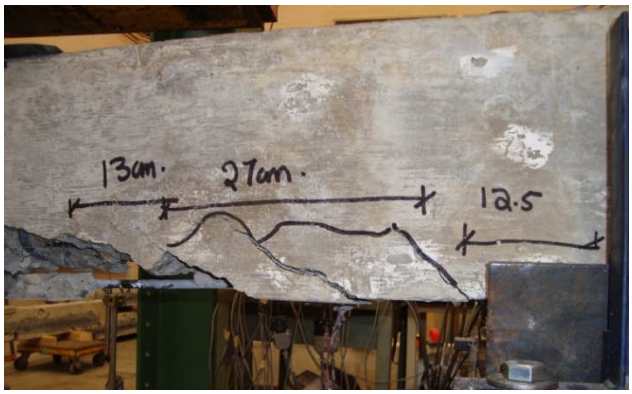

b-Cracks interconnecting horizontally

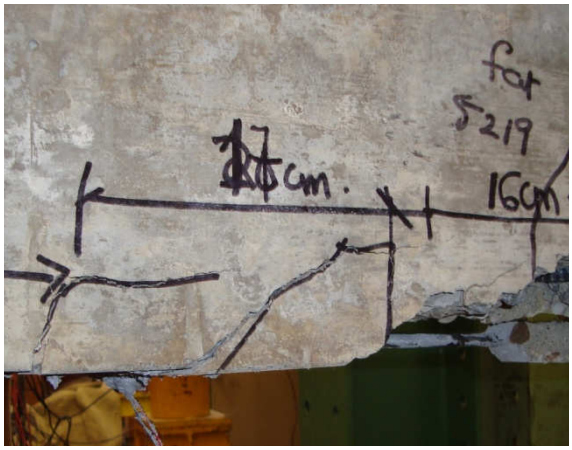

c-Region 2 with some chunks intact and other separated

d-Region 3 with concrete chunks separated from the beam

Figure 4.21: Beams after failure for Group F

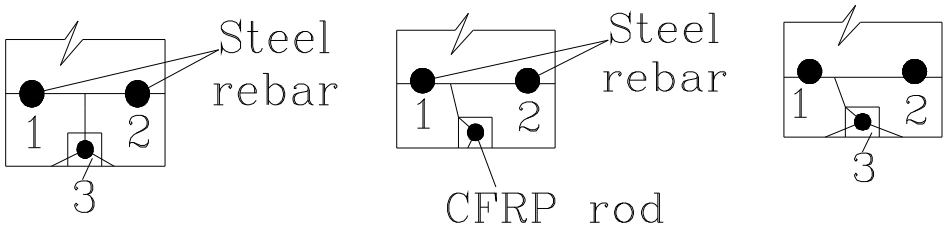

Figure 4.22: Illustrative drawing showing the observed chunks that separate from the beam at failure

Strain distribution in the shear span

Figure 4.23 shows the distribution of strain due to applied load and the total strain (strain due to prestressing plus strain due to applied load) in the CFRP rod at different percentages of life for beam S-SW-45%-70%. In the first cycle, the strain in the CFRP rod at all locations was tensile with no signs of slip of the CFRP rod from the epoxy. Yet, there was debonding of the CFRP rod from the epoxy between the midspan strain gauge and the gauge located at 500mm from the support. This is clear from the equal CFRP strain reading at 500mm and midspan. As the load was cycled until 10% of the fatigue life, the measured strain in the gauge located at 125mm was less than the reading in the first cycle. At 20 % of the fatigue life, gauges at 125mm and 250mm exhibited unloading in the form of a reduced strain reading. As the cycling continued strain readings in the gauges at 125mm and 250mm continued to decrease as shown in Figure 4.23-a. At 90% of the fatigue life, the slip between the CFRP rod and the concrete started to increase as shown in Figure 4.24. At the same time, the CFRP rod lost almost all the strain (at 125mm location) as shown in Figure 4.23-b at 98% of life. The readings of the strain gauges mounted on the steel rebar at 125 and 250 mm increased dramatically after 90% of the fatigue life as the CFRP strain decreased due to the slipping of the CFRP rod as shown in Figure 4.25. At 100% of the fatigue life, the tensile forces in the beam due to the applied load were mainly resisted by the

steel rebars. The slip between the CFRP rod and the epoxy increased to 10mm and the beam failed.

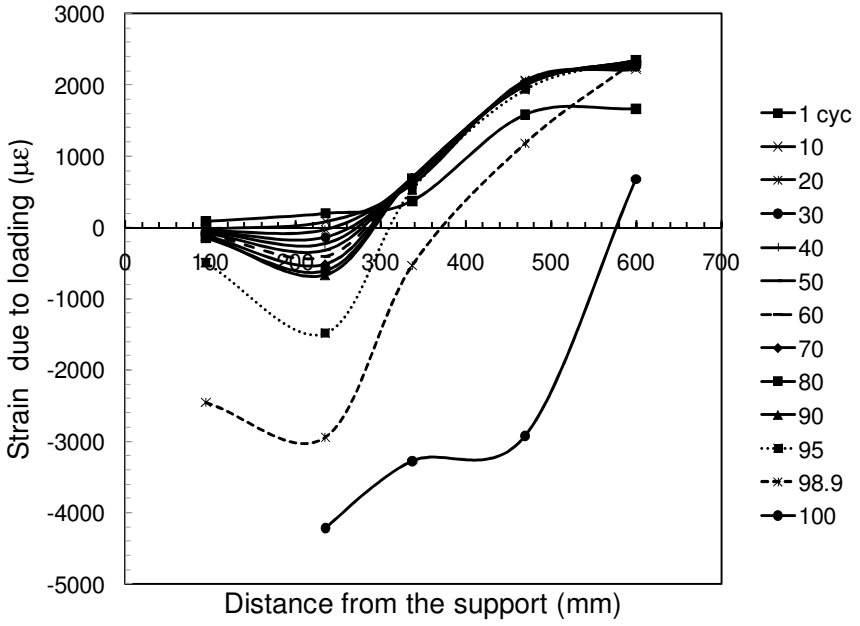

a- Strain due to applied load

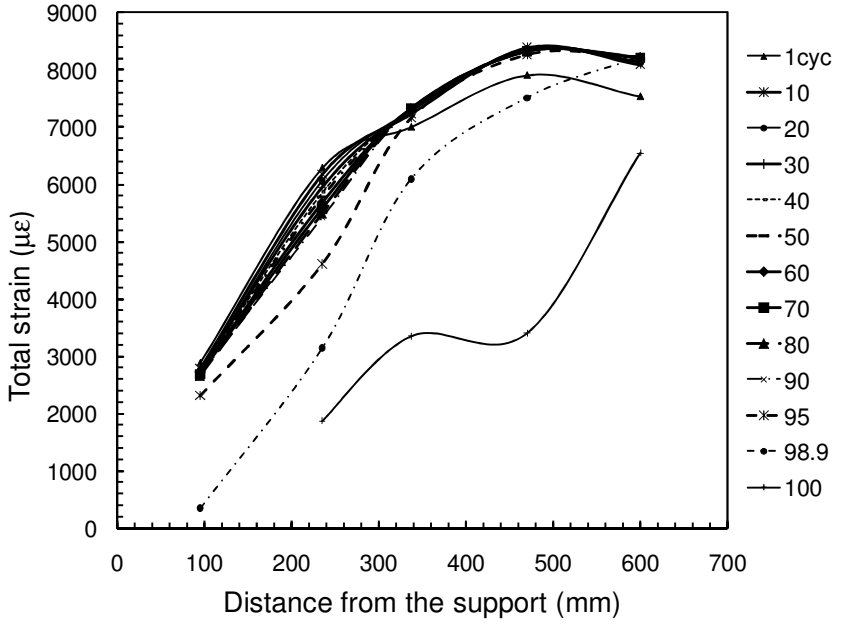

b- Total Strain

Figure 4.23: Strain distribution along CFRP rod at different percentages of life for beam S-SW-45%-70%

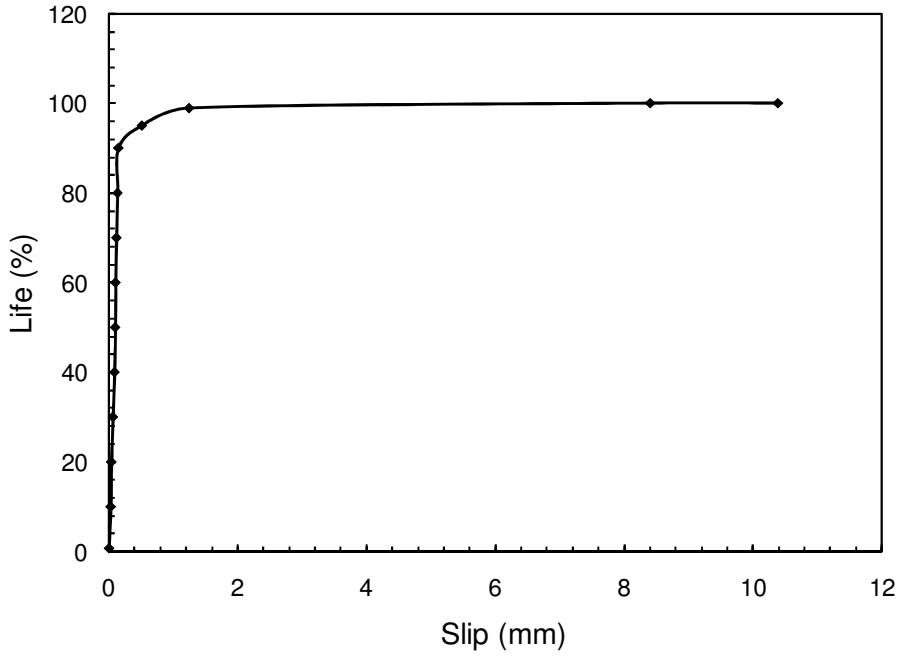

Figure 4.24: Life versus CFRP rod end slip from epoxy for beam S-SW-45%-70%

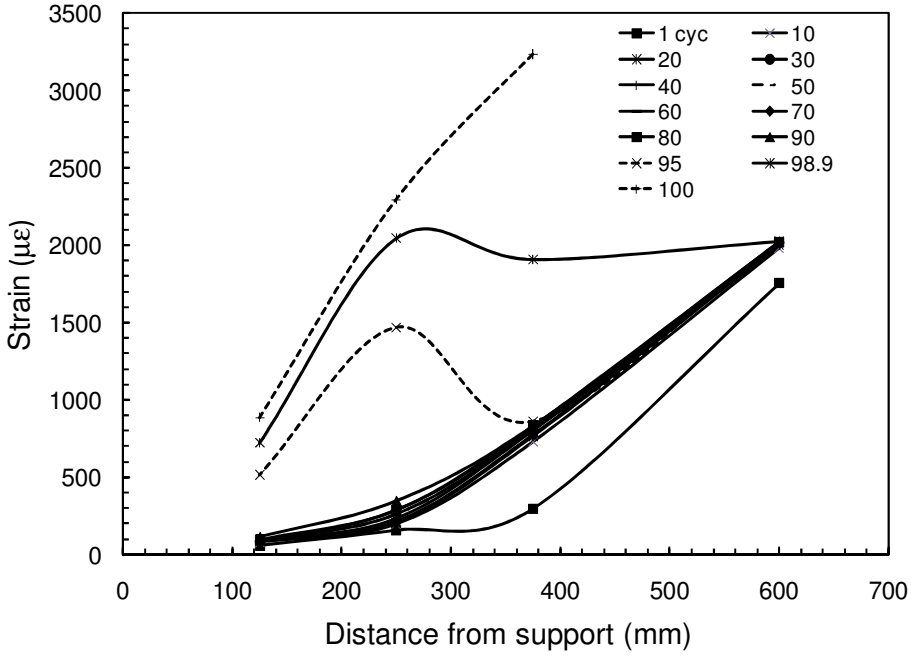

Figure 4.25: Strain distribution along steel rebar at different percentages of life for beam S-SW-45%-70%

4.5.4 Beams with internal steel and strengthened with prestressed sand coated CFRP rod

This section discusses the fatigue results of Group G beams with internal steel that were prestressed with sand coated CFRP rods.

Cracking behaviour

In the first cycle, the beam was loaded to the peak load monotonically. In this cycle, cracks occurred at midspan, underneath the loading points and just outside the constant moment region in the shear span. As the load was cycled, no further cracks were noticed until close to failure when the CFRP rod started slipping. At this point, a vertical crack close to the support located at about 85 mm from the support occurred. Then, this crack propagated horizontally towards midspan at the steel concrete interface and the CFRP rod separated from the beam.

After failure, the shear span could be divided into 2 regions; region 1 that extends from the support to the closest crack to the support and region 2 that extends after region 1 to the loading point (end of the shear span).

In region 1, epoxy cover together with concrete separated from the soffit of the beam and the CFRP rod separated from the beam as shown in Figure 4.26-a. Horizontal cracking propagated from the support to the midspan (Figure 4.26-b). In region 2, the CFRP rod together with chunks of concrete and epoxy separated from the beam as shown in Figure 4.26.

a-Bottom view showing the CFRP separation from the beam in region 1

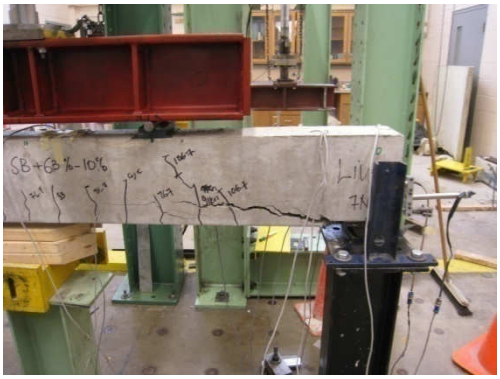

b-Horizontal crack propagation

Figure 4.26: Beams after failure

Strain distribution in the shear span

Similar to the beams in Group F, Figures 4.27-a and 4.27-b show the distribution of strain due to applied load and the total strain (the strain due to prestressing plus the strain due to load) in the CFRP rod at various percentages of the fatigue life of the beam S-SC-40%-63%. In the first cycle, the strain along the CFRP rod at all locations was tensile with no signs of slip. As the load was cycled to 90% of the fatigue life, there were no signs of slip and all the strain gauge readings were tensile. At 90% of the fatigue life, the CFRP rod started to slip from the epoxy and the CFRP strain gauge readings at 125mm and 250 mm decreased as shown in Figure 4.27-a. At 97% life, Figure 4.28 shows an increase in the steel strain gauge readings at 125 and 250mm. At 100% of the fatigue life, the slip reached 5.6mm as shown in Figure 4.29 and the beam failed.

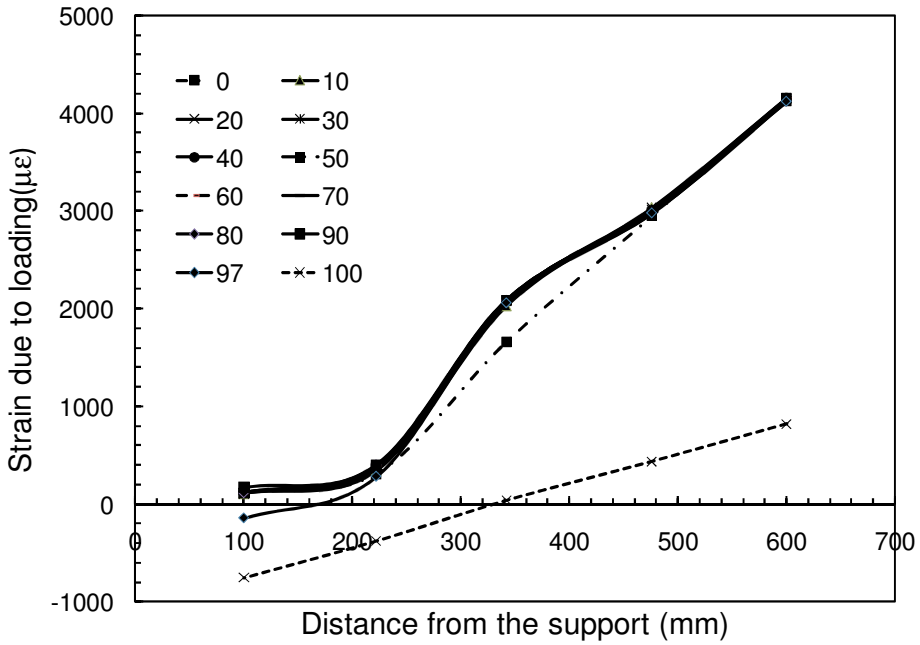

a-Strain distribution due to applied load

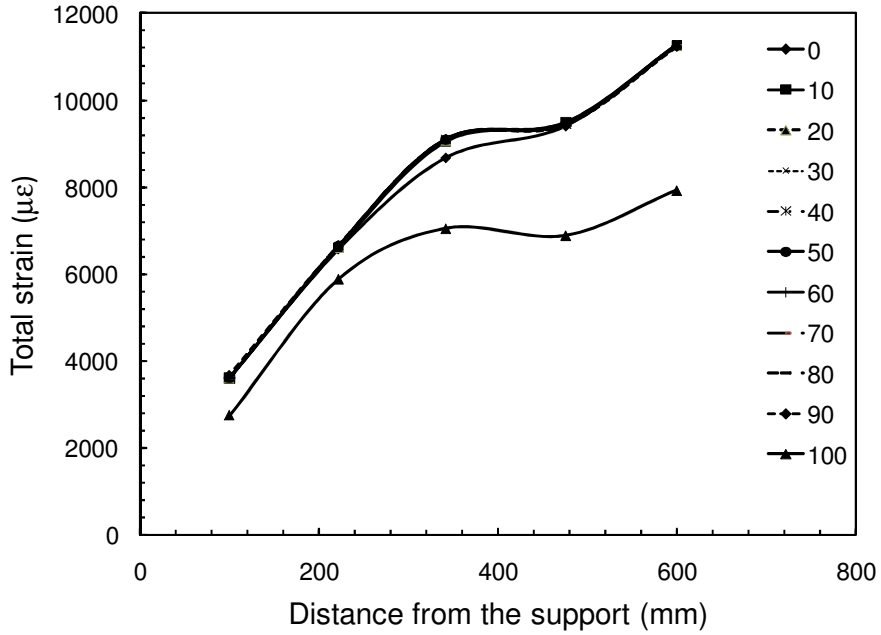

b-Total Strain distribution along CFRP rod

Figure 4.27: Strain distribution along the CFRP rod at different percentages of life for beam S-SC-40%-63%

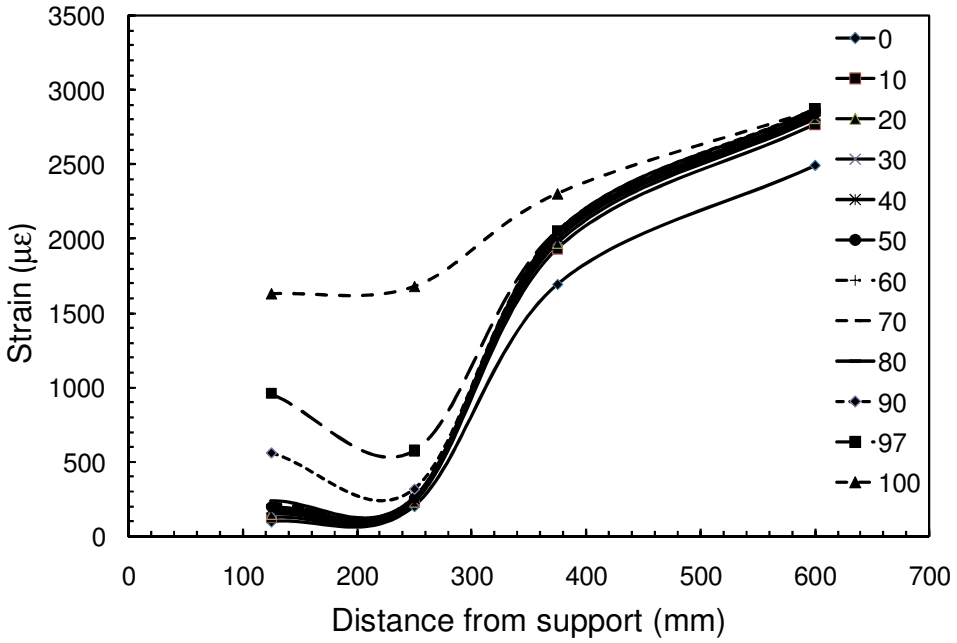

Figure 4.28: Strain distribution along steel rebar at different percentages of life for beam S-SC-40%-63%

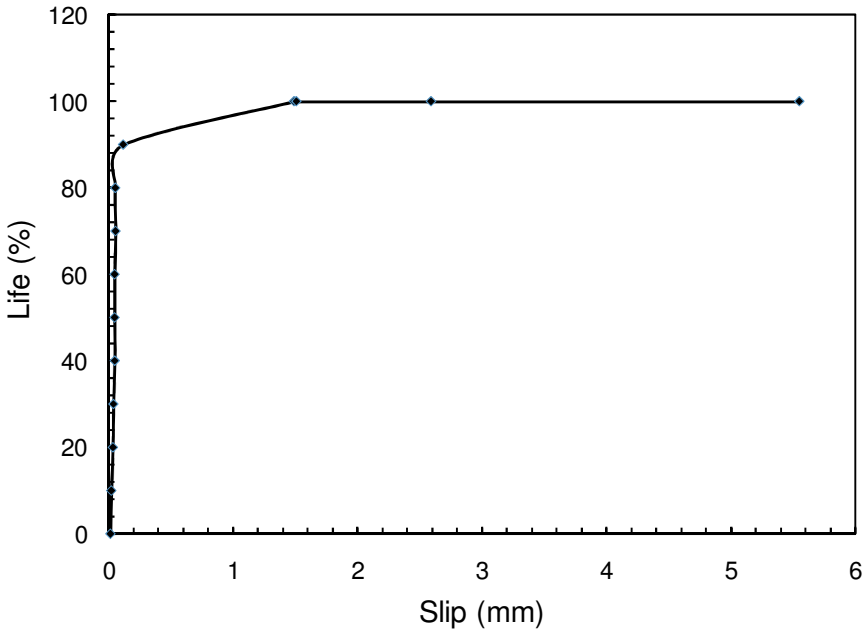

Figure 4.29: Life versus CFRP rod end slip from epoxy for beam S-SC-40%-63%

4.6 CFRP strain distribution

This section discusses the CFRP strain distribution at failure for the prestressed beams tested under monotonic loading (section 4.6.1) and those tested under fatigue (section 4.6.2).

4.6.1 Strain distribution in monotonic beams

Figure 4.30-a shows the strain distribution at failure (onset of excessive slip) for all the beams tested monotonically except beam S-SW-45%-M. Figure 4.30-b shows the strain distribution for beam S-SW-45%-M. In these figures, the x-axis represents the location of the strain gauges along the rod and the y-axis represents the strain gauge readings in micro strain. The strain values for all beams in Figure 4.30-a were at their peak load. For beam S-SW-45%-M, the strain distribution plotted is at the initiation of slip (onset of failure). At failure, the CFRP strain recorded in the fully bonded region had the same value and distribution for all beams strengthened with sand coated rods. The distribution was independent of the prestressing of the CFRP rod or presence of internal steel. This indicates that the force in the CFRP rod and the shear stress in the fully bonded region (ahead of the crack) at failure was the same for all beams strengthened with sand coated CFRP rods. Once the rod started slipping, the readings of the strain gauges at 125 mm and 250 mm from the centerline of the support decreased as the load increased. Thus, the CFRP rod starts to unload and failure occurs. Figure 4.30-a also shows that at failure, the fully debonded region for the beams strengthened with sand coated rods is longer than the fully debonded region for the beams strengthened with spirally wound rods. Thus, debonding between the CFRP rod and the epoxy has progressed more in beams strengthened with sand coated rods than the beams strengthened with spirally wound rods.

From Figure 4.30-a, the gauges closer to midspan sections, at 500 mm and 375 mm from the support, recorded almost the same strain as the strain gauge at midspan. This indicates as discussed in the previous chapter that the CFRP rod was fully debonded in this region. The gauges that are closer to the support, at 125 mm and 250 mm from the support, recorded strain values higher than the value expected based on strain compatibility analysis for a bonded cross section but lower than the strain value at midspan. This indicates that they are in the fully bonded region but the crack at the CFRP-epoxy interface has progressed towards the support.

Figure 4.30-b shows the strain distribution for beam S-SW-45%-M at the initiation of slip (onset of failure). This beam failed by pull-out of the CFRP rod from the epoxy in the end region, similar to the mode of failure reported by Badawi (2007). The CFRP rod started slipping from the epoxy in the region close to the support followed by regions closer to the loading point. Thus, the progress of failure is in the opposite direction when compared to all other beams tested under monotonic loading. This indicates that the critical shear stress causing failure for beam S-SW-45%-M is at the support as opposed to beam S-SC-40%-M where the critical shear stress is closer to the loading point. The shear stresses and their superposition will be discussed in Chapter 5.

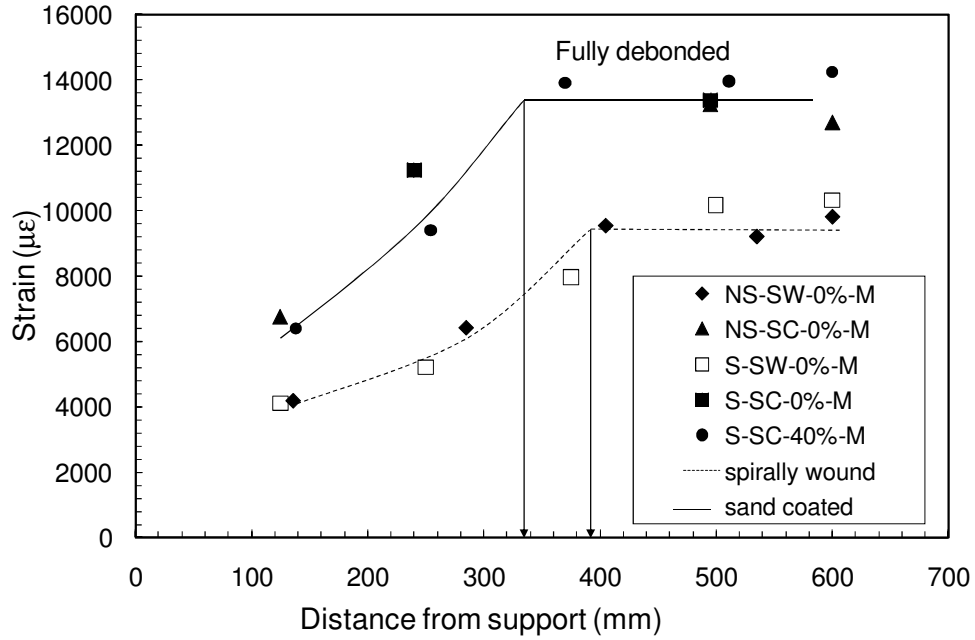

a- All monotonic beams except S-SW-45%-M

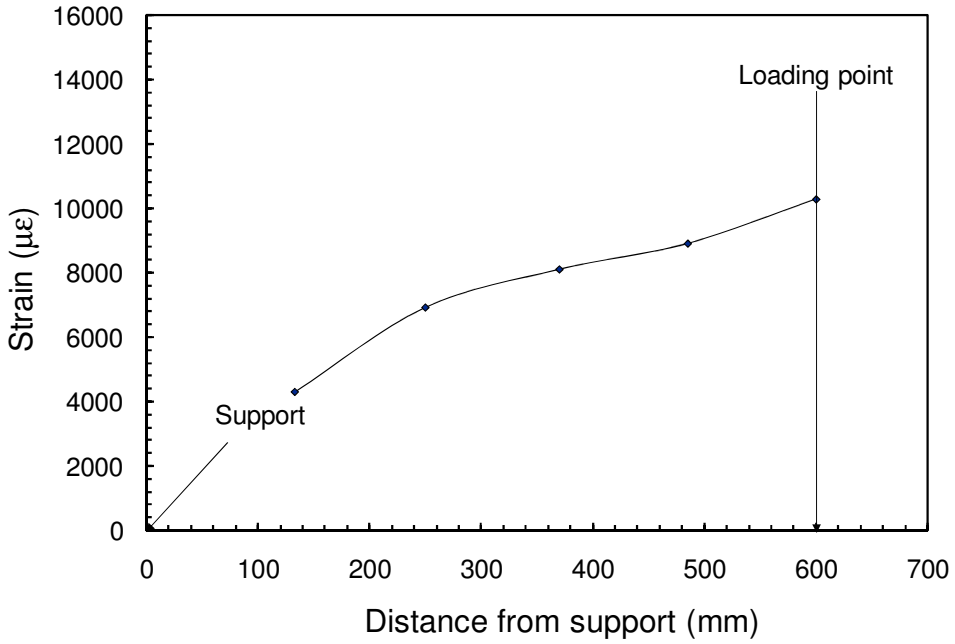

b- Beam S-SW-45%-M

Figure 4.30: CFRP Strain distribution at failure

4.6.2 Strain distribution in fatigue beams

All the beams strengthened with prestressed CFRP rods and tested under fatigue load had the same mode of failure. The failure started with slipping of the CFRP rod from the epoxy at the support followed by separation of the CFRP rod together with the concrete and epoxy from the beam in the shear span. During loading, there were 3 phases for the CFRP rod strain readings. Phase 1 was from the prestressing strain to first cycle or 10% of the life. In this phase, all the strain readings along the rod were increasing and the CFRP rod was fully bonded at all sections. Phase 2 was from cycle 1 to cycle at initiation of slip, where the strain at 125 mm and 250 mm decreased indicating that the CFRP rod was unloading at these locations. Beyond this phase, excessive slip occurs followed by failure. When the applied load was low enough, the unloading (as indicated by reduction in total force) at 125mm and 250 mm did not cause failure. Phase 3 extends from the initiation of slip until complete failure. Figure 4.31 shows the total strain distribution along the shear span for the beams at the onset of excessive slip. It is clear in both figures that the strain distribution was consistent where the strains at onset of excessive slip in the end region (where failure initiates) were the same regardless of the applied load. Thus, at onset of excessive slip (onset of failure), the force distribution in the CFRP rod in the end region is the same for a given rod type. The shear stress is the variation of the normal force in the rod over a given distance divided by the perimeter of the rod. Thus, the shear stress value and distribution in the region close to the support is the same at onset of excessive slip (failure) for a given rod type regardless of the applied load level. The shear stress value and distribution will be discussed in details in Chapter 5.

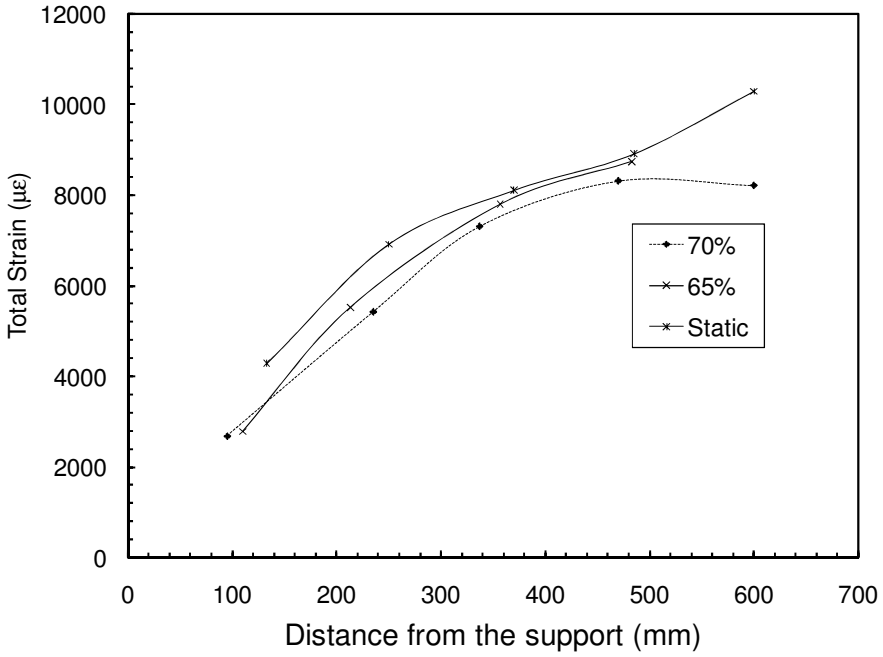

a- Spirally wound rods

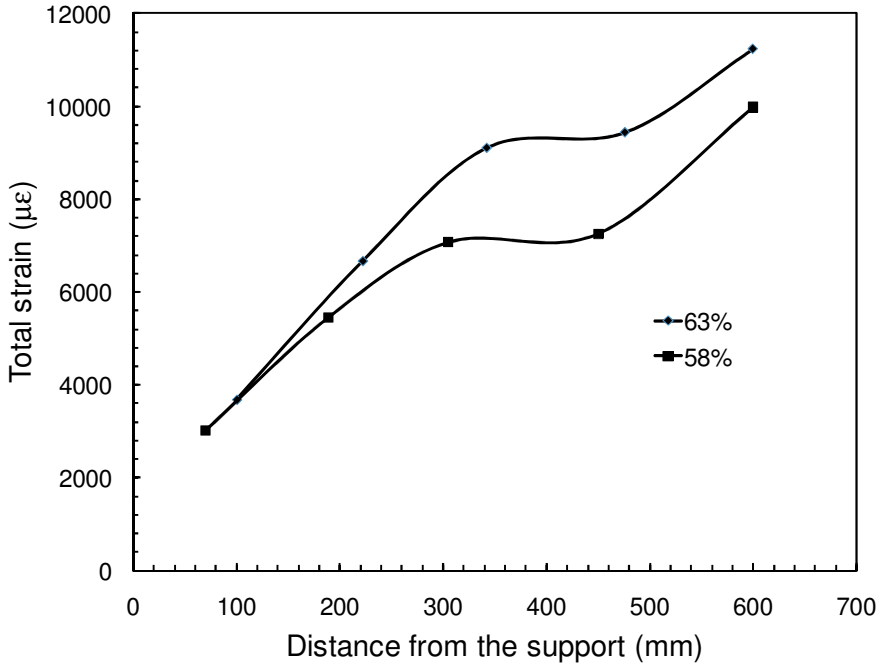

b- Sand coated rods

Figure 4.31: Total strain distribution along the CFRP rod at onset of excessive slip

Chapter 5: Modelling of the Experimental Results

5.1 Introduction

The model used to describe the experimental test results is presented here. An explanation of the model is presented first, followed by a comparison between the calculated and experimental forces and fatigue lives for all specimens tested under fatigue loading.

5.2 Bond failure

Two modes of bond failure were observed;

a- Debonding that starts at the loading point and spreads towards the support

This mode of failure occurred for the beams (with or without internal steel) strengthened with non-prestressed CFRP rods and tested under monotonic or fatigue load. It also occurred for one beam with internal steel, strengthened with prestressed sand coated CFRP rod and tested under monotonic loading.

b- Slipping between the CFRP rod and the epoxy that starts at the support and travels to the loading point

This mode of failure occurred for the beams with internal steel and strengthened with prestressed spirally wound rod, regardless of the type of applied loading. It also occurred for the beams with internal steel, strengthened with prestressed sand coated CFRP rods and tested under fatigue loading.

Examining the beams after failure (see Chapter 3 and 4), shows that the failure is caused by radial stresses (emitting from the CFRP rod outward in the beam cross section). Yet, since the radial stress is proportional to the shear stress along the rod, the shear stress along the rod will be considered here. Modelling of each mode of failure will be dealt with in a separate section.

5.3 Failure by debonding that starts at the loading point and spreads towards the support

In this mode of failure, debonding between the epoxy and the CFRP rod starts at the loading point after a flexure crack occurs at a low load level or at a low percentage of the fatigue life. As the load or the number of cycles is increased, debonding spreads towards the support. The arrival of the de-bonding crack is indicated by a sudden increase in the strain gauge reading at a gauge at the front of the debonded region to a strain equal to or slightly less than the midspan strain. Figure 5.1 shows typical CFRP strain distributions along the shear span at various fractions of the fatigue life of a beam.

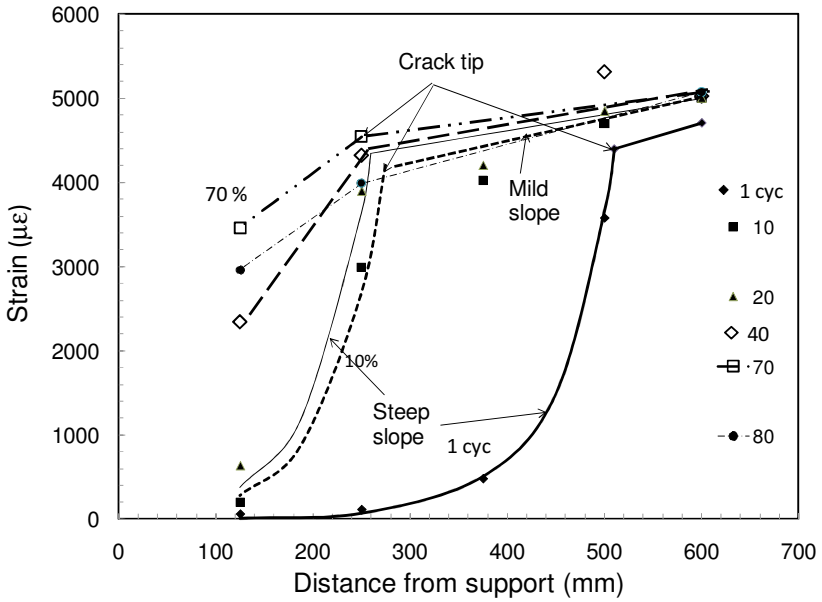

Figure 5.1: Strain distribution along the CFRP rod

The front of the debonded region can be modelled as a crack at the interface between the epoxy and the CFRP rod as shown in Figure 5.2. The crack grows longer (i.e. gets closer to the support) as the load is increased in a monotonic test or as the number of cycles is increased in a fatigue test. The action driving the crack growth is the shear stress between the CFRP rod and the epoxy at the crack tip. The shear stress distribution can be divided into 2 regions; one behind the crack tip and the other ahead of the crack tip as shown in Figure 5.2.

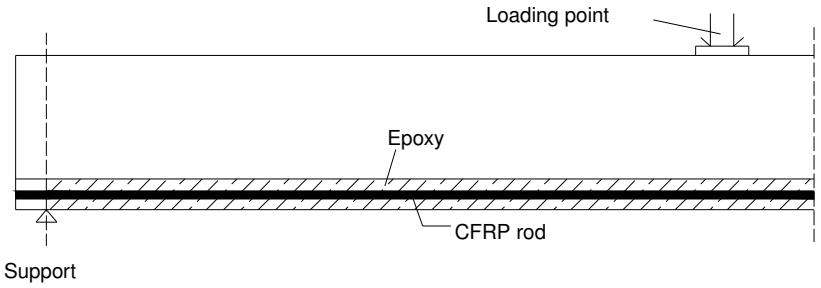

a- Fully bonded

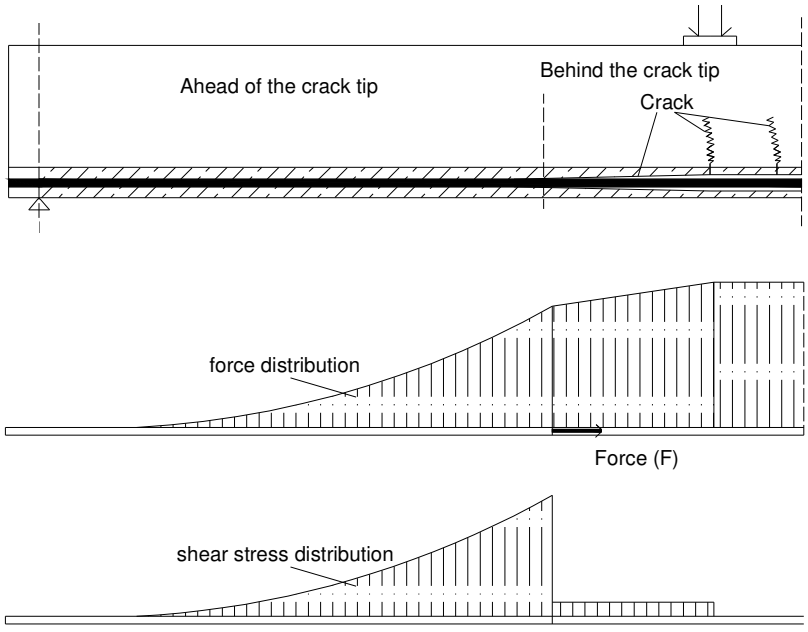

b- Partially debonded

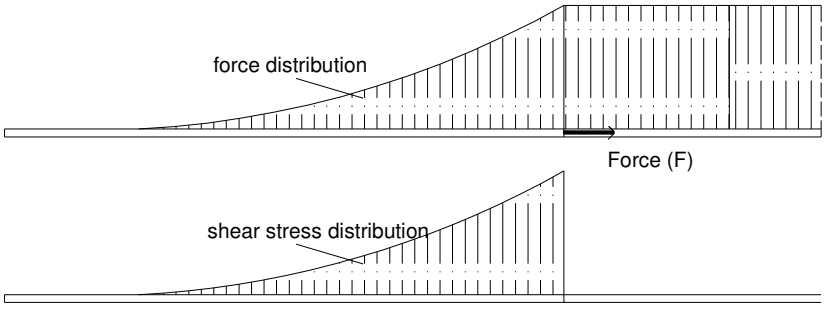

c- Fully debonded

Figure 5.2: Crack at the interface between the CFRP rod and the epoxy

a-Behind the crack tip:

This region can be either fully or partially debonded. If it is fully debonded then the CFRP rod is completely separated from the epoxy in this region behind the crack tip. If it is partially debonded, there is a debonded shear stress in all or part of this region between the crack tip and the loading point. If the strain in the CFRP rod at the crack tip is equal to the strain at the loading point (midspan), then the debonded stress is equal to zero and the region is fully debonded. If the strain at the crack tip is less than the strain at the loading point (midspan), then the debonded stress is not equal to zero.

b- Ahead of the crack tip:

This region extends from the crack tip to the center line of the support. In this region, the CFRP rod is fully bonded to the epoxy. The shear stress at the crack tip has to decay and reach zero at the center line of the support where the bond between the CFRP rod and the concrete ends.

Thus, the main parameters for the model become:

1- The shear stress versus slip model for the CFRP- epoxy material combination.
2- The force that drives the crack
3- The rate of crack propagation(i.e. how much the crack tip progresses per cycle)
4- The failure criterion (i.e. a definition of beam failure)

Each of these parameters will be discussed in detail.

5.3.1Parameters for the model

a- The shear stress versus slip model for the CFRP- epoxy material combination

The bond stress versus slip models proposed by De Lorenzis and Nanni 2002, De Lorenzis, L. et al. 2002 and 2004, based on their experimental pull out tests on CFRP rods, are shown in Figure 5.3. Figure 5.3-a represents the failure at the interface between concrete and groove filler (smooth grooves) and the splitting failure for CFRP ribbed rods in epoxy. Figure 5.3-b was obtained for splitting failure of GFRP ribbed rods and spirally wound rods in epoxy. Figure 5.3-c was obtained for pull out failure at the rod-epoxy interface for CFRP sand coated rods in epoxy. All the figures share an ascending branch until reaching the maximum bond stress. The shape of the descending branch depends on the strain distribution behind the crack tip.

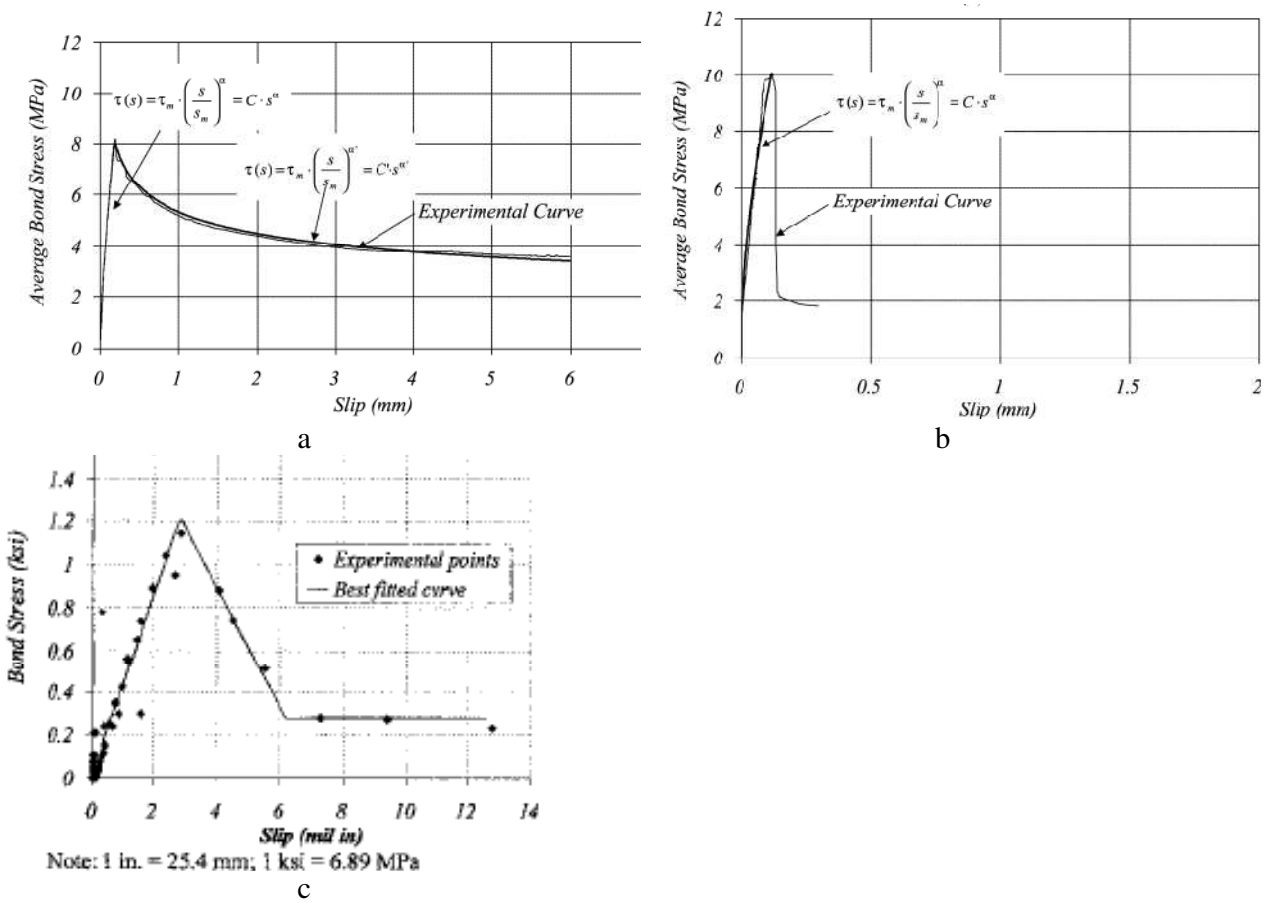

Figure 5.3: Different bond stress versus slip models
(De Lorenzis and Nanni 2002, De Lorenzis, L. et al. 2002 and 2004)

Two bond stress versus slip models are shown in Figure 5.4. The vertical axis represents the bond stress (MPa) and the horizontal axis represents the slip (mm). The shear stress in both figures increases until a peak shear stress is reached. Past the peak shear stress, the shear stress drops abruptly to zero (as in Figure 5.4-a) and drops suddenly to a lower value after which it remains constant (as in Figure 5.4-b).

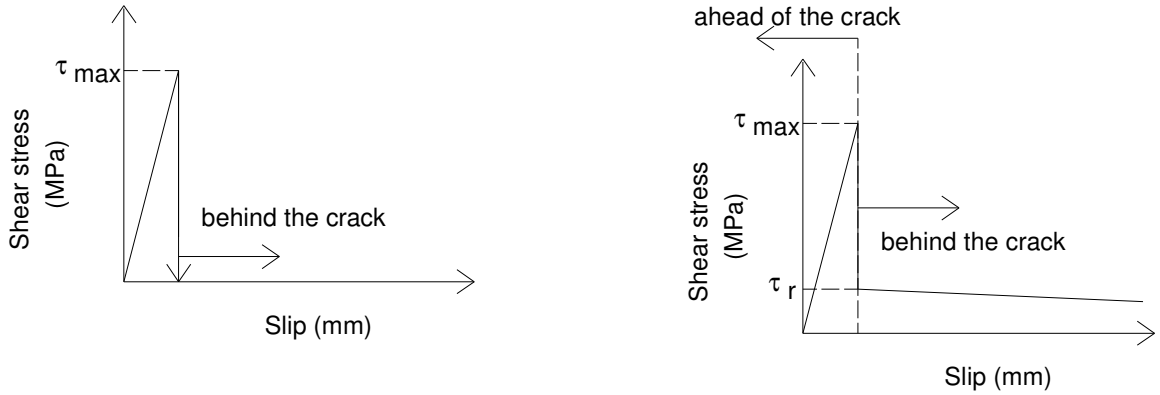

a b

Figure 5.4: Different shear stress versus slip models

The shape of the post maximum shear stress branch governs the CFRP strain distribution and therefore the CFRP normal stress distribution in the un-bonded region.

-If the CFRP normal stress distribution in the debonded region is constant and equal to the stress at the midspan as shown in Figure 5.5-a, then the debonded shear stress drops to zero from the peak shear stress as in Figure 5.4-a.

- If the CFRP normal stress distribution in the debonded region has a mild slope as given by Figure 5.5-b, then the debonded shear stress drops to a constant value from the peak shear stress as represented by Figure 5.4-b.

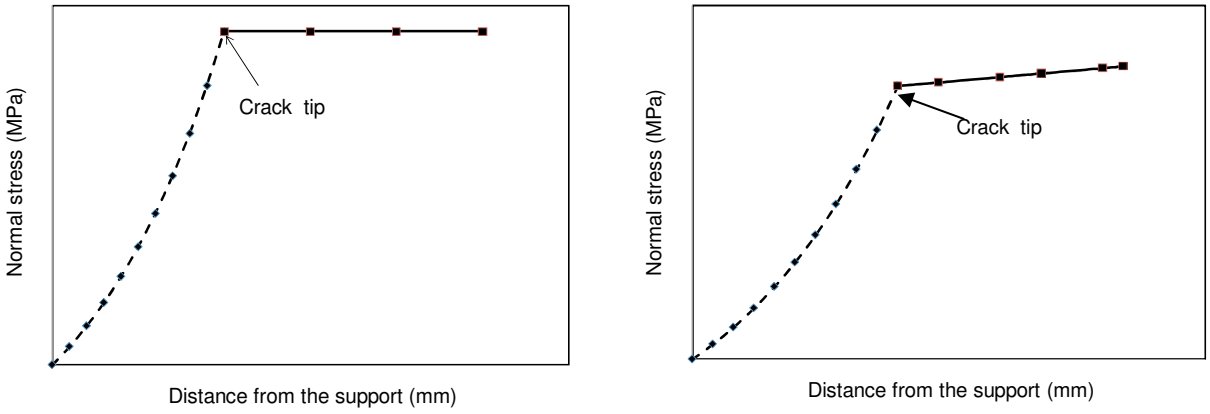

a b

Figure 5.5: CFRP normal stress distribution (MPa) with distance (mm) for different cases

The proposed model for the shear stress versus slip between the CFRP rod and the epoxy is shown in Figure 5.6. The shear stress is at the interface between the epoxy and the CFRP rod (bond-shear stress). The shear stress increases linearly until reaching the maximum shear stress at a slip (s_0) of 0.03mm (which is in the same order of magnitude as those reported in the literature) then it drops to a debonded shear stress value (τ_r). After the drop there is a descending branch in which the shear stress decreases as the slip increases. In the beam, the maximum stress occurs at the crack tip, while the debonded region behind the crack tip lies in the post peak debonded shear stress region of the stress slip curve. Since the CFRP rod is fully bonded to the epoxy ahead of the crack tip, the total slip between the crack tip and the loading point is equal to the change in length of the CFRP rod due to the change in CFRP rod stress due to the debonding. Since the slip that occurs due to de-bonding between the CFRP rod and the epoxy is small the descending branch in Figure 5.6 past the debonded shear stress can be assumed to be a horizontal line with a

constant value equal to the debonded shear stress. The debonded shear stress behind the crack tip is similar to friction between the rod and the epoxy.

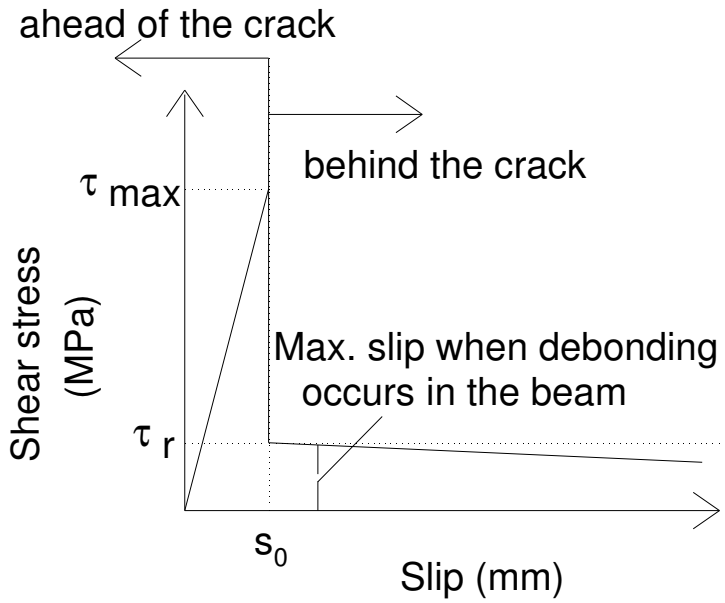

Figure 5.6: Shear stress versus slip model

Behind the crack tip

During loading, once a flexure crack appears and gives rise to a stress raiser at the loading point the shear stress distribution is as shown in Figure 5.7- a with a maximum in the shear stress at the crack location. Under monotonic loading a crack (debonding) forms between the CFRP rod and the epoxy when the monotonic maximum shear stress is exceeded, and as the load is further increased, the crack (debonded length) moves towards the support as partial debonding takes place (Figure 5.7-b). Under cyclic loading, the occurrence and propagation of crack (debonding) can take place with cycling at a stress lower than the maximum monotonic shear stress. In the partially debonded region behind the advancing crack, the shear stress along the CFRP rod is

equal to the debonded shear stress. The debonded shear stress depends on the type of the CFRP rod surface. If the CFRP rod surface is rough, the debonded shear stress will be higher than for a smooth rod.

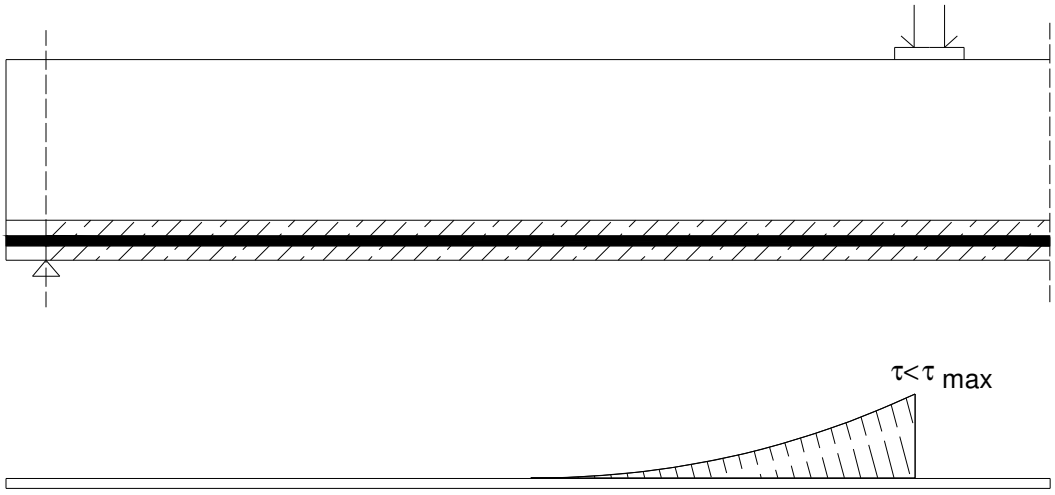

a- Shear stress at initial loading

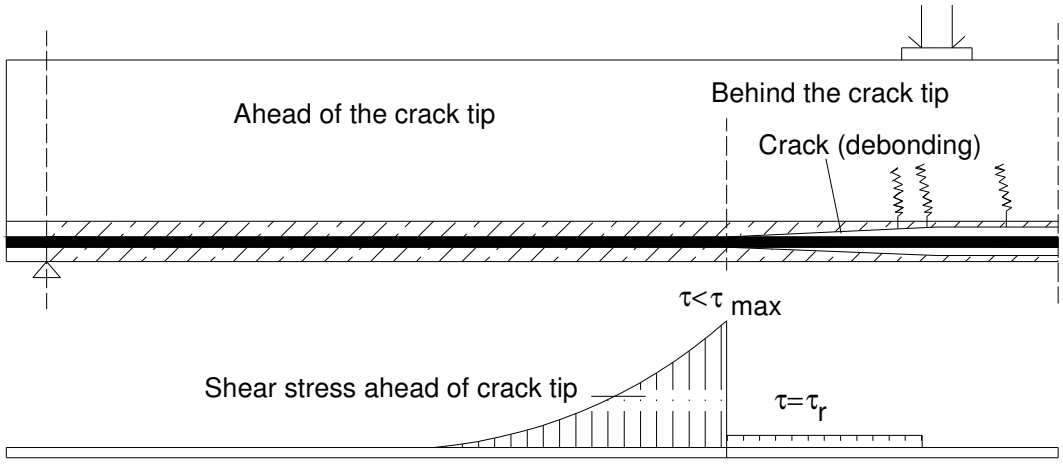

b- Shear stress after the crack (debonding) has propagated

Figure 5.7: Variation of shear stress along the CFRP rod

The value of the debonded shear stress was determined from the experimental results as follows. For each set of beams, the CFRP strain distribution in the shear span at different percentages of

life was plotted. As debonding propagates from the loading point with cycling, the maximum CFRP rod strain behind the crack tip increases (with full debonding it would be equal to the strain at midspan). Figure 5.1 shows the distributions of strains in the CFRP rod estimated from the strain gauge readings. The initial slope of the curves emanating from the loading point is low indicating a slow rate of transfer of force from the rod to the concrete and a low shear stress. The slope of the second segment of the curve is much steeper indicating a much more rapid transfer of force from the rod to the concrete and a much higher shear stress. The region of the beam covered by the first curve segment is identified with the region behind the crack where slip has taken place and the bond has been broken. The second region ahead of the crack is assumed to be fully bonded. The intersection of the two curve segments then gives the location of the crack tip. Once the difference in strain readings between the loading point (midspan) and any gauge in the partially debonded region is determined ($\Delta\varepsilon$), and if the distance between them is known (ΔX), the difference in force (ΔF) can be obtained and the shear stress can be calculated from Equation 5.1. This procedure was repeated at all load levels for ten per cent of the fatigue life of each beam and at failure. An average debonded shear stress value was then determined for each group as shown in Table 5.1. Also, Table 5.1 shows the number of values used in the calculations and the range of shear stress for each group.

$$\Delta F = \Delta\varepsilon \times E \times A$$
$$\tau = \frac{1}{\pi d} \times \frac{\Delta F}{\Delta X}$$
$$\Delta F = \pi d(\tau \times \Delta X) \qquad \text{E.q.(5.1)}$$

Where;

Δ is the difference in force or length or strain

F is the normal force in the rod (kN)

ε is the strain in the CFRP rod

E is Young's modulus of the rod

A is the area of the cross section of the rod

τ is the shear stress along the CFRP rod (MPa)

d is the CFRP rod diameter (mm)

X is the incremental length along the rod (mm)

Table 5.1: Average value of debonded shear stress for different rod types

Rod Type	Beam type	τ_r (MPa)	Number of values	Range (MPa)
Sand coated	No internal steel	1.25	5	Zero to 2.5
	With internal steel and strengthened with non-prestressed CFRP rods	2.25	9	0.87 to 2.82
	With internal steel and strengthened with prestressed CFRP rods			
Spirally wound	No internal steel	1.9	6	0.75 to 2.5
	With internal steel and strengthened with non-prestressed CFRP rods	2.5	6	1.95 to 2.86
	With internal steel and strengthened with prestressed CFRP rods	1*	6	0.3 to 1.5

*: This value is anomalous. It was expected to be equal to 2.5 as the beams with internal steel and strengthened with non-prestressed CFRP rods.

Ahead of the crack tip

In the region ahead of the crack tip, the CFRP rod is still fully bonded to the epoxy. At low load levels, when the beam is uncracked (no flexural cracks), the strain distribution along the CFRP rod is linear as shown in Figure 5.8 and the shear stress is uniform along the rod. When the load is increased and debonding between the epoxy and the FRP rod is initiated, the force increases in the CFRP rod at a crack location and decays exponentially over a distance ahead of the crack tip. Beyond a given distance (L), the force in the CFRP rod will be nearly equal to the force in a CFRP rod in an uncracked region (no flexural cracks). The shear stress is assumed to follow an exponential curve over the distance (L) beyond which the shear stress would be almost uniform as shown in Figure 5.8. This uniform shear stress value is small compared to the shear stress near the crack tip. The total force and shear stress in the rod is the superposition of the two shear stress distributions; a uniform distribution and an exponential distribution.

The value of the uniform shear stress was evaluated from the beams tested under monotonic load. Figures 5.9 and 5.10 show the strain distributions and the uncracked regions for beams strengthened with sand coated and spirally wound CFRP rods, respectively. For each beam, the un cracked region which is the end of the distance (L) over which the shear stress due to the stress raiser at this crack has decayed to a negligible value is marked by the circle in Figures 5.9 and 5.10. In this region, the uniform shear stress can be computed in terms of the CFRP strains using Equation 5.1. The uniform shear stress was computed in this region at the maximum load before the cracked force distribution extends into this region. The beams with no internal steel and strengthened with sand coated and spirally wound rods showed a uniform shear stress of 0.65 and 0.35 MPa, at 60 and 40 kN, respectively. The beams with internal steel and

strengthened with sand coated and spirally wound rods showed a uniform shear stress of 0.3 and 0.24 MPa, at 55 and 60 kN, respectively. Since the uniform shear stress value is so small, it will be ignored and the exponential shear stress distribution will be the only distribution considered. In this case, the normal force in the CFRP rod can be used to replace the shear stress as the force driving the crack.

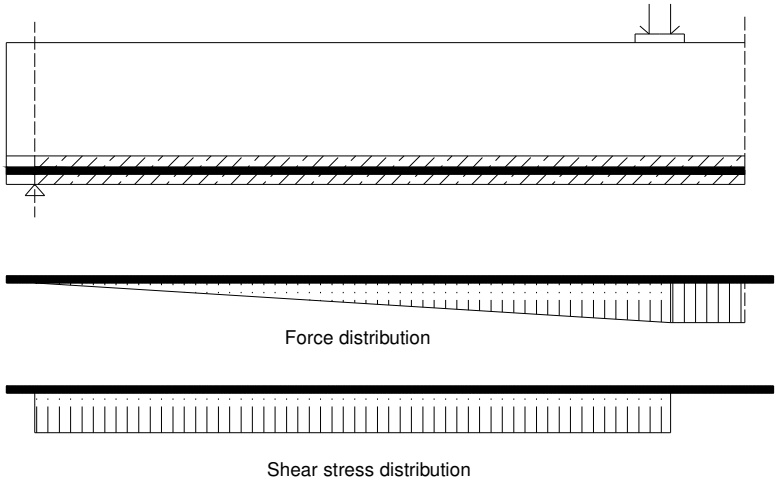

a- Uncracked beam

(No flexural cracks and full bond between the CFRP rod and the epoxy)

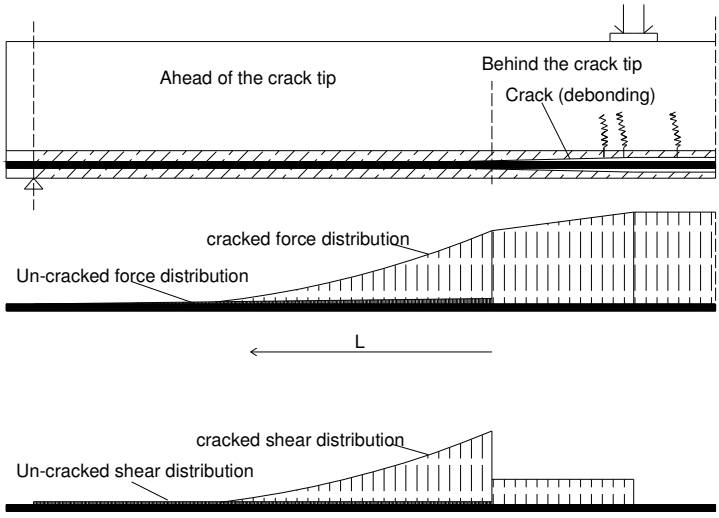

b- Cracked beam

(Some flexural cracks with debonding between the CFRP rod and the epoxy initiated)

Figure 5.8: The uncracked and cracked force and shear stress distribution

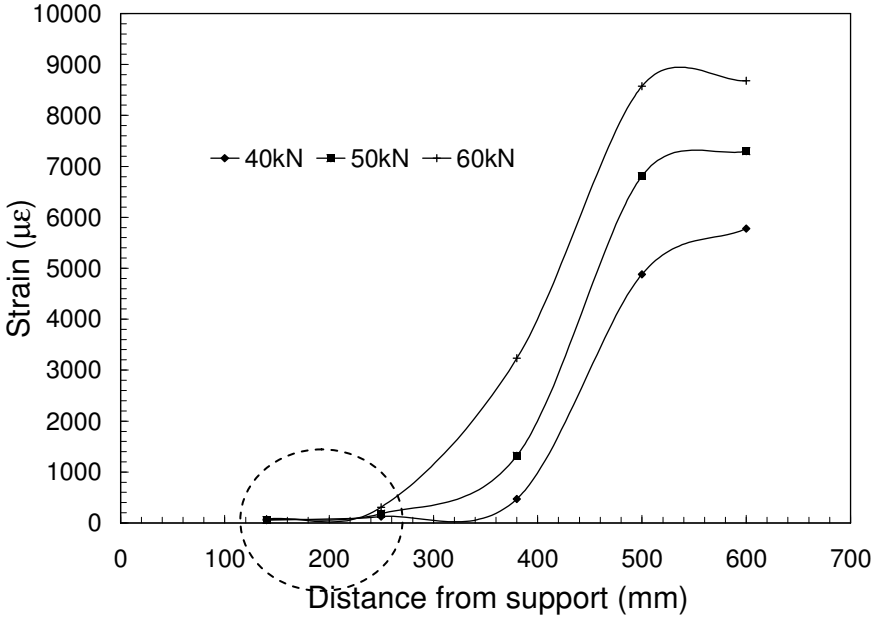

a-Beam NS-SC-0%-M

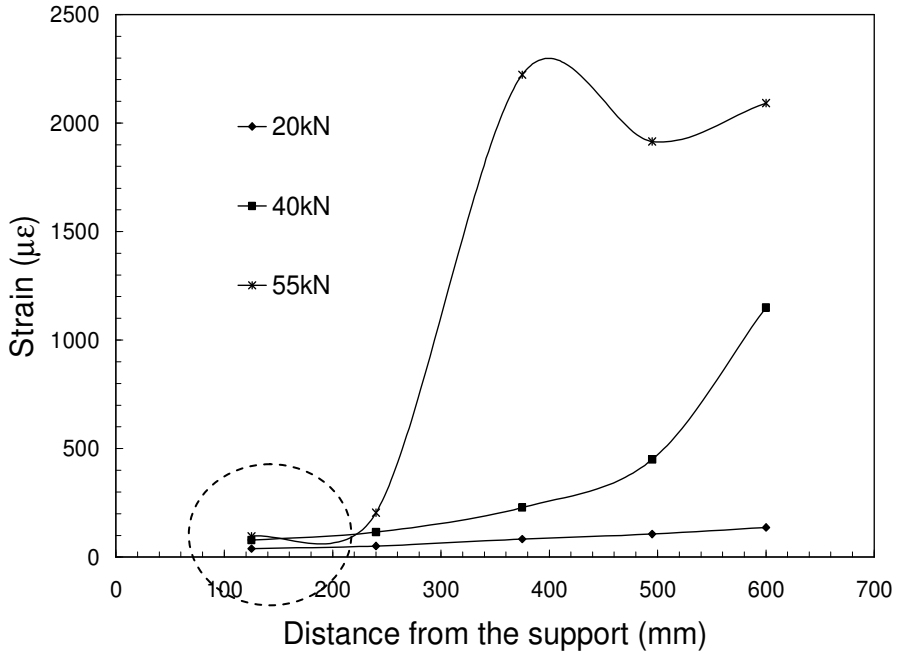

b- Beam S-SC-0%-M

Figure 5.9: CFRP strain distribution in the shear span for beams strengthened with sand coated rods

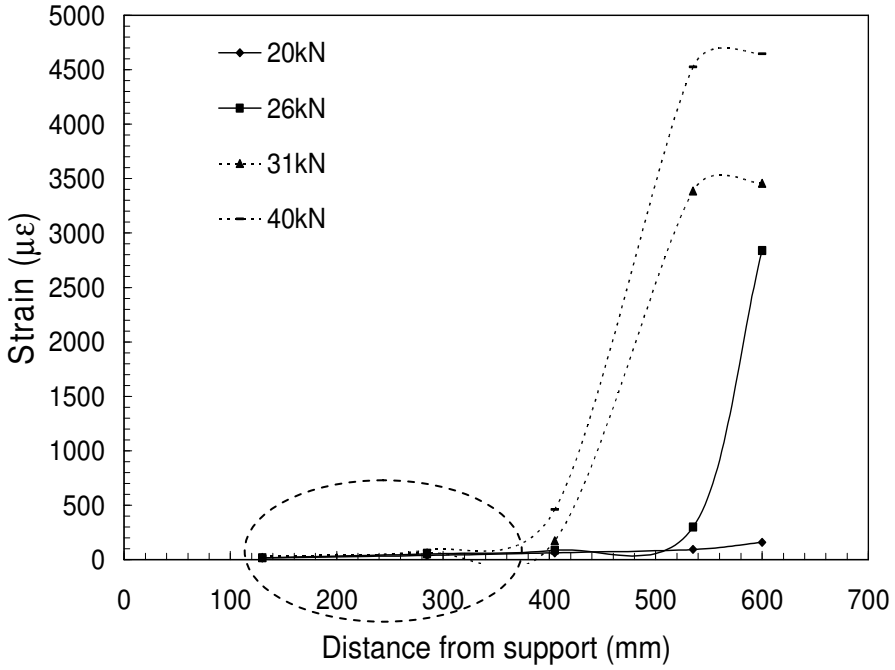

a- Beam NS-SW-0%-M

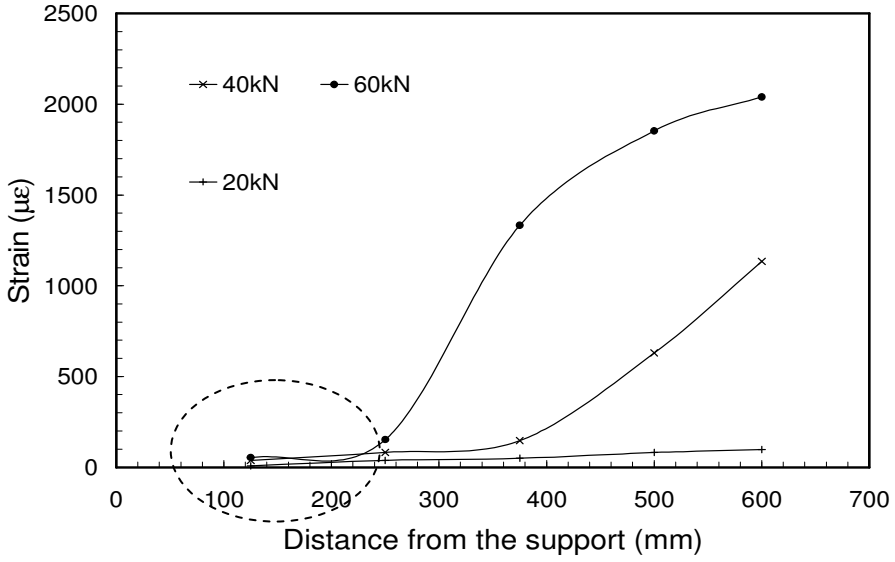

b- Beam S-SW-0%-M

Figure 5.10: CFRP strain distribution in the shear span for beams strengthened with spirally wound rods

From the strains in the CFRP rod in Figure 5.1, it is clear that the force (proportional to the strain) decreases slowly in the partially debonded region (as discussed earlier) and then decreases rapidly in the bonded region. The exponential curve given by Equation 5.2 is proposed to describe the descending branches of the rod force and shear stress curves.

$$F(x) = F\exp^{(-C\times X)}$$

$$\tau(x) = \tau_0 \exp^{(-C\times X)} \qquad \text{E.q.(5.2)}$$

Where:

F(x) is the normal force in the CFRP rod at any given distance (kN)

F is the force at the crack tip or the crack driving force (kN)

C constant that depends on the CFRP rod texture and beam configuration (presence of internal steel or not).

X is the distance from the crack tip (mm)

$\tau(x)$ is the shear stress along the CFRP rod at any distance (x) (MPa)

τ_0 is the peak shear stress at the crack tip (MPa)

The rapid or exponential decay was described in the literature for similar problems that studied the debonding between the CFRP and the concrete (Mazzotti et al., 2005, Huang and Lyons, 2007, Achintha and Burgoyne, 2008, Harries et al. 2010). The constant (C) in Equation 5.2 was determined by fitting the curve to the experimental results for each set of beams tested under fatigue load. For each beam in the set, the debonded region (crack length) was determined from the strain distribution in the shear span in the first cycle and at 10% of the fatigue life as explained earlier. Then, the CFRP rod force distribution in the bonded region was determined

from the measured strains in the first cycle and at 10% of the life. The force distributions ahead of the crack were then superimposed for all beams as shown in Figures 5.11 and 5.12. Within the same group, most of the curves had the same shape indicating that they all have the same exponent (C).For a given set, each curve was extended to intersect with the Y axis. Then, the forces in each curve were normalized by dividing them by the force given by the intercept of the curve with the Y axis. This resulted in the normalized data falling onto a single band as shown in Figures 5.13 and 5.14.

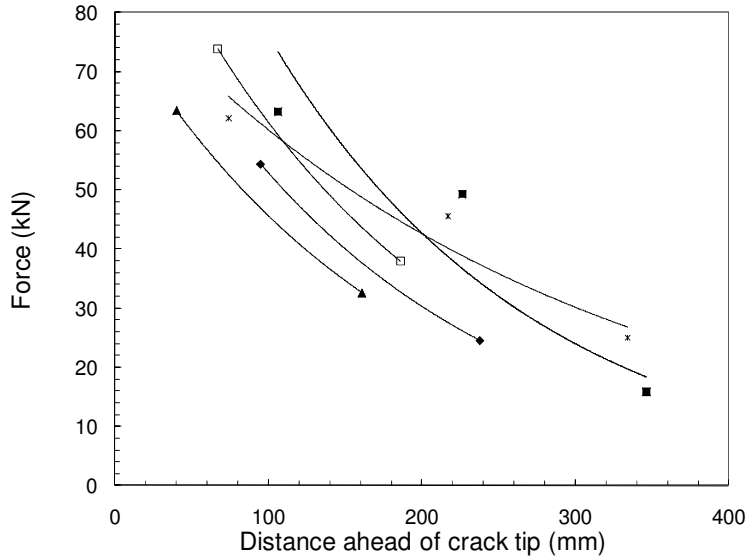

a- Beams with no internal steel and strengthened with non-prestressed sand coated rods

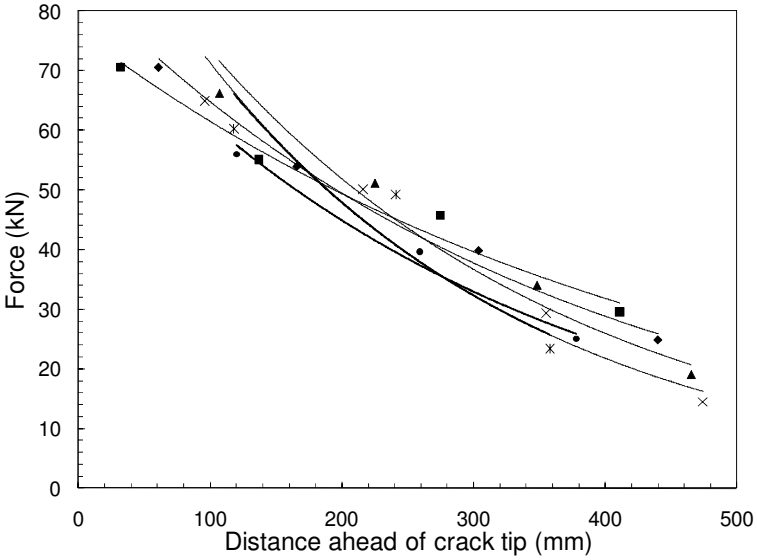

b- Beams with internal steel and strengthened with non-prestressed sand coated rods

Figure 5.11: Force distribution ahead of crack for beams strengthened with sand coated rods

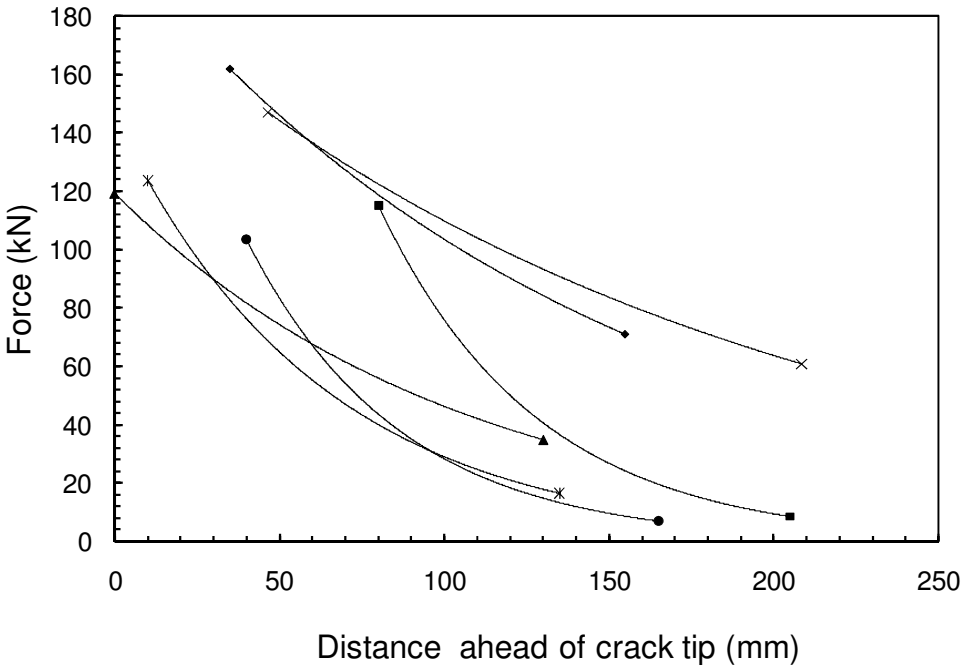

a- Beams with no internal steel and strengthened with non-prestressed spirally wound rods

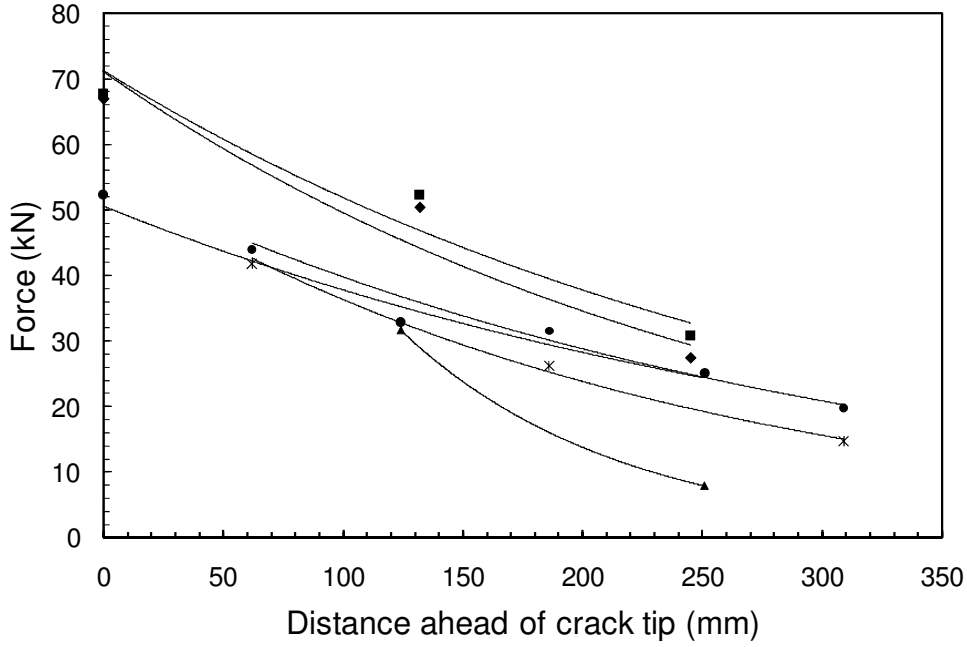

b- Beams with internal steel and strengthened with non-prestressed spirally wound rods

Figure 5.12: Force distribution ahead of crack for beams strengthened with spirally wound rods

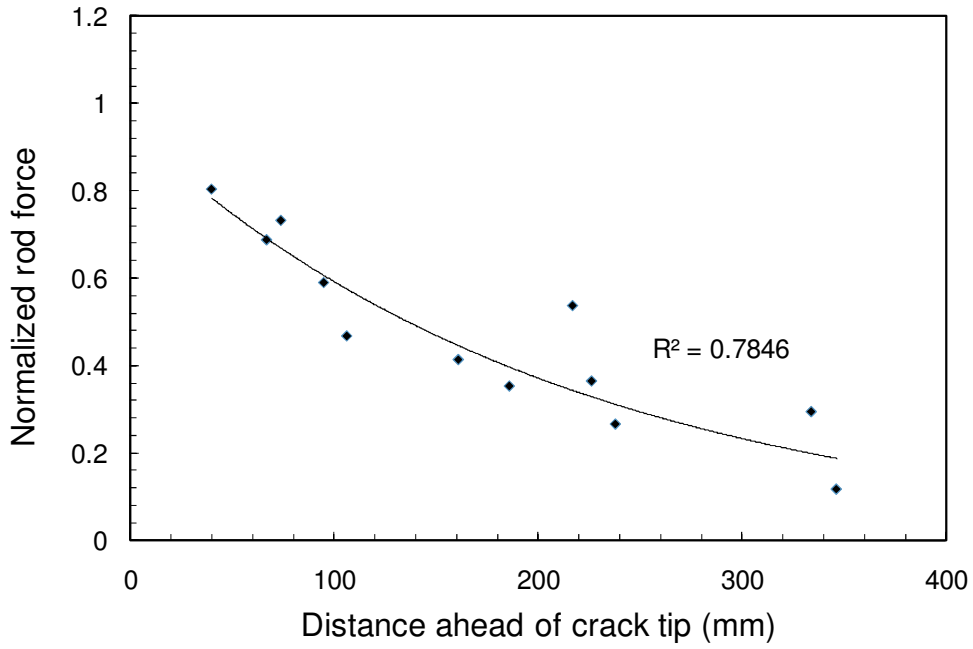

a- Beams with no internal steel and strengthened with non-prestressed sand coated rods

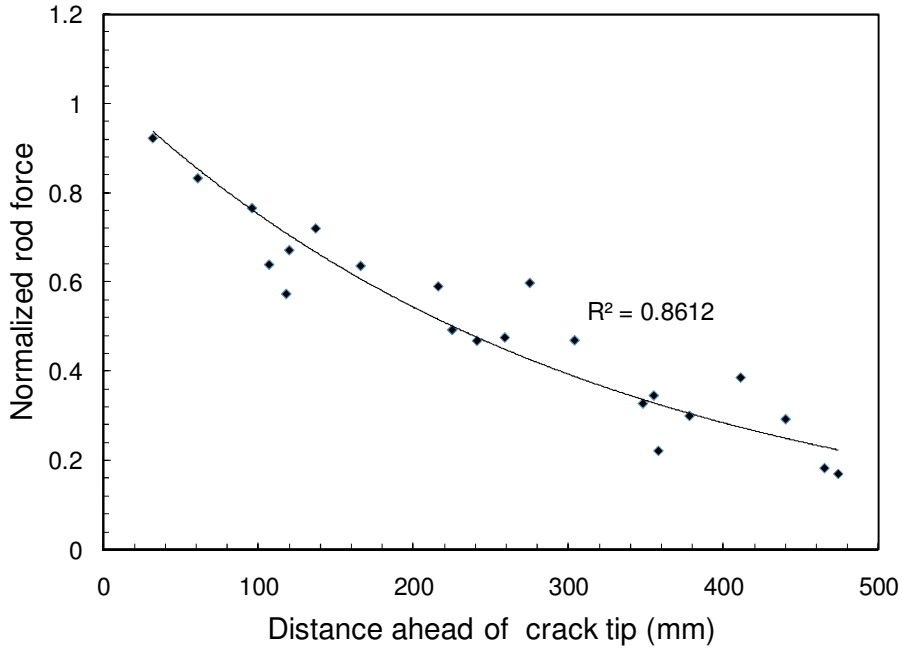

b- Beams with internal steel and strengthened with non-prestressed sand coated rods

Figure 5.13: Normalized distribution of rod force for beams strengthened with sand coated rods

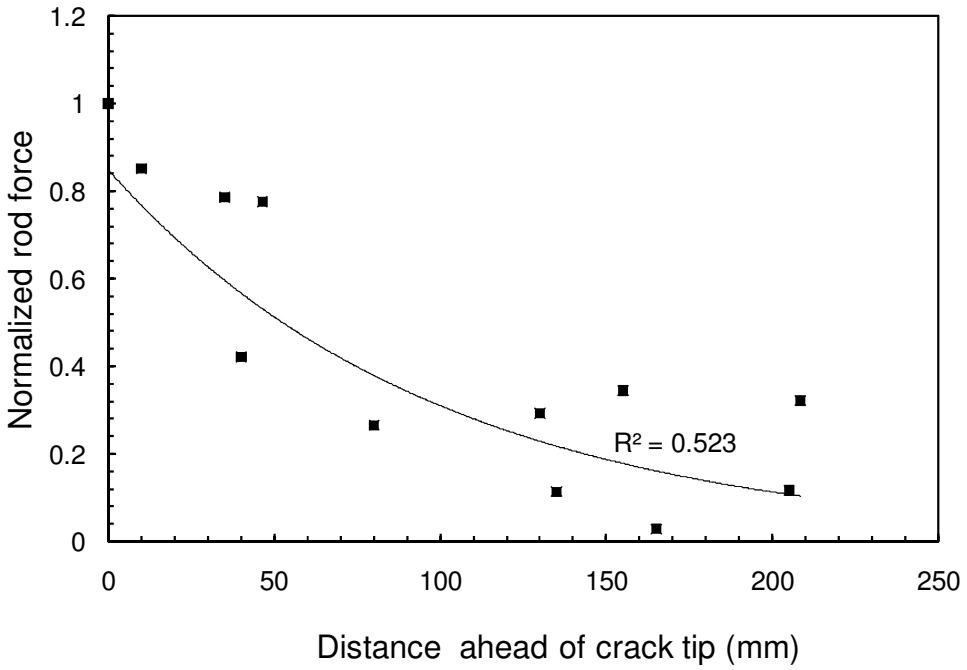

a- Beams with no internal steel and strengthened with non-prestressed spirally wound rods

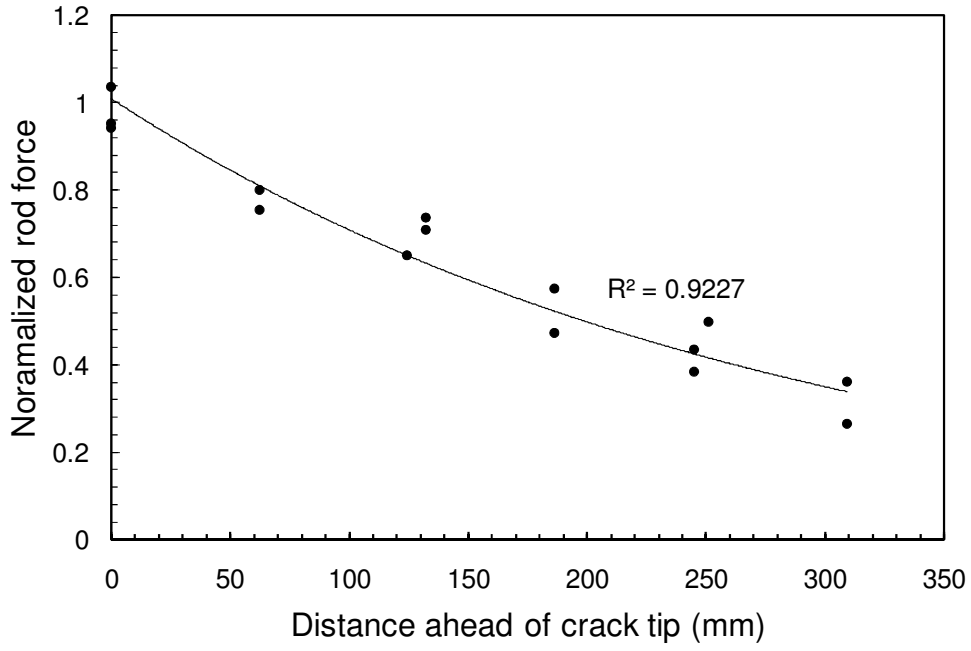

b- Beams with internal steel and strengthened with non-prestressed spirally wound rods

Figure 5.14: Normalized distribution of rod force for beams strengthened with spirally wound rods

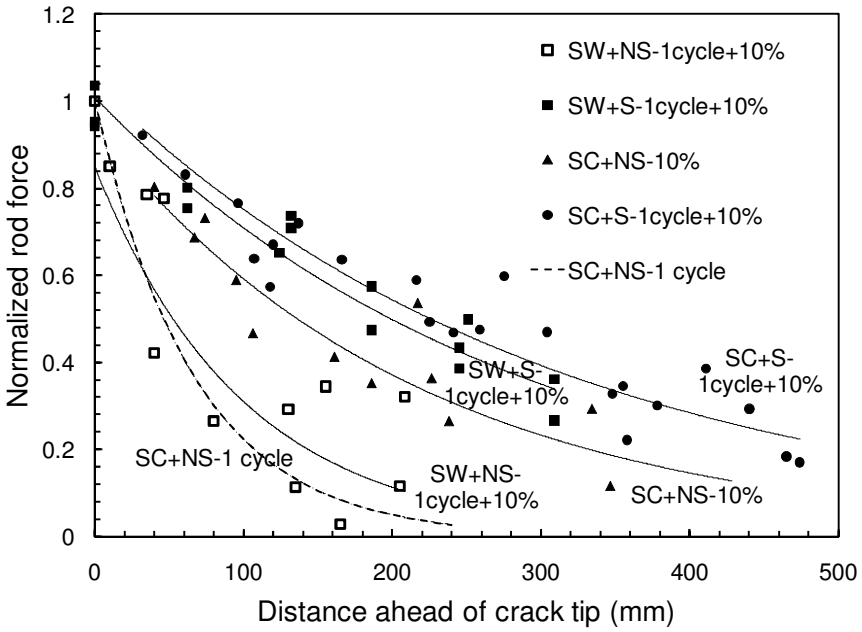

Figure 5.15: Normalized distribution of rod force for beams strengthened with non-prestressed rods

Figure 5.15 shows the normalized force distribution ahead of the crack tip for all beams (with or without steel) strengthened with non-prestressed CFRP rods (spirally wound or sand coated). It is clear that the presence of steel, especially for the spirally wound rods, leads to a reduction in the slope of the force distribution ahead of the crack tip.

Table 5.2 shows the different values of exponent "C" for the best fit curves to the normalized data. This exponent depends on the CFRP rod type and on the presence or lack of internal steel. In presence of the internal steel, some of the forces in the bonded region will be taken by the steel and that will change the value of the exponent. For the spirally wound rods, the beams with no steel had a curve with an exponent of -0.012. For the sand coated rods, the beams with no steel showed a strain under monotonic load (1 cycle) that differs from the ones under fatigue load

as shown in Figure 5.16. The main difference was that the distribution had an exponent "C" of -0.015 for the 1st cycle and an exponent of -0.004 for the fatigue loading. Since, the model is used to predict the fatigue test results, the distribution under fatigue loading is the one that was used. Therefore, the curve had an exponent of -0.004 and decayed over the shear span. For the beams with steel, the spirally wound rods had an exponent of -0.004 and the sand coated rods had an exponent of -0.005.

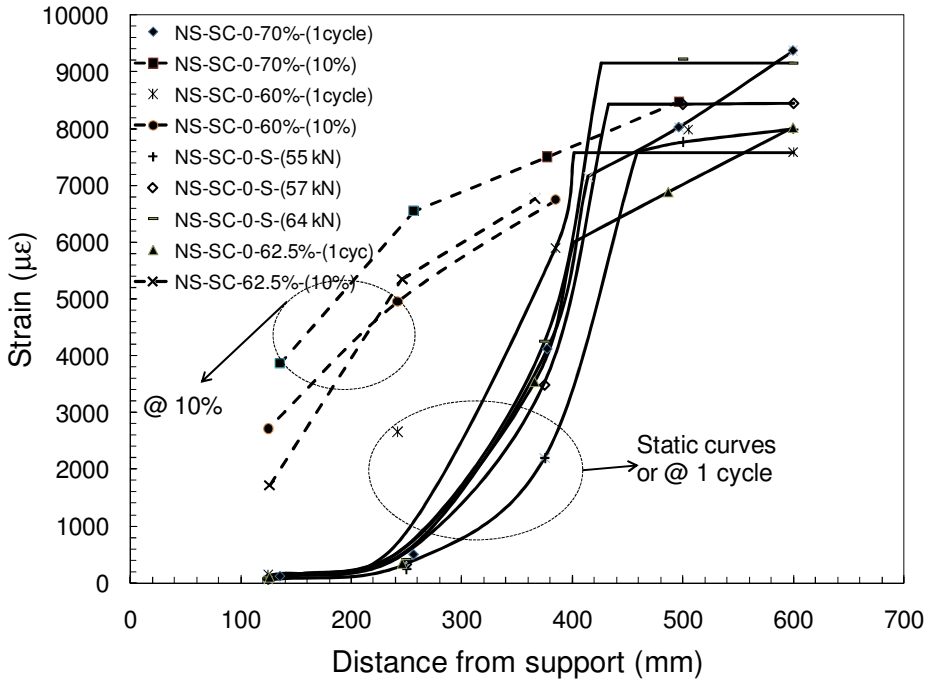

Figure 5.16: The strain distribution for beams with no internal steel and strengthened with non-prestressed sand coated rods at the first cycle and 10% life

Table 5.2: Values of exponent "C"

Rod Type	Beam type	C
Sand coated	No internal steel	-0.004
	With internal steel and strengthened with non-prestressed CFRP rods	-0.005
Spirally wound	No internal steel	-0.012
	With internal steel and strengthened with non-prestressed CFRP rods	-0.004

Since the integral of the shear stress multiplied by the circumference of the CFRP rod between the free end and the crack tip is equal the force at the crack tip as shown in Figure 5.17, substituting Equation 5.2 into Equation 5.1 gives Equation 5.3:

$$
\begin{aligned}
F &= \pi d \times \int \tau \Delta X \\
F &= \pi d \int \tau_0 \exp^{(-CX)}\, dX \\
F &= -\frac{\pi d}{C} \tau_0 \exp^{(-CX)} \Big|_0^L \\
F &= -\frac{\pi d}{C} \tau_0 (\exp^{(-CL)} - 1) \\
F &= \frac{\pi d}{C} \tau_0 (1 - \exp^{(-CL)}) \\
\tau_0 &= \frac{FC}{\pi d} \frac{1}{(1 - \exp^{(-CL)})}
\end{aligned}
\qquad \text{E.q.(5.3)}
$$

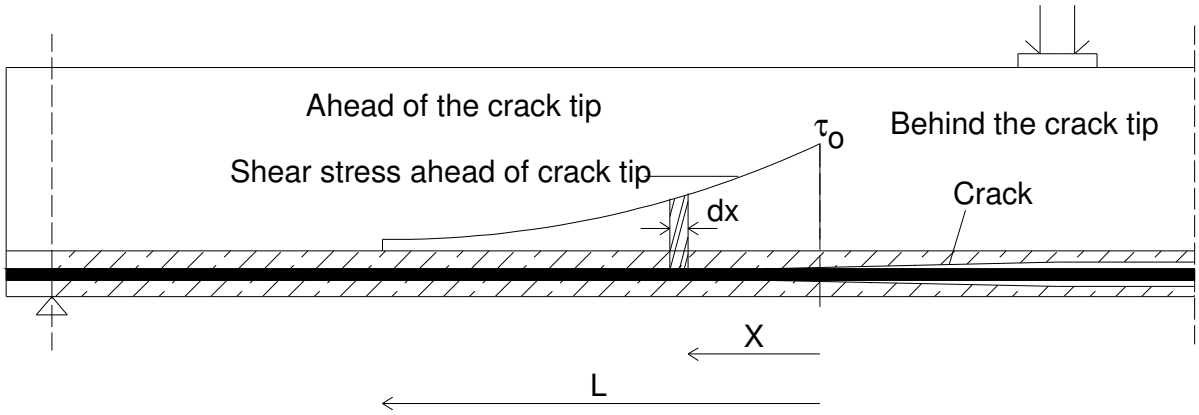

a- Short crack

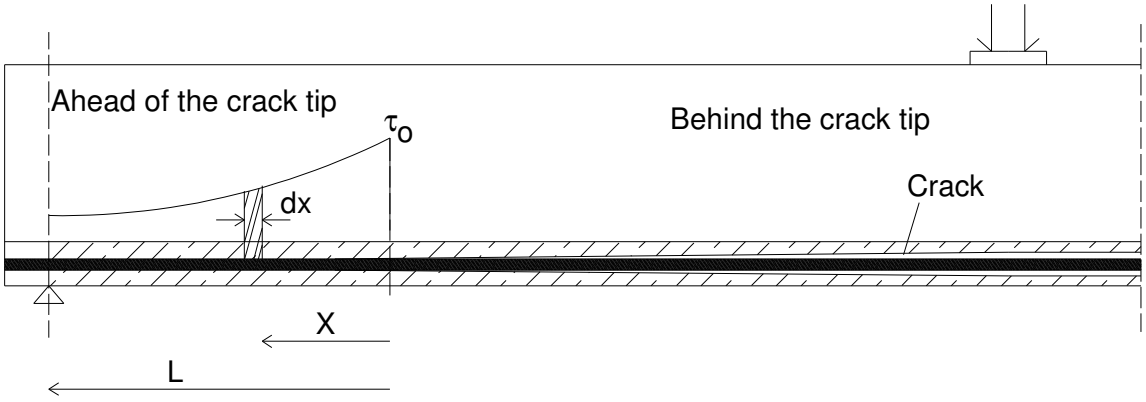

b- Long crack

Figure 5.17: Symbols used in integration

Thus, if the force at the crack tip and the distance ahead of the crack tip (L) are known the peak shear stress at the crack tip (τ_0) can be determined from Equation 5.3. The peak shear stress at the crack tip (τ_0) will be less than or equal to the maximum shear stress in Figure 5.6. As the force at the crack tip decreases, the peak shear stress at the crack tip (τ_0) decreases, but if this is accompanied by a decrease in the distance (L), the peak shear stress at the crack tip (τ_0) can increase.

The maximum shear stress for a given rod type is the monotonic shear stress. The maximum shear stress and the exponent for the monotonic curves were determined from the monotonic test results as follows. At any load level, the strains in the shear span were known and thus the force distribution in the shear span could be determined. The crack length can be predicted as explained earlier (See Figure 5.1), where the crack length is the distance between the crack tip and loading point). Then, the force ahead of the crack tip is fitted with an exponential curve as shown in Figure 5.18. The sand coated rods showed an exponent of -0.015 and the spirally wound rods showed an exponent of -0.012. The difference in the exponent between the sand coated and spirally wound rods is attributed to the difference in Young's modulus, where Young's modulus for the sand coated and spirally wound rods was 130 and 136 GPa, respectively. Using Equation 5.3, the maximum shear stress at the crack tip can be determined. It is estimated to be 30 MPa for the sand coated rods and 25 MPa for the spirally wound rods.

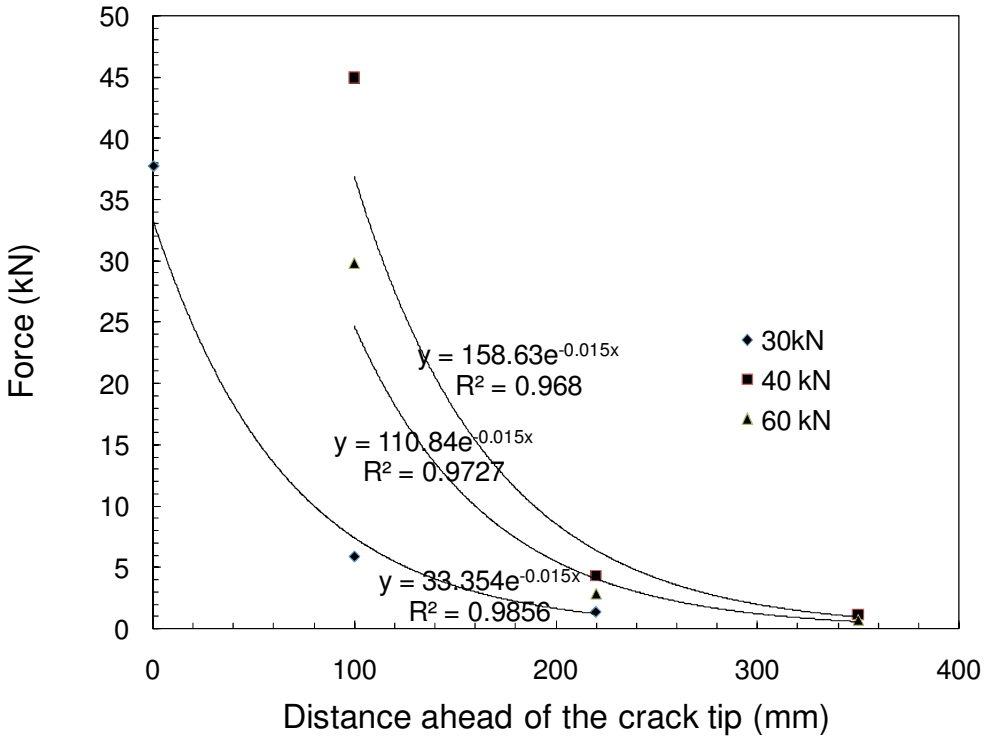

a- Sand coated rod in Beam NS-SC-0%-M

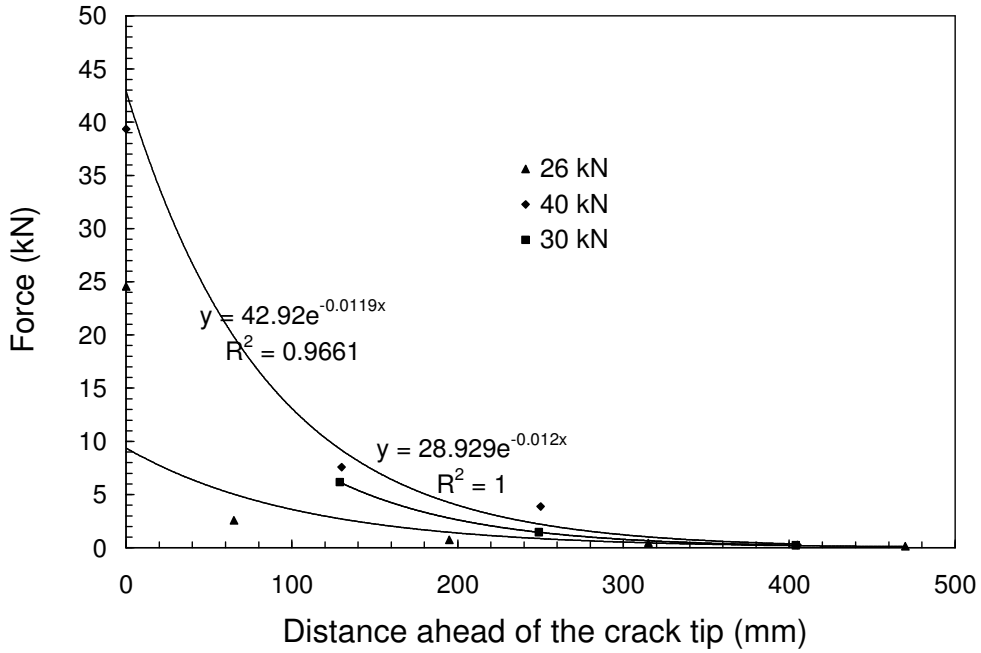

b- Spirally wound rod in Beam NS-SW-0%-M

Figure 5.18: Determination of the exponent "C" for the monotonic test results

b-The force that drives the crack

The variation of normal forces along the length of the CFRP rod creates shear stresses between the rod and the surrounding epoxy. The shear stress between the CRRP rod and the epoxy at the crack tip drives the crack. Yet, as discussed in the previous section, the uniform shear stress has a low value. Thus, it will be ignored and the only shear stress that will be considered is that given by the exponential curve and the shear stress will be replaced by the proportional normal force in the rod. The normal force in the CFRP rod at the crack tip will be used to represent the force driving the crack.

Debonding starts at a flexural crack near the loading point of the beam and propagates towards the support. Thus, the first crack that occurs underneath the loading point is driven by the normal force in the CFRP rod at the loading point which is equal to the normal force in the CFRP rod at midspan (equal moment region).

When the crack has already propagated as shown in Figure 5.7-b to a distance (x), the driving force then becomes the force at the crack tip at the distance x (F(x)). This force is equal to the force at the midspan minus the change in force over the distance x. This can be expressed by Equation 5.4.

$$F(x)=F-\tau_r \times\pi\times d\times x$$

and $x=\Delta a$ E.q.(5.4)

Where

F(x) is the force in the rod at the new crack location (kN)

F is the force in the rod at the previous crack location (kN)

τ_r is the debonded shear stress (MPa) from Table 5.1

d is the diameter of the CFRP rod

Δa is the incremental crack length (mm)

x is the distance from the loading point (mm)

Knowing the applied moment at midspan, the force in the CFRP rod at midspan can be computed. The force in the CFRP at the loading point (initial driving force) is equal to the force in the CFRP rod at midspan. When the crack has propagated a distance (Δa), the force in the rod at the crack tip can be computed using Equation 5.4 if the debonded shear stress is known.

c- The rate of crack propagation

If a growing crack increases its length by an amount (da) due to the application of a number of cycles (dn), the rate of crack growth can be characterized by the ratio (da/dn). A model is proposed where the rate of fatigue crack growth (da/dn) is dependent on the crack front shear stress between the CFRP rod and the epoxy. As discussed earlier, the uniform portion of the shear stress distribution is small and will be ignored. The normal force in the CFRP rod at the crack tip can then replace the shear stress in the model.

The relationship between the crack growth rate and the rod force at the crack tip is similar to the relationship between the applied load on the specimen and the life of the specimen. The load

versus life curve is a power function curve that is linear on the log-log scale. Thus, a power function was chosen to represent the relation between the crack growth rate and the force as described by Equation 5.5 and shown in Figure 5.19 where the integration of Equation 5.5 to get the life of the specimen will be a power function as shown from Equation 5.6.

$$\frac{da}{dn} = \alpha F^{\beta} \qquad \text{E.q.(5.5)}$$

Where:

da is the incremental crack length (mm)

dn is the incremental number of cycles (cycles)

F is the force in the CFRP rod at the crack tip or the force driving the crack (kN)

β is a constant that depends on the rod type. It is the slope of the crack growth versus force curve on a log-log scale.(Figure 5.19)

α is a constant that depends on the rod type, presence of internal steel and the prestressing force in the CFRP rod

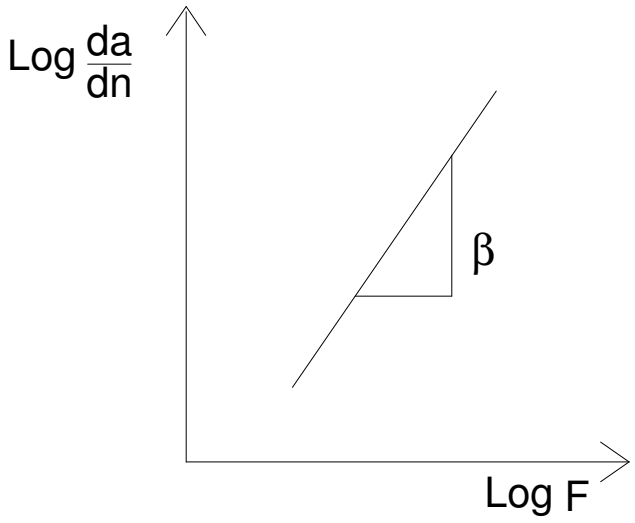

Figure 5.19: Rate of crack growth versus force on a log-log scale

$$\frac{da}{dn} = \alpha F^{\beta}$$

$$dn = \frac{da}{\alpha F^{\beta}}$$

$$\because F = F_m - \tau_r \times \pi \times d \times a$$

$$dn = \frac{da}{\alpha (F_m - \tau_r \times \pi \times d \times a)^{\beta}}$$

$$\int_0^N dn = \int_o^a \frac{da}{\alpha (F_m - \tau_r \times \pi \times d \times a)^{\beta}}$$

$$N = \frac{-1}{\alpha (1-\beta) \times \pi \times d \times \tau_r} (F_m - \tau_r \times \pi \times d \times a)^{(1-\beta)}$$

E.q. (5.6)

Where:

N is the total number of cycles or life of the specimen

a is the final crack length (mm)

F_m is the force in the CFRP rod at midspan (kN)

τ_r is the debonded shear stress (MPa)

d is the diameter of the CFRP rod (mm)

Determination of α and β

Figures 5.20-a and 5.20-b show the load range (kN) versus life curve for the spirally wound rods and the sand coated rods, respectively. It is clear that the intercept of the best fit line is different from one set of beams to another for the same rod type. Thus, constant " α" will differ from one set of beams to another for the same rod type. From Figure 5.20, it is clear that there are some differences in slope from one set of beams to another for the same rod type but nevertheless, using the same slope to for all the beams strengthened with the same rod type will give a reasonable fit to the data. Therefore, the constant β was fixed for a given rod type.

For a given rod type, constants α and β were first determined for the beams with no internal steel such that they satisfy the shortest and longest life. Then, using these values, the lives of the beams in between for the same group were calculated. The constant β was kept constant for groups of beams strengthened with the same rod type. The constant α was changed from one group to another to match the observed life. Table 5.3 shows the values for constants α and β. For all the beams in each set, the force distribution in the shear span and crack length at failure was computed and compared to the experimental values as will be discussed latter.

Table 5.3: Values of constants " α" and " β"

Rod Type	Beam type	β	α
Sand coated	No internal steel	8.5	4.4×10^{-19}
	With internal steel and strengthened with non-prestressed CFRP rods		8.8×10^{-16}
Spirally wound	No internal steel	6.4	1.2×10^{-12}
	With internal steel and strengthened with non-prestressed CFRP rods		7.1×10^{-12}

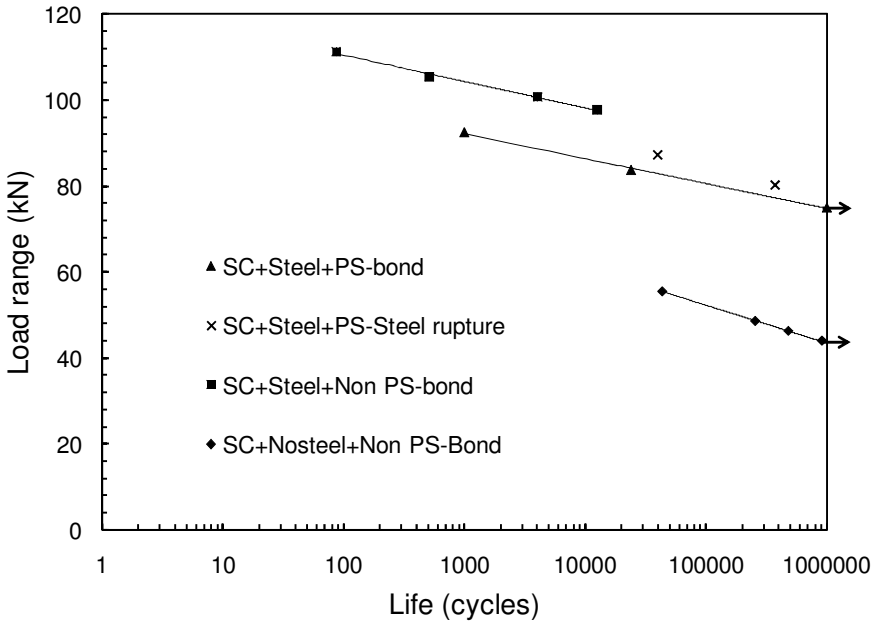

a- Sand coated rods

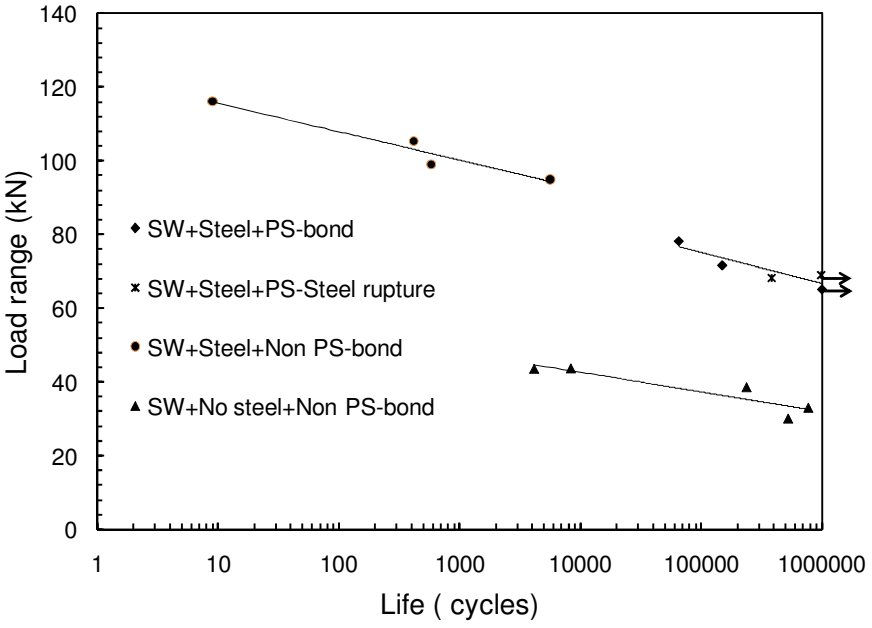

b- Spirally wound rods

Figure 5.20: Load range (kN) versus life (cycles) for all beams

d- Failure criterion

As discussed in previous sections, the debonding between the CFRP rod and the epoxy starts at midspan then extends towards the supports for the beams strengthened with non-prestressed CFRP rods. As the debonded length increases, the crack driving force decreases due to the presence of a debonded shear stress and this will in turn decrease the shear stress ahead of the crack. When the crack front approaches the support, the length of the bonded region ahead of the crack decreases and the peak shear stress ahead of the crack tip increases even though the force is still decreasing. In the model, the failure criterion was taken to be the peak shear stress at the crack tip.

The failure shear stress under fatigue loading is expected to be less than the monotonic failure shear stress. Wahab et al. (2008) found that the failure shear stress under fatigue loading is 70% of the monotonic failure shear stress for near surface mounted spirally wound CFRP rods. In the present investigation, it was found that using a failure shear stress under fatigue loading equal to 50% of the monotonic shear stress in the model gives the best fatigue life predictions. The monotonic shear stress was determined earlier to be 30 and 25 MPa for the sand coated and spirally wound rods, respectively. The fatigue failure shear stress was found to be 15 and 12.5 MPa for the sand coated and the spirally wound rods under fatigue loading, respectively as shown in Table 5.4.

Table 5.4: Failure shear stress for different CFRP rods

CFRP Rod		Failure shear stress (MPa)
Sand coated	Monotonic loading	30
	Fatigue loading	15
Spirally wound	Monotonic loading	25
	Fatigue loading	12.5

Figure 5.21 shows a typical curve of percentage of life versus slip. It shows the point where the experiment ended (100%life). In the model, failure was defined at the onset of large scale slip between the CFRP rod and the epoxy for the following reasons:

1-The fatigue experiments were conducted in a load controlled environment where the beam was cycled between pre-defined minimum and maximum loads. The termination of the experiment depended on a deflection limit set in the experiment. The deflection limit was set equal to the deflection at the peak load in the first cycle plus 20 mm. The maximum deflection at peak load in the first cycle for beams without internal steel was 11.5mm (about L/ 175, where L is the span) and for the beams with steel was about 22 mm (about L/ 90) and the deflection limit in these cases were set at 32 and 42 mm, respectively.

2-In the experiments, the onset of large scale slip between the CFRP rod and the epoxy on occurred between 80-90% of the total fatigue life of the beam.

3-After the CFRP rod slips excessively from the epoxy at the free end, the shear stress distribution given by Figures 5.6 and 5.7 is no longer valid.

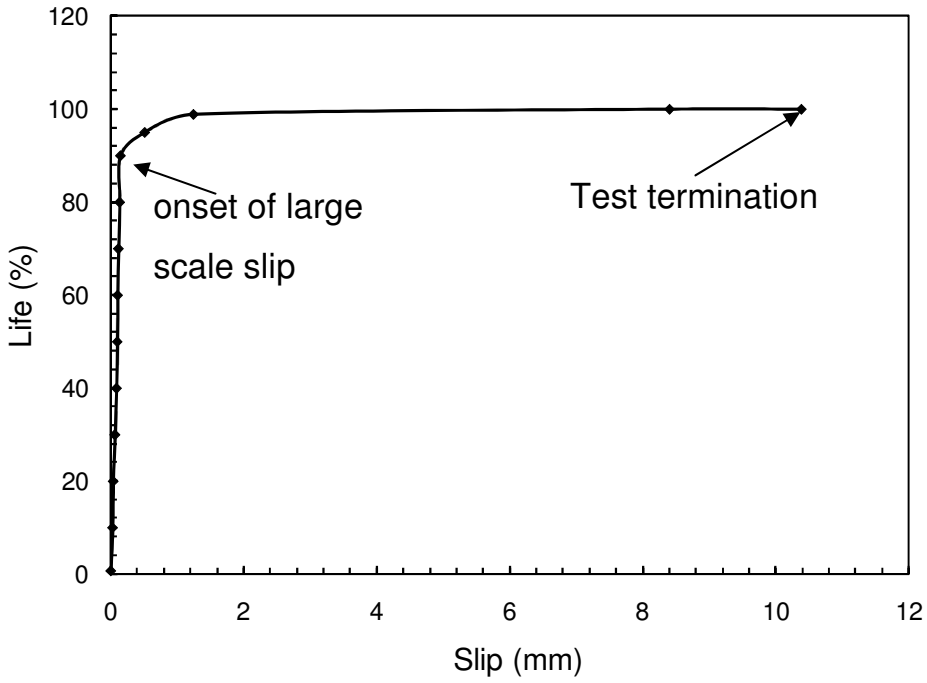

Figure 5.21: Life (%) versus slip (mm)

Therefore, at failure (the onset of large scale slip between CFRP rod and epoxy), the following parameters will be compared to one another;

1- The predicted and experimental number of cycles at onset of large scale slip will be compared.

2- The force distribution in the shear span at failure will be predicted and compared to the experimental forces in the shear span deduced from the strain gauge readings.

5.3.2 Calculation steps:

1-Using the external applied load, the moment at midspan is calculated.

2-Given the material properties, the strain in the CFRP rod at midspan is calculated. That is the initial driving force for the crack (F_0).

Force=strain × Young's modulus× cross sectional area of the rod= ε×E×A

3-The initial crack length (a_0) is set to be 10 mm. The initial crack length could be chosen any other value. The analysis is not sensitive to the initial crack length.

4-Using the equation for rate of crack growth, the incremental number of cycles (dn) is calculated.

$$\frac{da}{dn} = \alpha F^{\beta} \longrightarrow dn_1 = \frac{da_0}{\alpha F_0^{\beta}}$$

Where α and β are already known for a given beam configuration and CFRP rod type

5-At the new crack location ($a_1 = a_0$), calculate the force in the CFRP rod (F_i). This force will be the new driving force for the crack.

$F_i = F_0 - \tau_r \times \pi \times d \times a_i$ where i=1

6- Calculate the peak shear stress (τ_0) ahead of the crack tip.

$$\tau_0 = \frac{F_i C}{\pi d} \frac{1}{(1-\exp^{(-CL)})}$$

If τ_0 > the failure shear stress then the beam has failed.

If τ_0 < the failure shear stress then proceed to step7.

7-The crack is propagated in an increment (da) equal to 10 mm. The incremental crack length could be chosen any other value. The analysis is not sensitive to the incremental crack length.

da=10

i=i+1

8- Using the equation for the rate of crack growth the number of cycles is computed.

$$dn_i = \frac{da}{\alpha F_{(i-1)}^{\beta}}$$

9- At the new crack tip location, the total crack length (a_i) and the force driving the crack (F_i) are:

$a_i = i.da$

$F_i = F_0 - \tau_r \times \pi \times d \times a_i$

Then,

10-The peak shear stress ahead of the crack tip is calculated.

$$\tau_0 = \frac{F_i C}{\pi d} \frac{1}{(1 - \exp^{(-CL)})}$$

If $\tau_0 >$ the failure shear stress then the beam has failed.

If $\tau_0 <$ the failure shear stress then go to step 7 and repeat.

The total number of cycles will be given by Equation 5.7:

$N = \sum dn$ E.q.(5.7)

At failure, the force at the crack tip (F_f), the final crack length and the number of cycles are known. The force ahead of the crack tip is distributed exponentially according to Equation 5.8. Thus, the force at any location ahead of the crack tip can be determined. Behind the crack tip, the force at any location will be given according to Equation 5.9.

$F(x) = F_f \exp^{(-C \times X)}$ E.q.(5.8)

$F(x) = F_f + \tau_r \times \pi \times d \times x$ E.q.(5.9)

Where:

F_f is the force at the crack tip (kN)

x is the distance from the crack tip to the desired location(mm)

The forces along the CFRP rod in the shear span at failure are determined and compared to the actual forces from the experimental results.

5.4 Failure by slipping between the CFRP rod and the epoxy that starts at the support and travels to the loading point

This mode of failure occurs when the critical section with the highest stresses between the rod and the epoxy is close to the support. In this case, slipping between the CFRP rod and the epoxy at the support will occur before debonding at sections close to the loading point spreads to reach the support. This mode of failure occurred only for beams strengthened with prestressed CFRP rods. It occurred for the beams with internal steel and strengthened with prestressed spirally wound CFRP rods for both monotonic and cyclic applied loads. It also occurred for the prestressed beams with internal steel strengthened with sand coated CFRP rods and tested under fatigue loading.

5.4.1 Parameters and assumptions for the model

As discussed earlier, when the CFRP rod is prestressed, the forces in the transfer length increase from zero at the free end until reaching the prestressing force at the end of the transfer length. The variation in force in the transfer length will create shear stresses along the rod. The shear stress is largest at the free end and decreases along the rod as shown in Figure 5.22. During release, if there is no slip between the CFRP rod and the epoxy, the peak shear stress will be at

the free end. Yet, normally some slip occurs between the CFRP rod and the epoxy and the peak shear stress is at some distance from the center line of the support. This distance was estimated to be between 25 and 50mm depending on the rod type. The peak shear stress is equal to the maximum shear stress that can occur at the interface between the CFRP rod and the epoxy. Therefore, it is equal to the cracking shear stress calculated from the monotonic tests, which was 30 and 25 MPa for the prestressed sand coated and spirally wound rods, respectively. The shear stress distribution due to prestressing is represented by an exponential curve with an exponent equal to the exponent of the monotonic shear stress distribution (See Figure 5.18). The sand coated rods have an exponent of -0.015 and the spirally wound rods have an exponent of -0.012.

During loading, following flexural cracking, debonding occurs at the loading point and progresses towards the supports as the load is cycled. The stress distribution ahead of the crack tip is shown in Figure 5.22. It will be the same distribution as the one for the beams with internal steel and strengthened with non-prestressed CFRP rods. The overlap between the shear stress distribution due to loading and due to prestressing is shown in Figure 5.22. The overlapping of the shear stress distribution increases the shear stress near the end of the beam which becomes the critical shear stress that causes failure. Failure starts when the CFRP rod slips from the epoxy near the end of the beam. Then, the peak shear stress shifts inwards. The integration of the shear stress distribution multiplied by the rod perimeter within the transfer length is equal to the sum of the prestressing force and the force due to loading. As the beam is cycled, the CFRP rod continues to slip and the peak shear stress continues to shift inward until failure occurs by slippage of the CFRP rod from the epoxy.

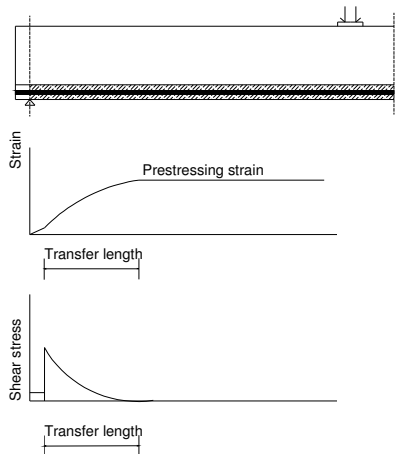

a- Shear stress due to prestressing

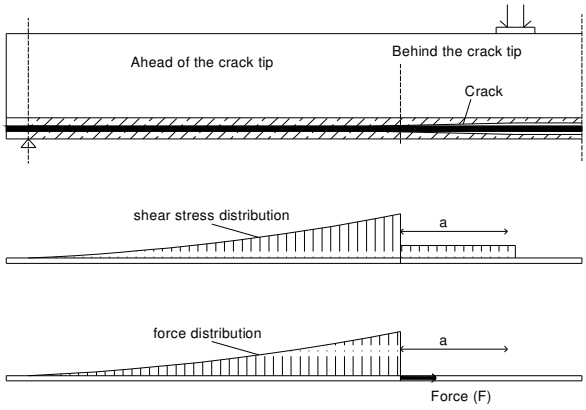

b- Shear stress due to loading

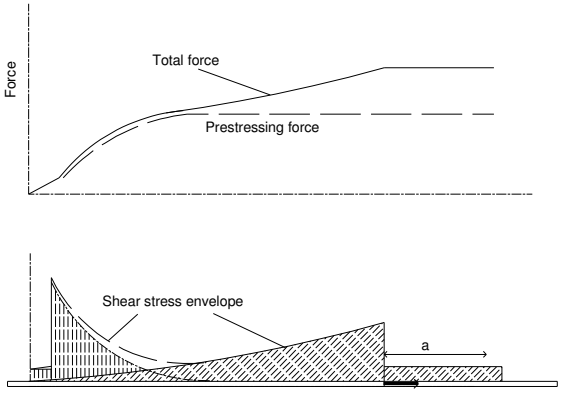

c- Total shear stress

Figure 5.22: Shear stress and force distribution in prestressed beams

The model used is based on the following assumptions:

1-During loading, no end slip occurs between the CFRP rod and the epoxy until failure. Thus, the distribution of the shear stress due to prestressing will remain the same from the beginning of loading until failure is reached. The distribution of the shear stress ahead of the crack tip occurring due to debonding between the CFRP rod and the epoxy shifts from the midspan towards the support until failure occurs. In the experimental beams, slip between the CFRP rod and the epoxy was small and thus the initial shear stress distribution due to prestressing would not change greatly. Because only 2 strain gauge readings were located in the transfer zone (so as not to unduly affect the bond between the CFRP rod and the epoxy), the experimental data was not sufficient to calculate accurately the change in the shear stress due to prestressing due to slip. The shear stress distributions due to loading and prestressing will be superimposed (elasticity is assumed). Once the shear stress at the end exceeds the failure shear stress, failure occurs.

2-The failure shear stress at the end is higher than the prestressing shear stress. It is estimated to be 25.5 MPa for the spirally wound rods and 30.4MPa for the sand coated rods, whereas the maximum prestressing shear stress was 25 and 30 MPa for the spirally wound and the sand coated rods, respectively. Table 5.5 summarizes the failure shear stress for prestressed CFRP rods under fatigue loading.

A Goodman diagram showing the effect of mean stress as expressed by Equation 5.10 is shown in Figure 5.23(Dowling, 1998). Figure 5.23 shows the normalized shear stress amplitude (shear stress amplitude divided by the shear stress amplitude at the fatigue limit for zero mean stress) on

the vertical axis versus the mean shear stress as a function of the ultimate shear stress on the horizontal axis.

$$\frac{\tau_a}{\tau_{ar}} + \frac{\tau_m}{\tau_u} = 1 \qquad \text{E.q.(5.10)}$$

Where;

τ_a shear stress amplitude (MPa)

τ_{ar} shear stress amplitude at the fatigue limit for zero mean stress (MPa)

τ_m mean shear stress (MPa)

τ_u ultimate shear stress (MPa)

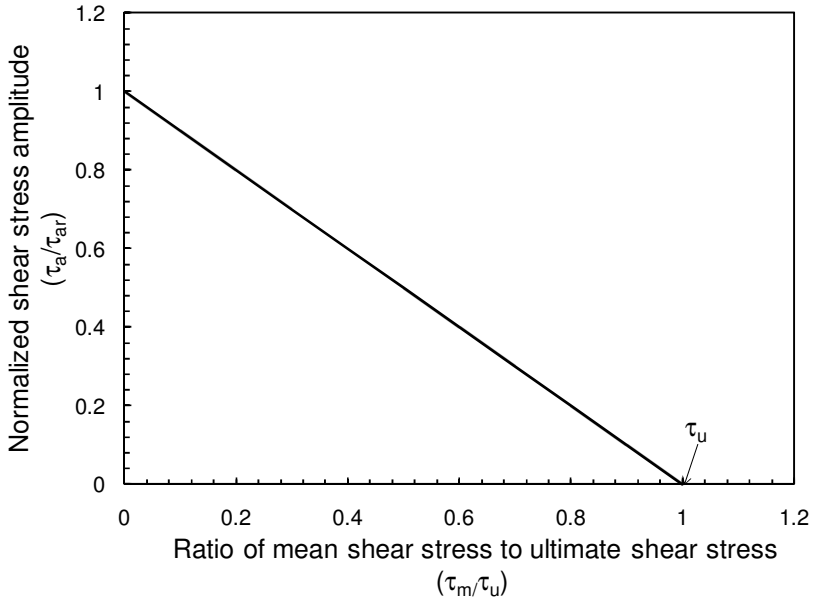

Figure 5.23: Goodman diagram

Figure 5.23 shows that the failure envelope (solid straight line) intersects the horizontal axis when the mean stress equals the ultimate stress. Thus, failure is achieved with a stress amplitude

of zero and a mean stress equal to the ultimate capacity. Since the shear stress due to prestressing is already nearly equal to the cracking shear stress, the expected contribution from the stress distribution due to loading will be small.

Table 5.5: Failure shear stress for prestressed CFRP rods under fatigue loading.

Rod type	Failure shear stress
Sand coated	30.4 MPa
Spirally wound	25.5 MPa

The same model used for the beams that fail by debonding that starts at the loading point and spreads towards the support will be used here with some modifications.

5.4.2 Steps in the calculations

1-The shear stress distribution due to prestressing can be determined from Equation 5.11. It depends on the CFRP rod type. That distribution will be fixed during the iterations.

$$\tau(x)=\tau_m \times \exp(-\mu \times (x-s_i)) \qquad \text{E.q.(5.11)}$$

Where:

x is measured from the center line of the support to the desired location along the CFRP rod

τ_m is the maximum shear stress due to prestressing.

It is equal to 30 and 25 MPa for the sand coated and spirally wound rods, respectively.

$\tau(x)$ is the shear stress at any distance x

μ exponent of the shear stress distribution due to prestressing. It was taken equal to the exponent of the monotonic shear stress distribution due to loading in the non-prestressed beams. It is equal to 0.015 or 0.012 for the sand coated and spirally wound rods, respectively.

s_i distance ranges from 25-50mm. It is 25mm for sand coated rods and 50mm for spirally wound rods.

2-Using the external applied load, the moment at midspan is calculated.

3-Given the material properties and the prestressing strain, the strain in the CFRP rod at midspan is calculated. The prestressing strain is then subtracted from the total strain calculated at midspan where that is the initial driving strain and thus force for the crack (F_0).

4-The initial crack length measured from the loading point (a_0) is assumed to be 10 mm.

5-Using the equation for rate of crack growth, the incremental number of cycles (dn) is calculated.

$$\frac{da}{dn} = \alpha F^{\beta} \longrightarrow dn_1 = \frac{da_0}{\alpha F_0^{\beta}}$$

Where α and β are given by Table 5.6.

Table 5.6: Values of constants "α" and "β" for prestressed CFRP rods

Rod Type	Beam type	β	α
Sand coated	With internal steel and strengthened with prestressed CFRP rods	8.5	1.4×10^{-13}
Spirally wound	With internal steel and strengthened with prestressed CFRP rods	6.4	7.1×10^{-12}

6-At the new crack location ($a_1=a_0$), calculate the force in the CFRP rod (F_i). This force will be the new driving force for the crack if the crack will propagate further.

$F_i= F_0-\tau_r \times\pi\times d\times a_0$ where i=1

7-Calculate the peak shear stress (τ_0) ahead of the crack tip.

$$\tau_0 = \frac{F_i C}{\pi d} \frac{1}{(1-\exp^{(-CL)})}$$

Where C and τ_r are given by Table 5.7

Table 5.7: C and τ_r for beams with internal steel and strengthened with prestressed CFRP rods

Rod type	C	τ_r
Sand coated	-0.005	2.25
Spirally wound	-0.004	1.0

8- Calculate the shear stress due to debonding using Equation 5.12 at the location of peak shear stress due to prestressing. That will be at 25 or 50 mm from the support for the beams strengthened with prestressed sand coated and spirally wound CFRP rods, respectively.

$\tau (x)=\tau_o \exp^{(-CX)}$ E.q.(5.12)

Where;

x =shear span(600mm)-crack length-25mm for sand coated rods

x =shear span(600mm)-crack length-50mm for spirally wound rods

9-Add the shear stress calculated in step 8 to the shear stress due to prestressing

-If the total shear stress > the failure shear stress then the beam has failed.

-If the total shear stress < the failure shear stress then proceed to step10.

10-The crack is propagated towards the support in an increment (da) equal to 10 mm.

da=10mm

i=i+1

11-Then, using the equation for the rate of crack growth the number of cycles can be computed.

$$dn_i = \frac{da}{\alpha F_{(i-1)}{}^{\beta}}$$

12- At the new crack location, the crack length (a_i) and the force driving the crack (F_i) are:

$a_i = i.da$

$F_i = F_0 - \tau_r \times \pi \times d \times a_i$

13-The peak shear stress ahead of the crack tip and at the location of peak shear stress due to prestressing end is calculated and added to the shear stress due to prestressing.

$$\tau_0 = \frac{F_i C}{\pi d} \frac{1}{(1 - \exp^{(-CL)})}$$

$\tau(x) = \tau_o \exp^{(-CX)}$

-If the total shear stress > the failure shear stress (see Table 5.5) then the beam has failed.

-If the total shear stress < the failure shear stress (see Table 5.5) then go back to step 10 and repeat.

The total number of cycles will be given by Equation 5.13:

$N = \sum dn$ E.q.(5.13)

At failure, the force at the crack tip (F_f), the final crack length and the number of cycles are known. The force ahead of the crack tip due to loading is distributed exponentially according to

Equation 5.14. Thus, the force due to loading at any location ahead of the crack tip can be determined. Behind the crack tip, the force due to loading at any location will be given according to Equation 5.15.

$$F(x) = F_f \exp^{(-C \times X)} \quad \text{E.q.(5.14)}$$

$$F(x) = F_f + \tau_r \times \pi \times d \times x \quad \text{E.q.(5.15)}$$

Where:

F_f is the force in the rod at the crack tip (kN)

x is the distance from the crack tip to the desired location (mm)

The forces due to loading and prestressing will be superimposed to get the total force at any location in the shear span. The forces along the CFRP rod in the shear span at failure are determined and compared to the actual forces from the experimental results.

5.5 Comparison between the experimental and the calculated values

5.5.1 Beams with no steel and strengthened with non-prestressed sand coated CFRP rods

Table 5.8 shows the experimental and calculated force in the CFRP rod in the shear span and the number of cycles at the onset of excessive slip. Figure 5.24 shows both the experimental and the predicted number of cycles to the onset of excessive slipping versus the applied load. Figure 5.25 shows plots of the calculated force (from the model) and the experimental (actual) force in the CFRP rod in the shear span for the beams with no steel and further strengthened with non-prestressed sand coated CFRP rods at the onset of excessive slip. The vertical axis represents the

force in the CFRP rod and the horizontal axis represents the distance along the beam from the support.

The model predicts the number of cycles until onset of excessive slipping with good accuracy with the trend lines for the experimental and predicted number of cycles falling on one another. The model also predicts the forces in the shear span with a reasonable accuracy where the maximum error in the force is 15kN (19.2 % of the experimental reading).

Table 5.8: Comparison between the experimental and calculated results for beams with no steel and strengthened with non-prestressed sand coated CFRP rods

Specimen		Distance from the support (mm)				Number of cycles at onset of excessive slip
		125	250	375	500	
NS-SC-0%-60%	Experimental force (kN)	44	64.17	----	73.47	434,224
	Calculated force (kN)	46.24	59.46	63.73	67.31	434,900
NS-SC-0%-62.5%(a)	Experimental force (kN)	50.5	------	73.85	73.85	231,206
	Calculated force (kN)	46.03	63.26	66.84	70.45	235,008
NS-SC-0%-70%	Experimental force (kN)	50.75	82.8	76.6	------	39,520
	Calculated force (kN)	41.19	66.84	80.15	83.7	34,141

(--------): indicates that the strain gauge was damaged
(NA): stands for not applicable

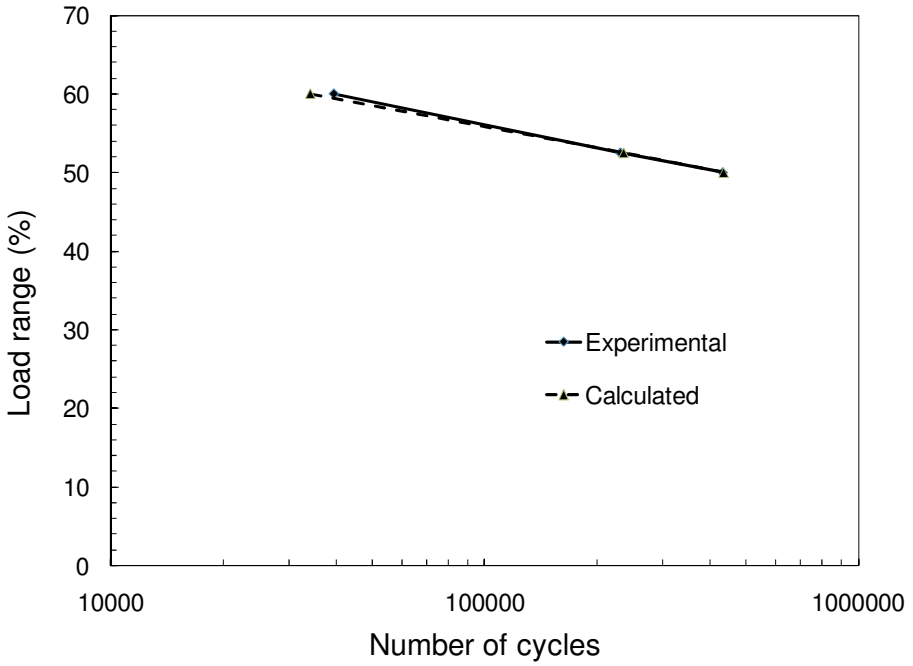

Figure 5.24: The experimental and calculated number of cycles to onset of excessive slip for beams with no steel and strengthened with non-prestressed sand coated CFRP rods

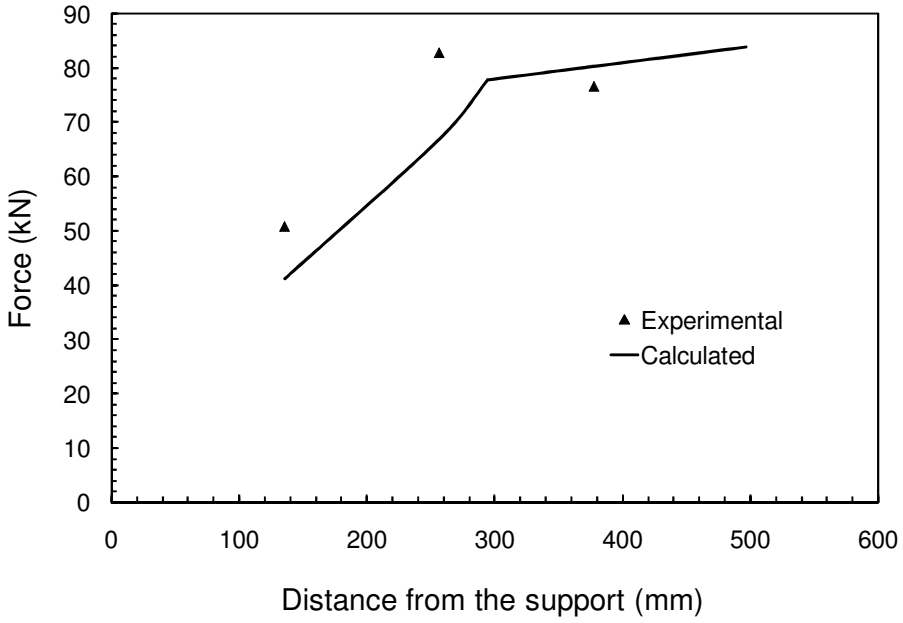

a-Beam NS-SC-0%-70%

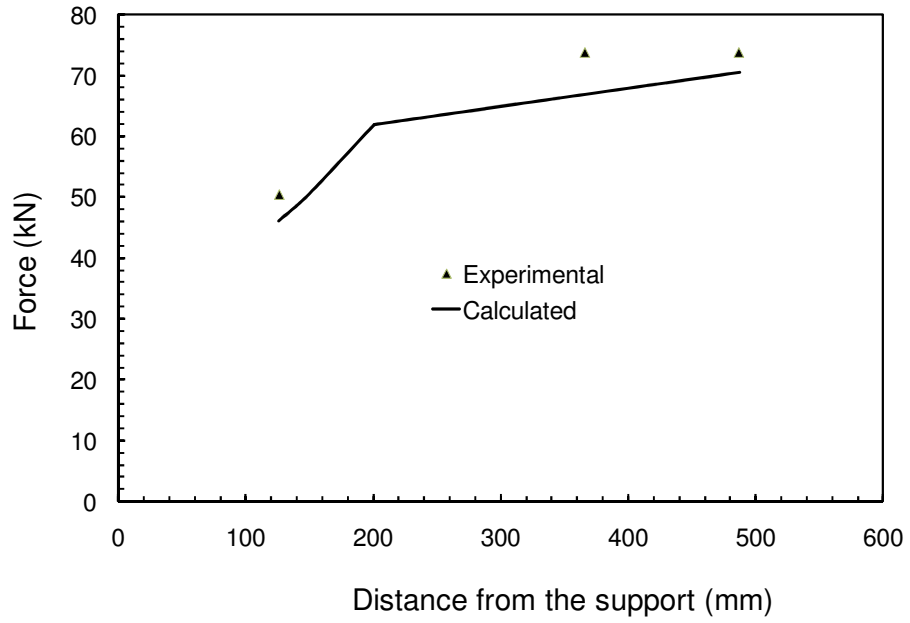

b-Beam NS-SC-0%-62.5%(a)

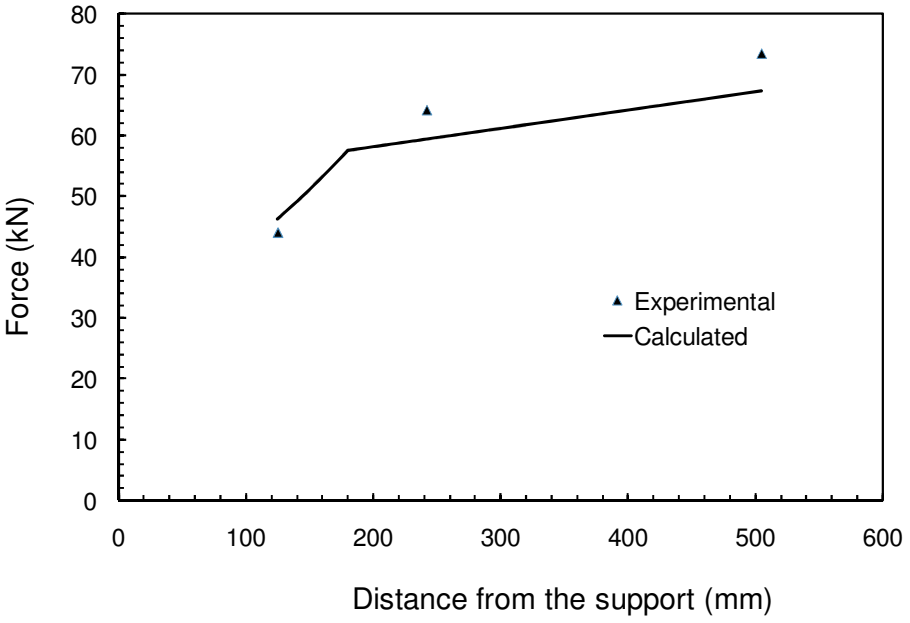

c- Beam NS-SC-0%-60%

Figure 5.25: Experimental and calculated forces in the CFRP rod in the shear span for beams with no steel and strengthened with non-prestressed sand coated CFRP rods

5.5.2 Beams with steel and strengthened with non-prestressed sand coated CFRP rods

Similar to the previous set, Table 5.9 shows the experimental and calculated force in CFRP rod in the shear span and number of cycle at the onset of excessive slipping for beams with steel and strengthened with non-prestressed sand coated CFRP rods. Figure 5.26 shows both the experimental and the predicted number of cycles at the onset of excessive slip versus the applied load. Figure 5.27 shows plots for the calculated force (from the model) and the experimental (actual) force in the CFRP rod in the shear span for the beams with steel and strengthened with non-prestressed sand coated CFRP rods.

The calculated and actual number of cycles to the onset of excessive slip are in good agreement with the trend lines coinciding except for a small error for the beam tested at a load range of 66% (longest life). The model also predicts the forces in the shear span at the onset of excessive slip with a good accuracy. The maximum error is 12 kN (25% of the experimental force). For beam S-SC-0%-76%, the force obtained from the strain gauge reading at the failing end is in doubt where the experimental force at 125mm at failure was measured to be 29.62 kN at the end that failed but at the end that did not fail at the same location the force was 36.4 kN. Thus, it is probable that the actual force at the failure location was 36.4 kN.

Table 5.9: Comparison between the experimental and calculated results for beams with steel and strengthened with non-prestressed sand coated CFRP rods

Specimen		Distance from the support (mm)				Number of cycles at onset of excessive slip
		125	250	375	500	
S-SC-0%-85%	Experimental force (kN)	48.47	60.8	79.1	76	87
	Calculated force (kN)	36.6	62.5	70.1	79.02	94
S-SC-0%-81.3%	Experimental force (kN)	37.4	54.72	55.8	69.79	460
	Calculated force (kN)	41.73	56.13	65.4	72.4	466
S-SC-0%-78%	Experimental force (kN)	29.62*	56	60.2	69	3637
	Calculated force (kN)	41.13	48.9	57.1	65.08	2304
S-SC-0%-76%	Experimental force (kN)	32.84	45.35	53.31	54.38	11305
	Calculated force (kN)	36.41	44.8	53.1	61.85	7246

*: At the non failing end, it was 36.4 kN

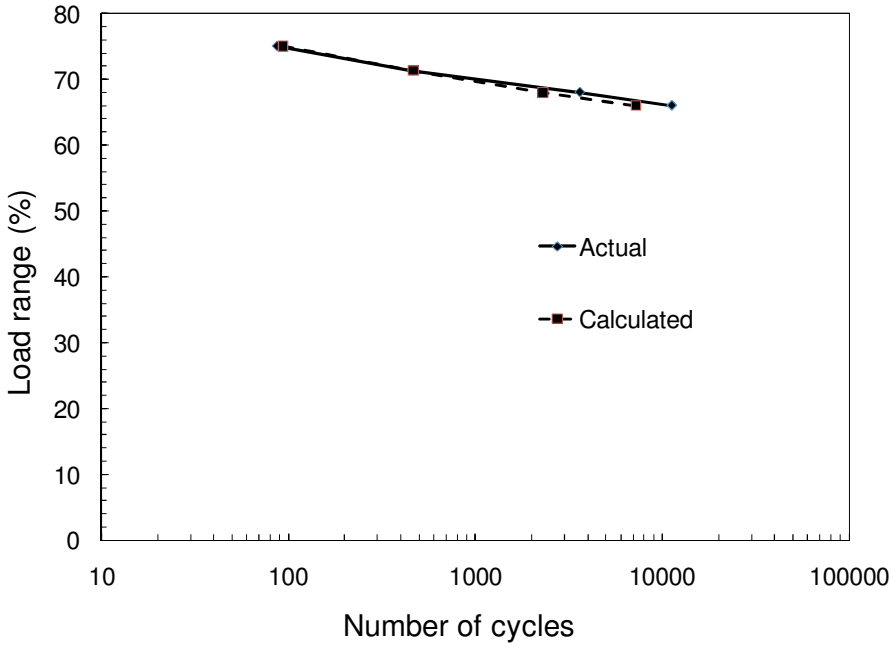

Figure 5.26: The experimental and calculated number of cycles to onset of excessive slip for beams with steel and strengthened with non-prestressed sand coated CFRP rods

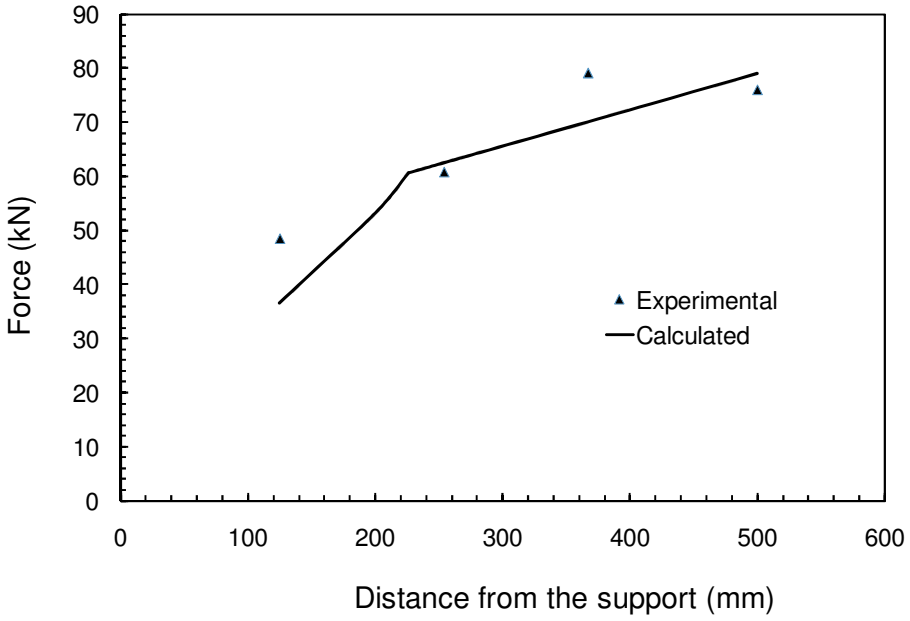

a-Beam S-SC-0%-85%

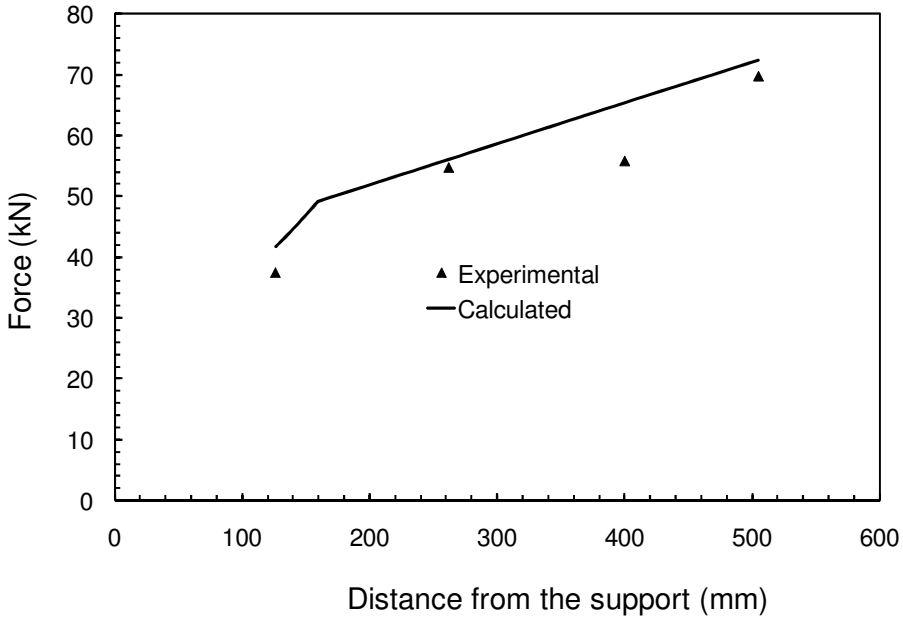

b- Beam S-SC-0%-81.3%

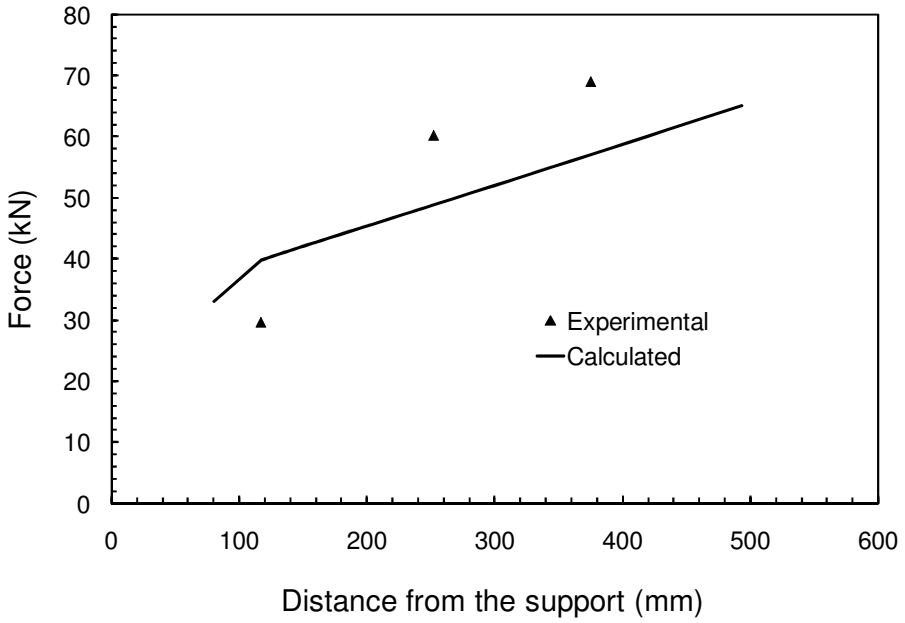

c-Beam S-SC-0%-78%

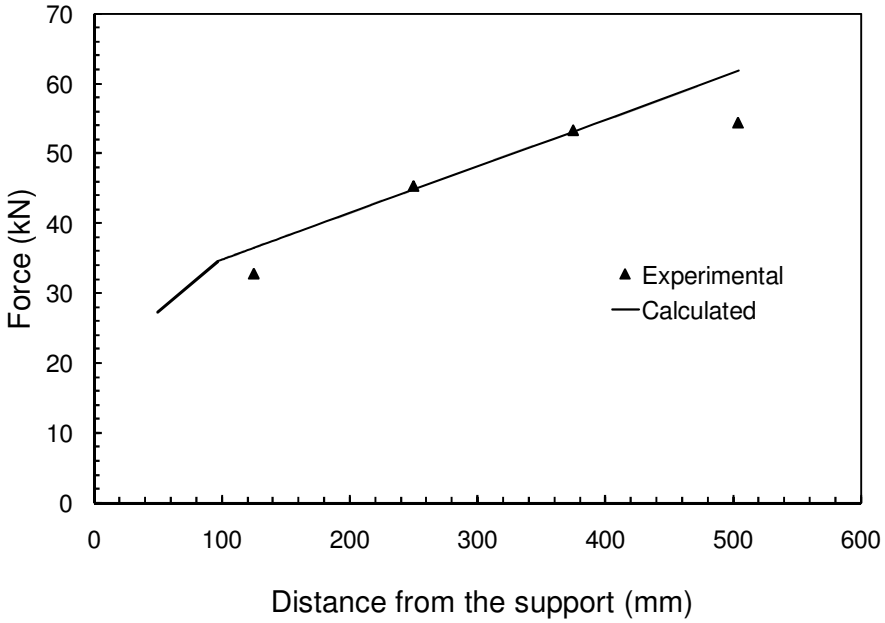

d-Beam S-SC-0%-76%

Figure 5.27: Experimental and calculated forces in the CFRP rod in the shear span for beams with steel and strengthened with non-prestressed sand coated CFRP rods

5.5.3 Beams with steel and strengthened with prestressed sand coated CFRP rods

Figure 5.28 shows a comparison between the experimental and calculated life for the beams with steel and strengthened with prestressed sand coated CFRP rods. Figure 5.29 shows the experimental and calculated prestressing forces. Table 5.10 and Figure 5.30 shows the experimental and calculated total forces in the CFRP rod in the shear span for the same group.

The force distribution in the rod due to prestressing depends on the rod type and the total prestressing force. Thus, the force distribution due to prestressing is constant for all beams with sand coated CFRP rods prestressed to the same load level. Experimental measurements for prestressing force showed some scatter but an average curve was chosen that fits all data as shown in Figure 5.29. Detailed discussions regarding the transfer length can be found in Chapter 4.

Table 5.10 shows the total force in the CFRP rod in the shear span. From the experimental forces within the transfer length (125 and 250mm), the prestressing force constitutes more than 95% of the total force at any location. Meanwhile, outside the transfer length the prestressing force is on average 76 % of the force. Thus, force due to loading in the transfer length is not more than 5% the total force in that zone and increases to 24% outside the transfer length. The model gives values of the forces with a reasonable accuracy. The experimental forces are less than the calculated forces. Figure 5.28-b and Figure 5.28-c show clearly the region behind the crack tip indicated by the flat part in the calculated curve (See dotted circle Figure 5.28-b). Then, ahead of the crack tip there is a transition from the force at the crack tip to a lower force. Then, finally the

last curved part of the calculated curve (See solid circle Figure 5.28-b) falls within the transfer length where there is a less prestressing force.

Table 5.10 and Figure 5.28 show a comparison between the experimental and calculated number of cycles at the onset of excessive slipping. The predicted and the actual values are in good agreement with one another.

Table 5.10: Comparison between the experimental and calculated total forces in the shear span for beams with steel and strengthened with prestressed sand coated CFRP rods

Specimen		Distance from the support (mm)				Number of cycles at onset of excessive slip
		125	250	375	500	
S-SC-40%-63%	Experimental force (kN)	33.6	60.94	76.4	88.82	900
	Calculated force (kN)	43.27	62.05	69.44	79.17	845
S-SC-40%-58%	Experimental force (kN)	28.81	51.03	63.97	65.31	21600
	Calculated force (kN)	31.74	59.02	66.73	75.76	24,352
S-SC-40%-56%	Experimental force (kN)	44	64.94	----	----	375,000
	Calculated force (kN)	47.61	61.09	67.02	74.34	375,000

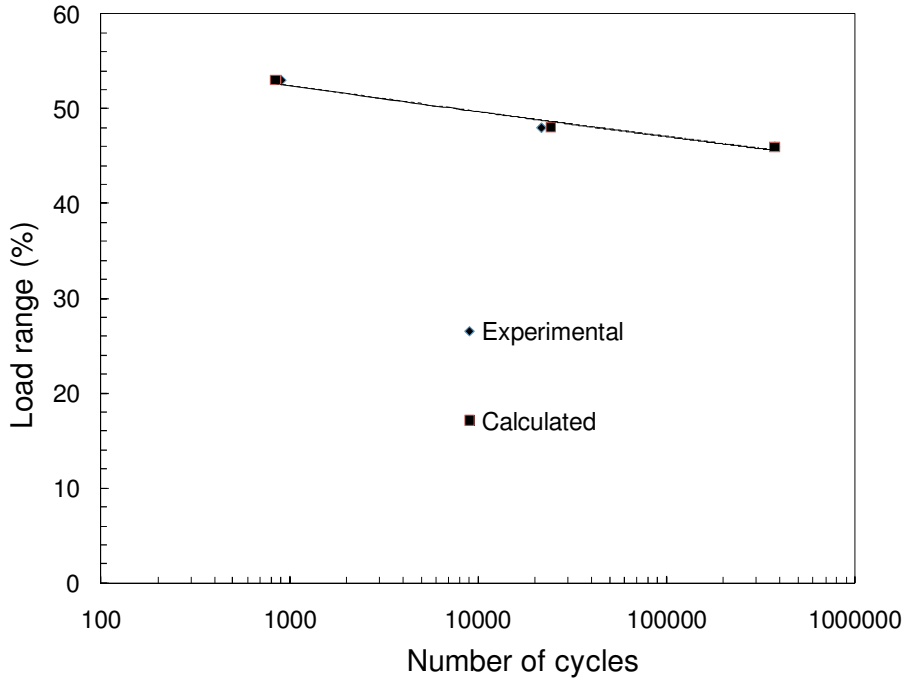

Figure 5.28: The experimental and calculated number of cycles to onset of excessive slip for beams with steel and strengthened with prestressed sand coated CFRP rods

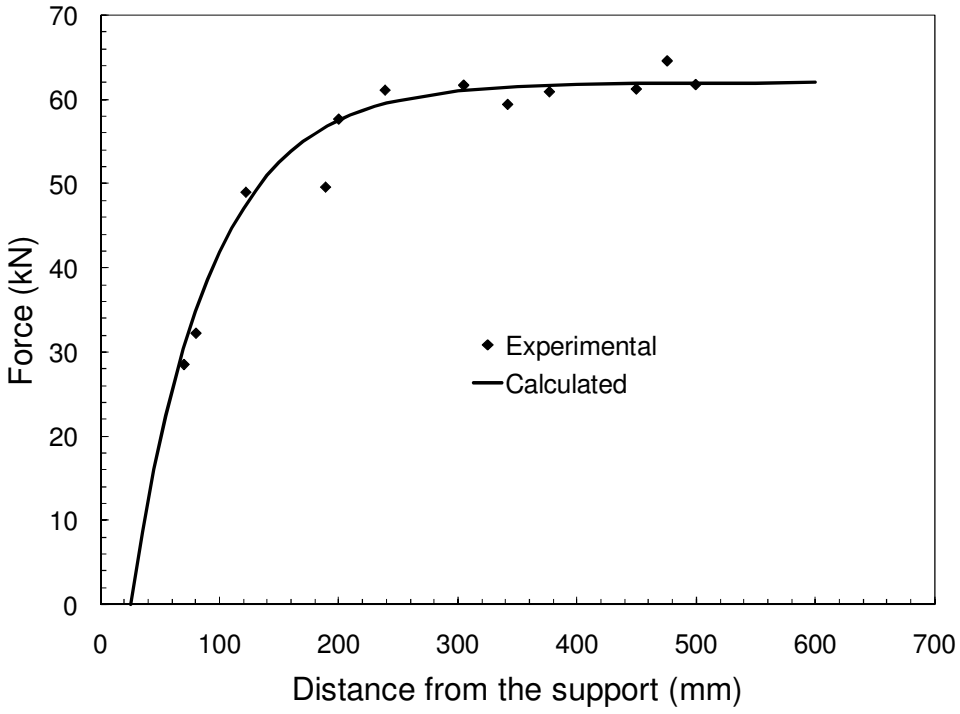

Figure 5.29: Experimental and calculated forces due to prestressing

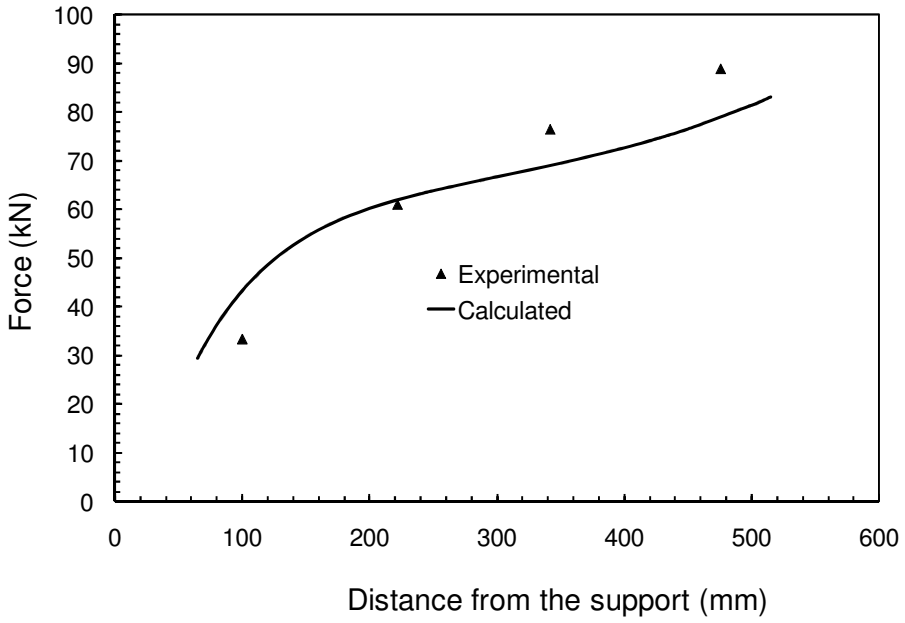

a-Beam S-SC-40%-63%

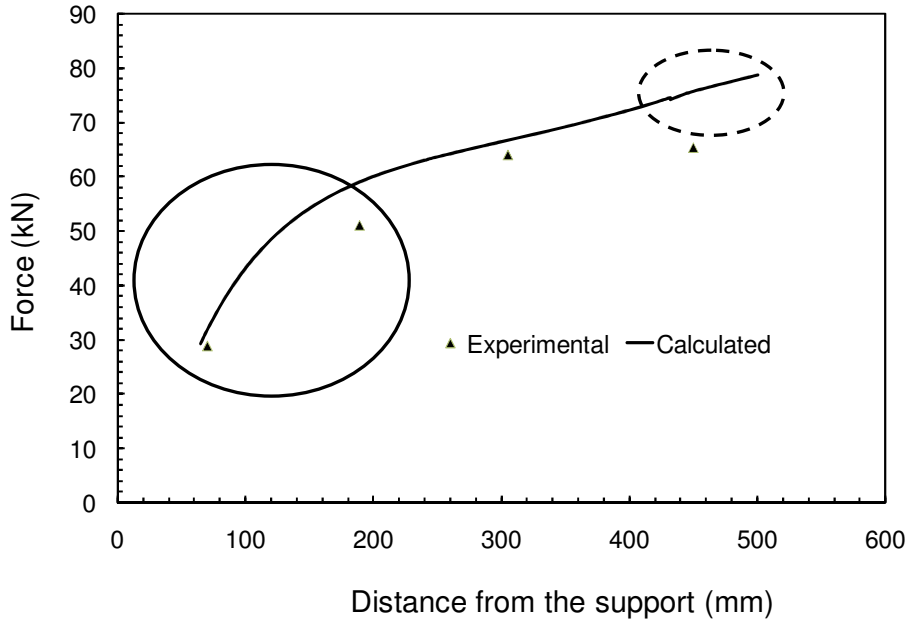

b-Beam S-SC-40%-58%

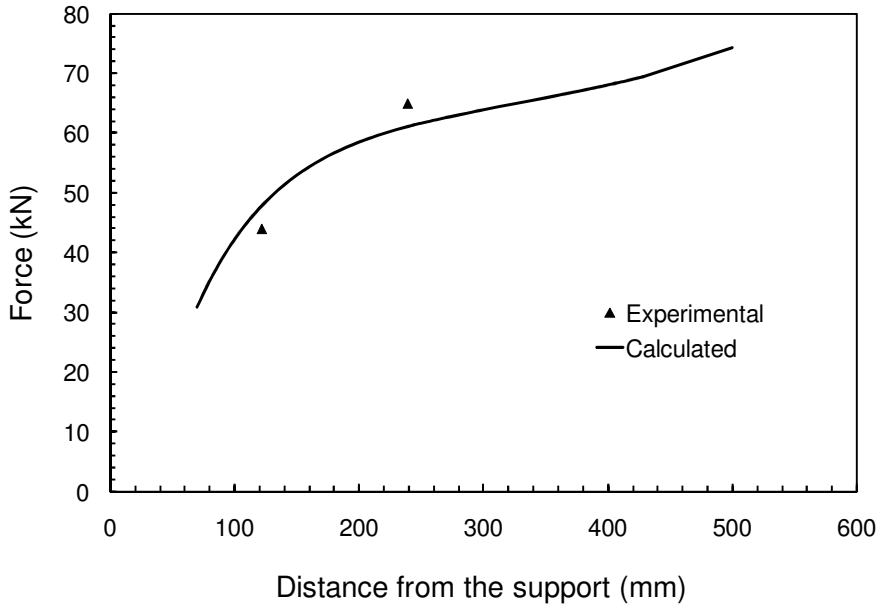

c-Beam S-SC-40%-56%

Figure 5.30: Experimental and calculated total forces in the CFRP rod in the shear span for beams with steel and strengthened with prestressed sand coated CFRP rods

5.5.4 Beams with no steel and strengthened with non-prestressed spirally wound CFRP rods

Similar to previous groups, Table 5.11 shows a comparison between the experimental and calculated force in the CFRP rod in the shear span and number of cycles at the onset of excessive slipping for the beams with no steel and strengthened with non-prestressed spirally wound CFRP rods. Figure 5.31 shows both the experimental and the predicted number of cycles to the onset of excessive slip versus the applied load. The solid line represents the trend line for the experimental data and the dotted line represents the trend line of the calculated data. Figure 5.32 shows plots of the calculated force (from the model) and the experimental (actual) force in the CFRP rod in the shear span for the beams with no steel and further strengthened with non-prestressed spirally wound CFRP rods. The vertical axis represents the force and the horizontal

axis represents the distance from the support. The model predicts the number of cycles until the onset of excessive slipping together with the forces in the shear span with reasonable accuracy. Figure 5.31 shows that there is scatter in the experimental life. However, the experimental and calculated trend lines for the life coincide on one another. The forces predicted from the model were at all locations for all beams less than the experimental forces. For Beams NS-SW-0%-60%, NS-SW-0%-54% and NS-SW-0%-47%, the forces predicated at 250, 375 and 500mm were only slightly less than the experimental forces but at 125mm the calculated force was considerably less than the experimental force. For beam NS-SW-0%-44%, gauges at 375 and 500 mm were damaged and the calculated force at 125 and 250mm was considerably less than the experimental force.

Table 5.11: Comparison between the experimental and calculated results for beams with no steel and strengthened with non-prestressed spirally wound CFRP rods

Specimen		Distance from the support (mm)				Number of cycles at onset of excessive slip
		125	250	375	500	
NS-SW-0%-60%	Experimental force (kN)	34.4	43.89	51.64	50.5	5600
	Calculated force (kN)	23.29	40.26	46.99	53.7	12160
NS-SW-0%-54%	Experimental force (kN)	31.3	40	50.35	51.13	141864
	Calculated force (kN)	20.42	36.35	41.35	48.33	35726
NS-SW-0%-47%	Experimental force (kN)	20.17	34.84	36.1	49.1	306850
	Calculated force (kN)	11.03	26.42	32	43.77	150356
NS-SW-0%-44%	Experimental force (kN)	29.95	39.28	----	----	365049
	Calculated force (kN)	18.3	24.96	31.7	38.83	1814817

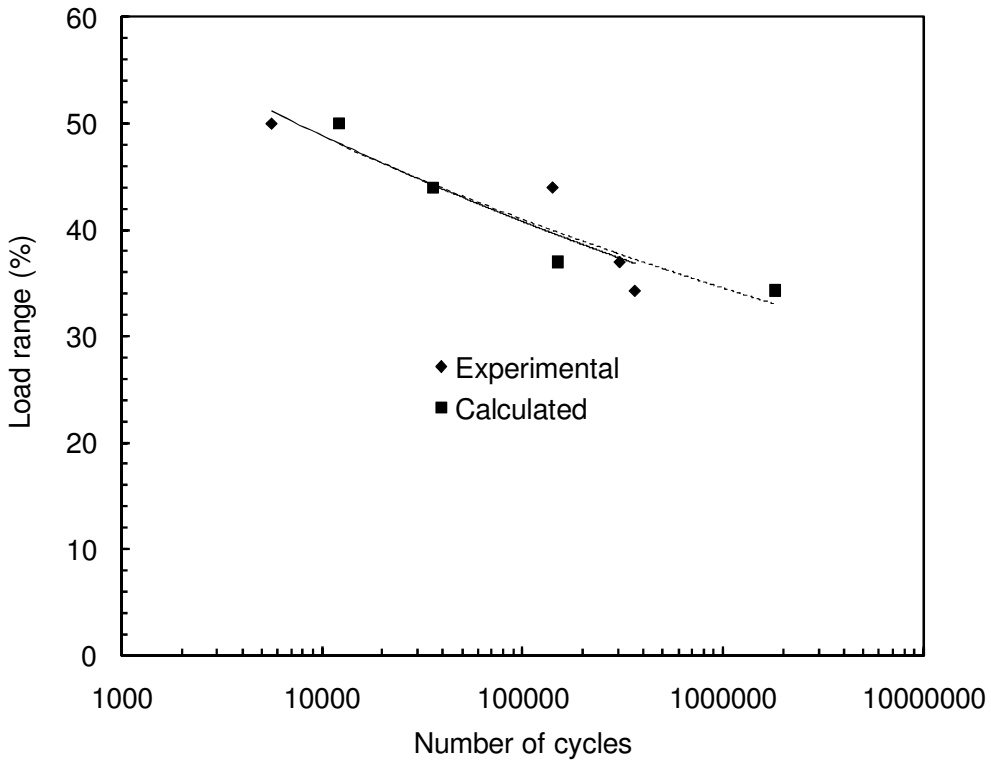

Figure 5.31: The experimental and calculated number of cycles to onset of excessive slip for beams with no steel and strengthened with non-prestressed spirally wound CFRP rods

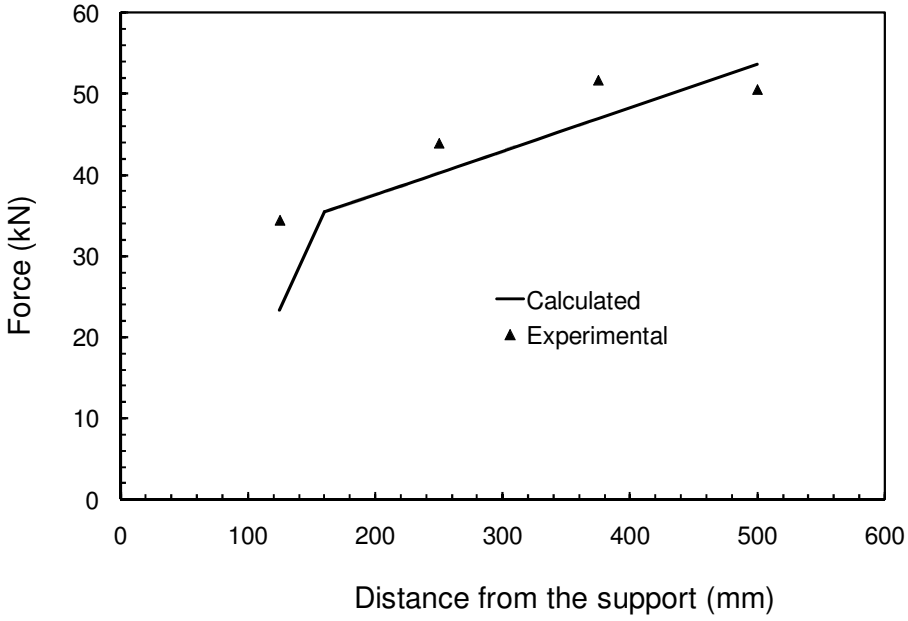

a-Beam NS-SW-0%-60%

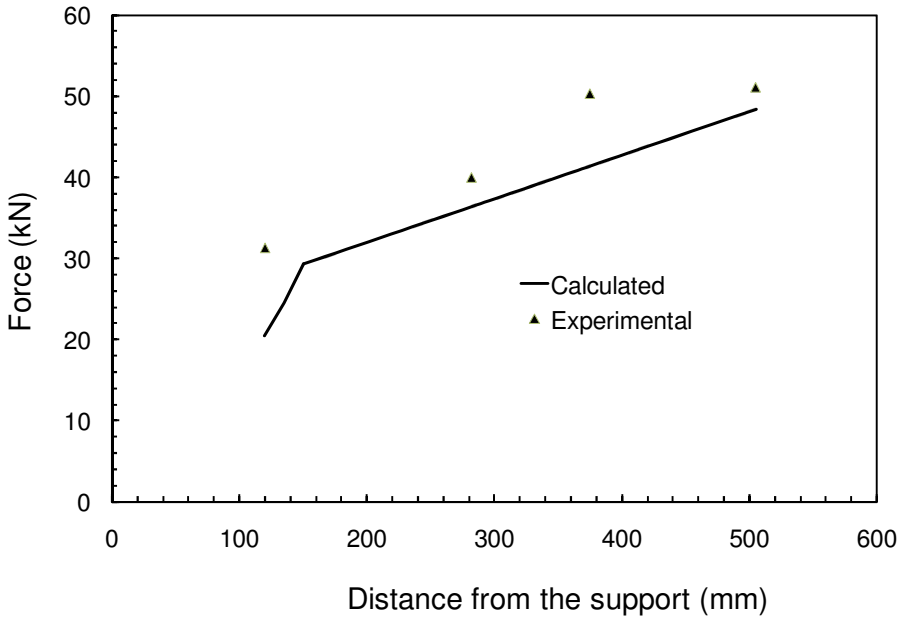

b-Beam NS-SW-0%-54%

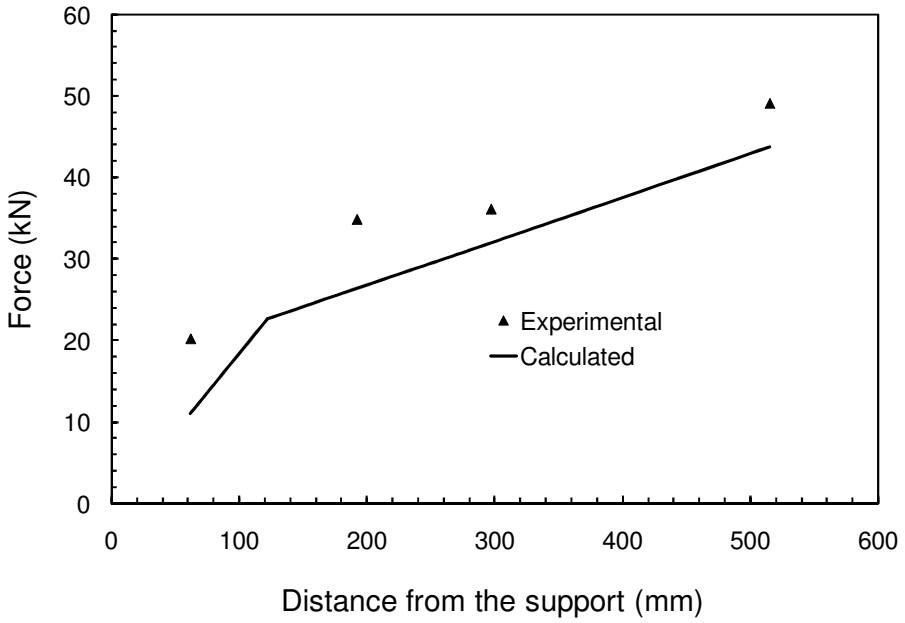

c- Beam NS-SW-0%-47%

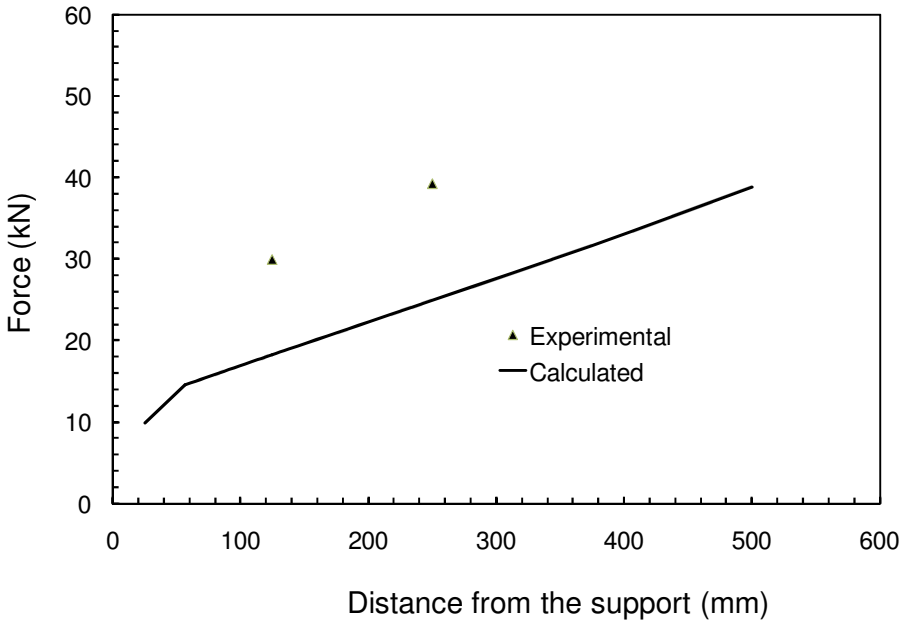

d- Beam NS-SW-0%-44%

Figure 5.32: Experimental and calculated forces in the CFRP rod in the shear span for beams with no steel and strengthened with non-prestressed spirally wound CFRP rods

5.5.5 Beams with steel and strengthened with non-prestressed spirally wound CFRP rods

Table 5.12 shows a comparison between the experimental and calculated forces in the CFRP rod in the shear span and number of cycles at onset of excessive slipping for beams with internal steel and further strengthened with non-prestressed spirally wound CFRP rods. Figure 5.33 shows both the experimental and the predicted number of cycles to the onset of excessive slip versus the applied load for the same group. The solid line represents the trend line for the experimental data and the dotted line represents the trend line for the calculated data. Figure 5.34 shows plots for the calculated force (from the model) and the experimental (actual) force in the CFRP rod in the shear span for the beams with steel and strengthened with non-prestressed spirally wound CFRP rods. The calculated and actual number of cycles until onset of excessive slipping are in good agreement. The model predicts the forces in the CFRP rod at all locations in the shear span with reasonable accuracy. The greatest difference between the experimental and predicted values was at the 125 mm location where the difference was 9 kN between the actual and predicted force (40% of the experimental force).

Table 5.12: Comparison between the experimental and calculated results for beams with steel and strengthened with non-prestressed spirally wound CFRP rods

Specimen		Distance from the support (mm)				Number of cycles at onset of excessive slip
		125	250	375	500	
S-SW-0%-81.6%	Experimental force (kN)	35.8	41.2	68.2	71.9	7
	Calculated force (kN)	27.73	43.28	68.42	77.32	5.5
S-SW-0%-75.1%	Experimental force (kN)	27.5	34.1	53.35	58.67	292
	Calculated force (kN)	33.16	45.1	53.91	62.74	132
S-SW-0%-71.4%	Experimental force (kN)	21.5	35	47.5	52.1	464
	Calculated force (kN)	30.08	38.77	47.53	56.3	841
S-SW-0%-68.75%	Experimental force (kN)	17.6	33.89	45.6	---	2796
	Calculated force (kN)	24.19	33.3	42.2	51.6	4582

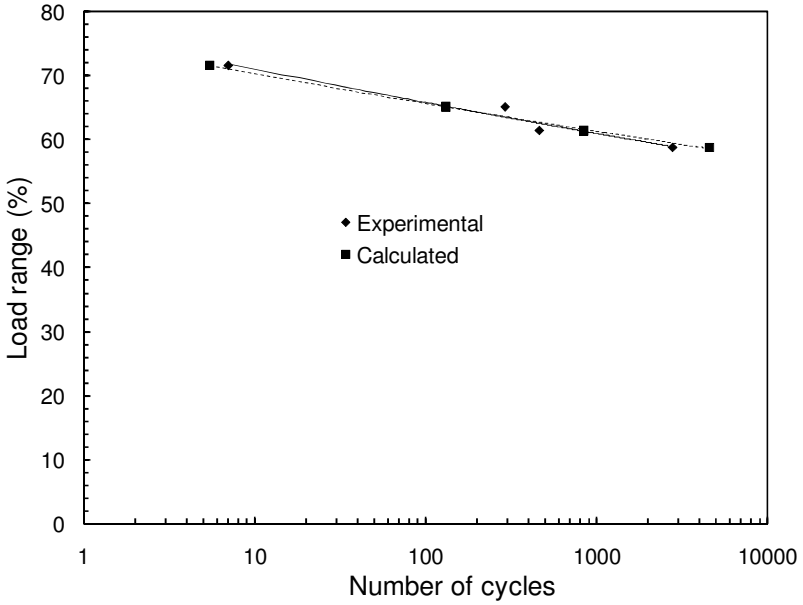

Figure 5.33: The experimental and calculated number of cycles to onset of excessive slip for beams with steel and strengthened with non-prestressed spirally wound CFRP rods

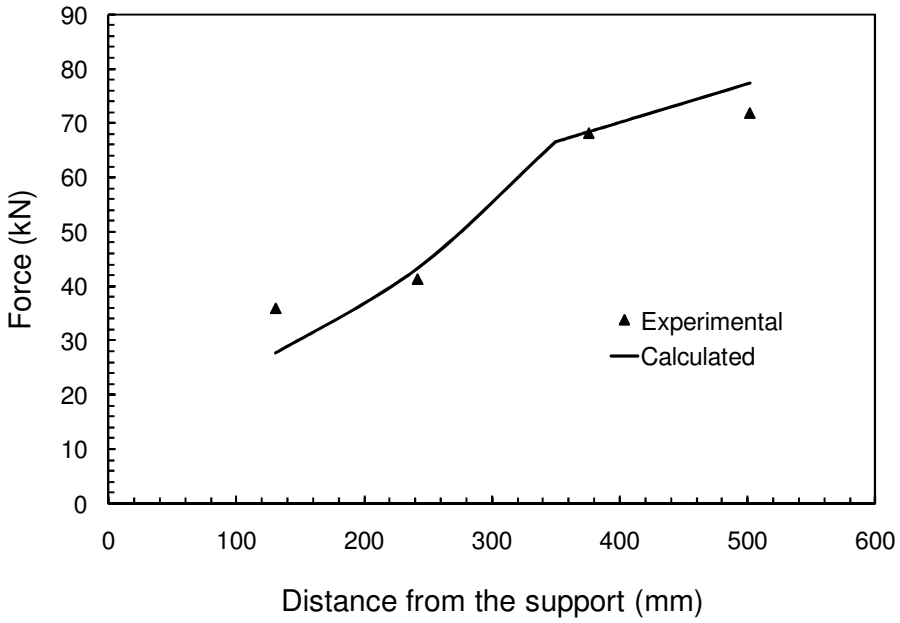

a-Beam S-SW-0%-81.6%

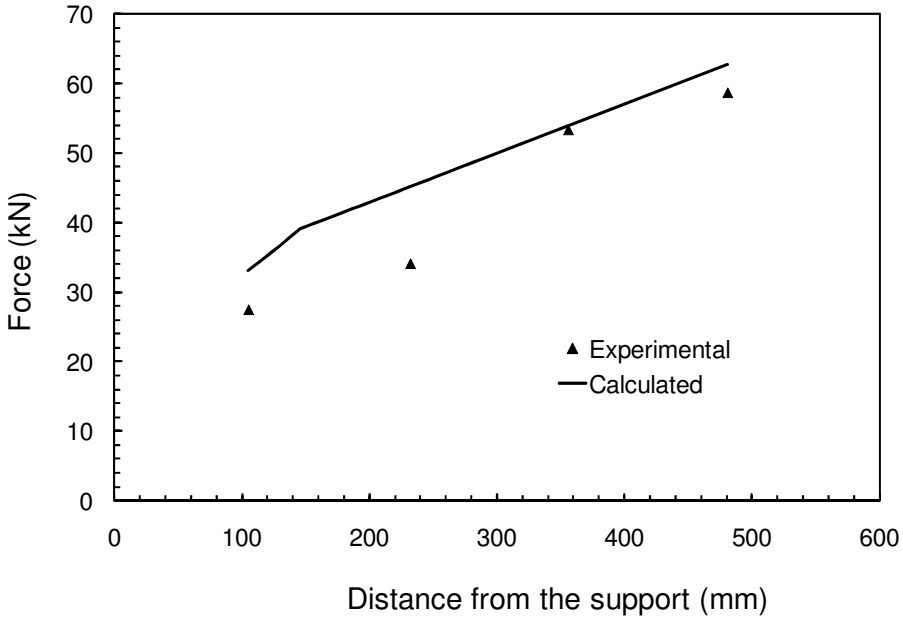

b- Beam S-SW-0%-75.1%

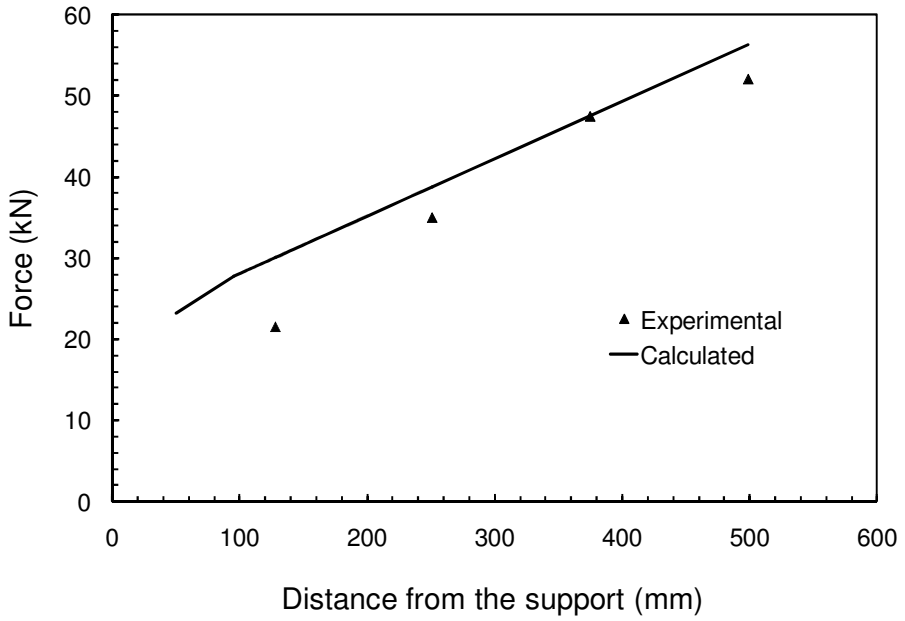

c-Beam S-SW-0%-71.4%

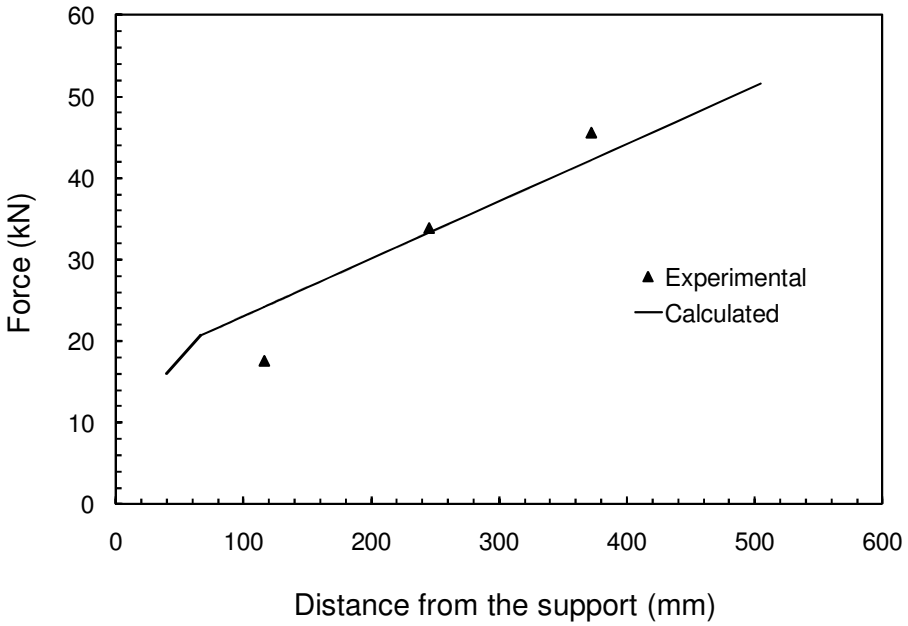

d-Beam S-SW-0%-68.75%

Figure 5.34: Experimental and calculated forces in the CFRP rod in the shear span for beams with steel and strengthened with non-prestressed spirally wound CFRP rods

5.5.6 Beams with steel and strengthened with prestressed spirally wound CFRP rods

Figure 5.35 shows the experimental and calculated lives for the beams strengthened with prestressed spirally wound CFRP rods. Figure 5.36 shows the experimental and calculated prestressing forces. Table 5.13 and Figure 5.37 show a comparison between the experimental and calculated total forces in the CFRP rod in the shear span for the same group.

Table 5.13 and Figure 5.36 show the experimental and calculated number of cycles at the onset of excessive slipping. The predicted and the actual values are in good agreement. The biggest difference was for the beam S-SW-45%-65% where the experimental number of cycles was considerably less than the predicted number of cycles. During testing, the CFRP rod started slipping from the epoxy at 60,000 cycles but complete failure occurred at 153,771 cycles. It was expected that the CFRP slip from epoxy will start at a higher number of cycles.

From Figure 5.37, the total predicted and experimental forces at the onset of excessive slipping were the same at 375 and 500mm. At 125 and 250mm, the total experimental force was less than the calculated force and the maximum difference was 12kN (26% of the experimental force). The difference between the experimental and calculated forces at 125 and 250mm for beams S-SW-45%-70% and S-SW-45%-65% is due to the slippage of the CFRP rod from the epoxy that occurred in the experiments.

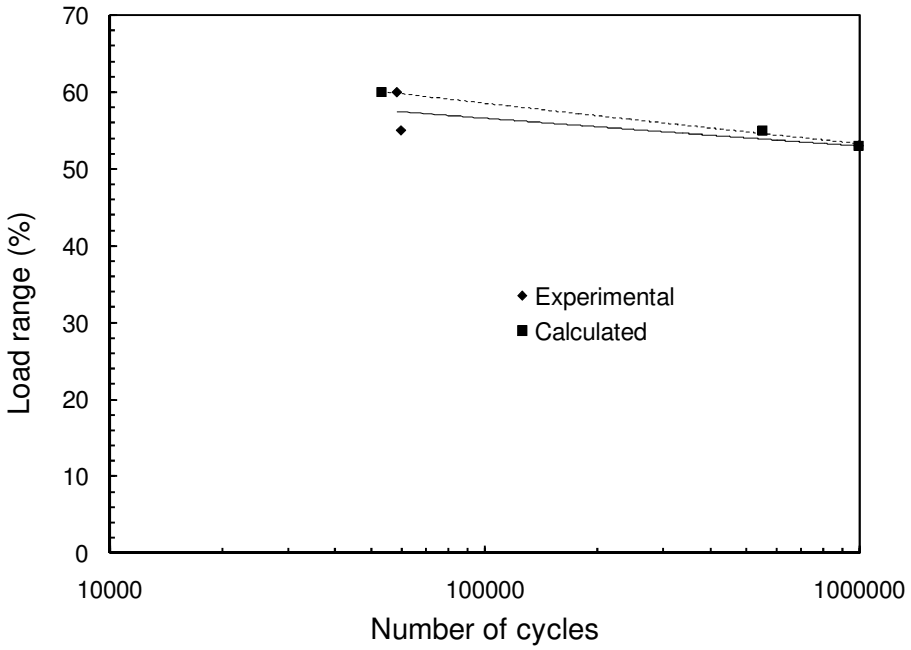

Figure 5.35: The experimental and calculated number of cycles to onset of excessive slip for beams with steel and strengthened with prestressed spirally wound CFRP rods

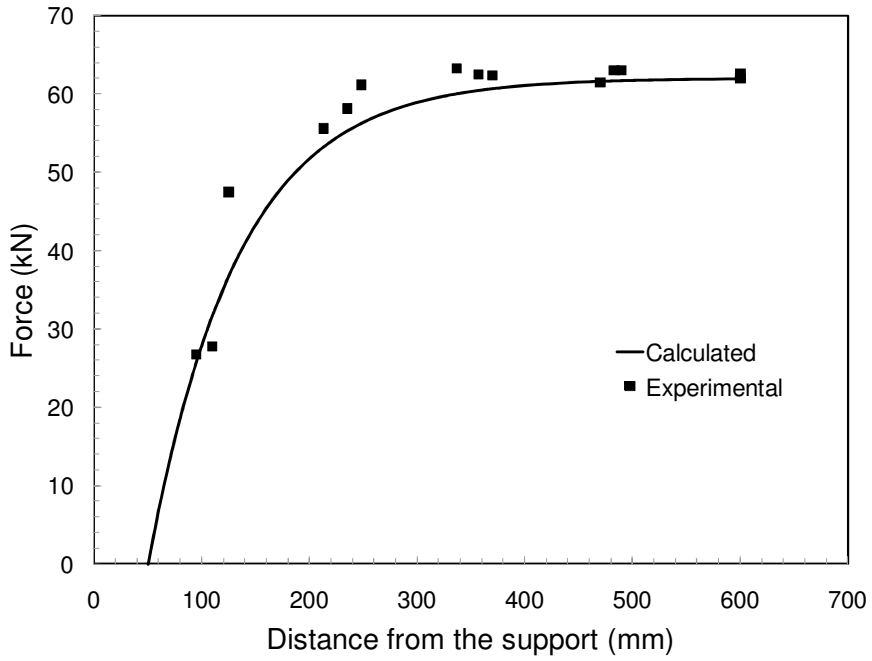

Figure 5.36: Experimental and calculated forces due to prestressing

Table 5.13: Comparison between the experimental and calculated total forces in the shear span for beams with steel and strengthened with prestressed spirally wound CFRP rods

Specimen		Distance from the support (mm)				Number of cycles at onset of excessive slip
		125	250	375	500	
S-SW-45%-70%	Experimental force (kN)	23.2	46.88	63.23	71.91	58500
	Calculated force (kN)	28.23	58.92	66.67	74.97	53020
S-SW-45%-65%	Experimental force (kN)	15.82	38.61	64.76	74.54	60000
	Calculated force (kN)	33.98	56.15	67.37	73.61	551250
S-SW-45%-63%	Experimental force (kN)	40.47	61.33	74.68	-----	996000
	Calculated force (kN)	38.67	59.53	67.58	72.75	996000

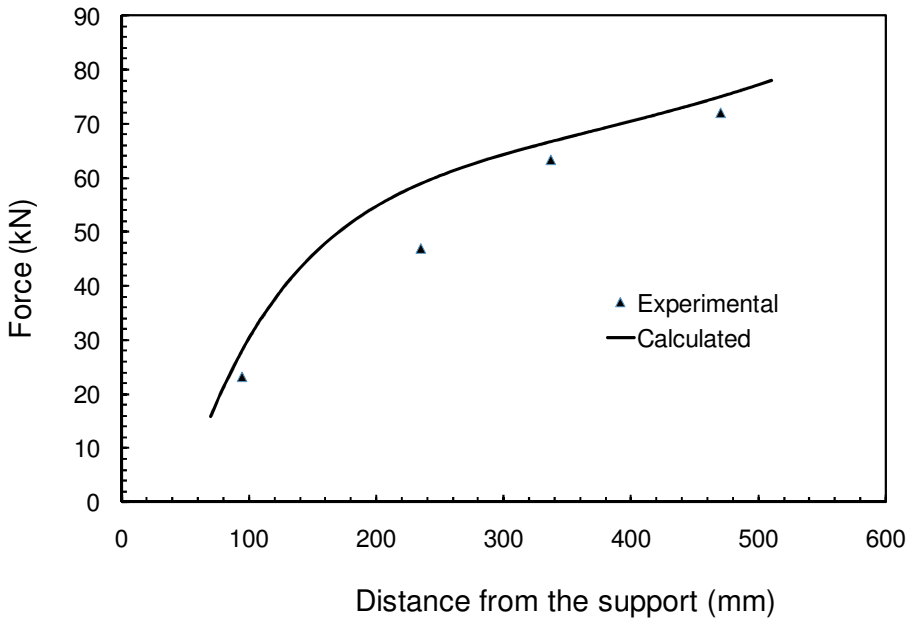

a-Beam S-SW-45%-70%

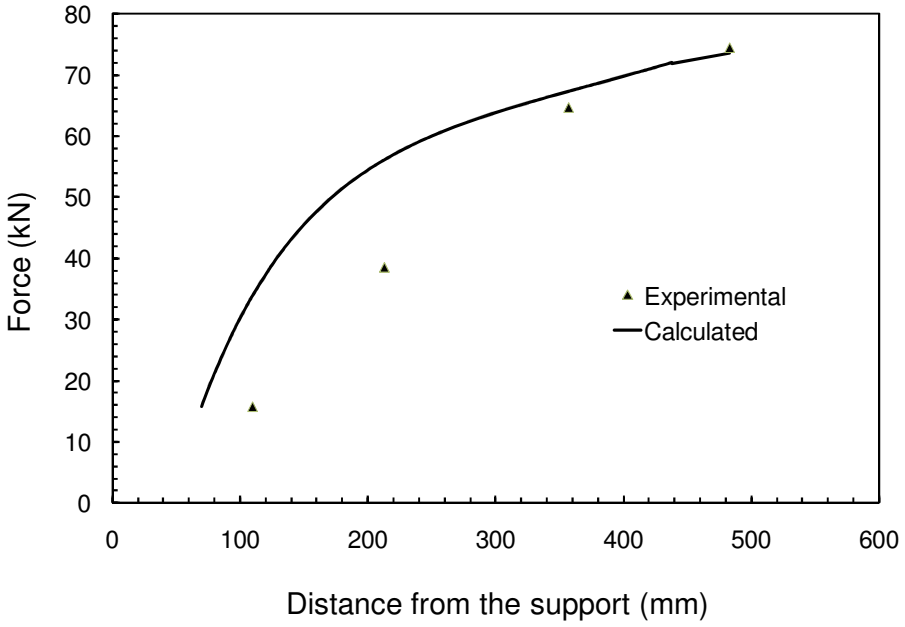

b-Beam S-SW-45%-65%

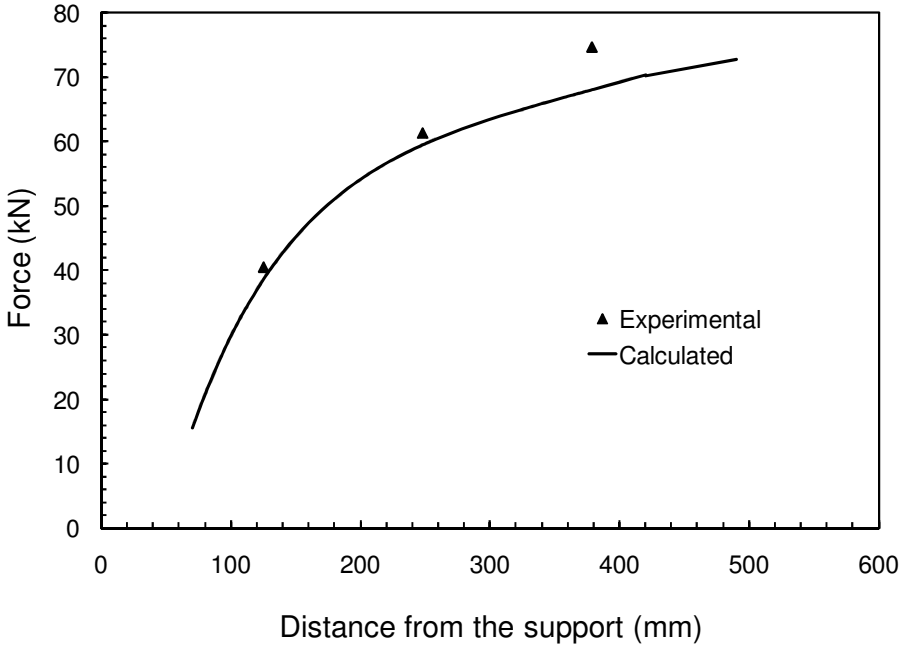

c-Beam S-SW-45%-63%

Figure 5.37: Experimental and calculated total forces in the CFRP rod in the shear span for beams with steel and strengthened with prestressed spirally wound CFRP rods

Chapter 6: Conclusions and Recommendations

6.1 Introduction

This chapter presents the conclusions drawn from this thesis for the monotonic beams test results, the prestressing and transfer length, the beam fatigue test results and the modelling of test results.

6.2 Conclusions

1-Beams with and without internal steel, strengthened with CFRP rods (sand coated or spirally wound) when tested under monotonic and fatigue loads failed in bond in a similar way. They all failed by debonding between the CFRP rod and the epoxy that started at the loading point and as the load was increased or cycled, the debonding spread towards the support until failure occurred.

2- A comparison of the load range versus life for the beams with and without steel, strengthened with CFRP rods and tested under fatigue load, revealed that the sand coated rod had better bond characteristics than the spirally wound rod (at the same load range the beam strengthened with sand coated rod had a longer life than the beam strengthened with spirally wound rod).

3- Beams with internal steel, strengthened with non-prestressed CFRP rods and tested under fatigue loading showed two modes of failure; bond failure and steel rebar rupture.

-The beams failed in bond at high load levels (short fatigue lives) and by rupture of the steel rebar at low load levels (long fatigue lives). The load level at which the failure mode

changed was at 66% of the monotonic capacity for beams with internal steel and strengthened with spirally wound CFRP rods.

- On the load range versus fatigue life plot, the slope of the bond failure data curve was flatter than the slope of the steel rupture data curve.

4-The CFRP rods used for strengthening the beam were prestressed to a force of 62 kN which corresponds to 45% of the monotonic capacity of the spirally wounded rods and to 40% of the monotonic capacity of the sand coated rods. The main conclusions that can be drawn are:

-The transfer length for the 45% prestressed spirally wound CFRP rods ranged between 150 and 210 mm measured from the end of bonded length (free end) while the transfer length for the 40% prestressed sand coated CFRP rods varied from 140 to 185 mm measured from the end of bonded length (free end) based on the experimental data.

-A semi- empirical exponential equation proposed by Badawi (2007) was modified and used to model the stresses in the transfer length. These curves provide a good fit to the experimental data for both spirally wound and sand coated CFRP rods.

-The crack front for the CFRP rod is estimated to be at 25mm and 50mm from the support for the sand coated and spirally wound CFRP rods, respectively.

-The maximum prestressing shear stress was found to be equal to the cracking shear stress under monotonic load that is 25 and 30 MPa for the spirally wound and the sand coated rods, respectively.

5- The beam with internal steel strengthened with sand coated CFRP rod and tested under monotonic loading failed by debonding between the CFRP rod and the epoxy that started at the loading point and as the load increased, the debonding spread towards the support until failure was reached.

6- The beam with internal steel strengthened with spirally wound CFRP rod and tested under monotonic loading failed by slipping between the CFRP rod and the epoxy that started at the support and propagated inwards towards the loading point.

7- Beams with internal steel, strengthened with prestressed CFRP rods and tested under fatigue load encountered 2 modes of failure; bond failure and steel rebar rupture. The bond failures occurred at high load levels (short fatigue lives) and the steel rupture occurred at low load levels (long fatigue lives). The load range at which the failure mode changed was 63% and 60% of the monotonic capacity for beams strengthened with prestressed spirally wound and sand coated CFRP rods, respectively.

8- Bond failures for the beams with internal steel that were strengthened with prestressed CFRP rods (sand coated or spirally wound) and tested under fatigue was by slipping between the CFRP rod and the epoxy that started at the support and propagated inwards towards the loading point.

9- Comparing the load range (kN) versus life curve for the beams with steel, strengthened with prestressed spirally wound and sand coated rods that failed in bond, shows that the beam strengthened with sand coated rod has longer fatigue lives than beam strengthened with spirally wound rod.

10-Beams that failed by debonding between the CFRP rod and the epoxy that started at the loading point and spread towards the support cracked first at the loading point and later cracks appeared at progressively increasing distances from the loading point. After failure, decohesion between the CFRP rod and the epoxy in the cross section of the beam at the free end was observed in most of the specimens.

11-Beams that failed by slip between the CFRP rod and the epoxy at the support usually had two cracks; one cracked at the loading point and another close to the loading point, followed by a crack at failure (when the CFRP rod started slipping excessively from the epoxy) that occurred close to the support. Once the CFRP rod slipped from the epoxy, the bottom epoxy together with the concrete cover separated from the rod in the region close to the support.

12-A model was developed to describe the progress of the debonding crack until excessive slipping occurred. The model predicted the number of cycles until excessive slipping between the CFRP rod and the epoxy occurred and the forces in the CFRP rod at all locations in the shear span at the onset of failure with reasonable accuracy.

6.3 Recommendations for future work

Based on the work done, the following can be recommended for future work:

1-Experimental work that investigates the failure of CFRP rods embedded in groove sizes that are larger than 1.5 times the CFRP rod diameter. Failure mode is expected to change as the groove size changes.

2-Experimental work that investigates the effect of spacing between multiple rods placed in multiple grooves and their interaction on the failure mode.

3- An investigation of the transfer length of prestressed CFRP rods and how the crack front shifts under fatigue loading. This will enable an accurate modelling for failure of beams strengthened with prestressed FRP rods.

4- Four point bending tests with longer shear spans and different internal steel ratios should be conducted. The longer shear span will change the fatigue life than the one reported here. Yet, a relation between the shear span and expected fatigue life can be established.

5- Pull out tests on the same rod type under fatigue loading to verify the calibrated parameters in the model. The minimum load level should be varied as well which will result in variation in the model parameters. Co-relation between the parameters of the model and the applied load level can be established. Also, in pull out tests, the free and end slip can be measured which should help verify the proposed shear stress versus slip model.

6- Finite element analysis to verify the shape of the ascending branch in the proposed model.

7- Four point bending tests with different internal steel ratios should be conducted. The different steel reinforcement will result in different values for parameters of the proposed model.

Appendices

Figures for each beam are provided in the appendix. They include load versus deflection, load versus CFRP, steel and concrete strain. They also include load versus end slip. The appendix is divided into two sections; appendix A and appendix B. Appendix A includes the data for the beams without internal steel and strengthened with non-prestressed CFRP rods followed by the data for beams with internal steel and strengthened with non-prestressed CFRP rods. Appendix B includes the data for beams with internal steel and strengthened with prestressed CFRP rods.

Appendix A: Beams strengthened with non-prestressed CFRP rods

Beams with no internal steel and strengthened with CFRP rods

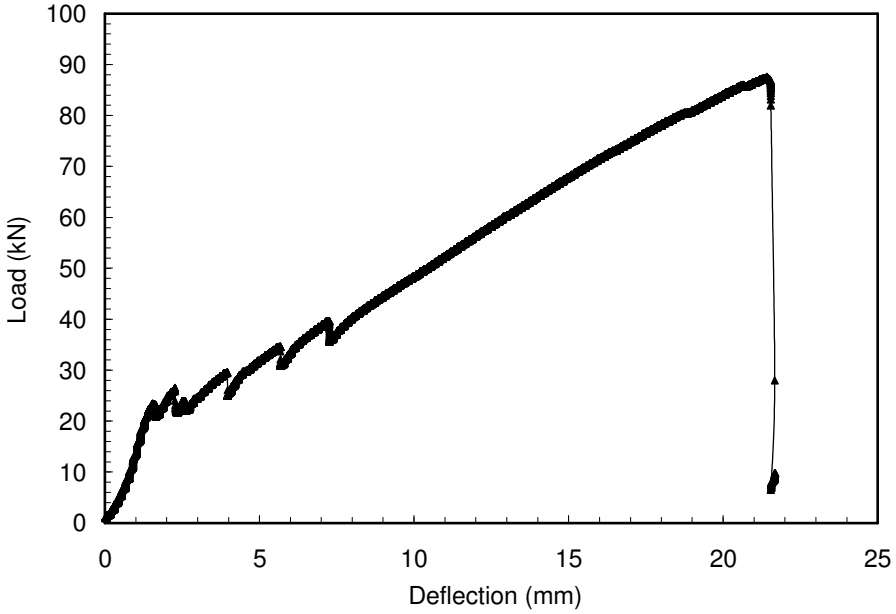

a-Load versus mid-span deflection

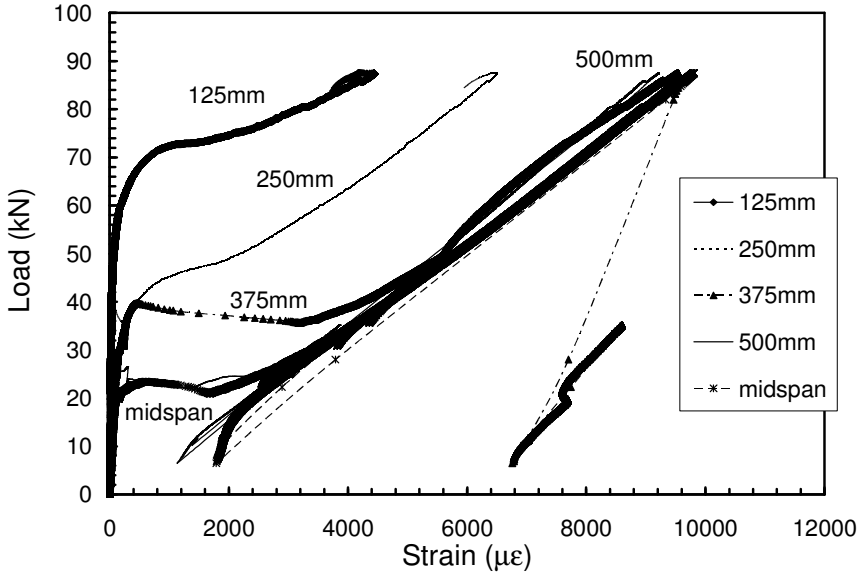

b-Load versus CFRP rod strain

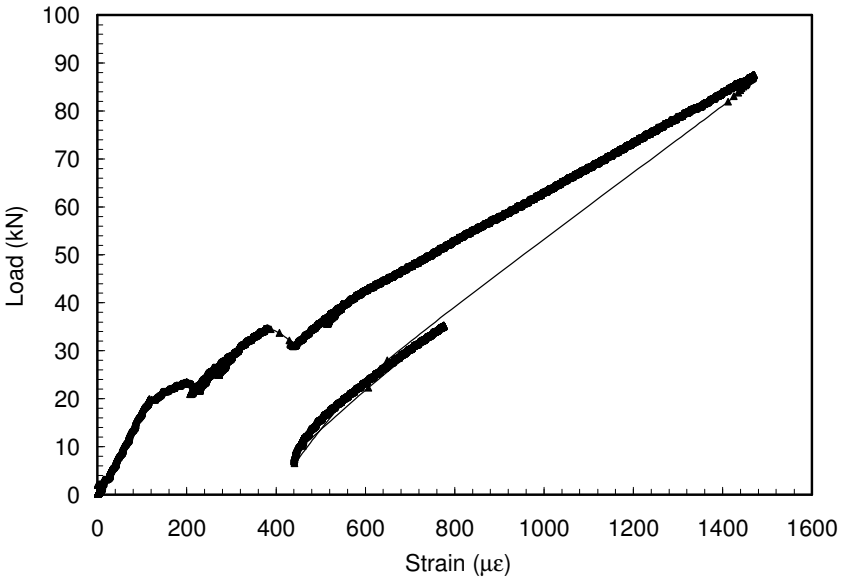

c- Load versus mid-span concrete strain

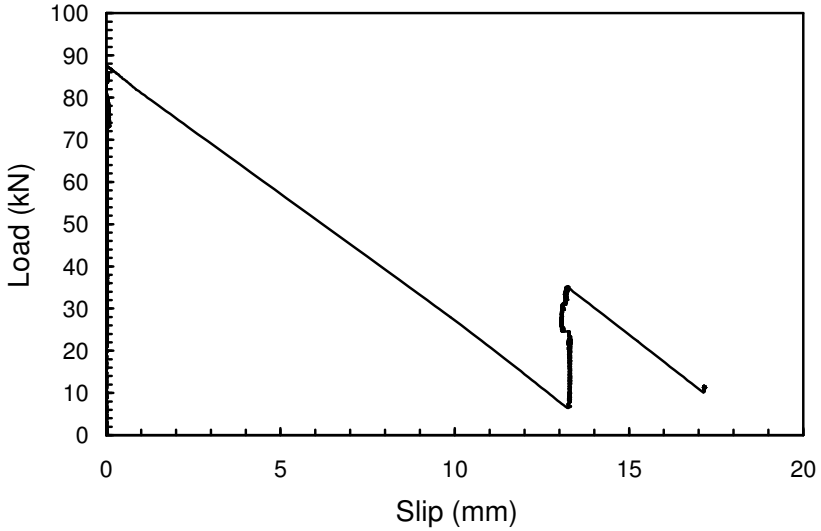

d-Load versus slip

Figure A-1: Test results for beam NS-SW-0%-M

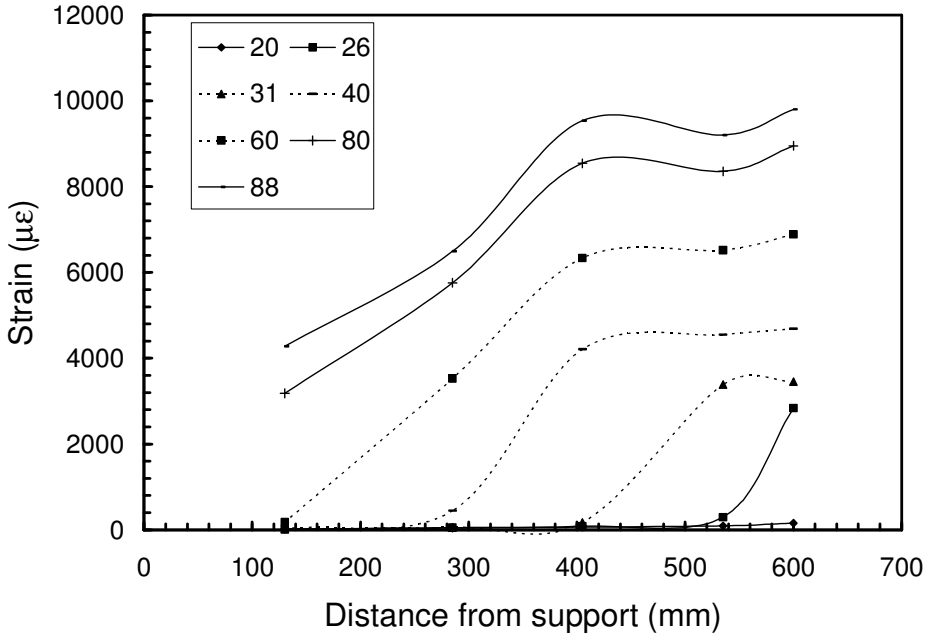

Figure A-2: Strain distribution along the CFRP rod for beam NS-SW-0%-M

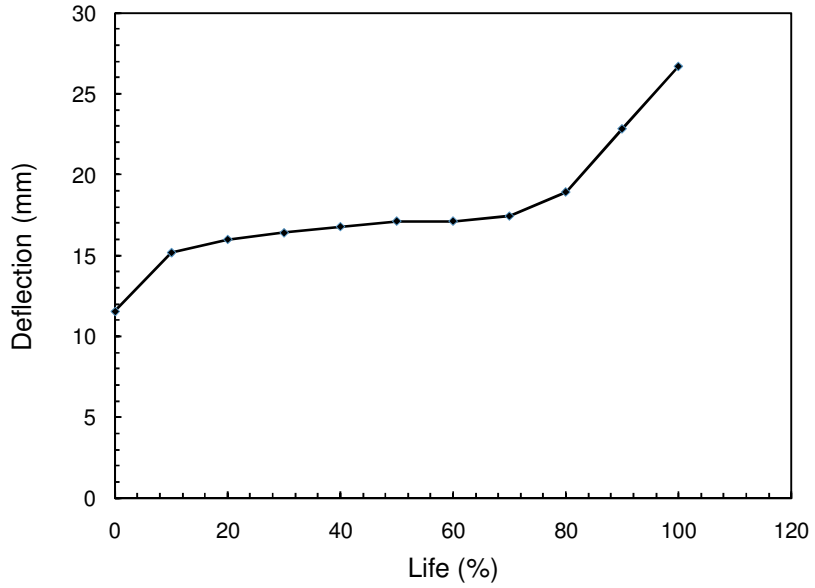

a-Mid-span deflection versus life

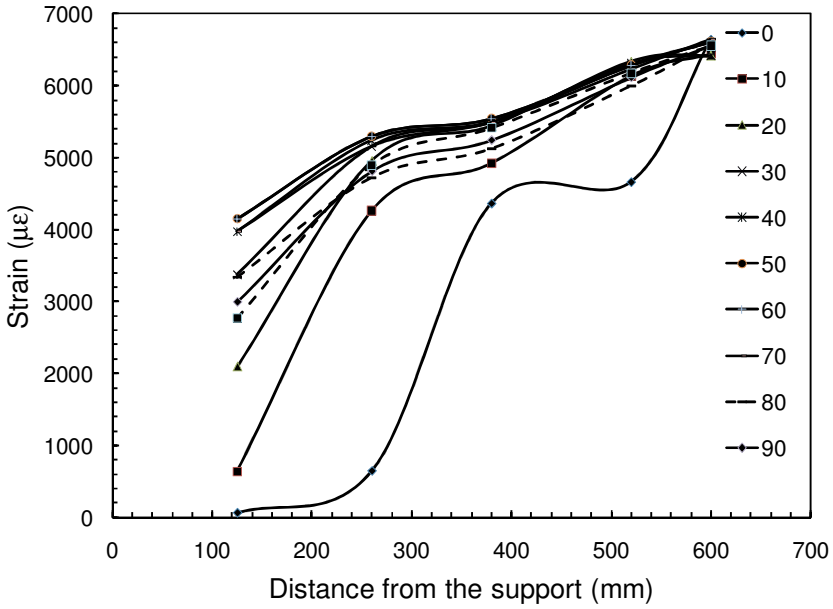

b-Strain distribution along the CFRP rod

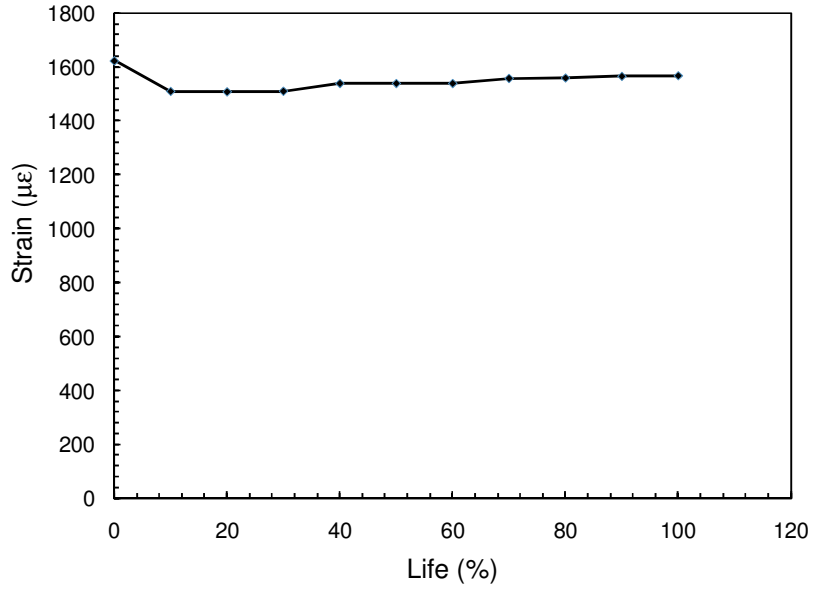

c-Mid-span concrete strain versus life

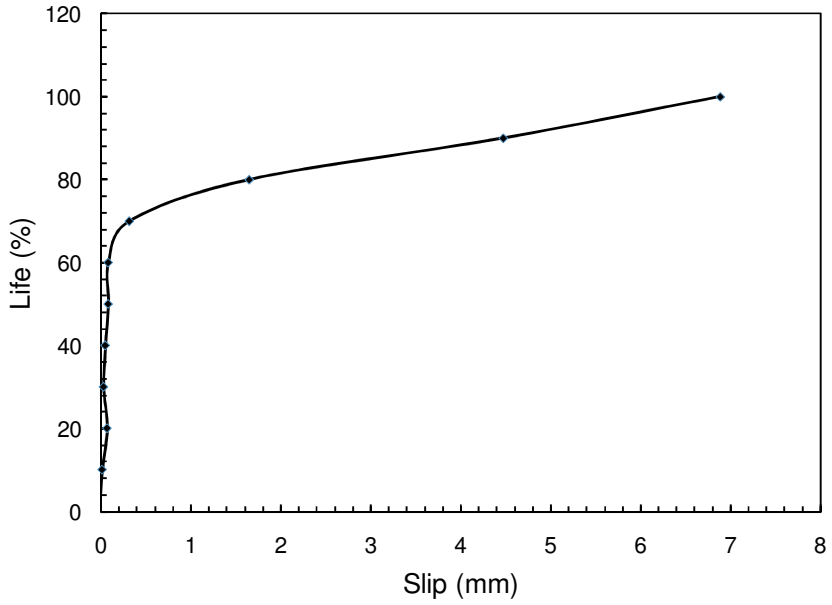

d- Life versus slip

Figure A-3: Test results for beam NS-SW-0%-65%

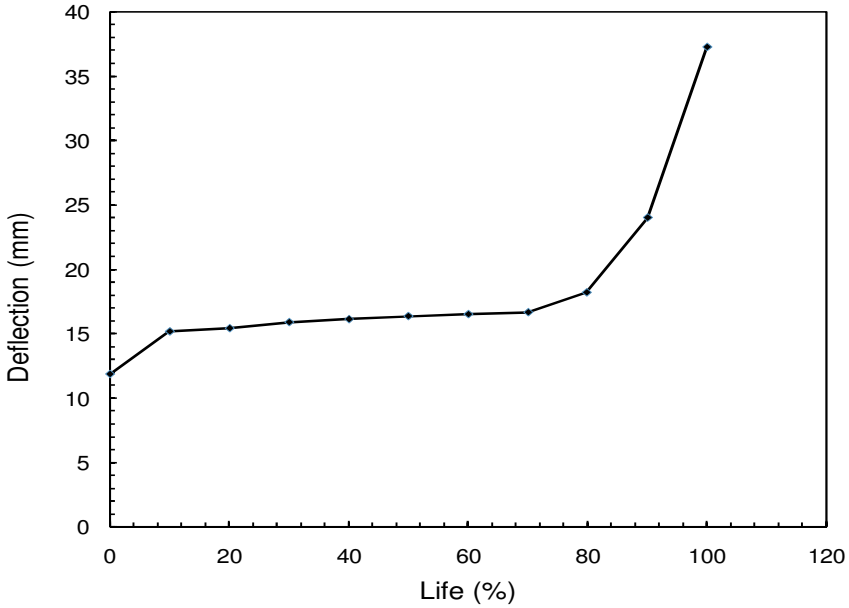

a-Mid-span deflection versus life

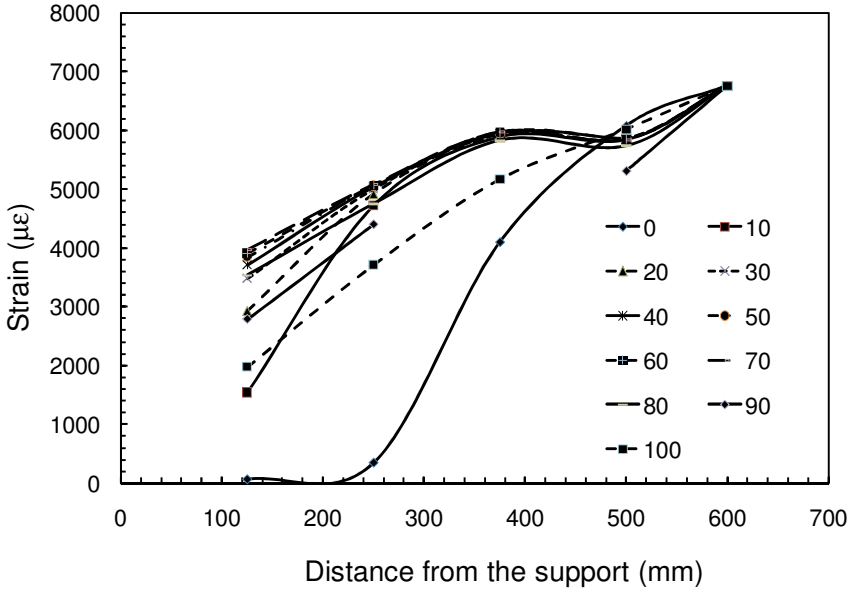

b-Strain distribution along the CFRP rod

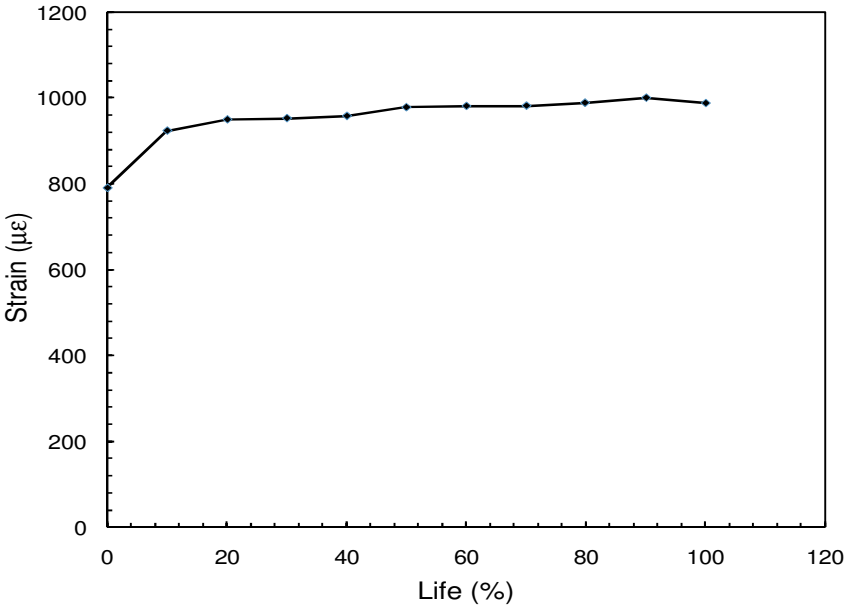

c-Mid-span concrete strain versus life

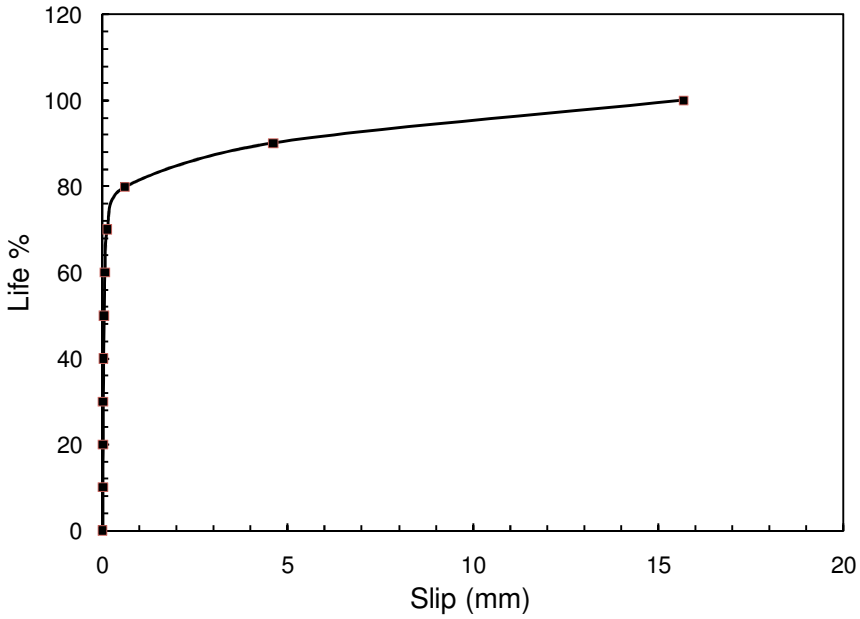

d- Load versus slip

Figure A-4: Test results for beam NS-SW-0%-60%(a)

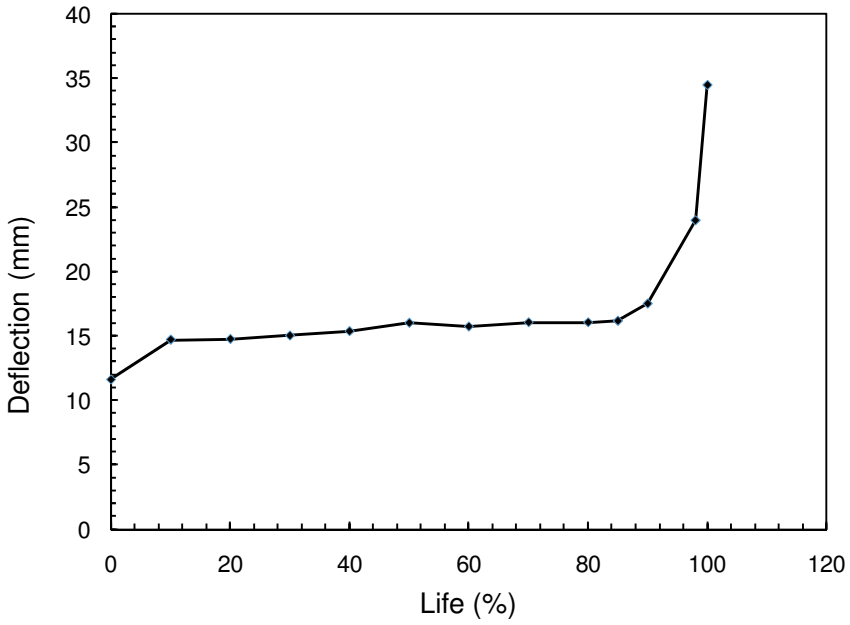

a-Mid-span deflection versus life

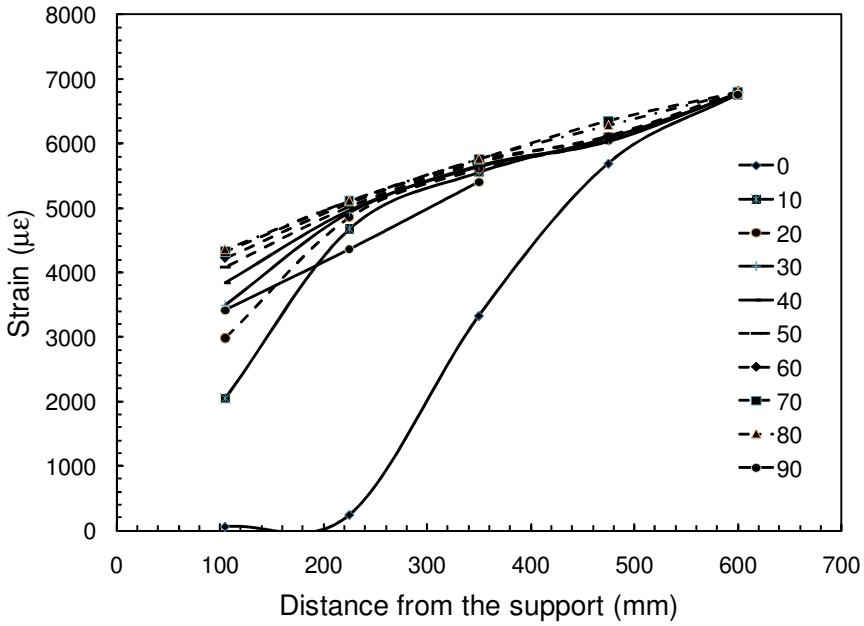

b-Strain distribution along the CFRP rod

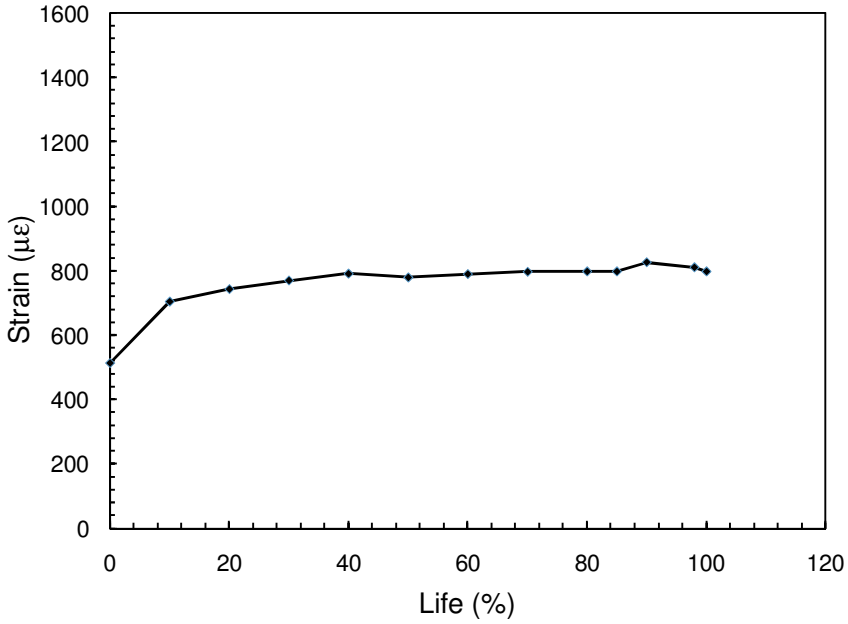

c-Mid-span concrete strain versus life

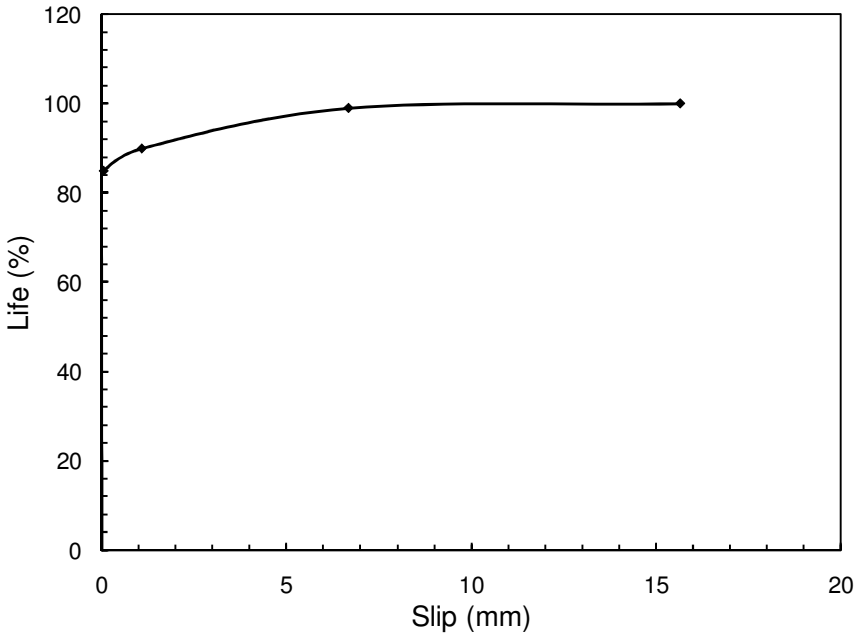

d- Load versus slip

Figure A-5: Test results for beam NS-SW-0%-60%(b)

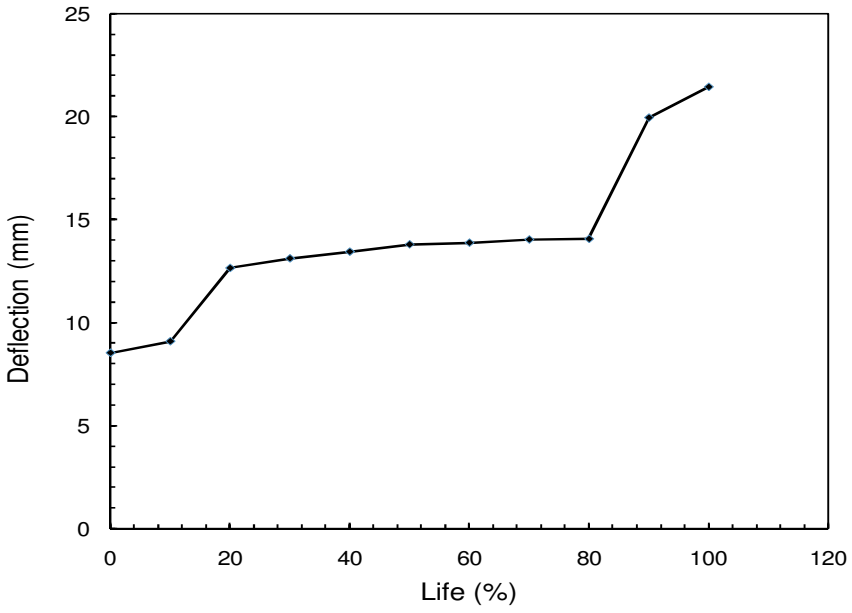

a-Mid-span deflection versus life

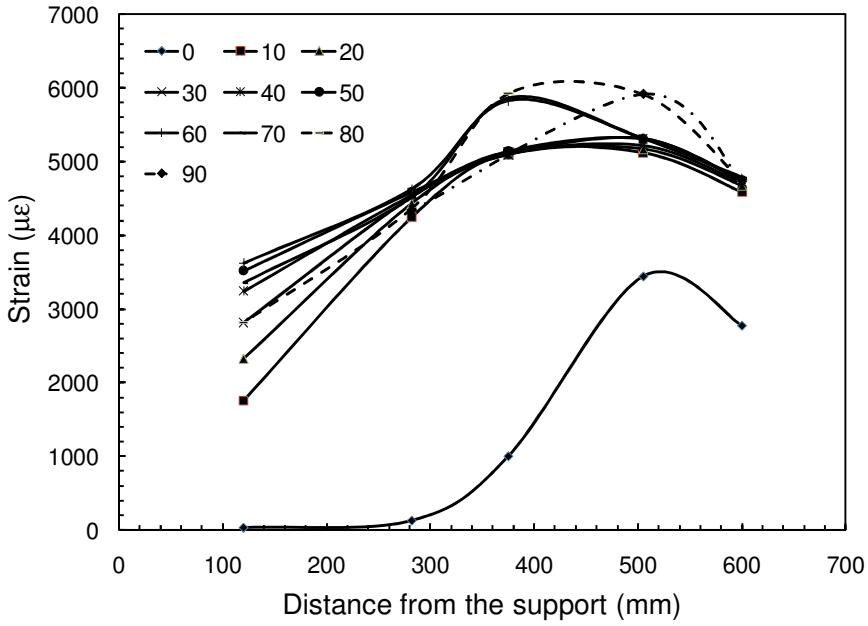

b-Strain distribution along the CFRP rod

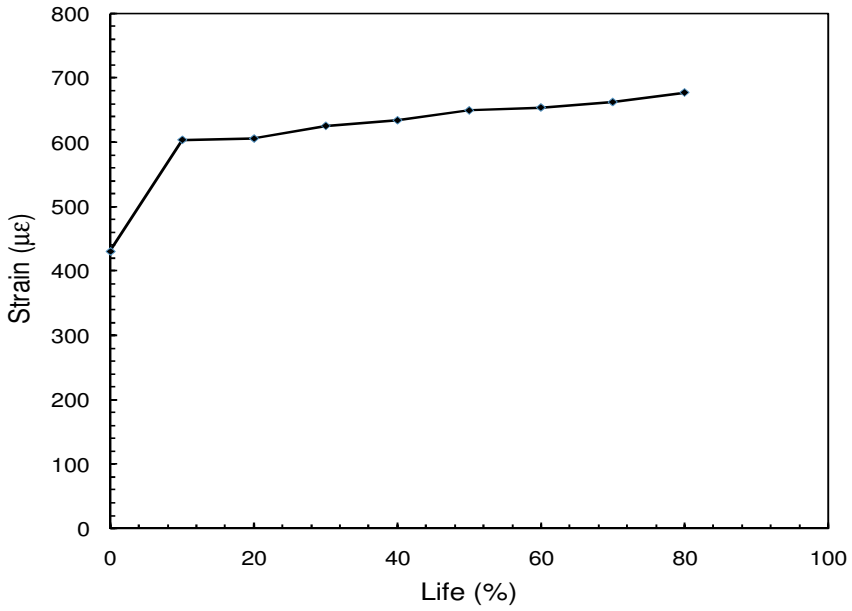

c-Mid-span concrete strain versus life

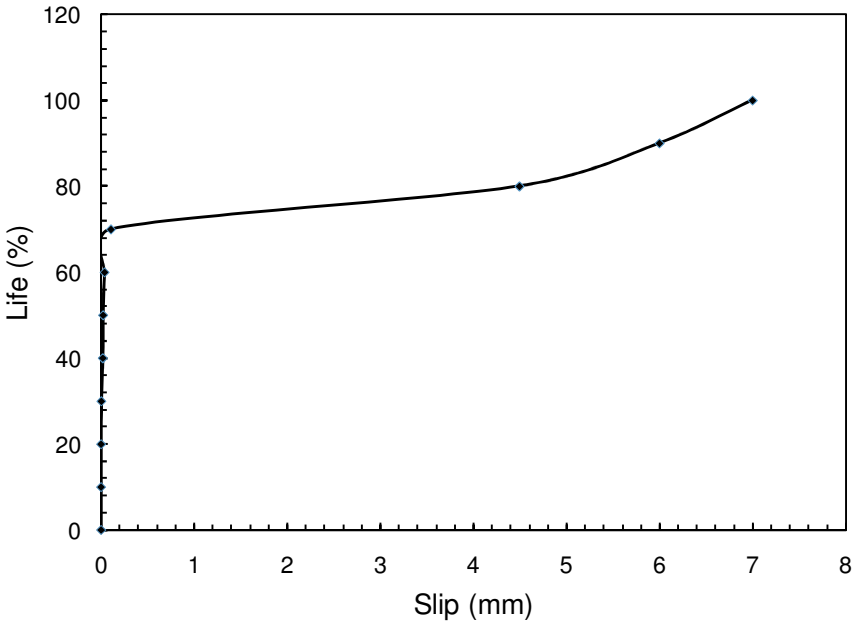

d- Load versus slip

Figure A-6: Test results for beam NS-SW-0%-54%

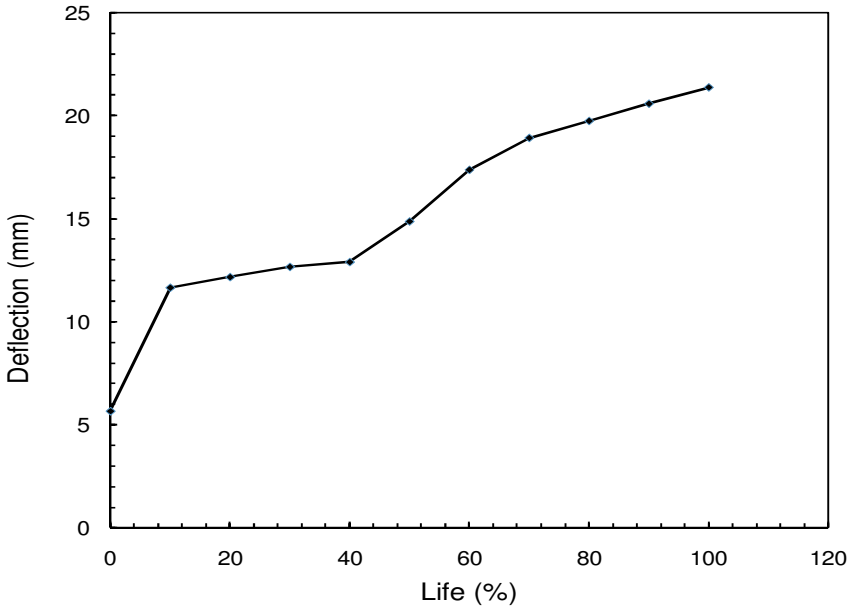

a-Mid-span deflection versus life

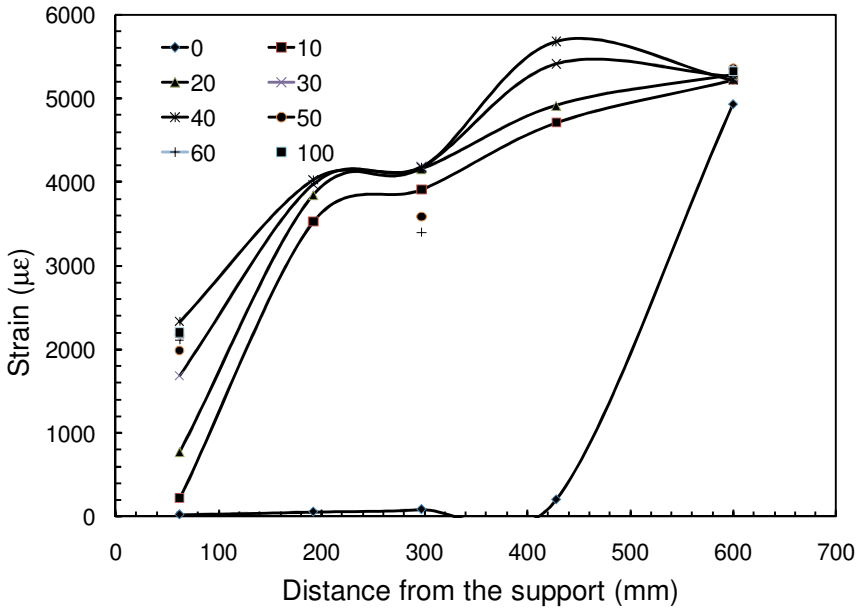

b-Strain distribution along the CFRP rod

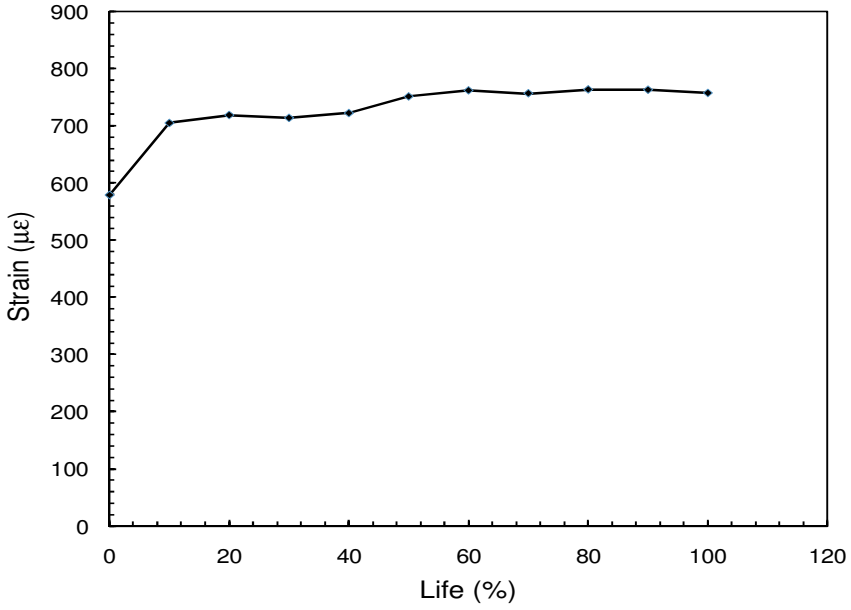

c-Mid-span concrete strain versus life

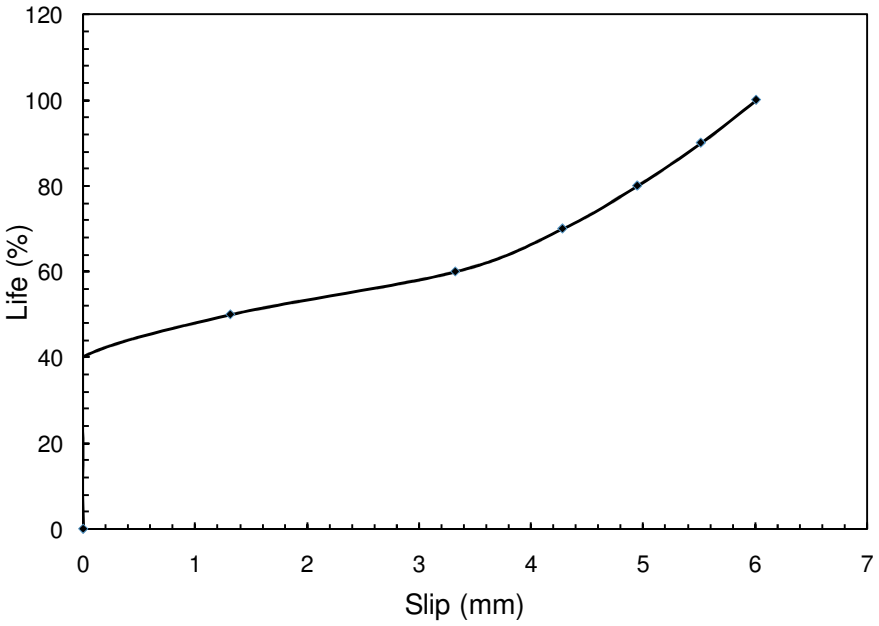

d- Load versus slip

Figure A-7: Test results for beam NS-SW-0%-47%

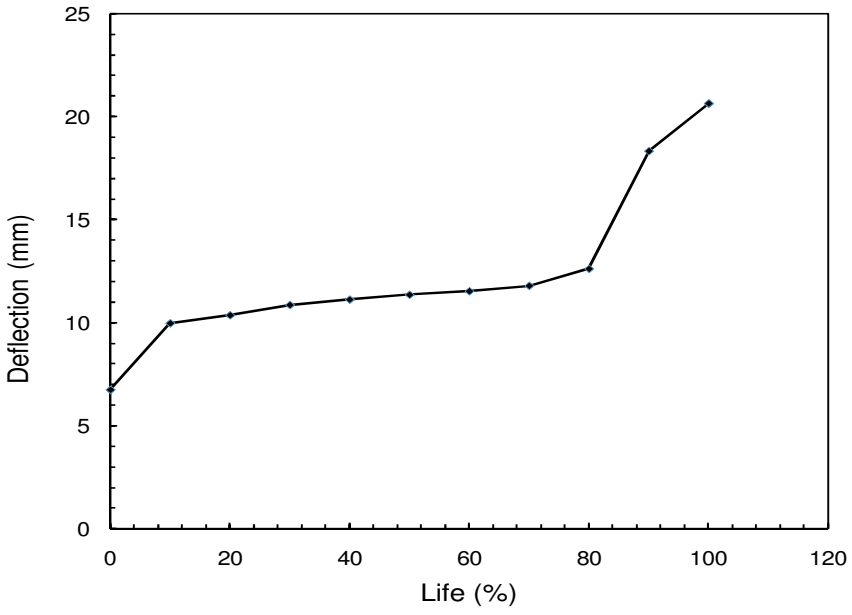

a-Mid-span deflection versus life

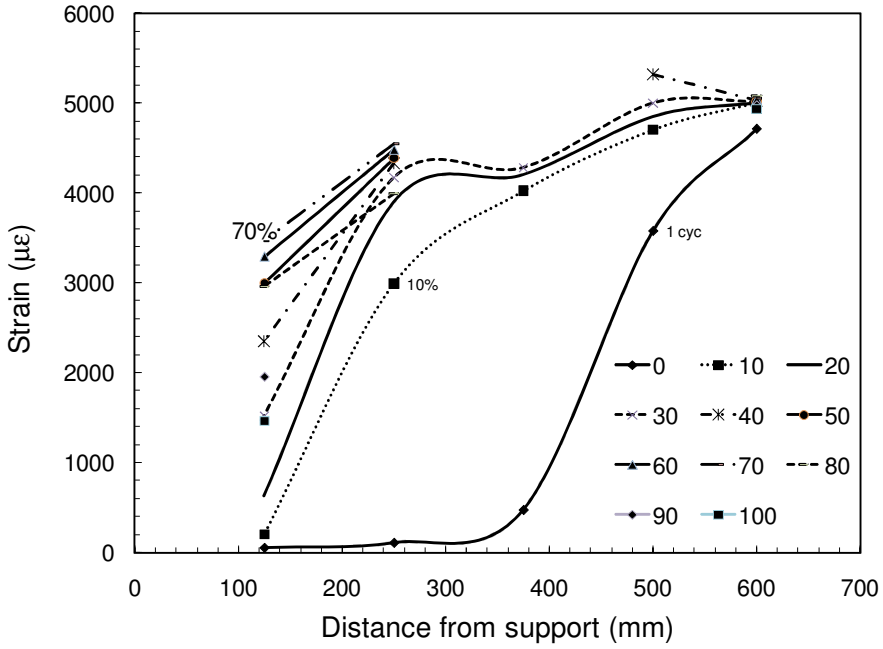

b-Strain distribution along the CFRP rod

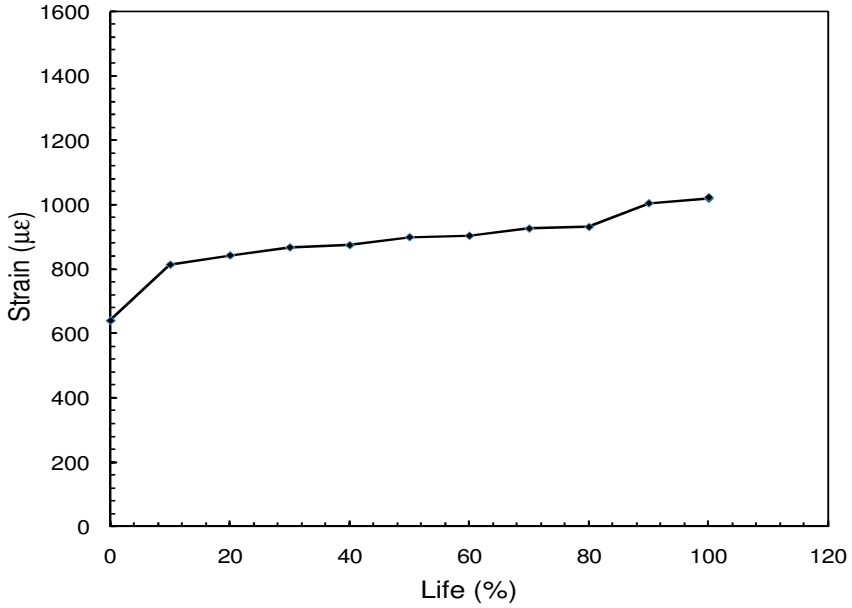

c-Mid-span concrete strain versus life

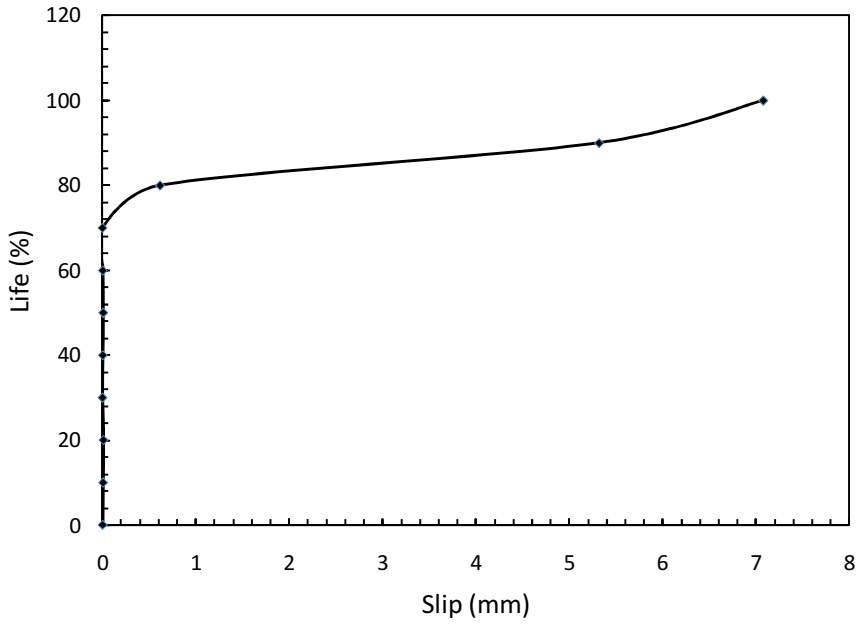

d- Load versus slip

Figure A-8: Test results for beam NS-SW-0%-44%

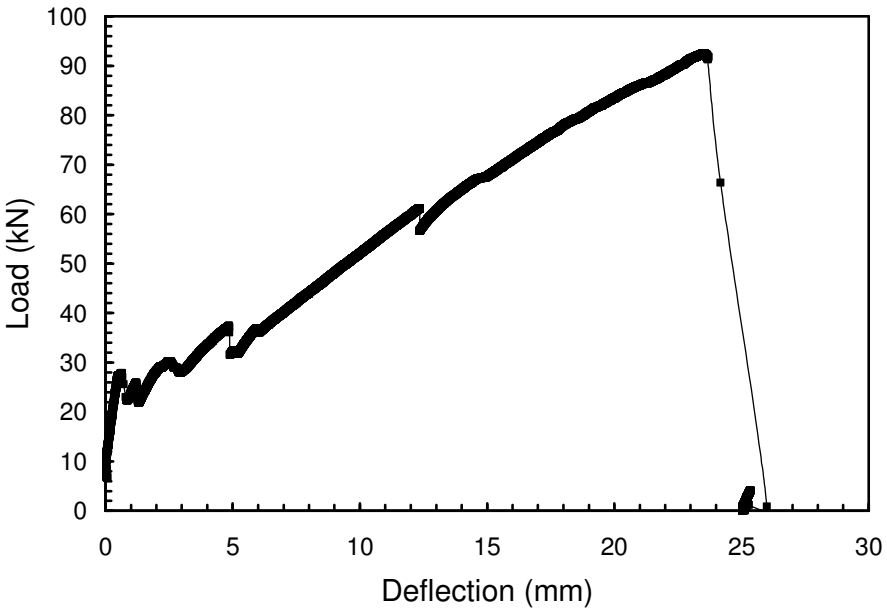

a-Load versus mid-span deflection

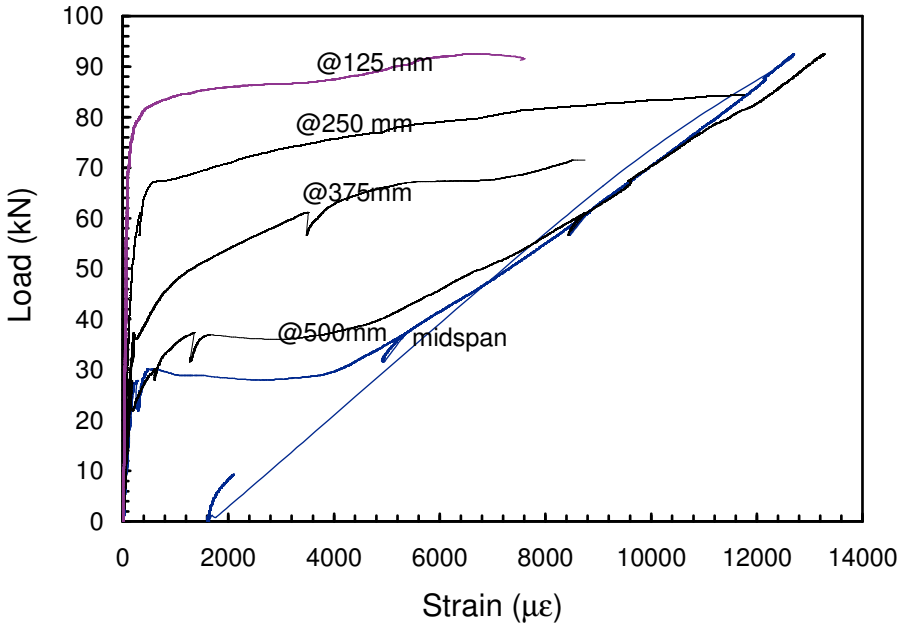

b-Load versus CFRP rod strain

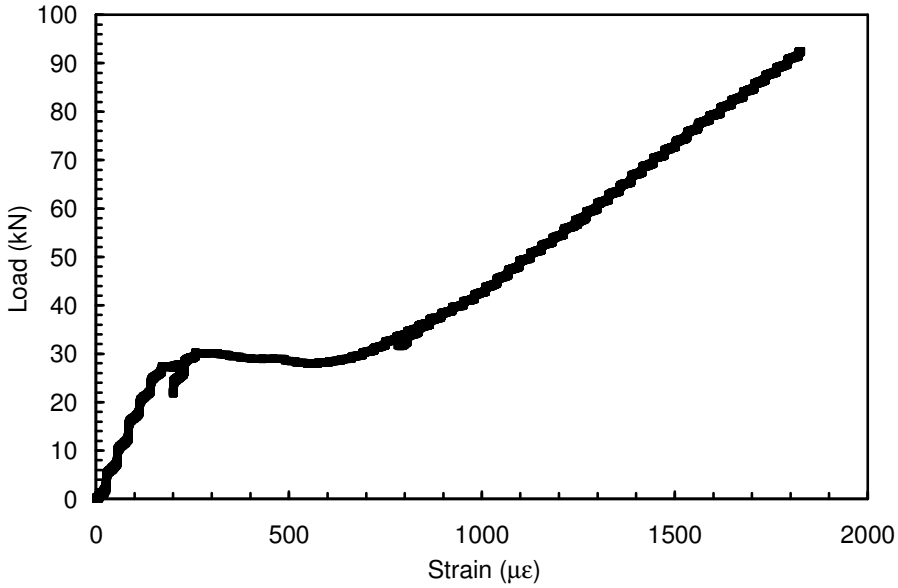

c-Load versus mid-span concrete strain

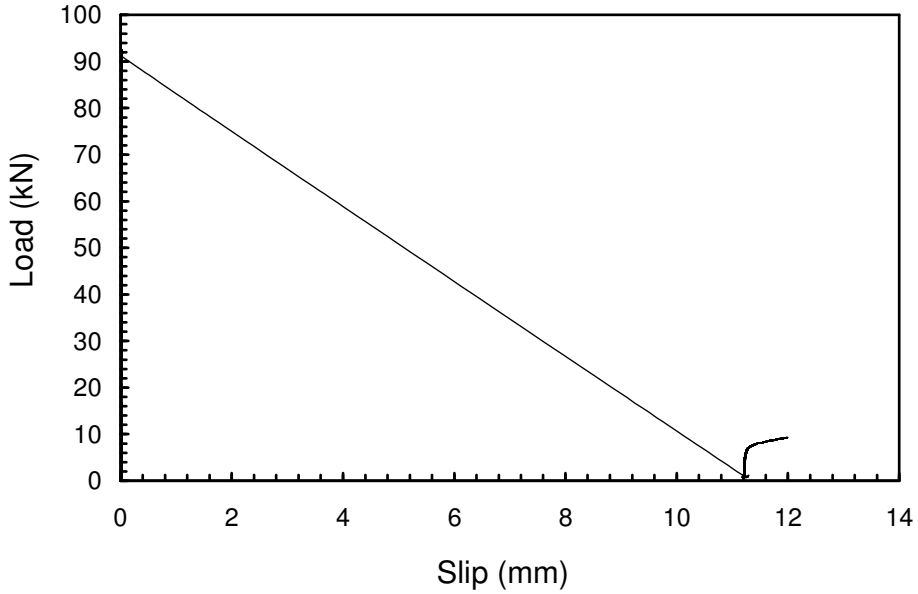

d-Load versus slip between the CFRP rod and the concrete

Figure A-9: Test results for beam NS-SC-0%-M

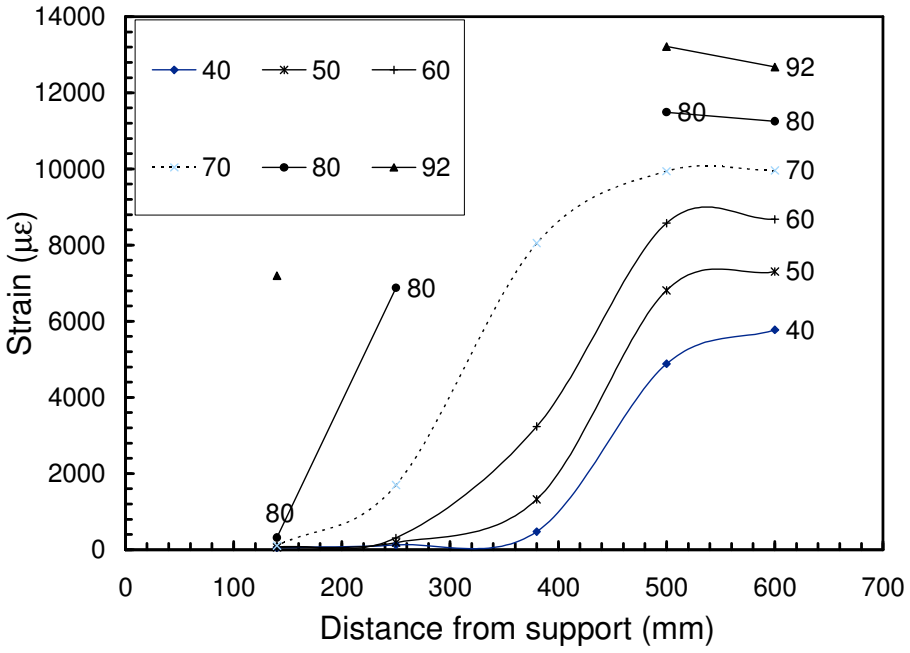

Figure A-10: Strain distribution along the CFRP rod for beam NS-SC-0%-M

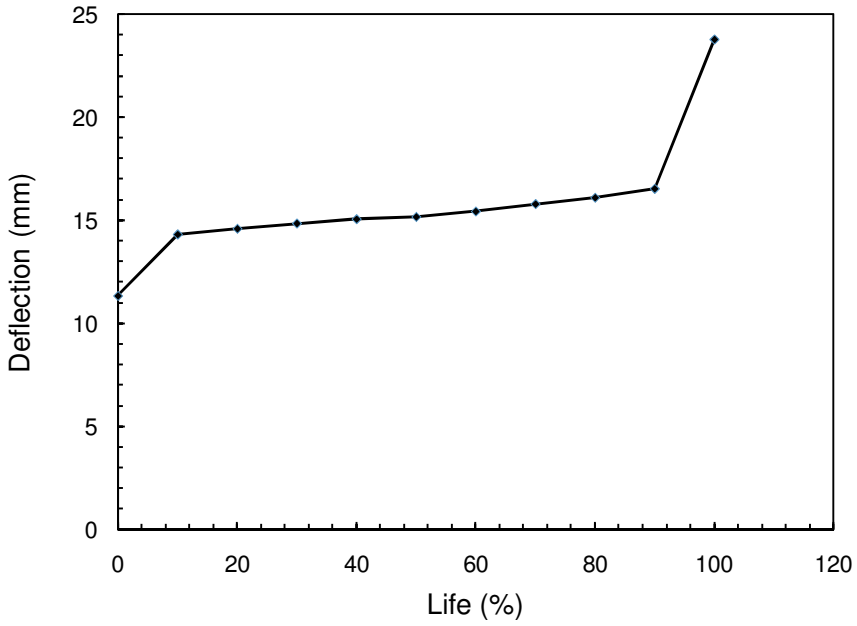

a-Mid-span deflection versus life

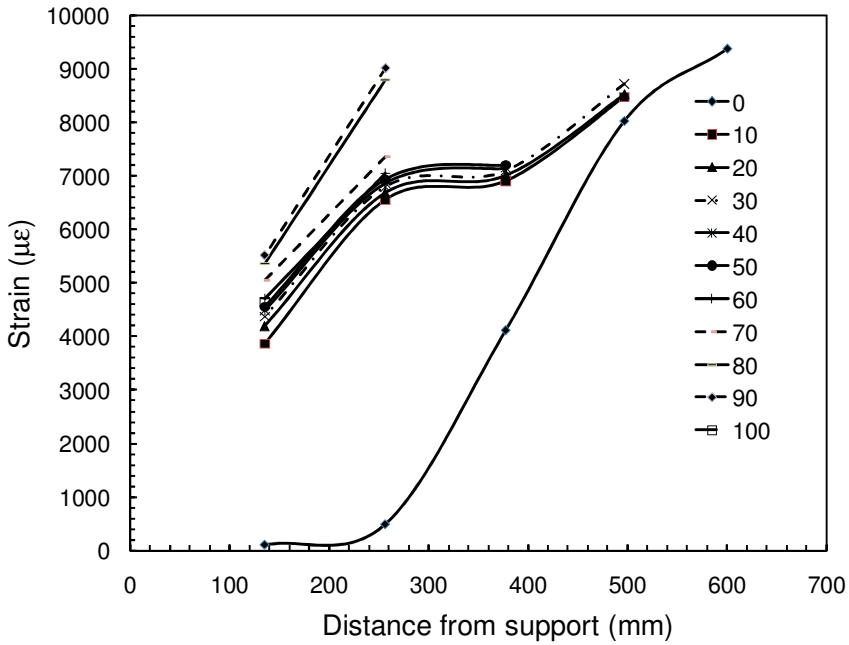

b-Strain distribution along the CFRP rod

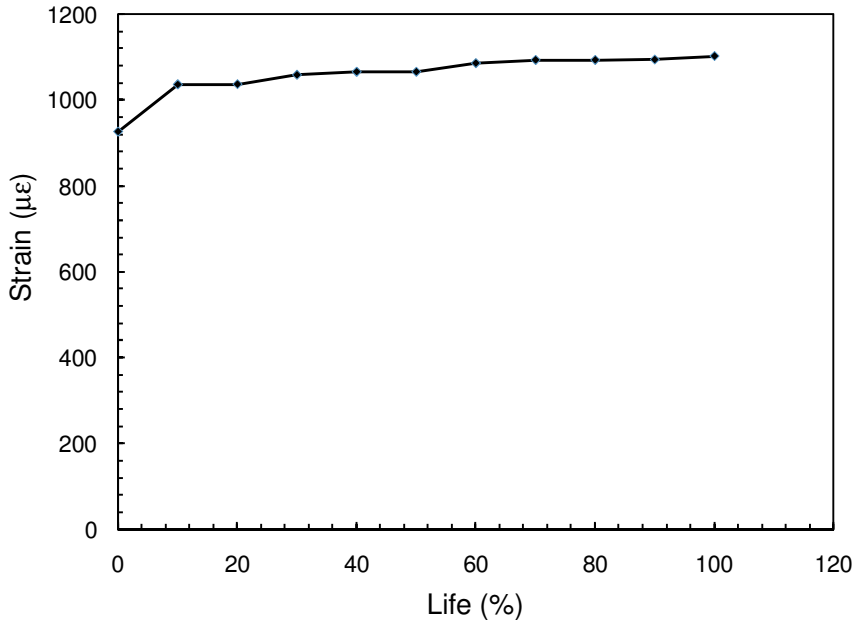

c-Mid-span concrete strain versus life

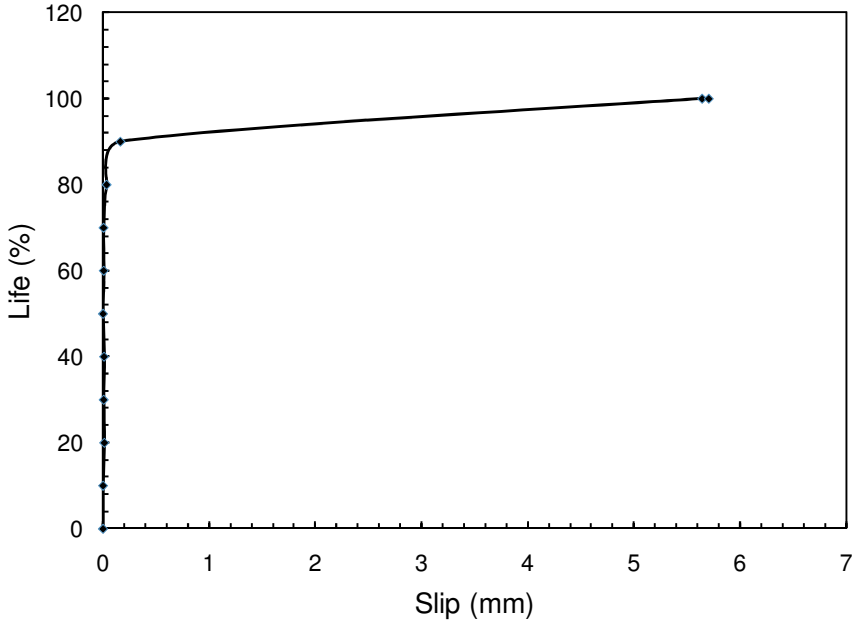

d- Load versus slip

Figure A-11: Test results for beam NS-SC-0%-70%

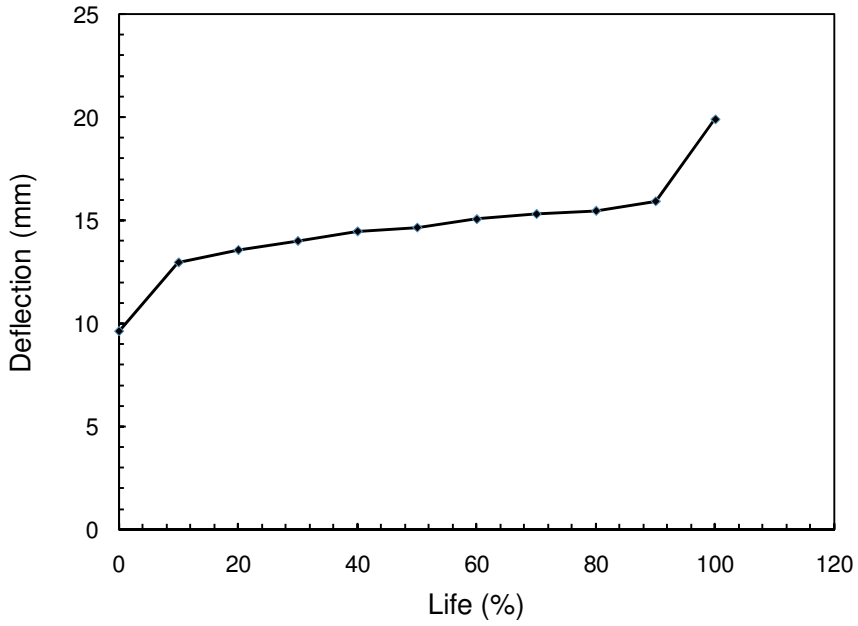

a-Mid-span deflection versus life

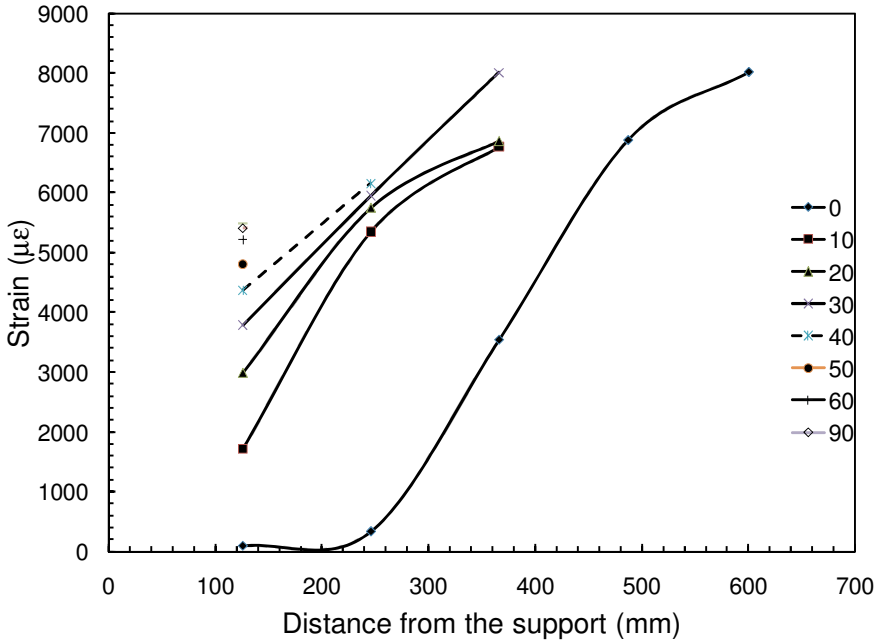

b-Strain distribution along the CFRP rod

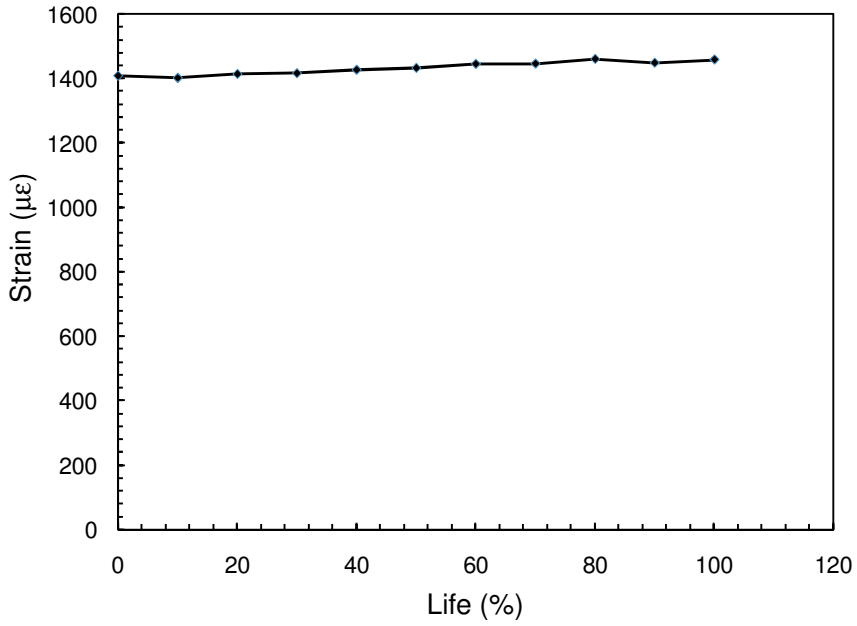

c-Mid-span concrete strain versus life

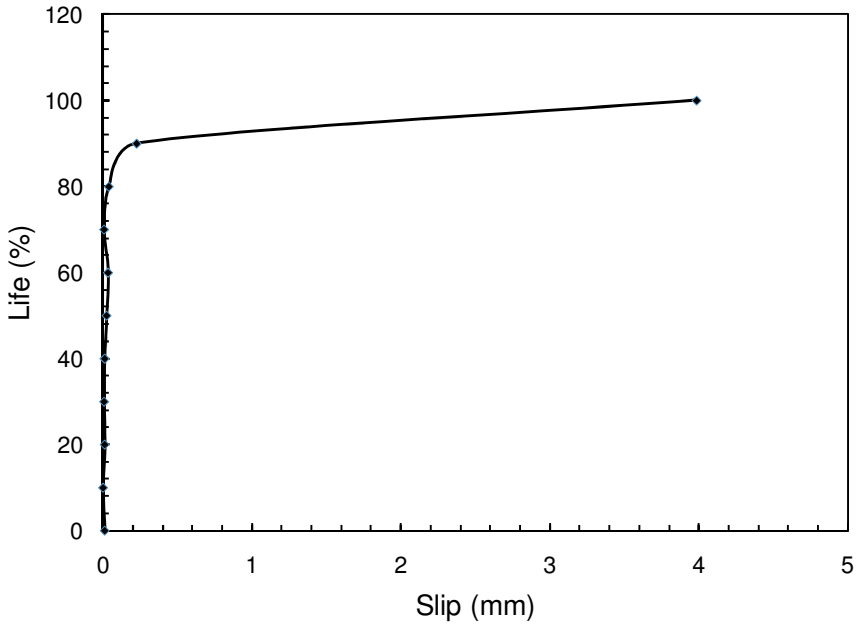

d- Load versus slip

Figure A-12: Test results for beam NS-SC-0%-62.5%(a)

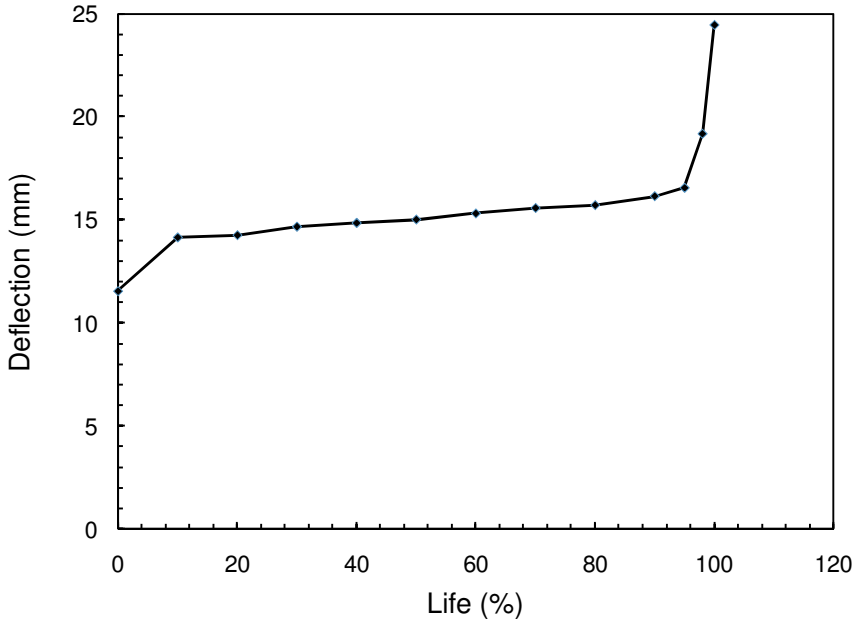

a-Mid-span deflection versus life

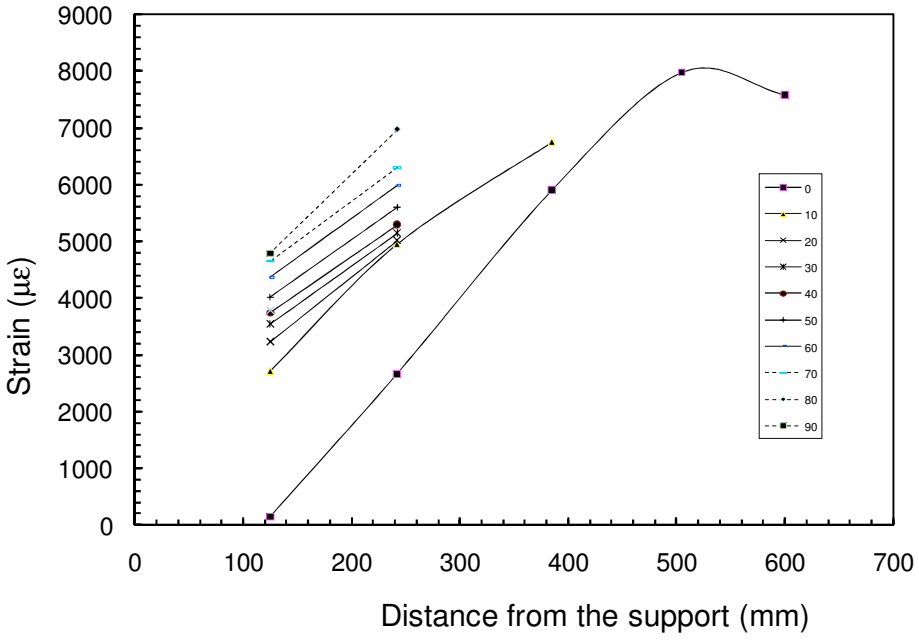

b-Strain distribution along the CFRP rod

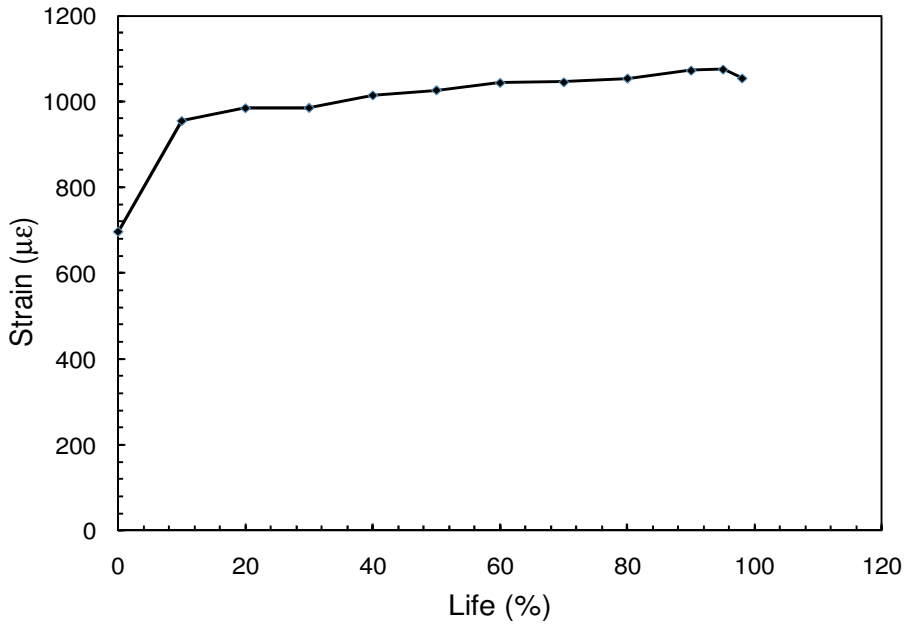

c-Mid-span concrete strain versus life

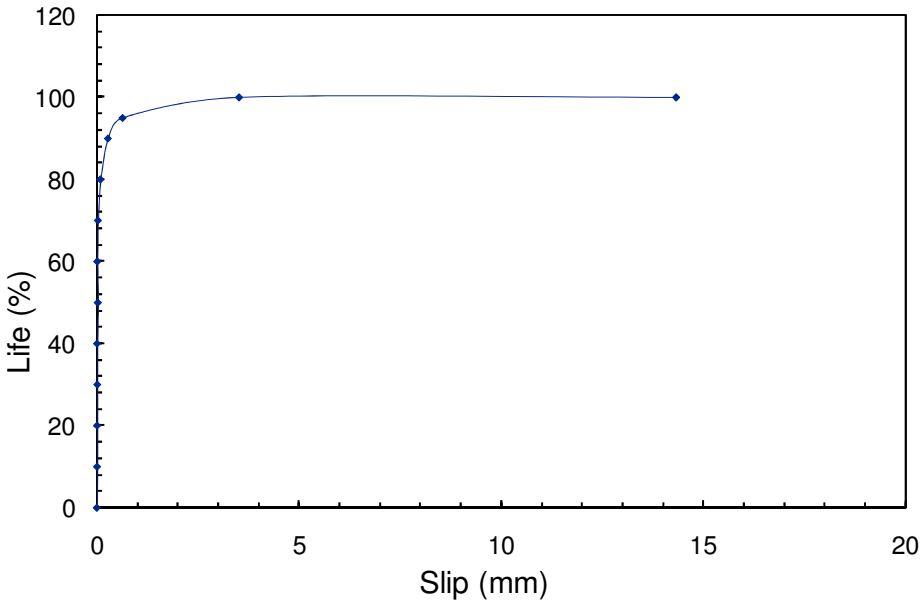

d- Load versus slip

Figure A-13: Test results for beam NS-SC-0%-60%

Beams with internal steel and strengthened with CFRP rods

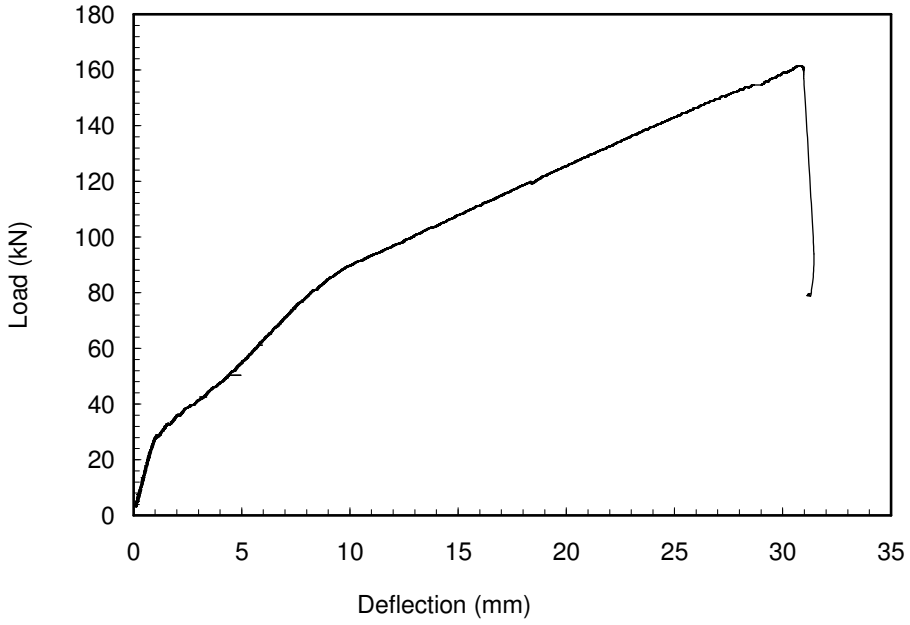

a- Mid-span deflection

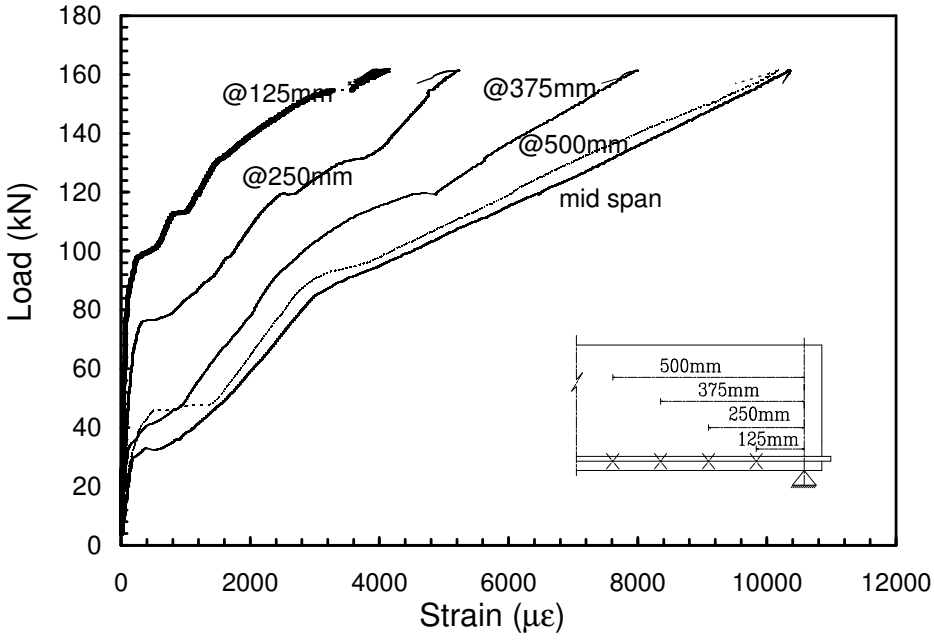

b-CFRP strain

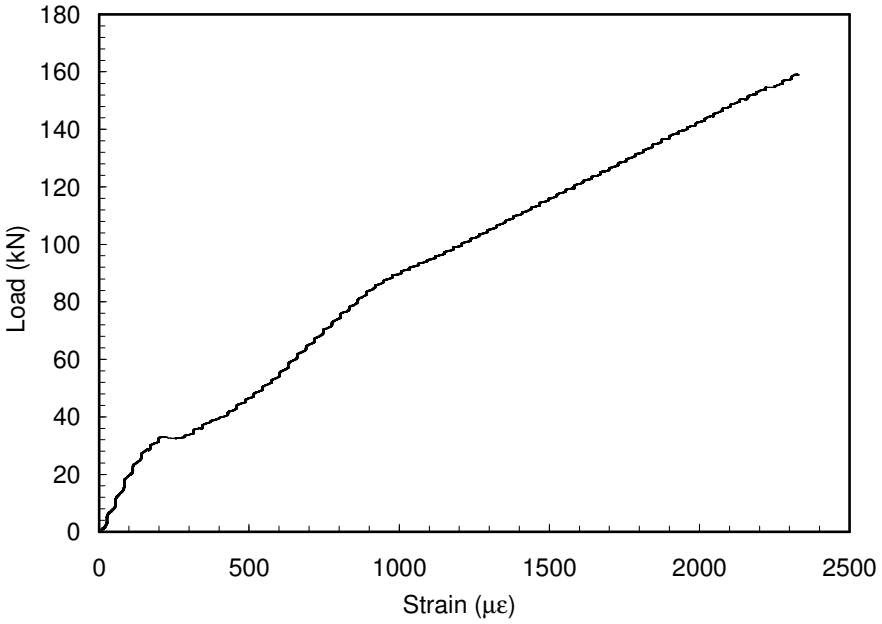

c-Mid-span concrete strain

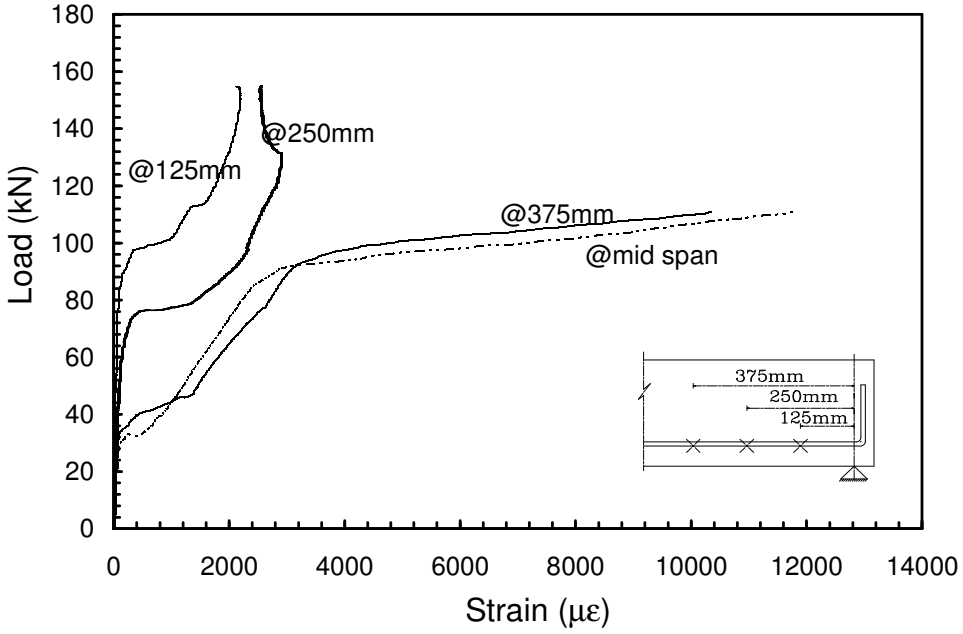

d- Steel strain

Figure A-14: Load versus deflection and strain response for beam S-SW-0%-M

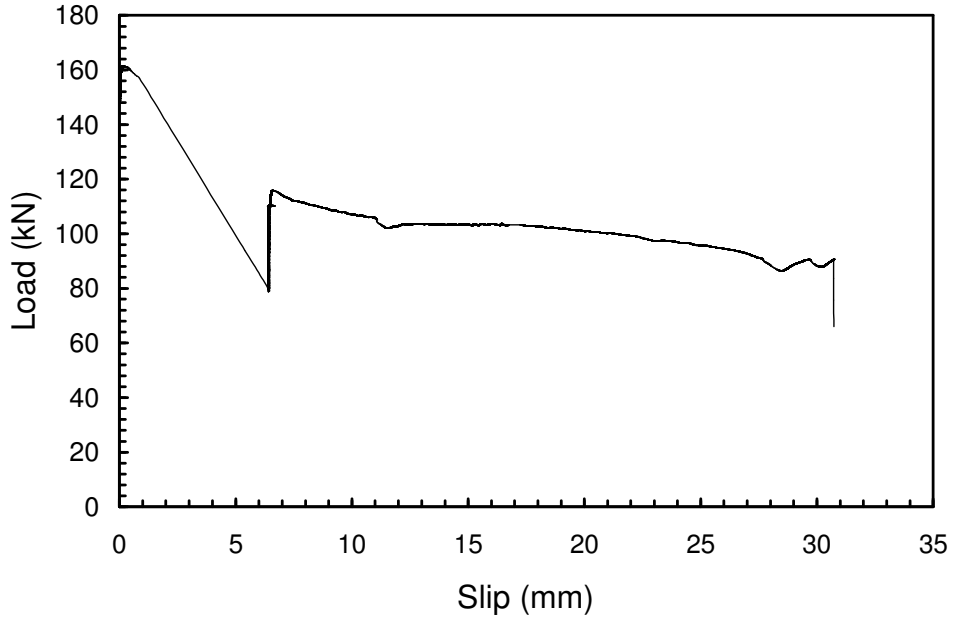

Figure A-15: Load versus end slip for beam S-SW-0%-M

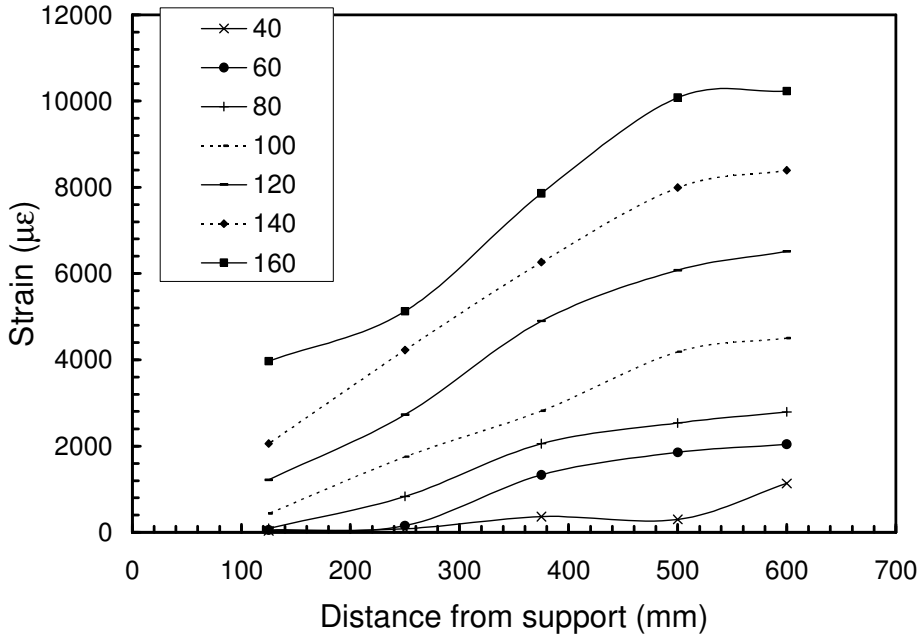

Figure A-16: Strain distribution along the CFRP rod for beam S-SW-0%-M

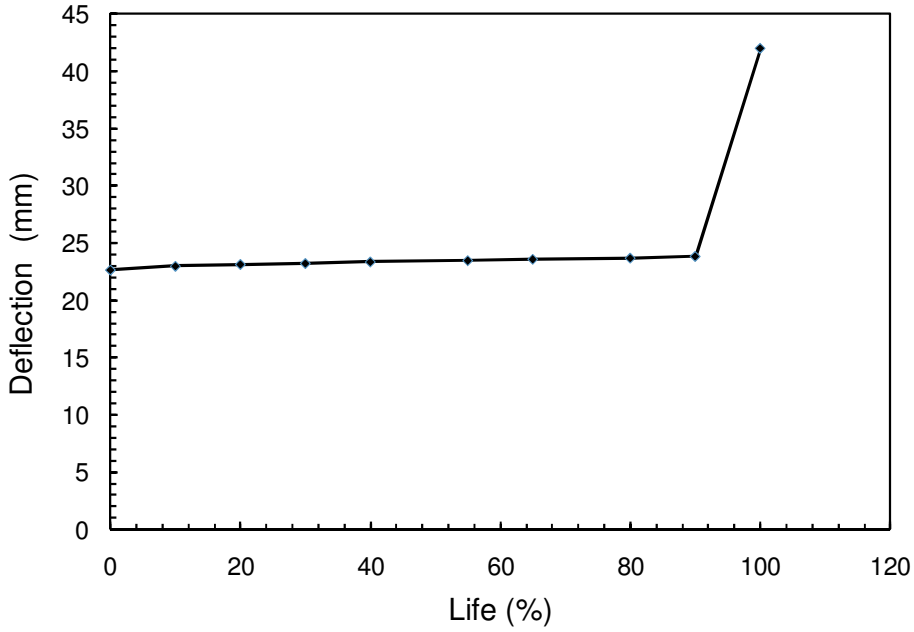

a-Mid-span deflection versus life

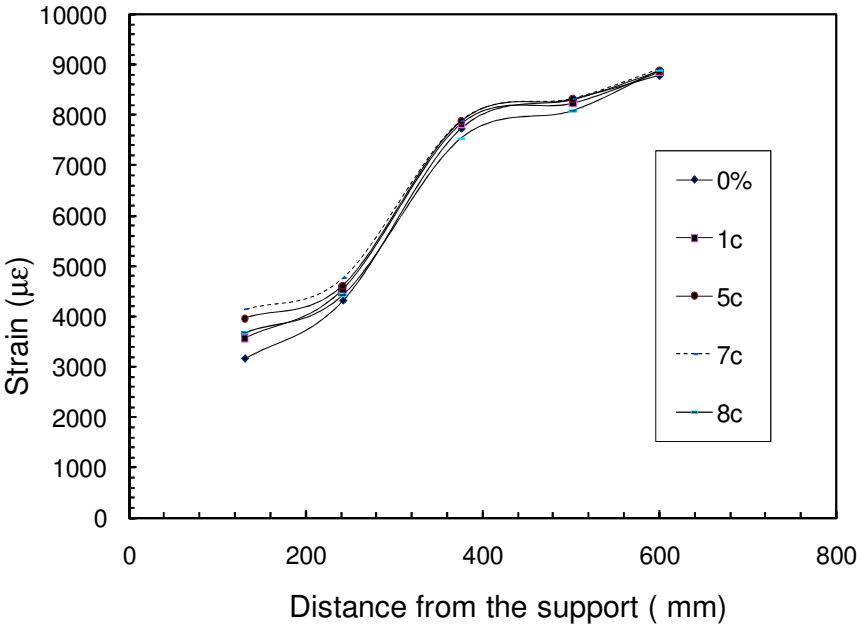

b-Strain distribution along the CFRP rod at different life

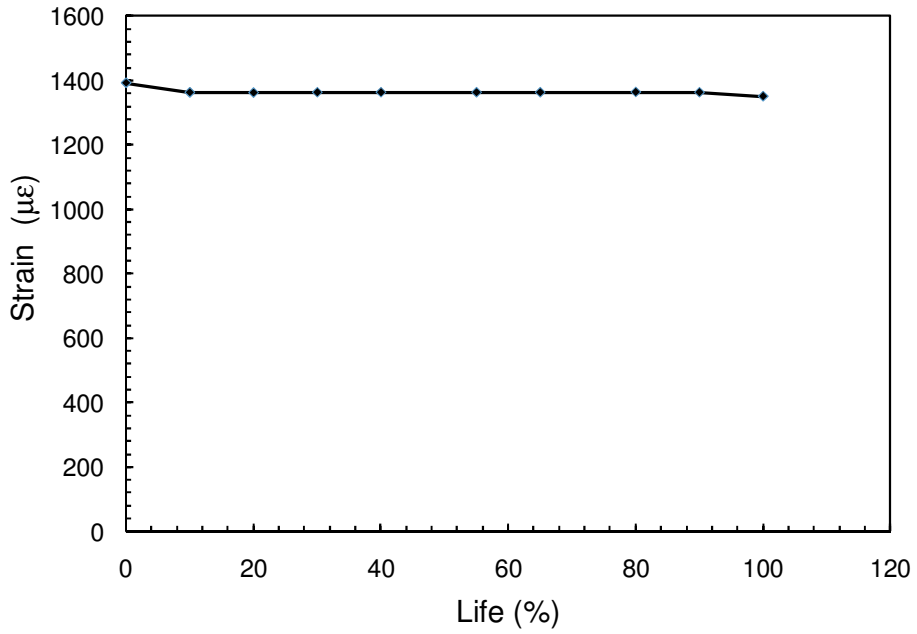

c-Mid-span concrete strain versus life

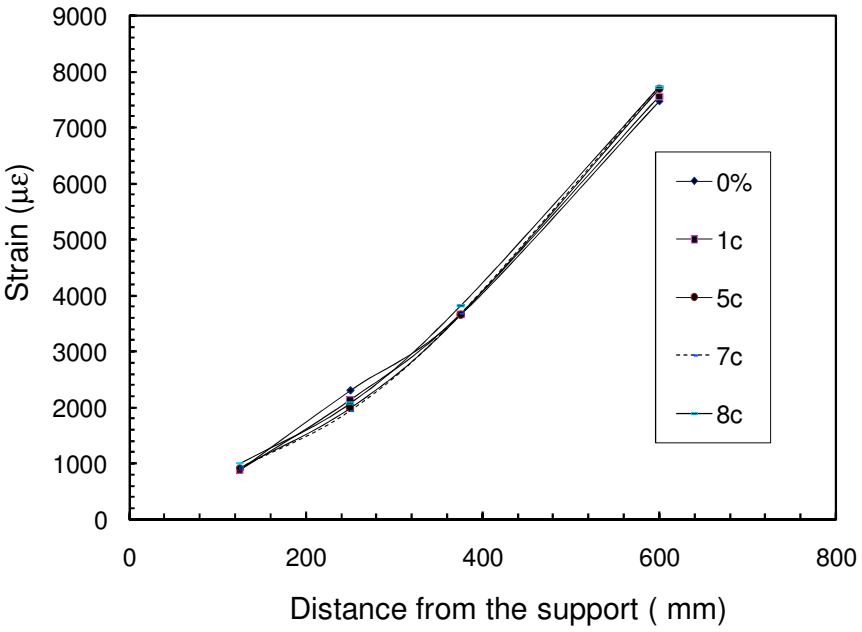

b-Strain distribution along steel rebar at different life

Figure A-17: Deflection and strains for beam S-SW-0%-81.6%

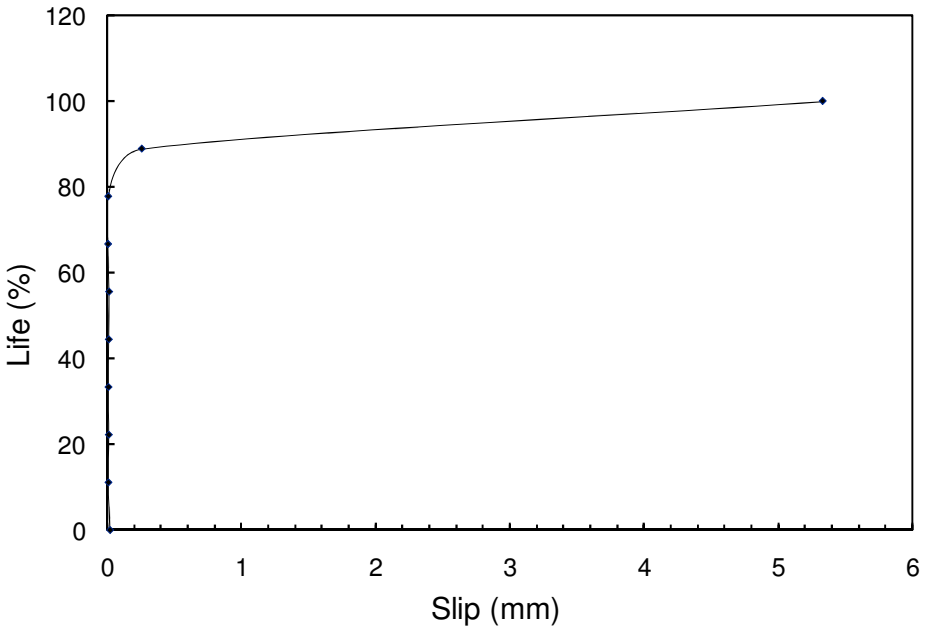

Figure A-18: Life versus CFRP rod end slip from epoxy for beam S-SW-0%-81.6%

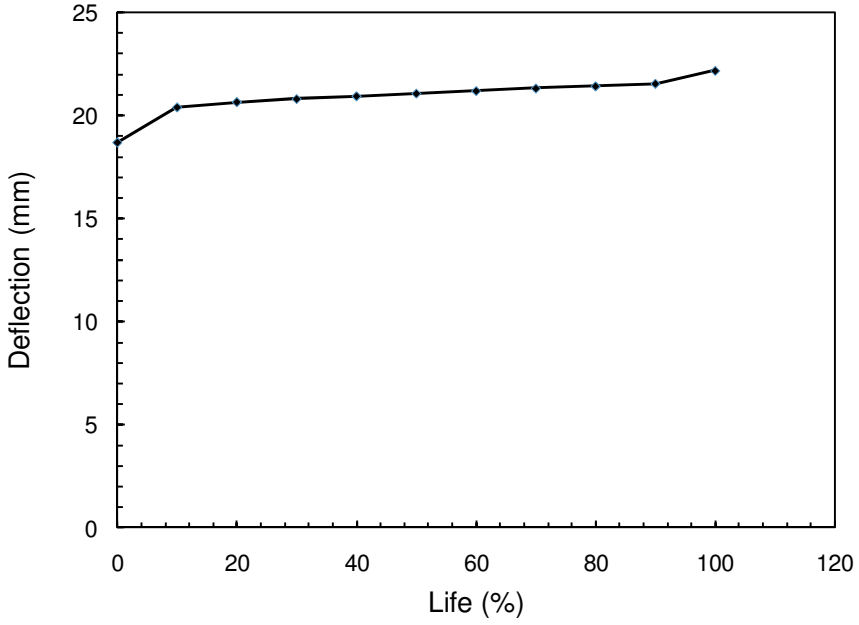

a-Mid-span deflection versus life

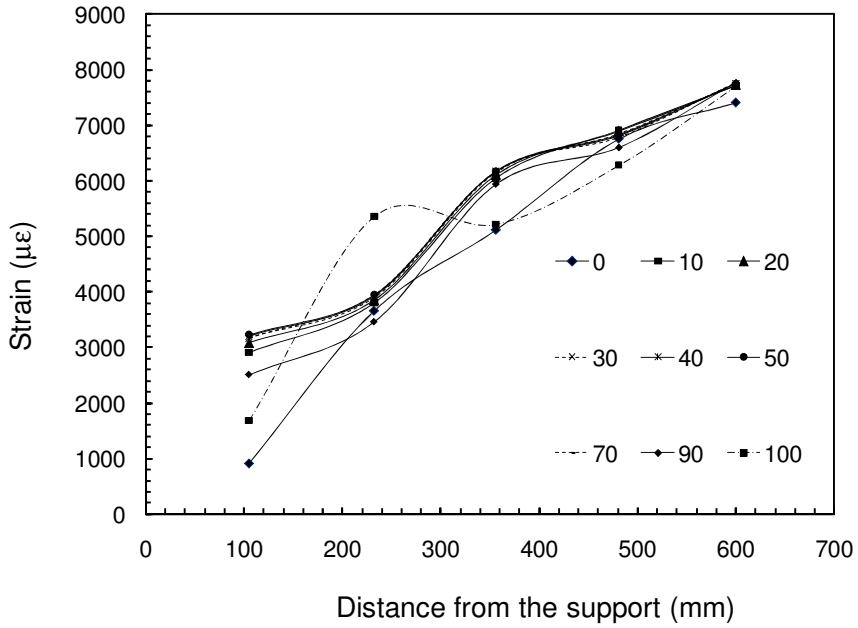

b-Strain distribution along the CFRP rod at different life

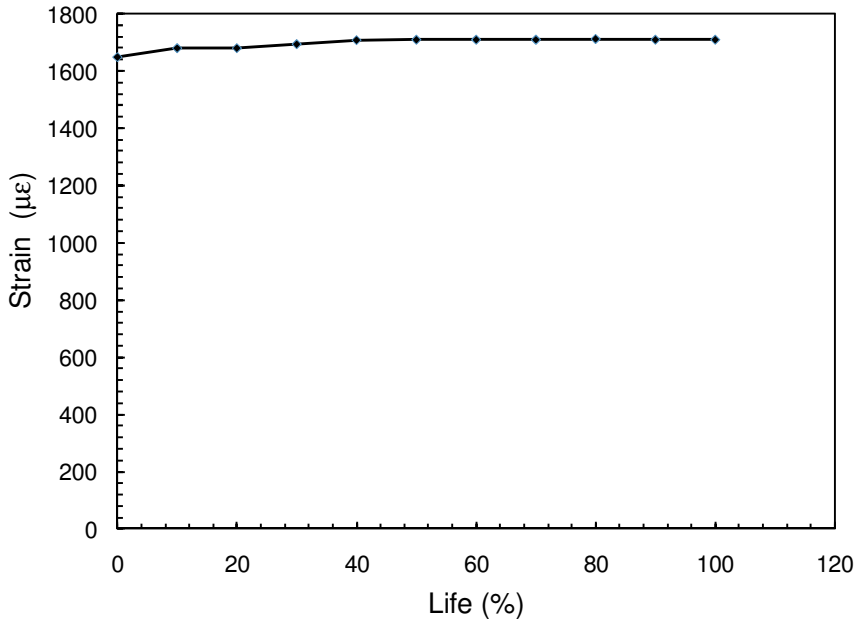

c-Mid-span concrete strain versus life

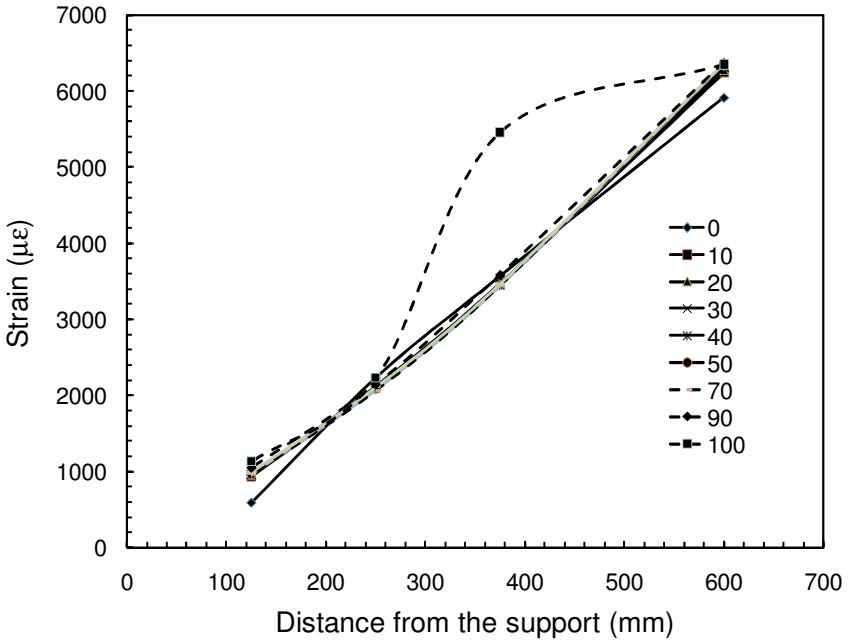

d-Strain distribution along steel rebar at different life

Figure A-19: Deflection and strains for beam S-SW-0%-75.1%

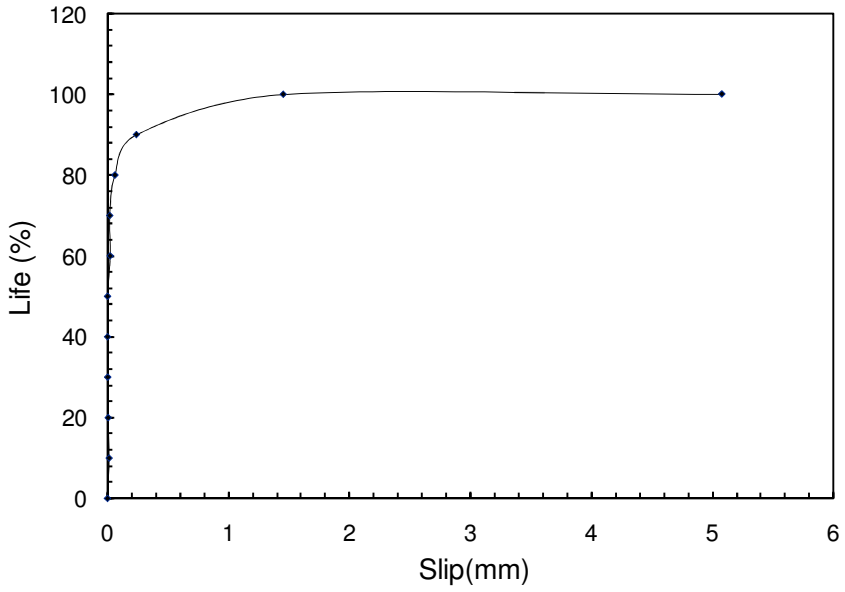

Figure A-20: Life versus CFRP rod end slip from epoxy for beam S-SW-0%-75.1%

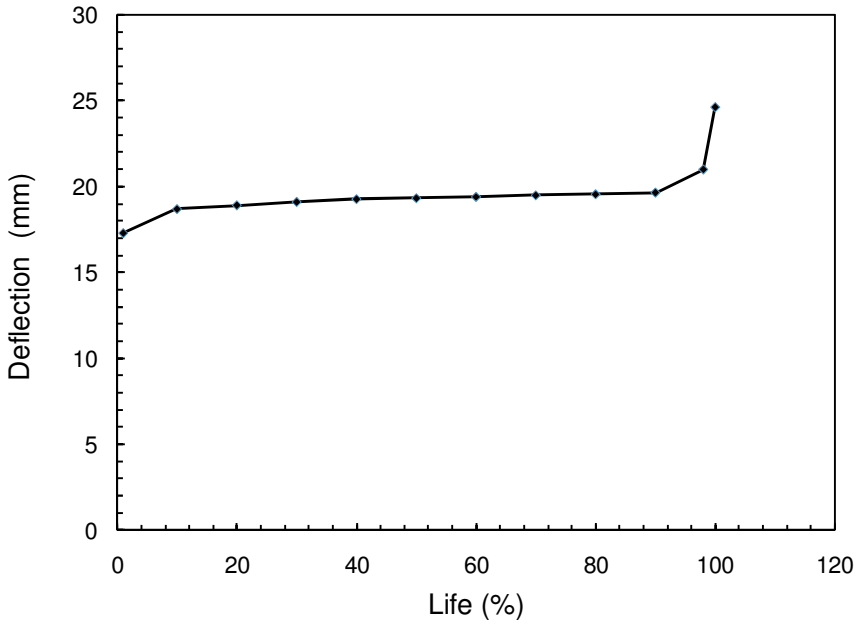

a-Mid-span deflection versus life

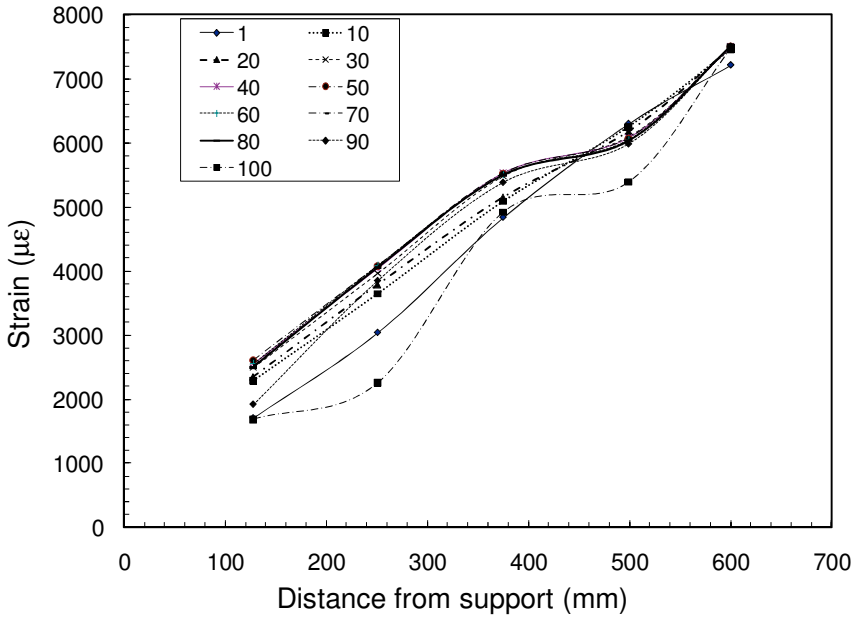

b-Strain distribution along the CFRP rod at different life

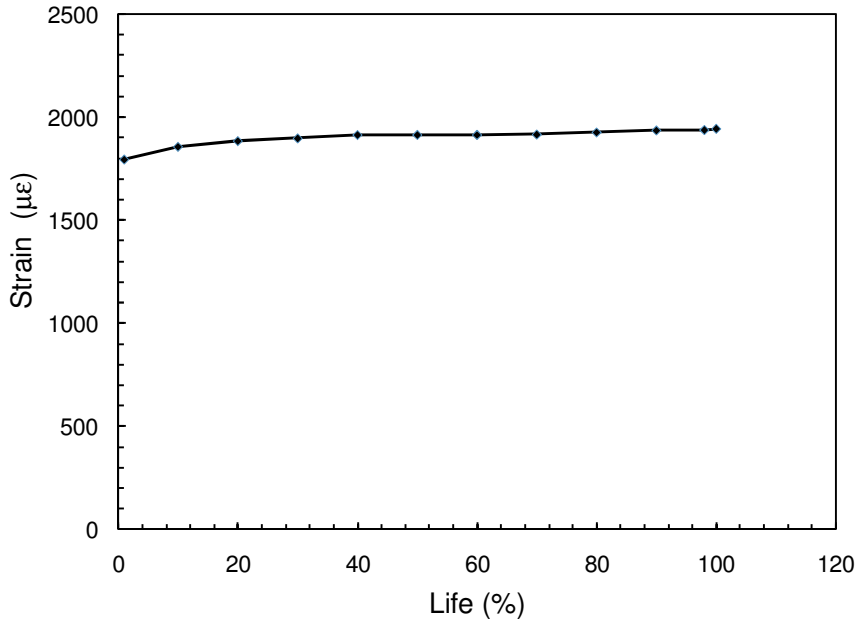

c-Mid-span concrete strain versus life

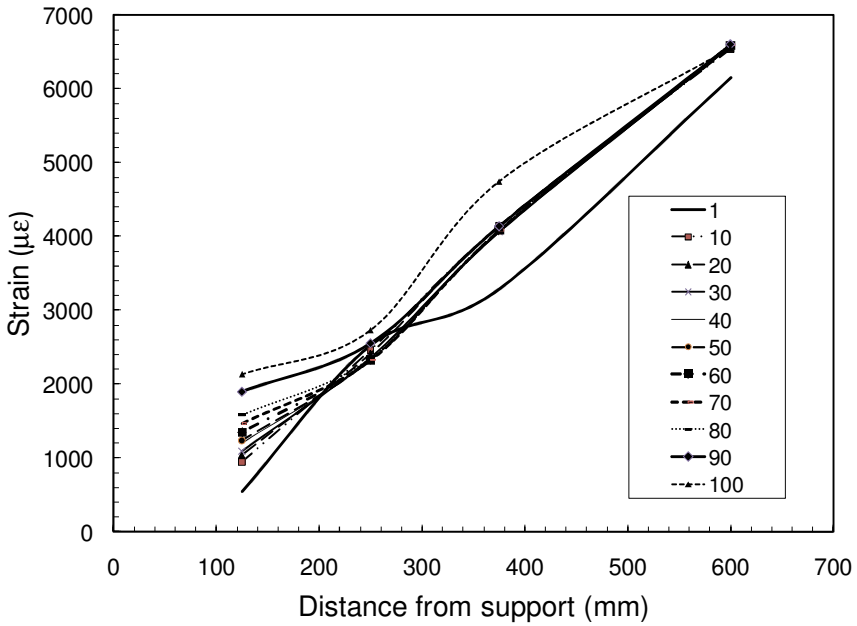

d-Strain distribution along steel rebar at different life

Figure A-21: Deflection and strains for beam S-SW-0%-71.4%

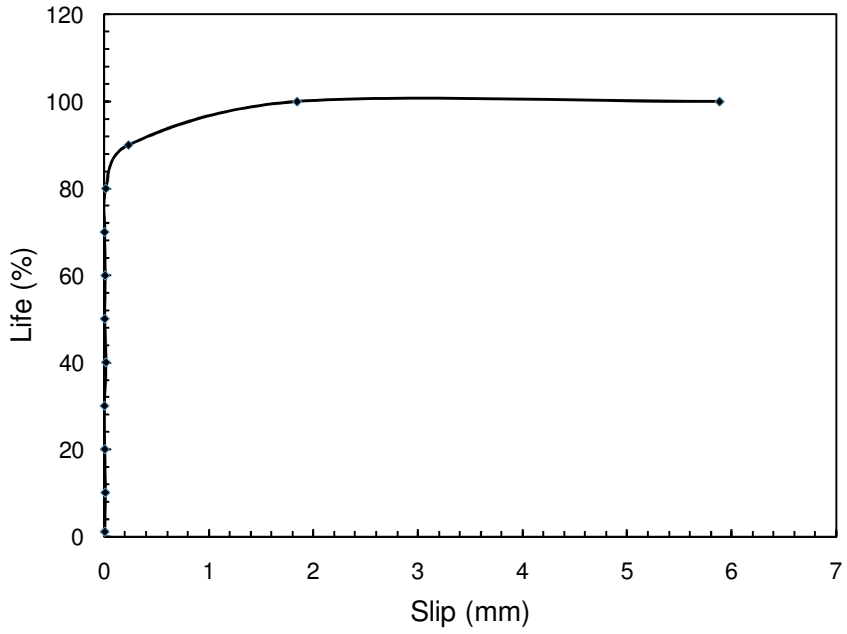

Figure A-22: Life versus CFRP rod end slip from epoxy for beam S-SW-0%-71.4%

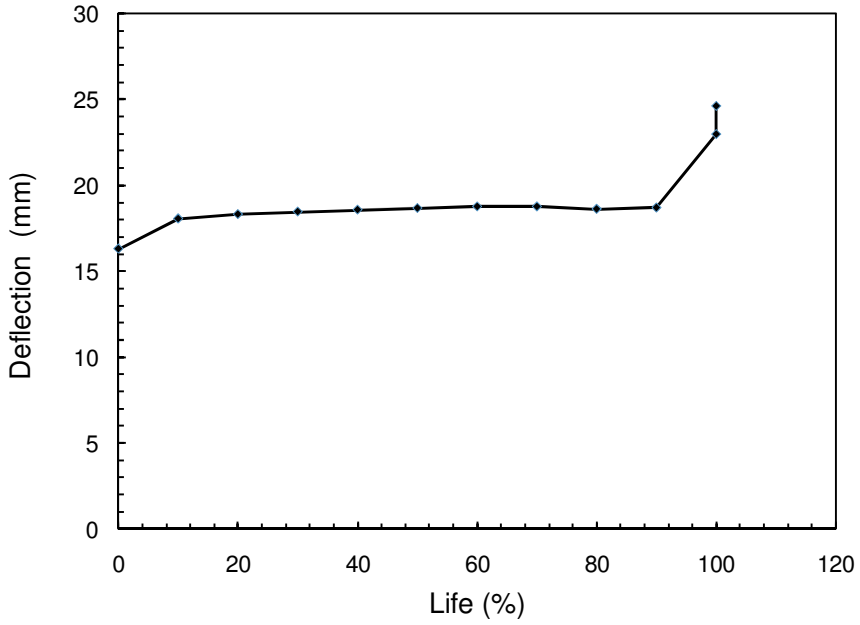

a-Mid-span deflection versus life

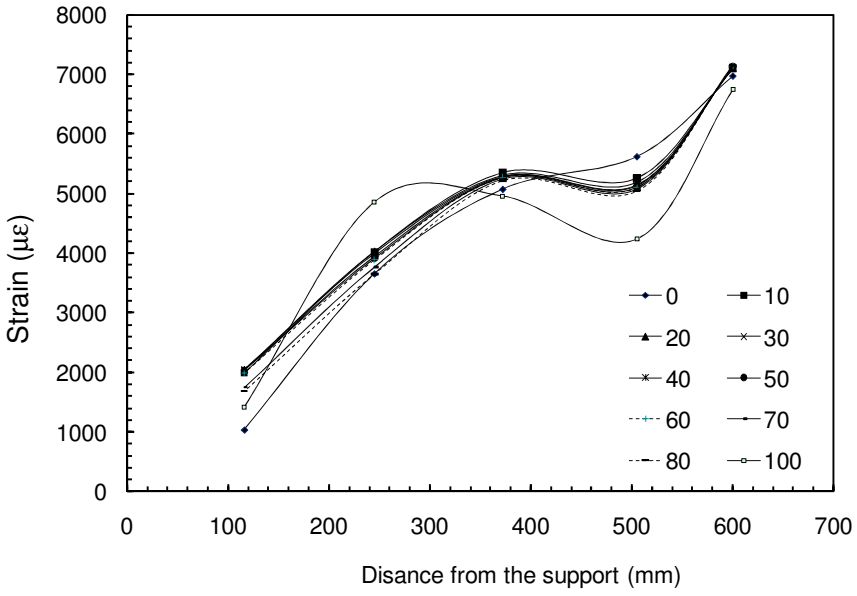

b-Strain distribution along the CFRP rod at different life

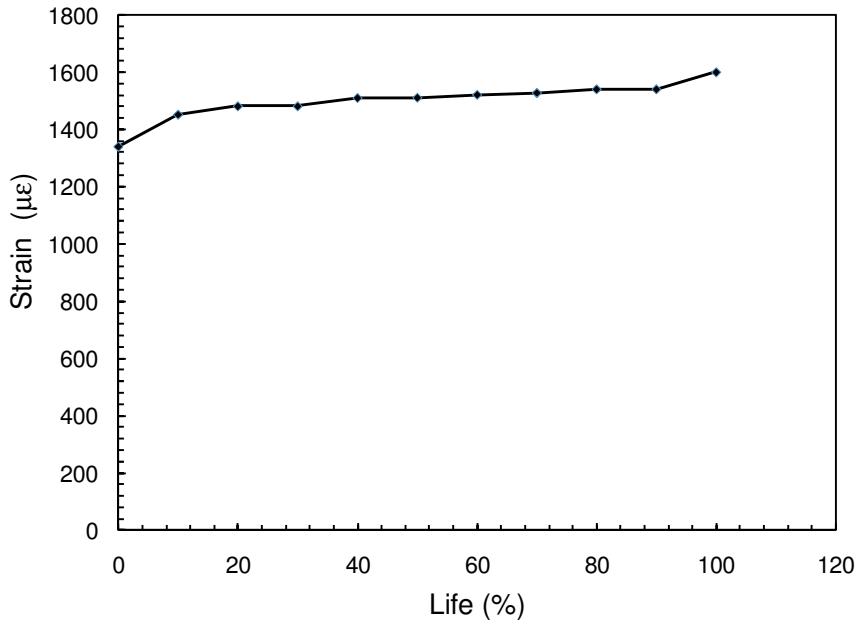

c-Mid-span concrete strain versus life

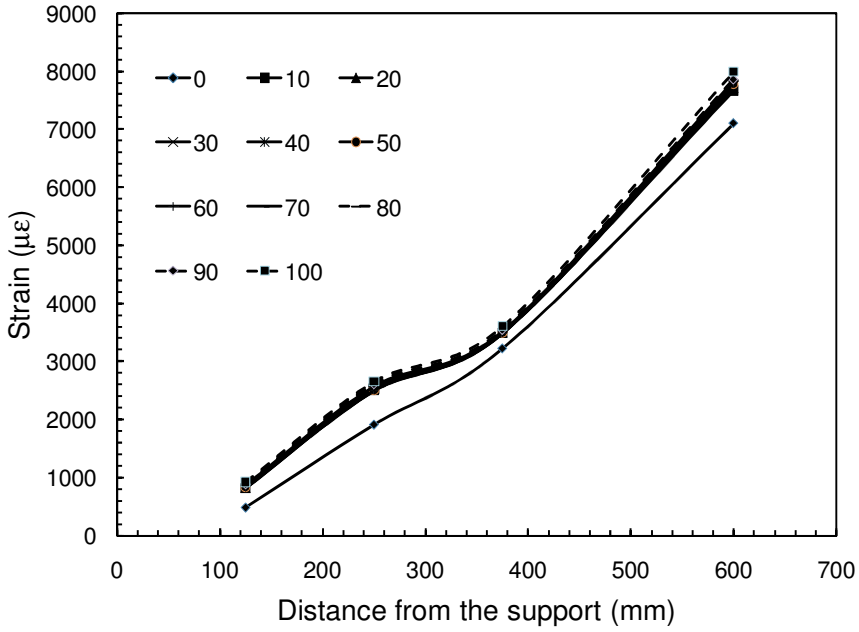

d-Strain distribution along steel rebar at different life

Figure A-23: Deflection and strains for beam S-SW-0%-68.75%

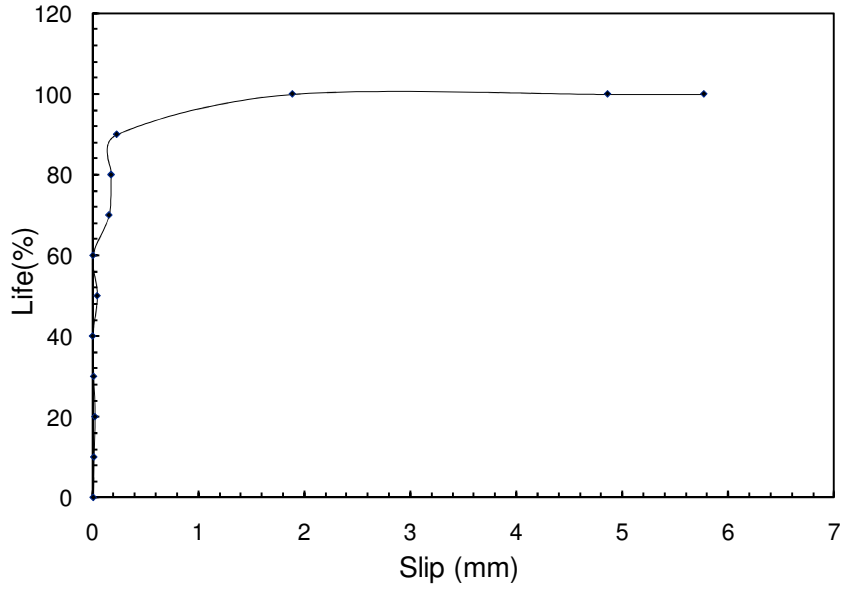

Figure A-24: Life versus CFRP rod end slip from epoxy for beam S-SW-0%-68.75%

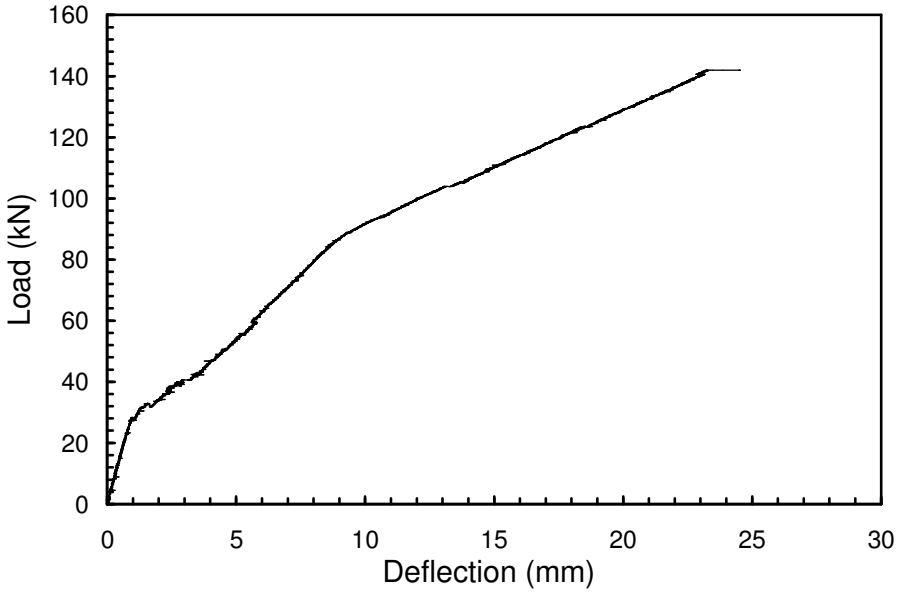

a-Mid-span deflection

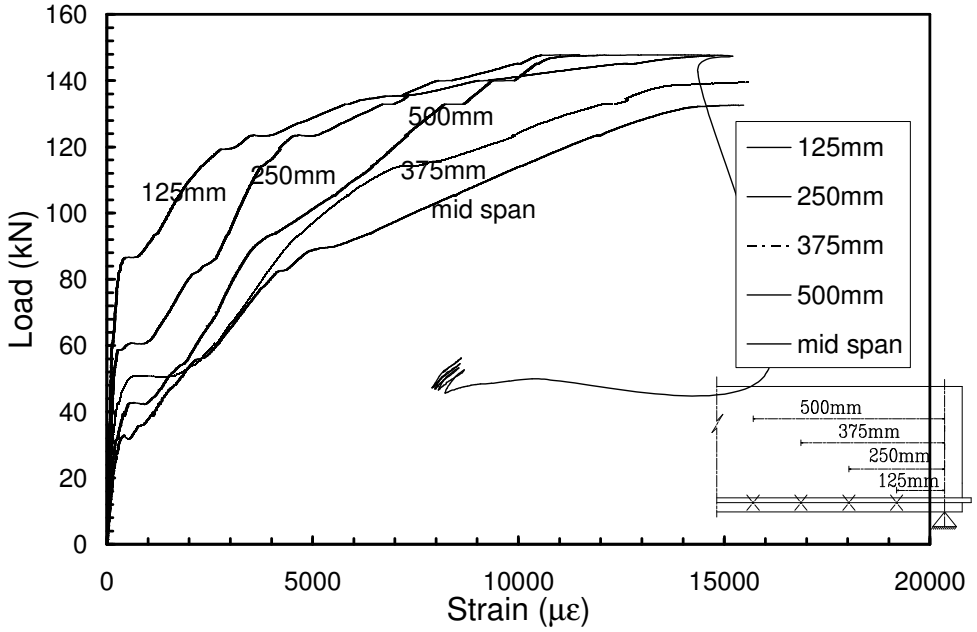

b-CFRP rod strain

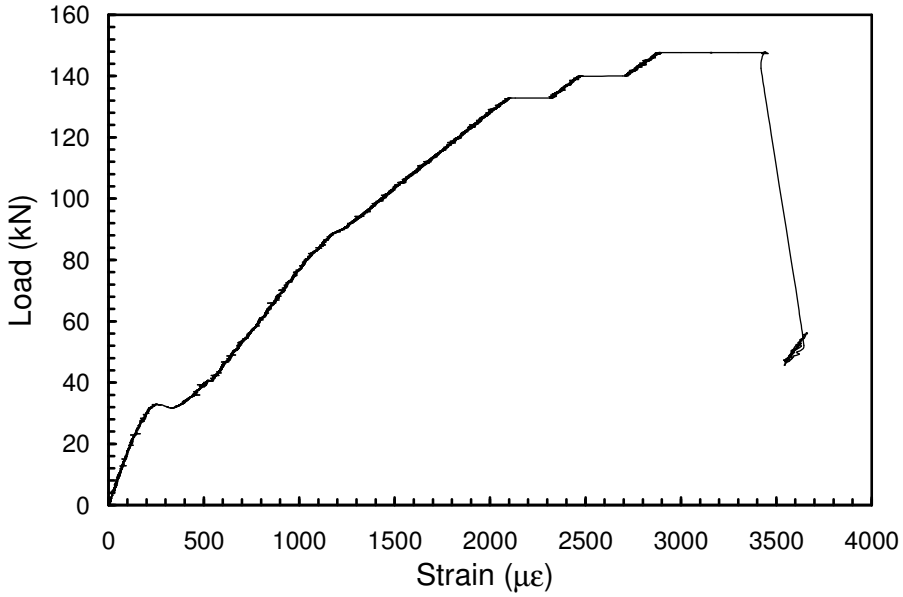

c-Mid-span concrete strain

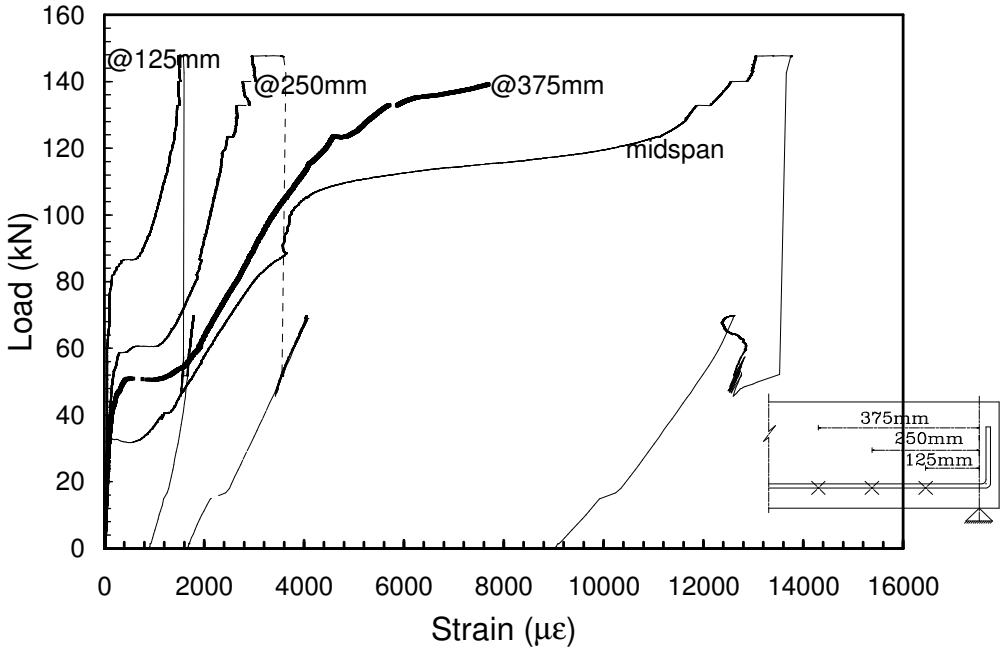

d-Steel rebar strain

Figure A-25: Load versus deflection and strain response for beam S-SC-0%-M

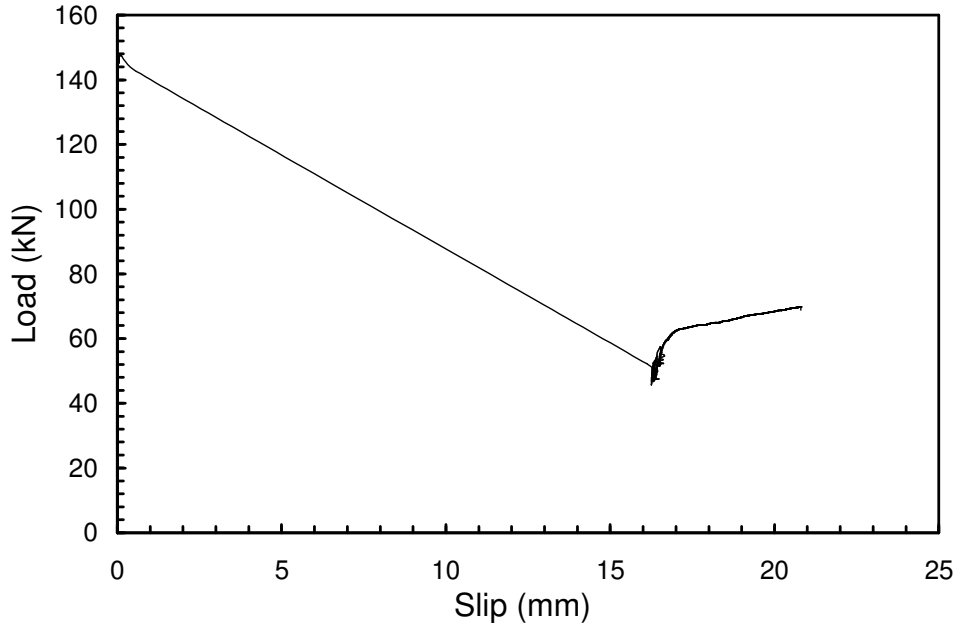

Figure A-26: Load versus slip for beam S-SC-0%-M

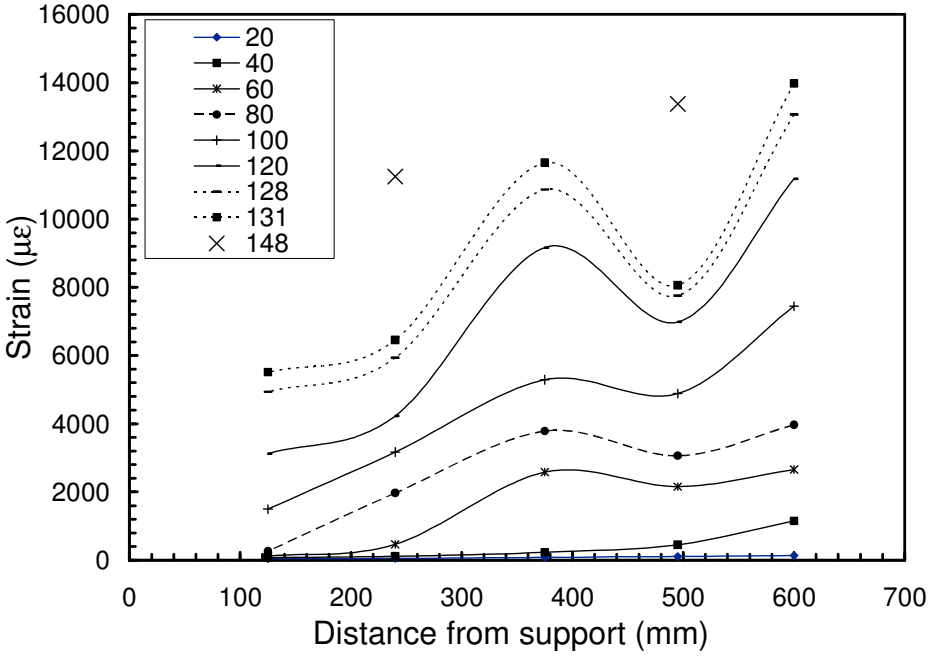

Figure A-27: Strain along the CFRP rod for beam S-SC-0%-M

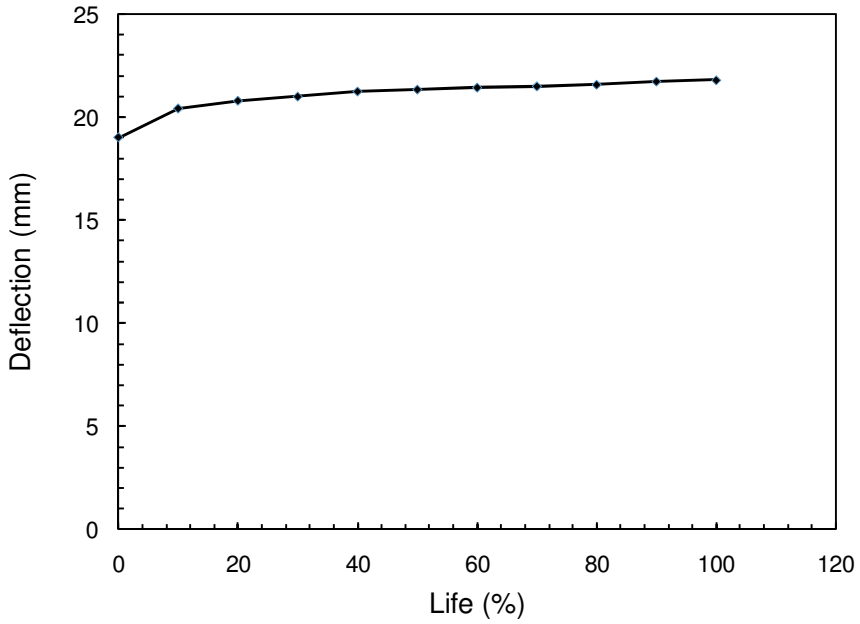

a-Mid-span deflection versus life

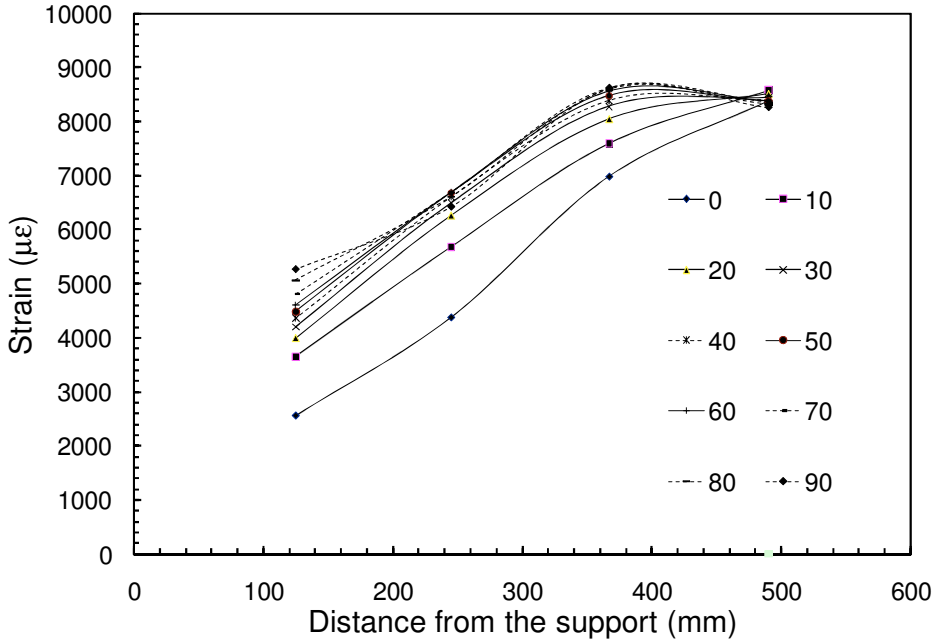

b-Strain distribution along the CFRP rod at different life

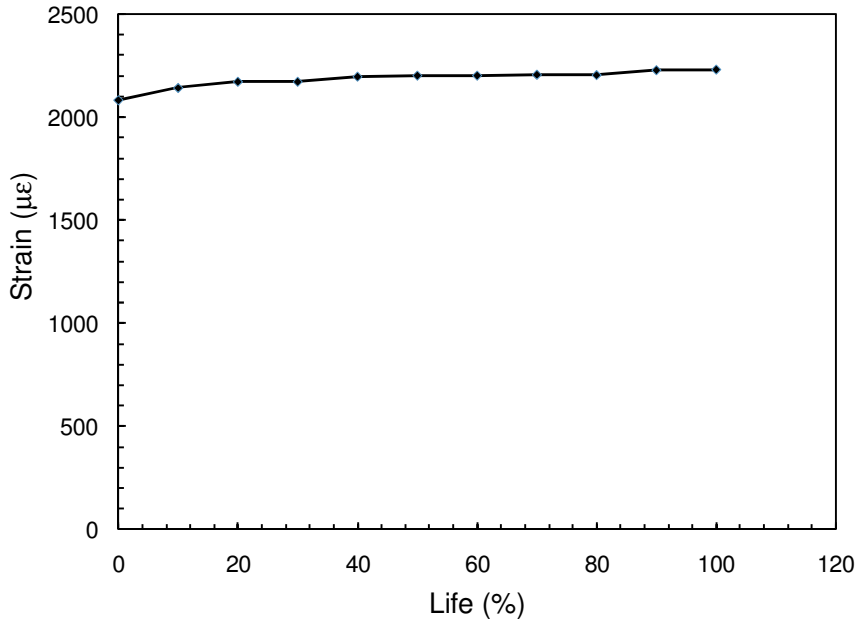

c-Mid-span concrete strain versus life

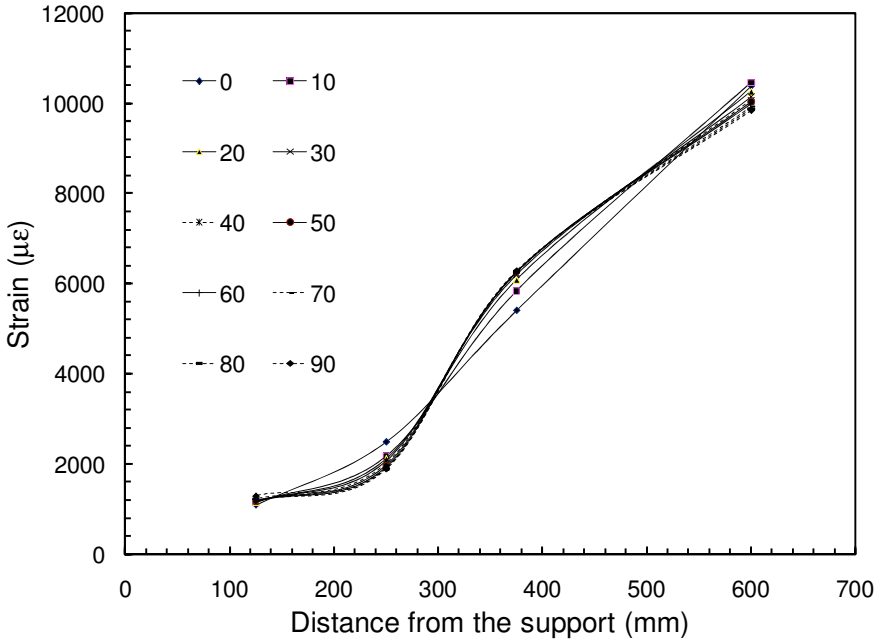

d-Strain distribution along steel rebar at different life

Figure A-28: Deflection and strains for beam S-SC-0%-85%

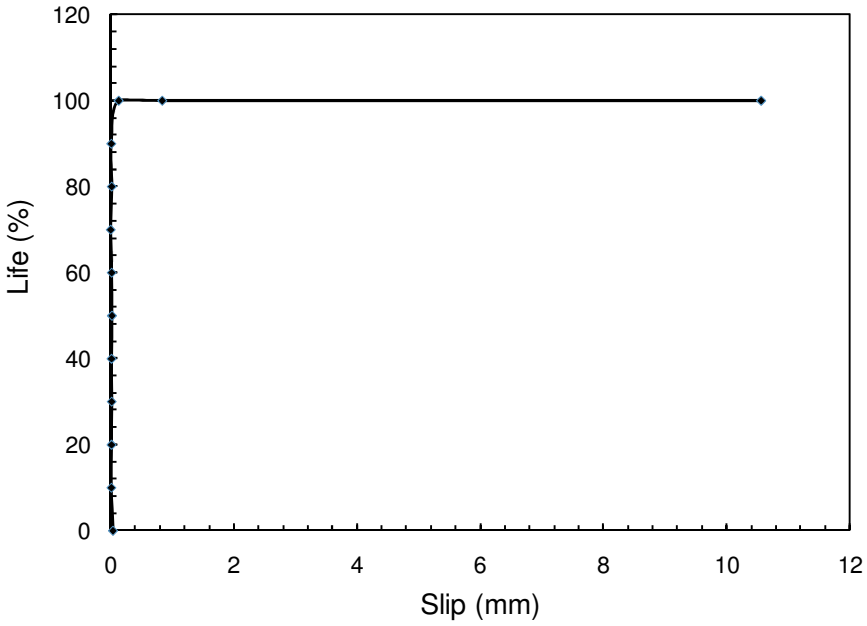

Figure A-29: Life versus CFRP rod end slip from epoxy for beam S-SC-0%-85%

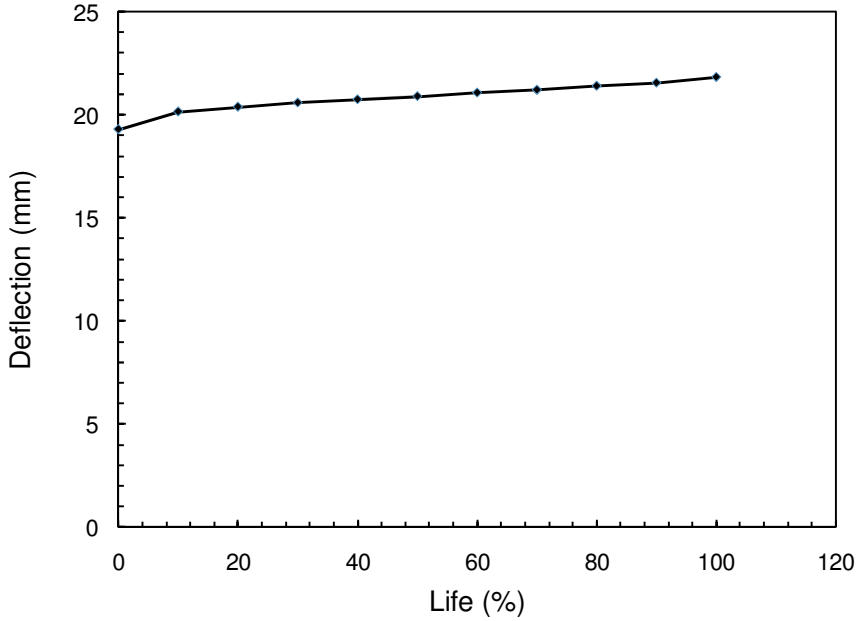

a-Mid-span deflection versus life

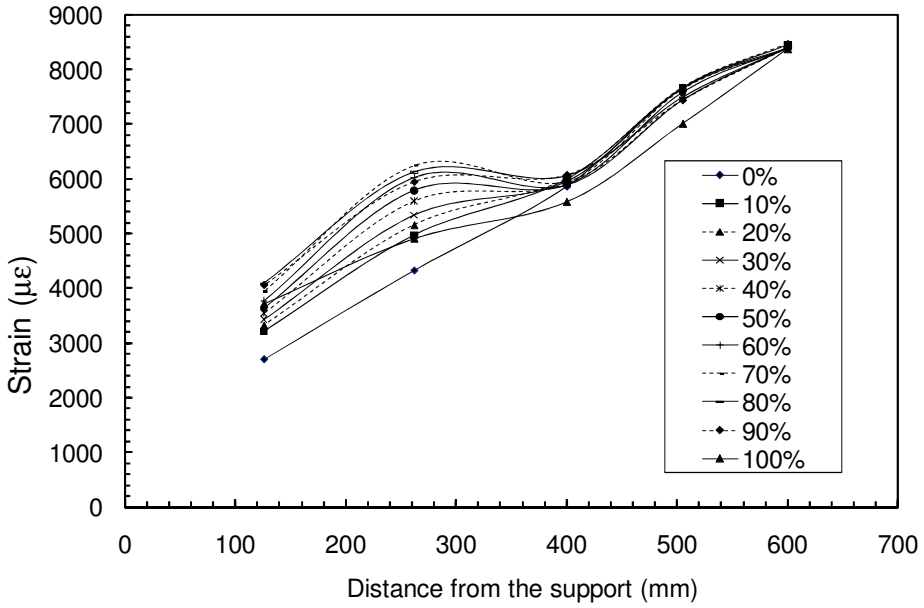

b-Strain distribution along the CFRP rod at different life

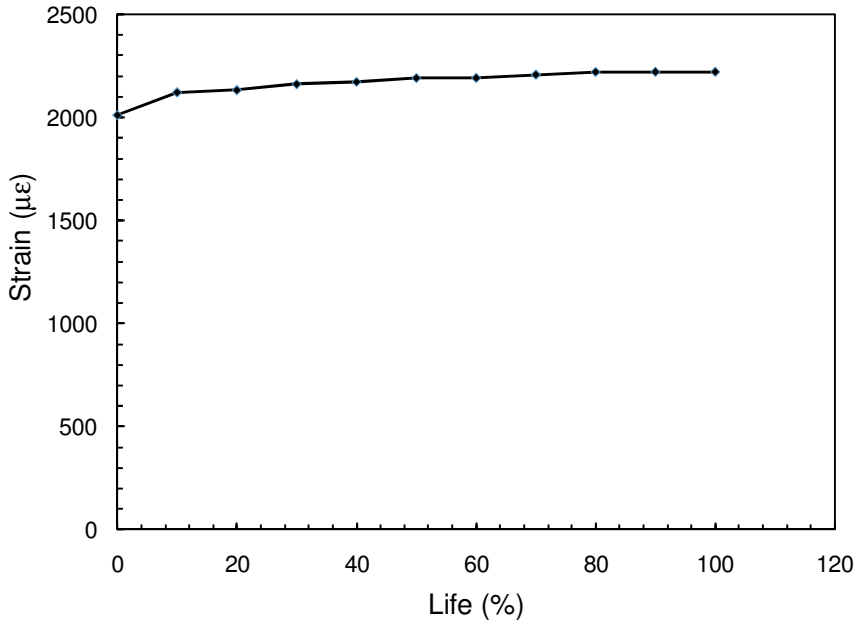

c-Mid-span concrete strain versus life

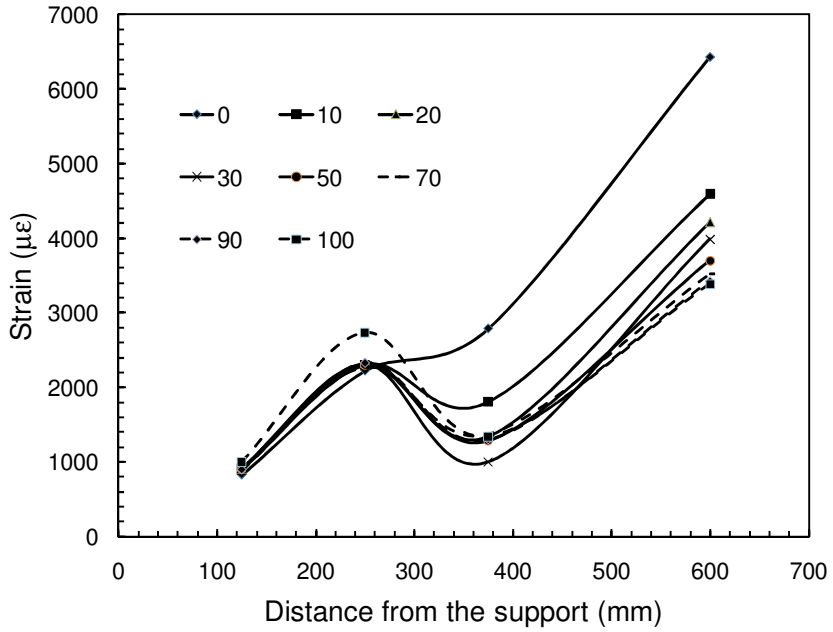

d-Strain distribution along steel rebar at different life
Figure A-30: Deflection and strains for beam S-SC-0%-81.3%

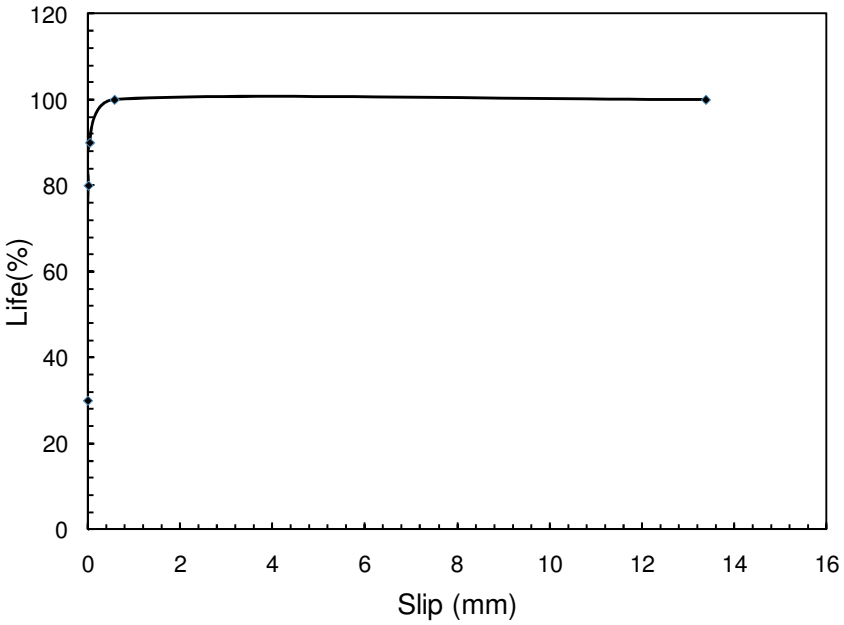

Figure A-31: Life versus CFRP rod end slip from epoxy for beam S-SC-0%-81.3%

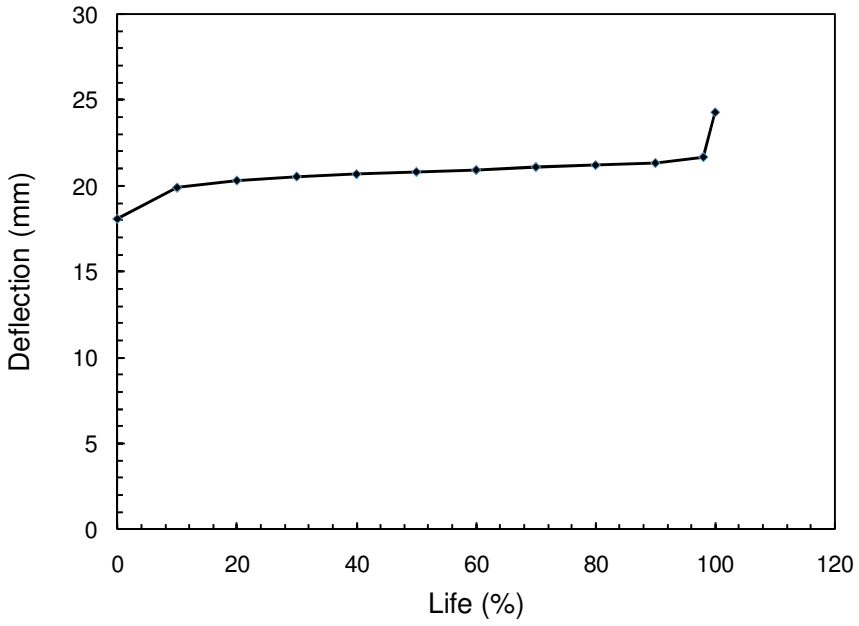

a-Mid-span deflection versus life

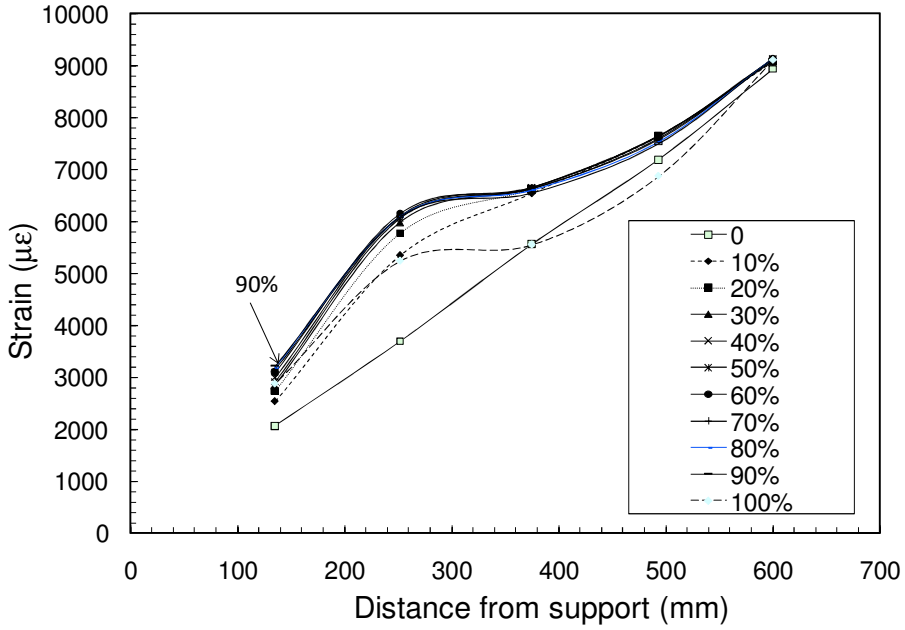

b-Strain distribution along the CFRP rod at different life

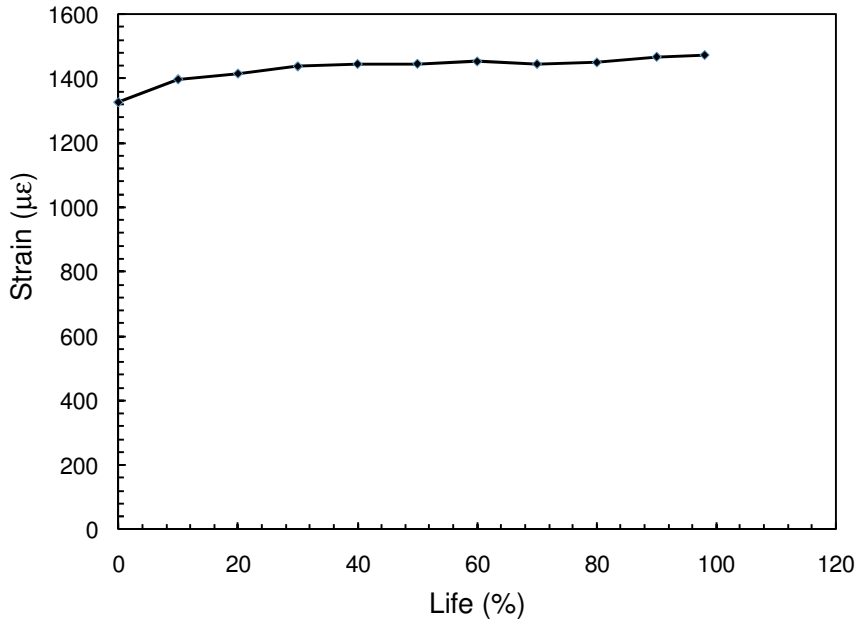

c-Mid-span concrete strain versus life

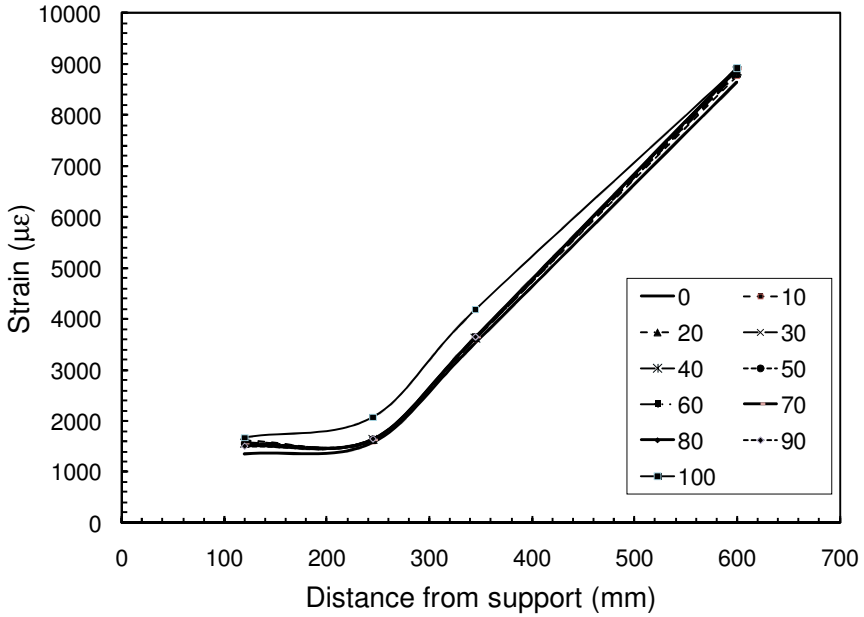

d-Strain distribution along steel rebar at different life

Figure A-32: Deflection and strains for beam S-SC-0%-78%

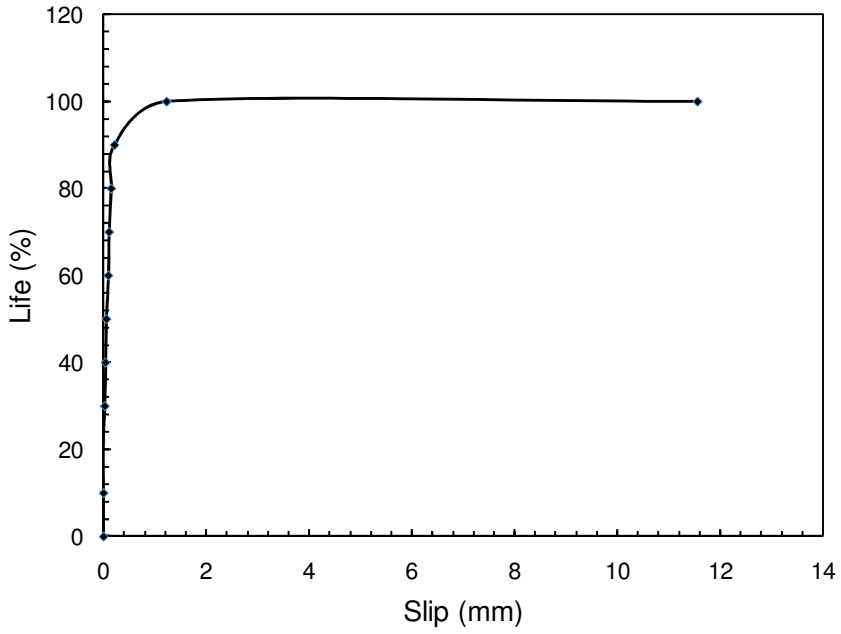

Figure A-33: Life versus CFRP rod end slip from epoxy for beam S-SC-0%-78%

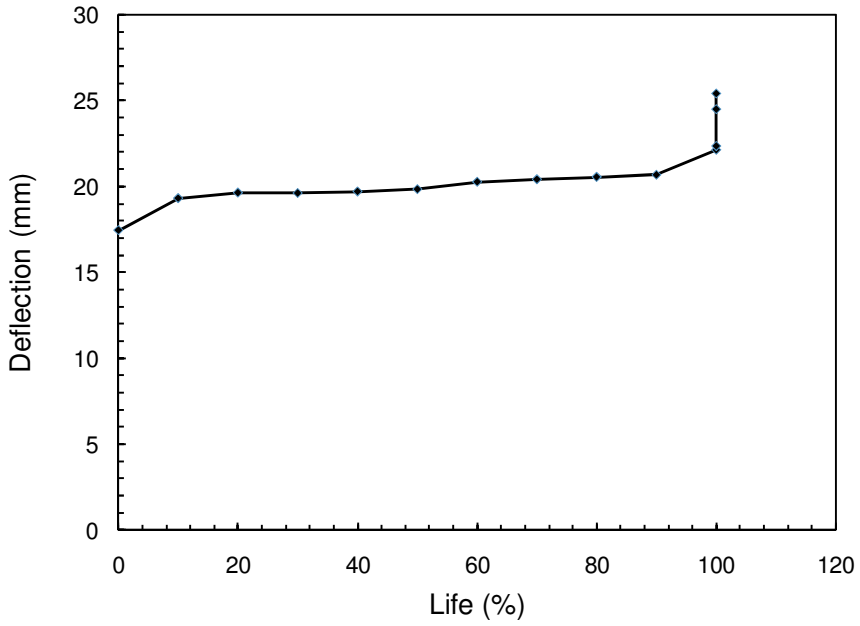

a-Mid-span deflection versus life

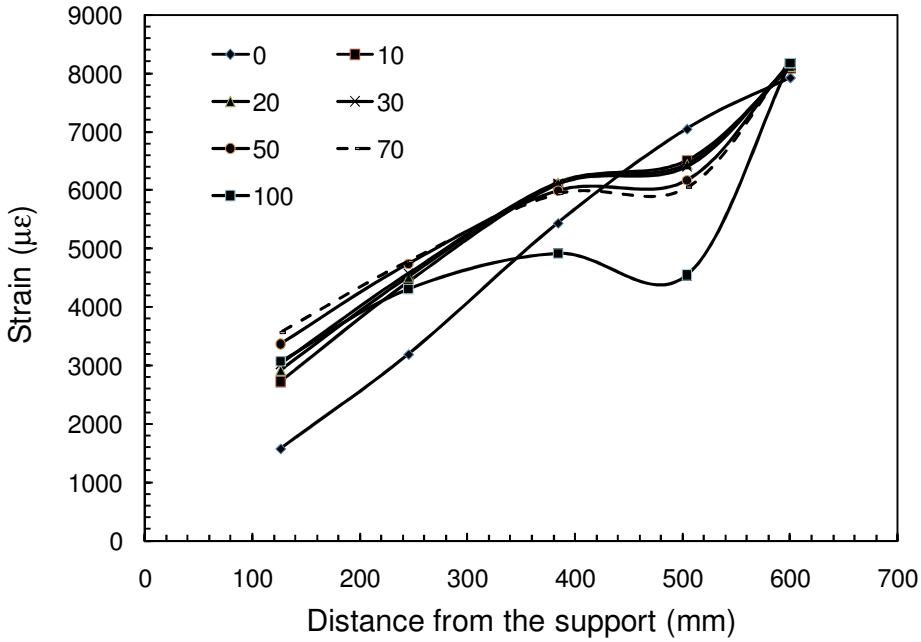

b-Strain distribution along the CFRP rod at different life

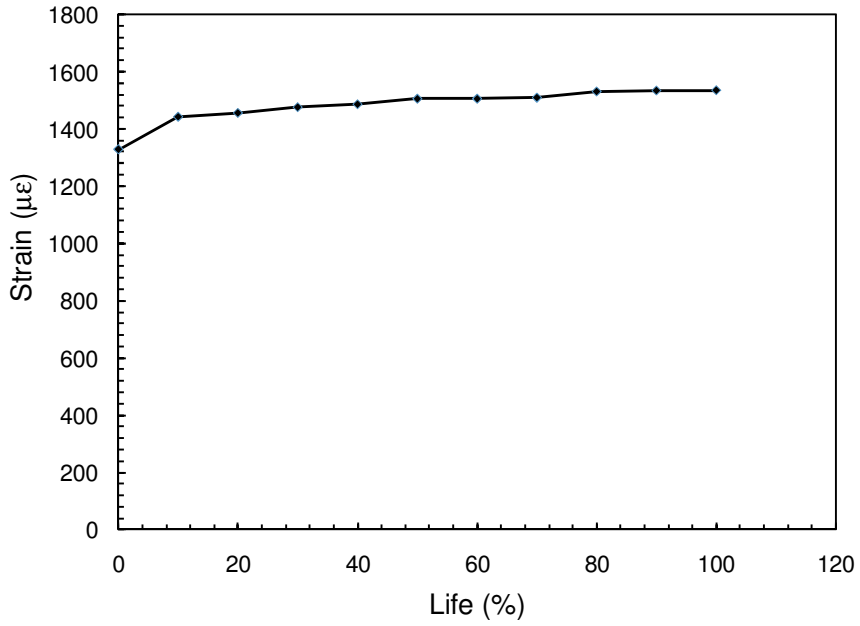

c-Mid-span concrete strain versus life

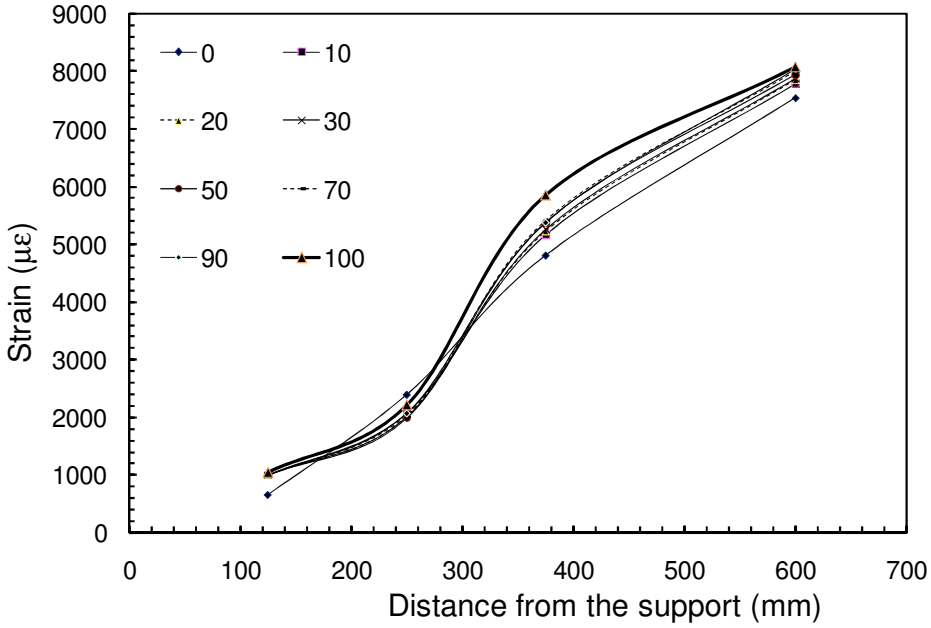

d-Strain distribution along steel rebar at different life

Figure A-34: Deflection and strains for beam S-SC-0%-76%

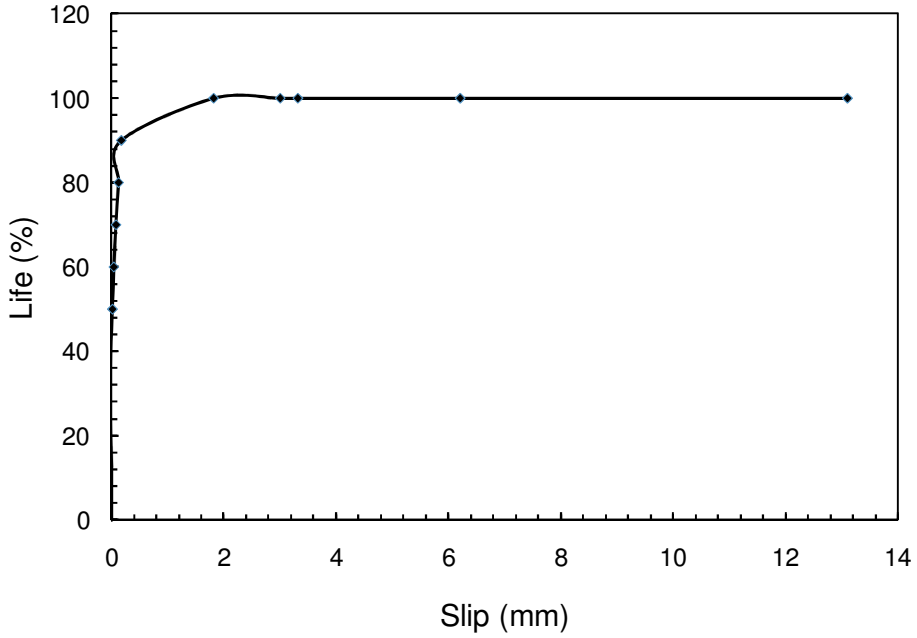

Figure A-35: Life versus CFRP rod end slip from epoxy for beam S-SC-0%-76%

Appendix B: Beams strengthened with prestressed CFRP rods

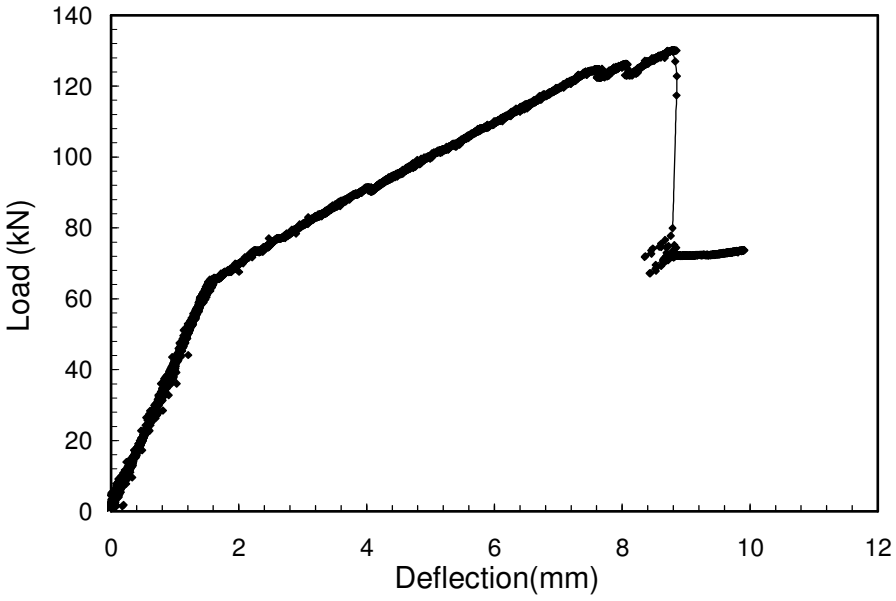

a-Mid span deflection

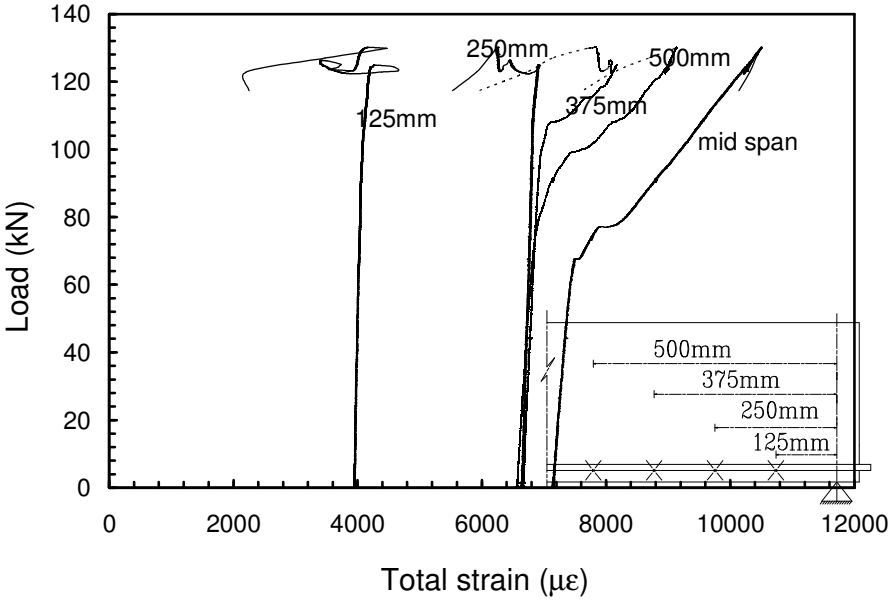

b-Total CFRP strain

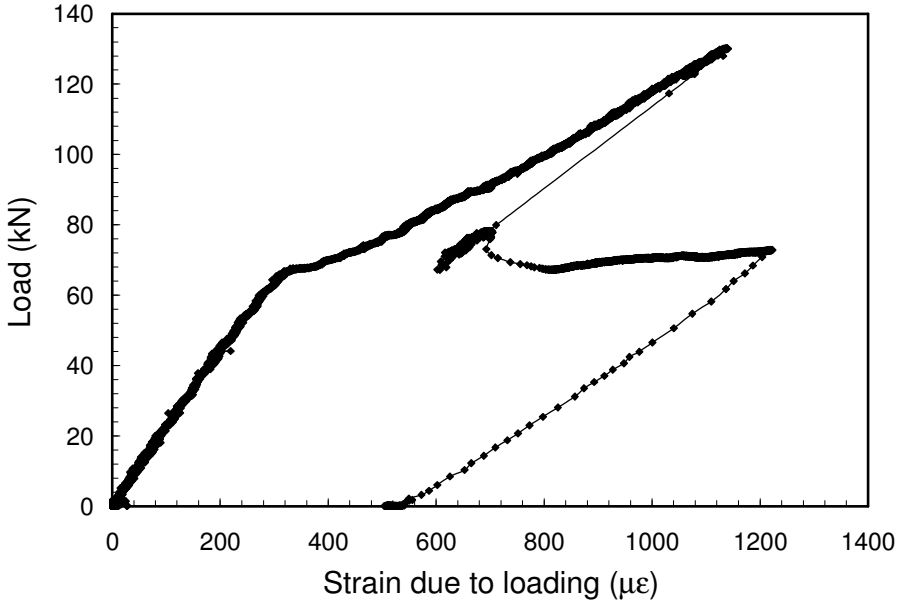

c-Mid-span concrete strain

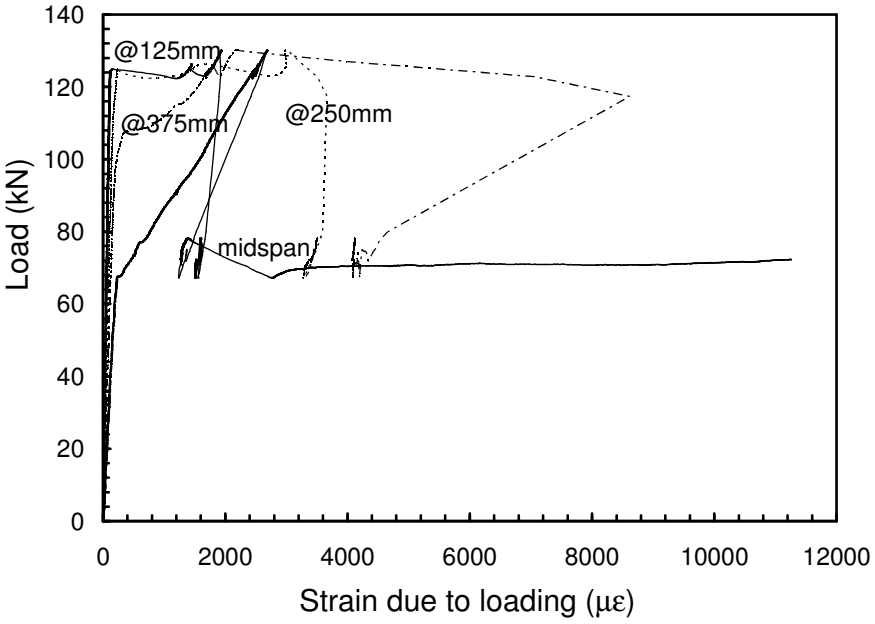

d- Steel rebar strain

Figure B-1: Load versus deflection and strains for beam S-SW-45%-M

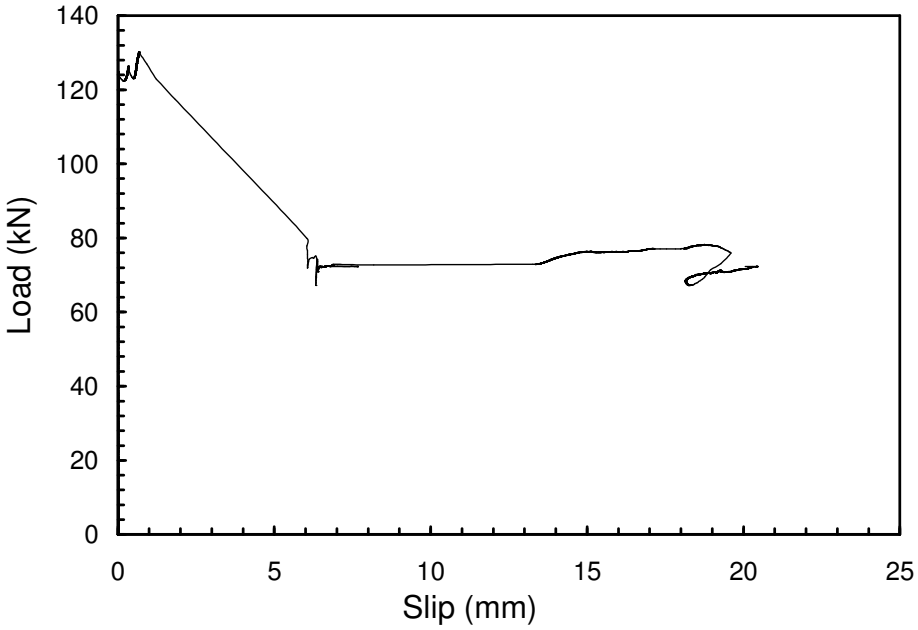

Figure B-2:Load versus end slip for beam S-SW-45%-M

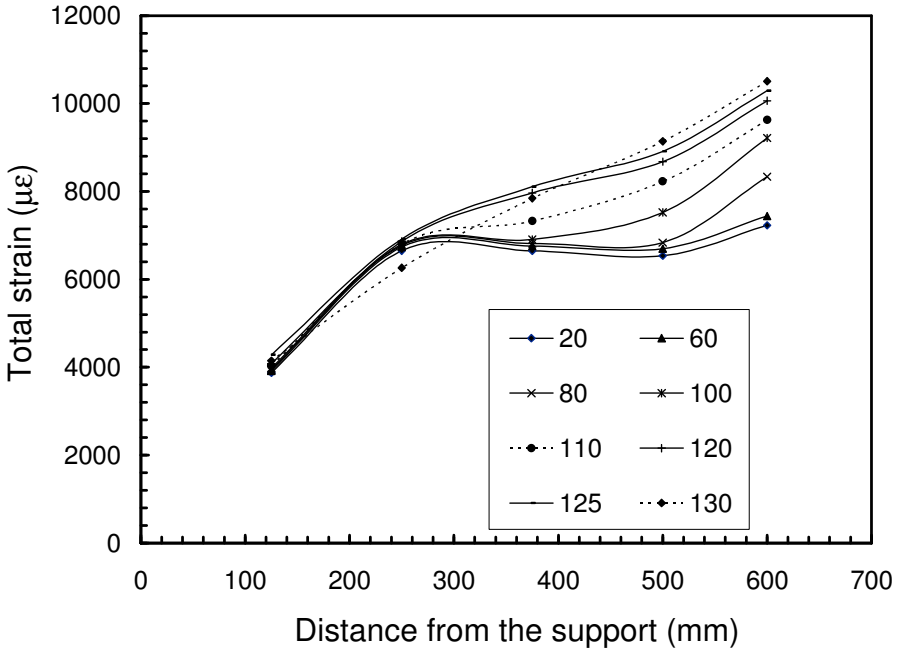

a-Total Strain in the CFRP rod at different load levels

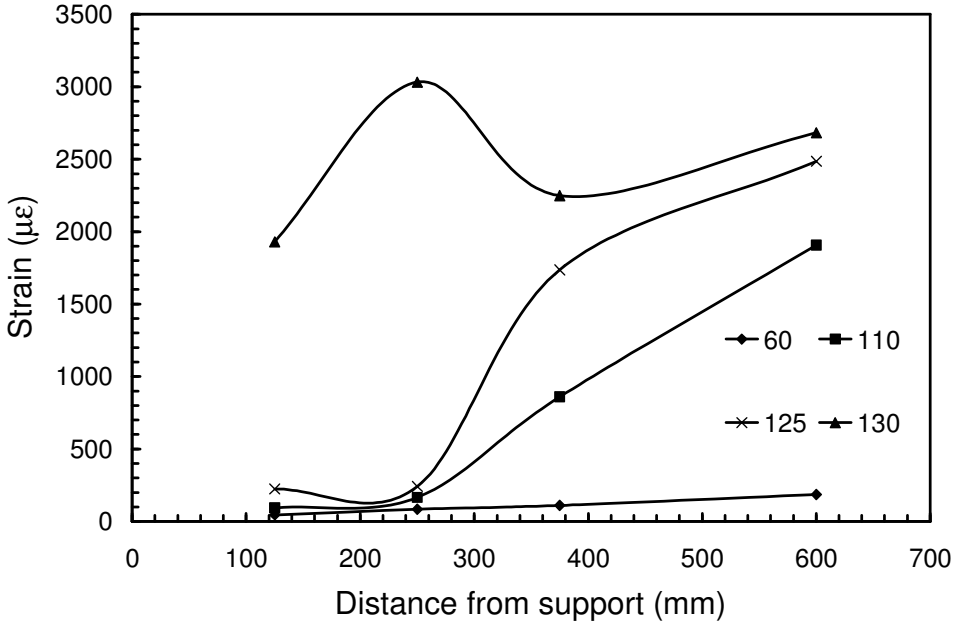

b- Strain in the steel rebar at different load levels

Figure B-3: Strain along the shear span for Beam S-SW-45%-M

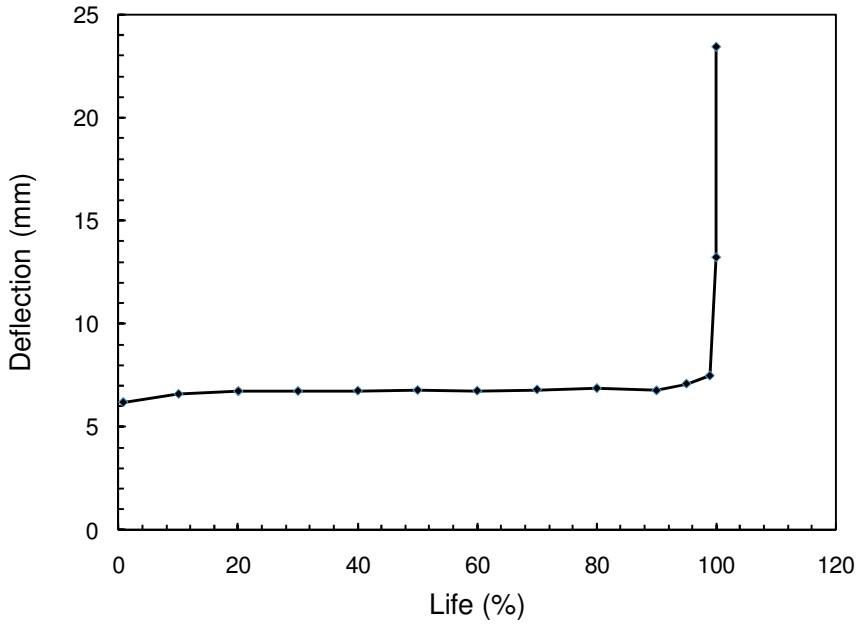

a-Mid-span deflection versus life

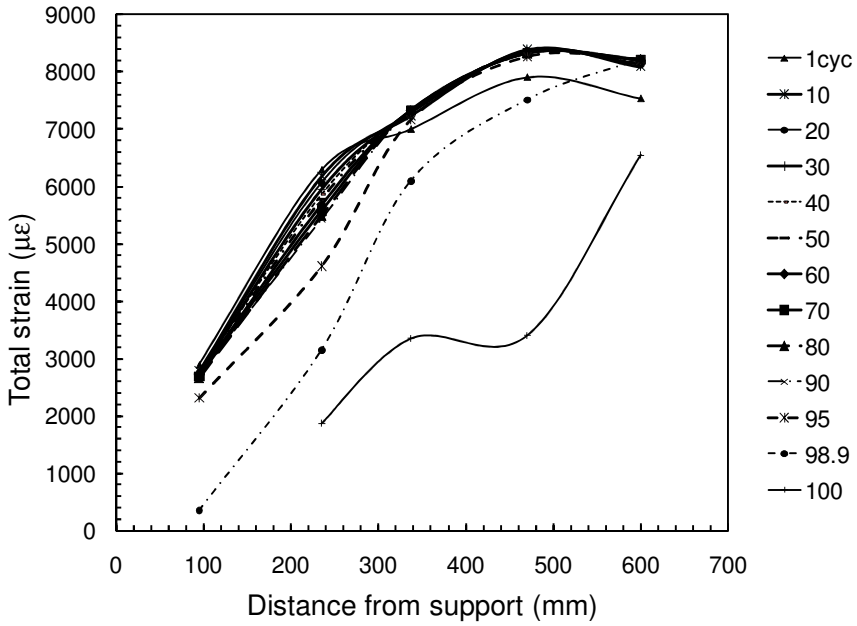

b-Total Strain in the CFRP rod at different load levels

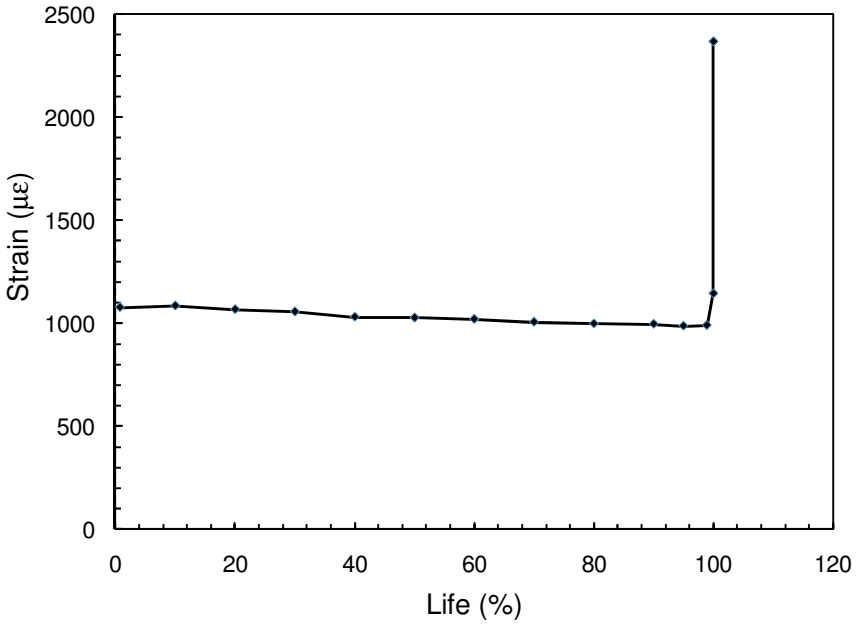

c-Mid-span concrete strain versus life

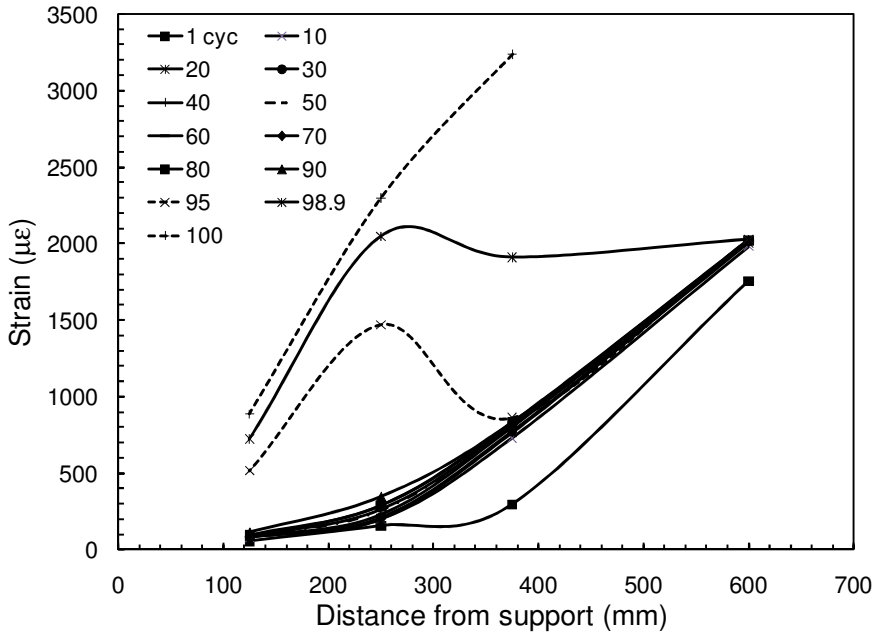

d- Strain in the steel rebar at different load levels

Figure B-4: Deflection and strains for Beam S-SW-45%-70%at different percentages of life

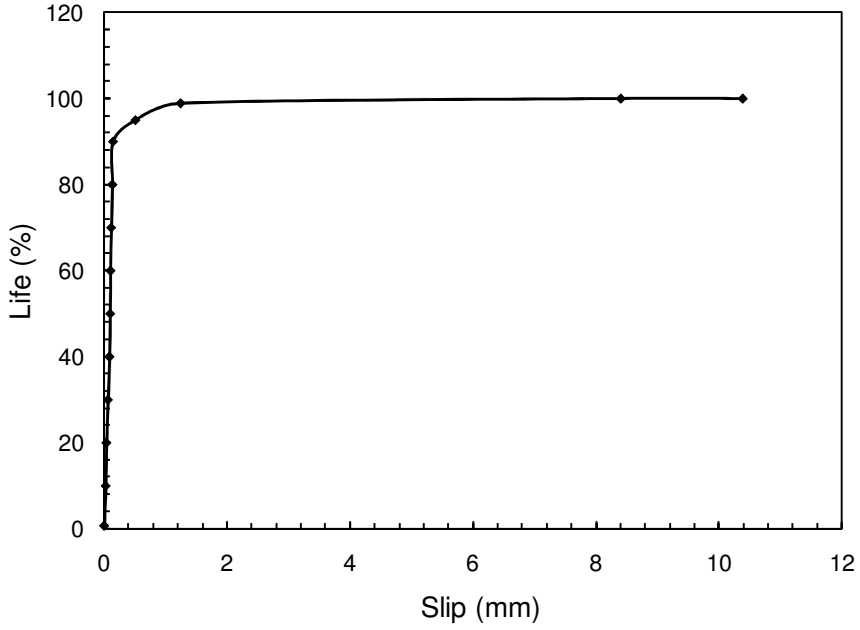

Figure B-5: Life versus CFRP rod end slip from epoxy for beam S-SW-45%-70%

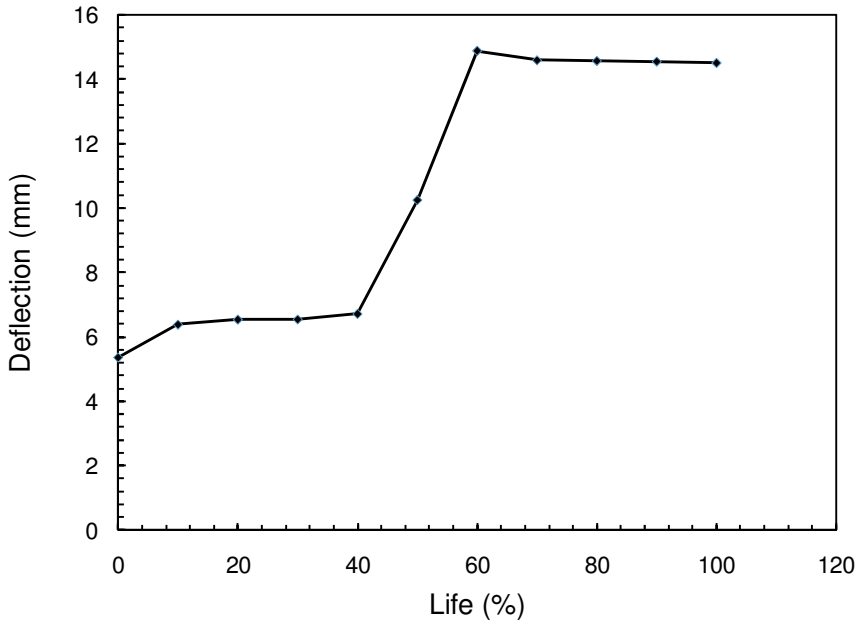

a-Mid-span deflection versus life

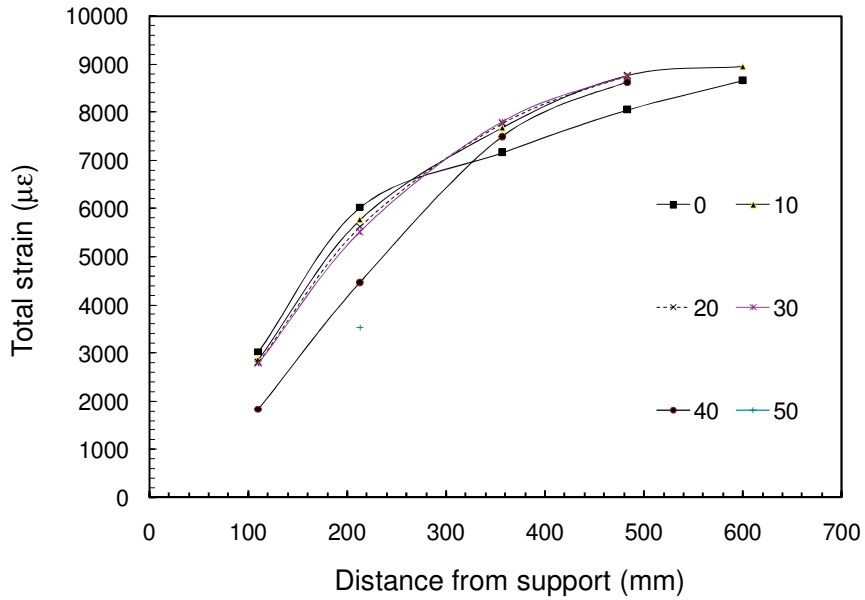

b-Total Strain in the CFRP rod at different load levels

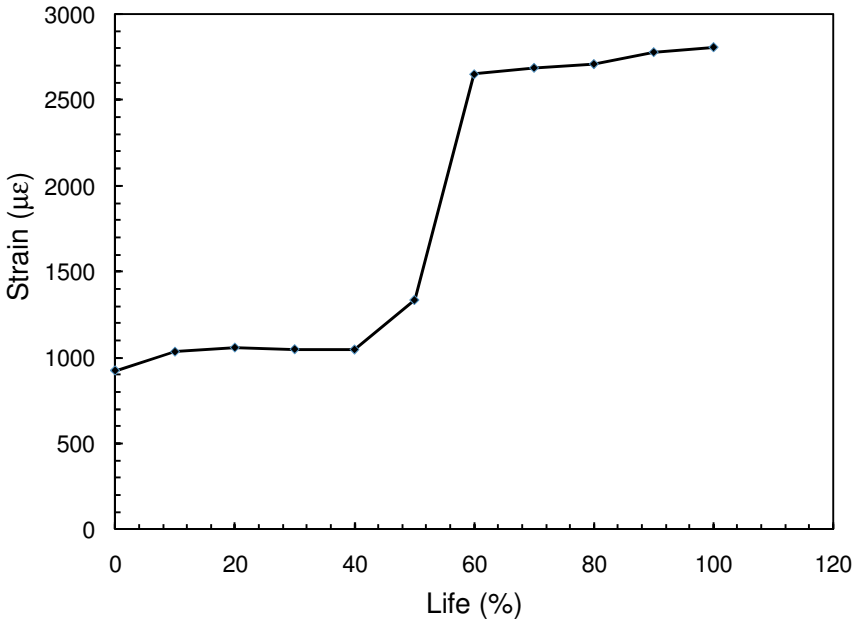

c-Mid-span concrete strain versus life

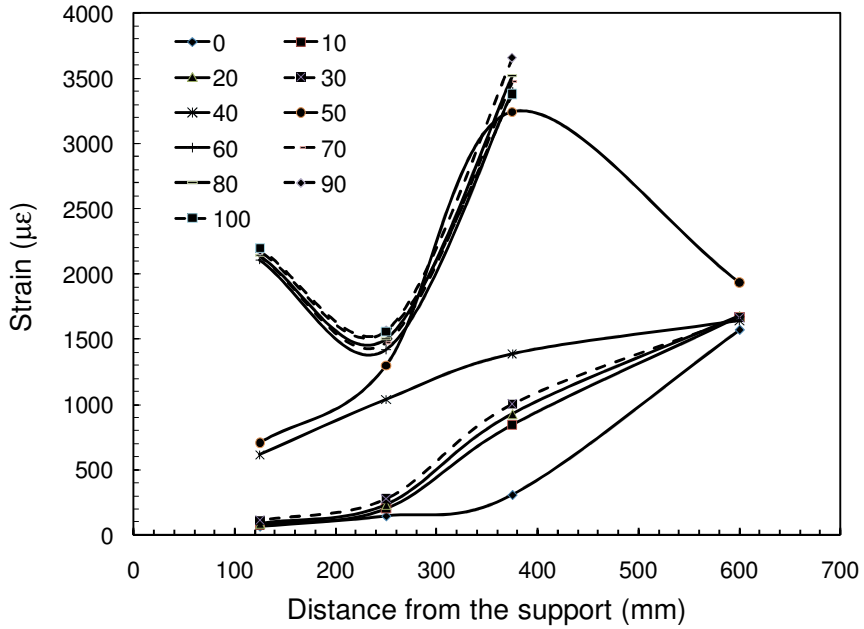

d- Strain in the steel rebar at different load levels

Figure B-6: Deflection and strains for Beam S-SW-45%-65% at different percentages of life

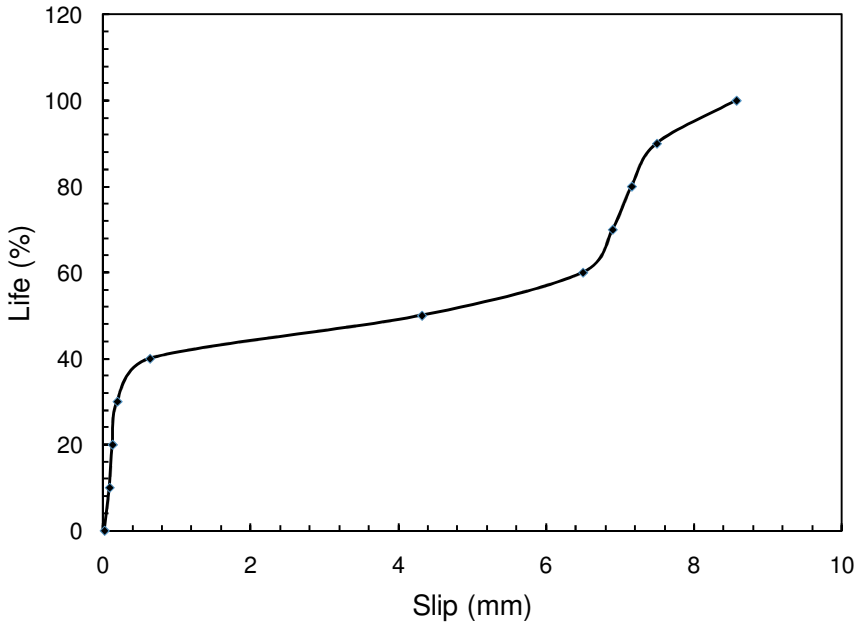

Figure B-7: Life versus CFRP rod end slip from epoxy for beam S-SW-45%-65%

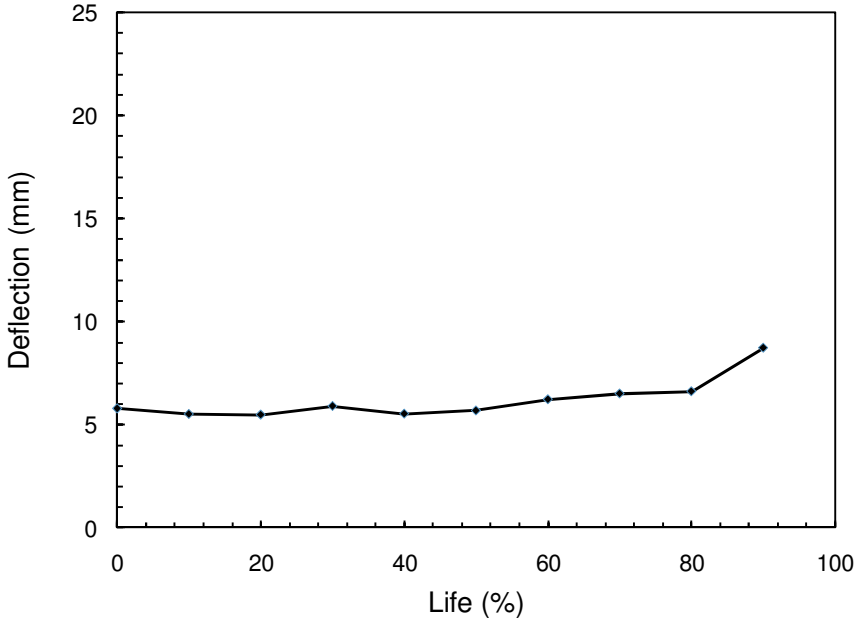

a-Mid-span deflection versus life

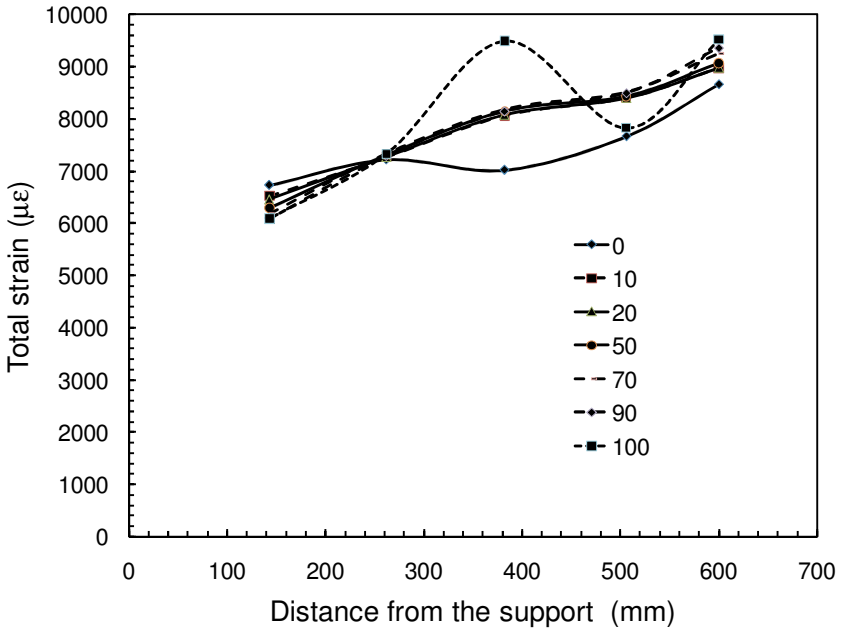

b-Total Strain in the CFRP rod at different load levels

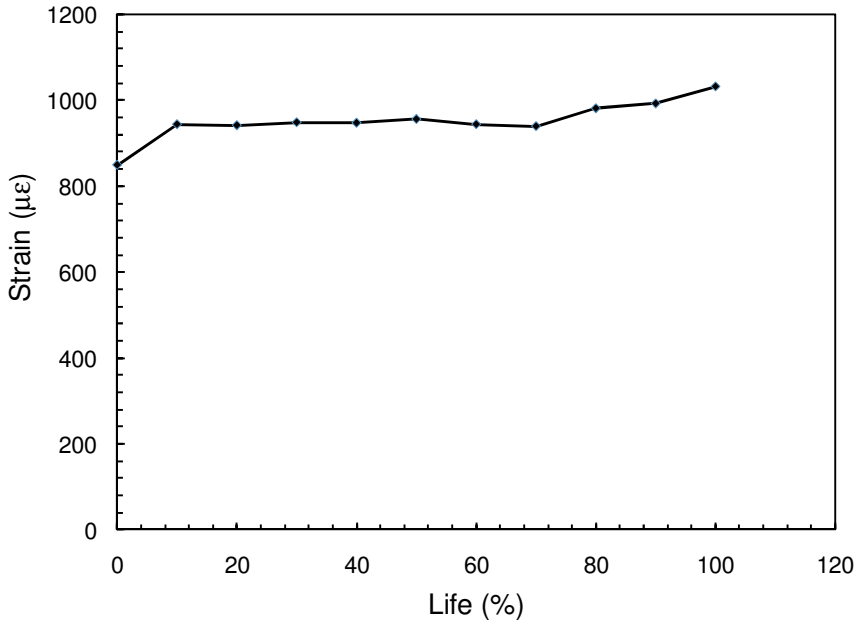

c-Mid-span concrete strain versus life

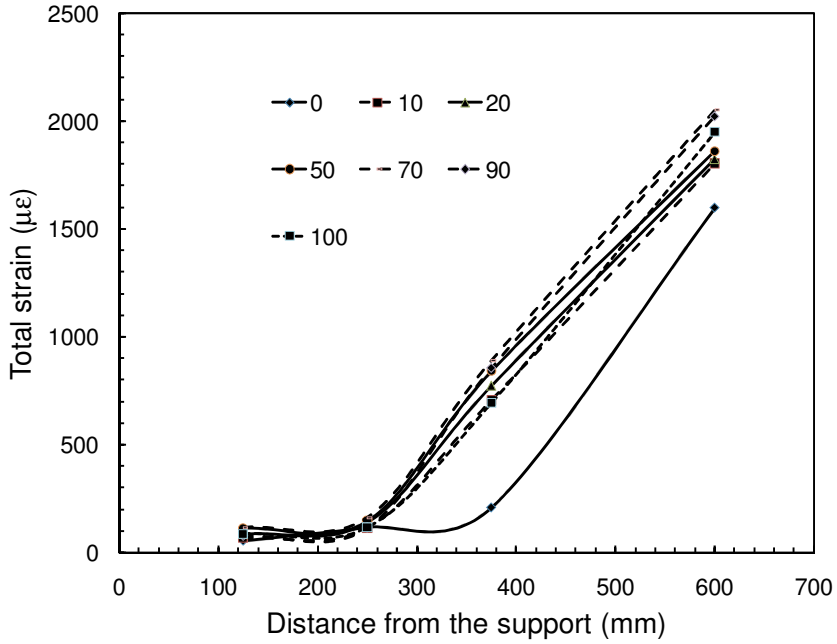

d- Strain in the steel rebar at different load levels

Figure B-8: Deflection and strains for Beam S-SW-45%-63% at different percentages of life

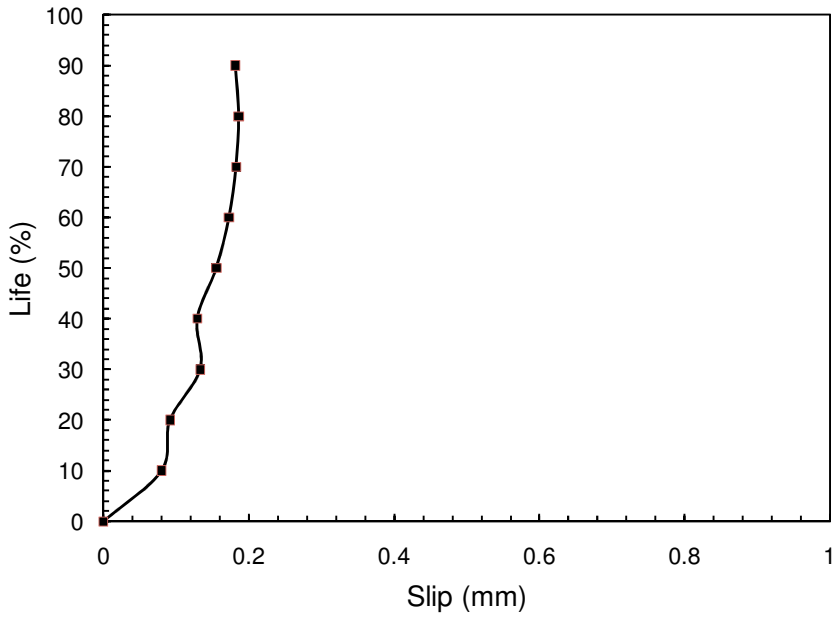

Figure B-9: Life versus CFRP rod end slip from epoxy for beam S-SW-45%-63%

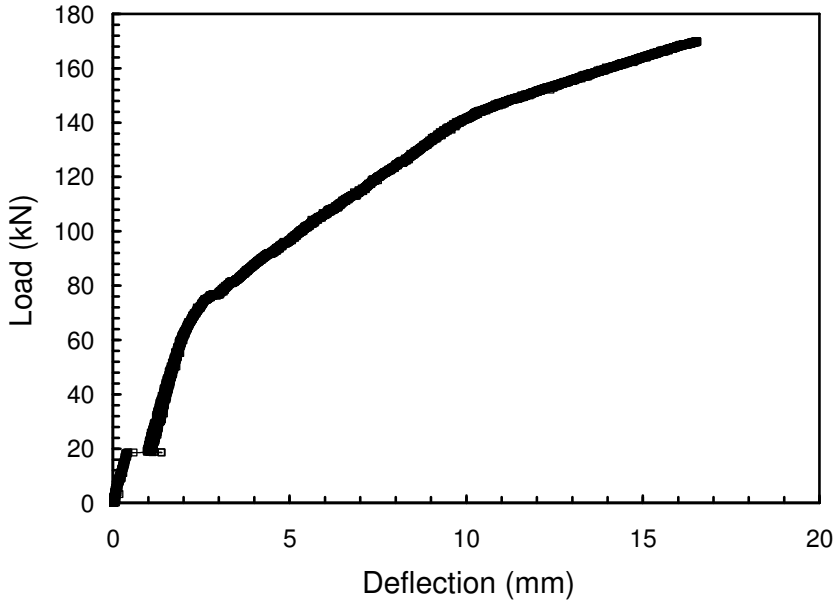

a-Mid-span deflection

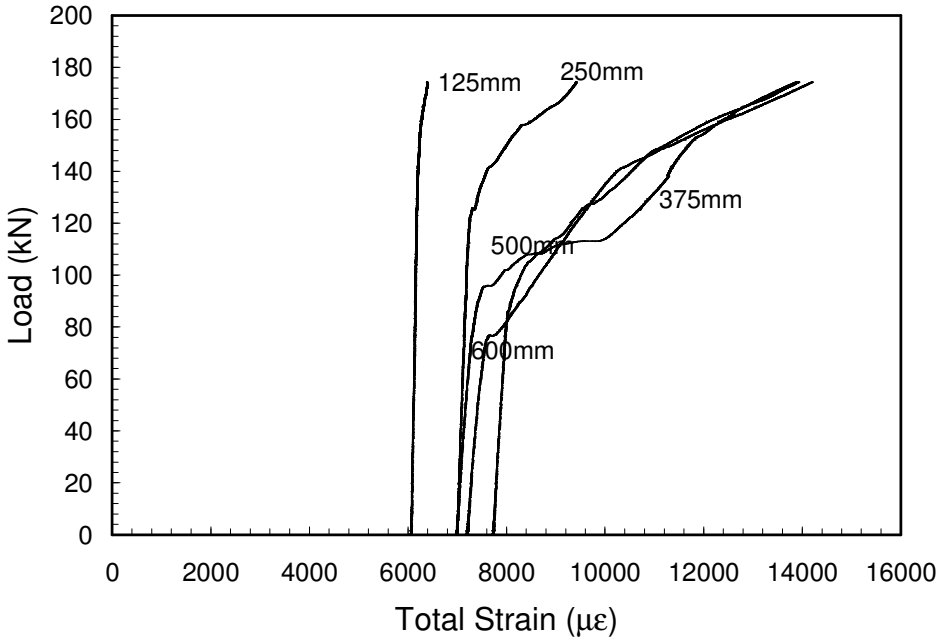

b-Total CFRP strain

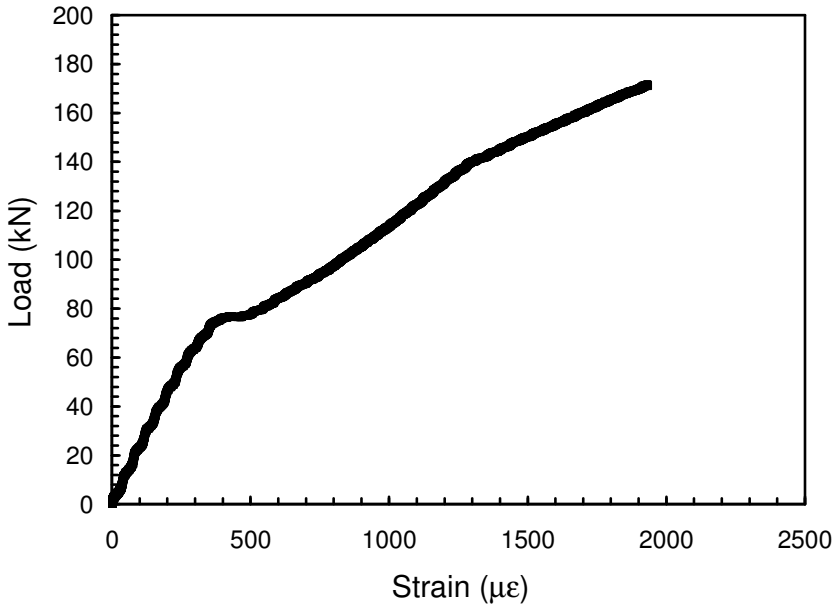

c-Mid-span concrete strain

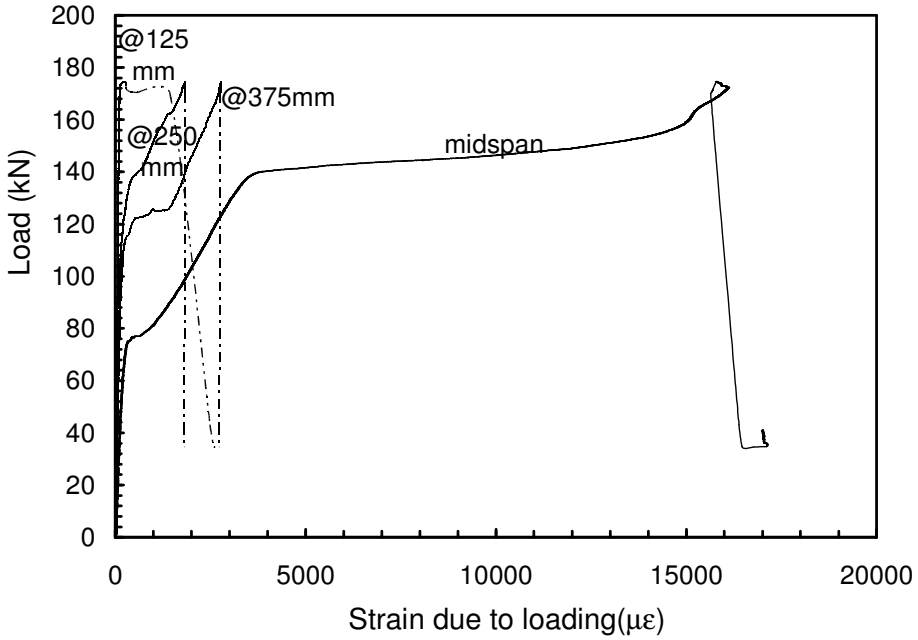

d- Steel rebar strain

Figure B-10: Load versus deflection and strains for Beam S-SC-40%-M

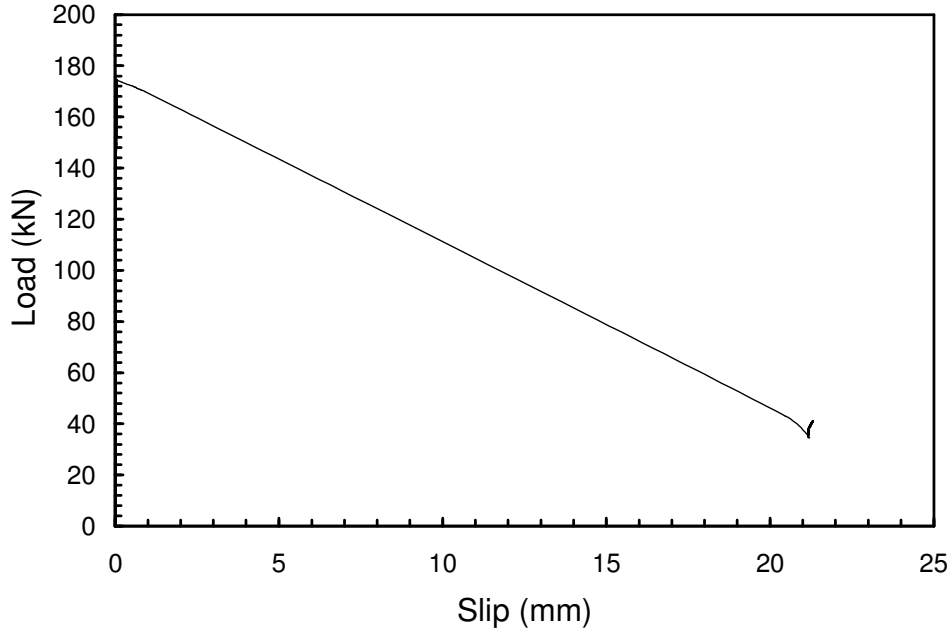

Figure B-11: Load versus end slip for Beam S-SC-40%-M

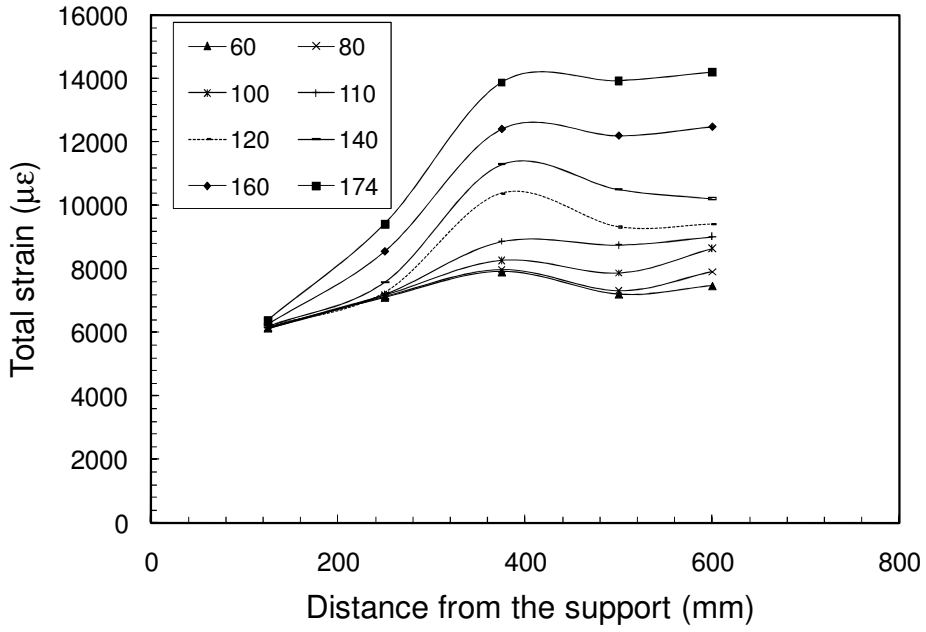

a-CFRP total strain

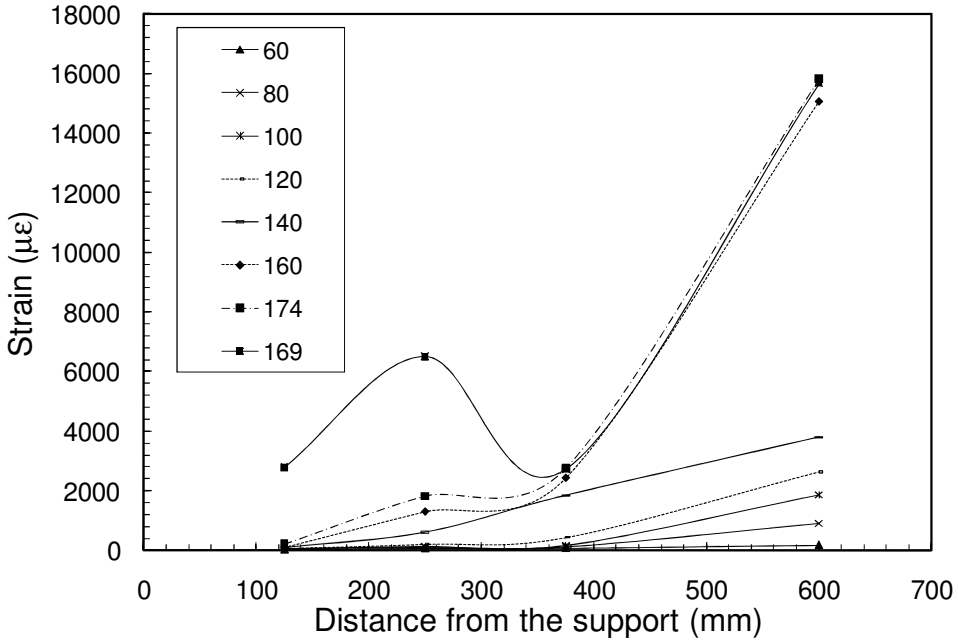

b-Steel rebar strain

Figure B-12: Strain profiles along the shear span for Beam S-SC-40%-M

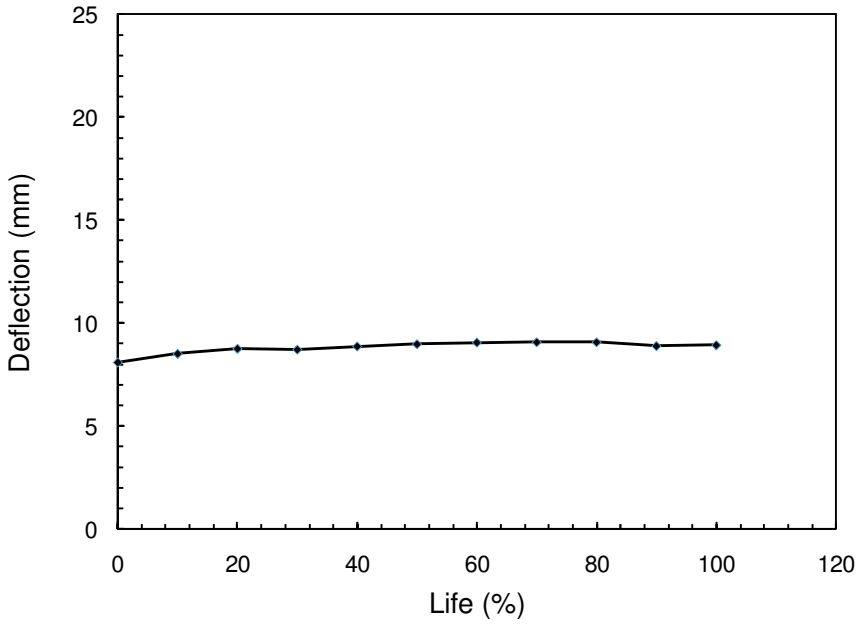

a-Mid-span deflection versus life

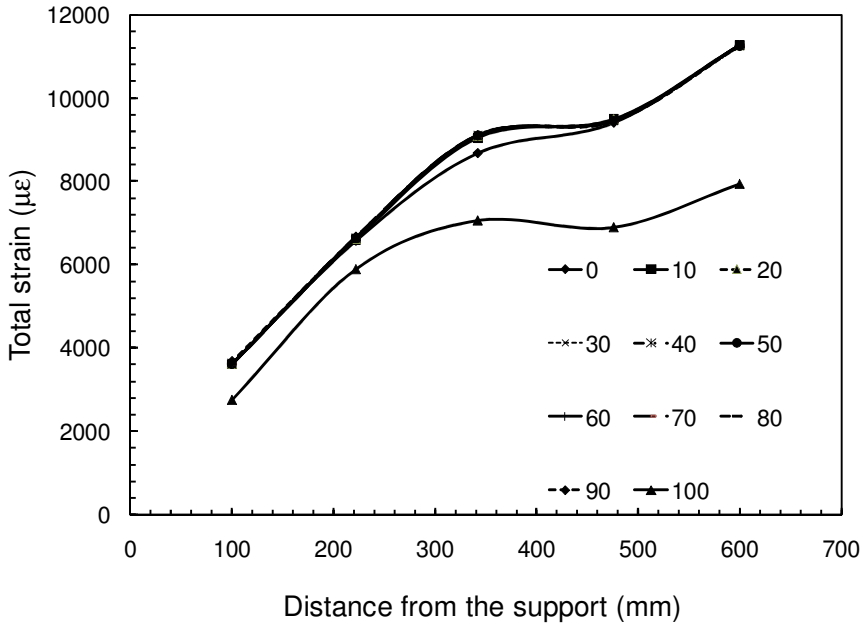

b-Total Strain in the CFRP rod at different load levels

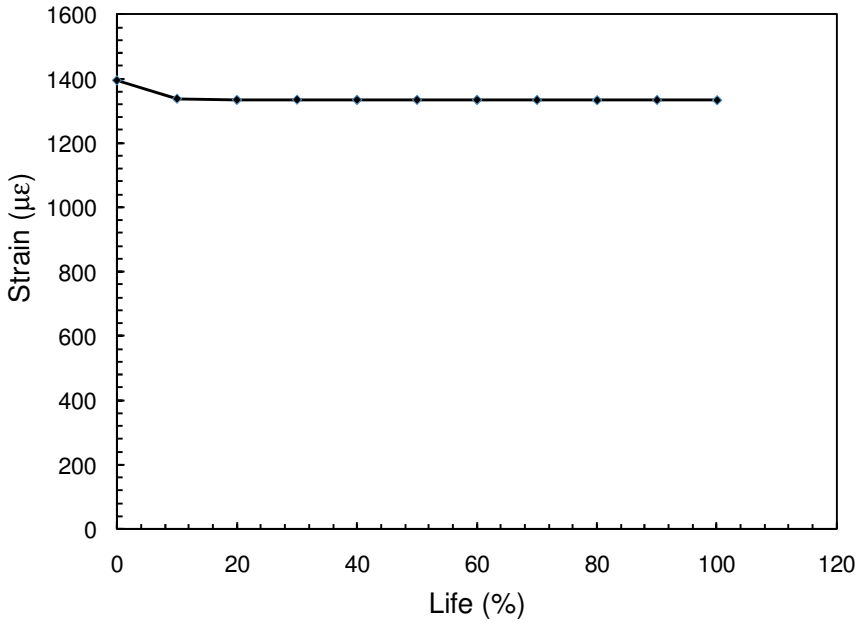

c-Mid-span concrete strain versus life

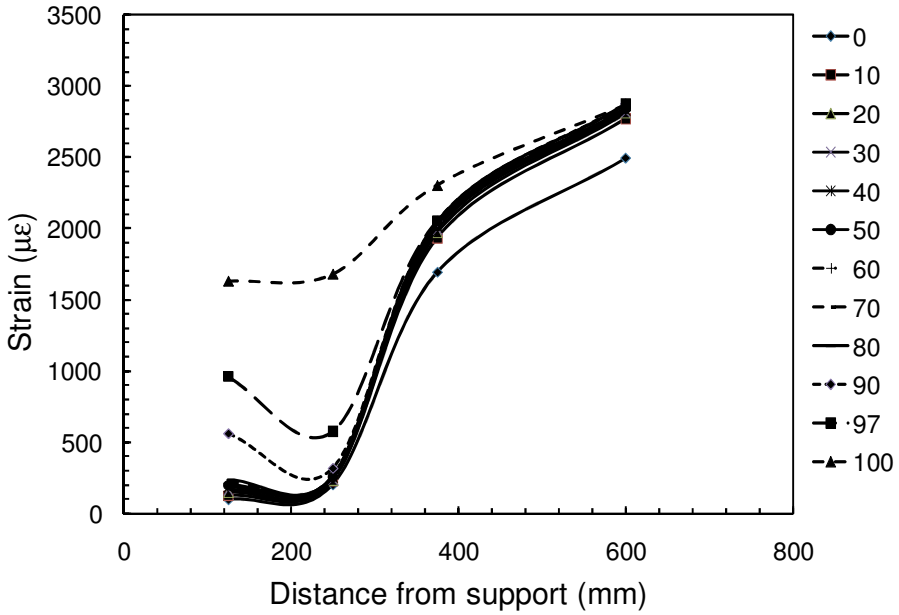

d- Strain in the steel rebar at different load levels

Figure B-13: Deflection and strains for Beam S-SC-40%-63% at different percentages of life

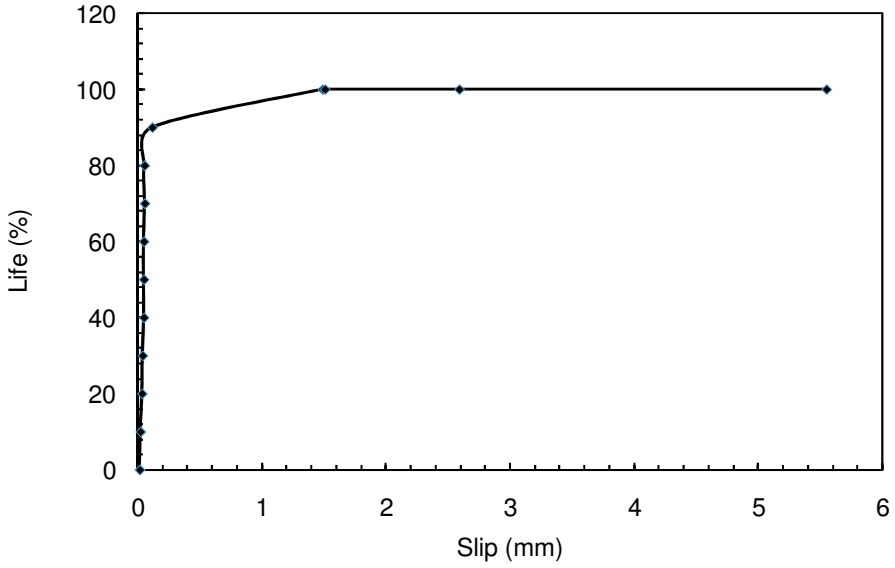

Figure B-14: Life versus CFRP rod end slip from epoxy for beam S-SC-40%-63%

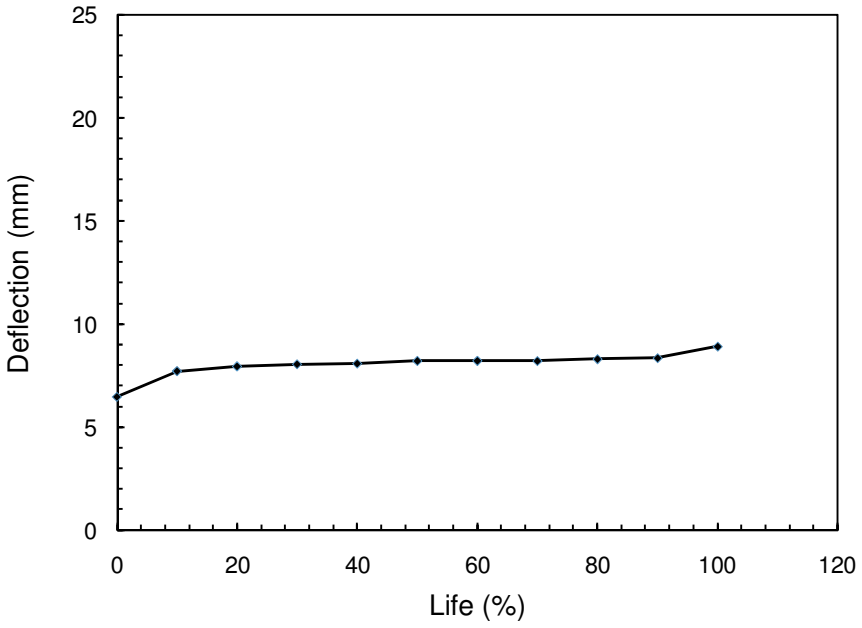

a-Mid-span deflection versus life

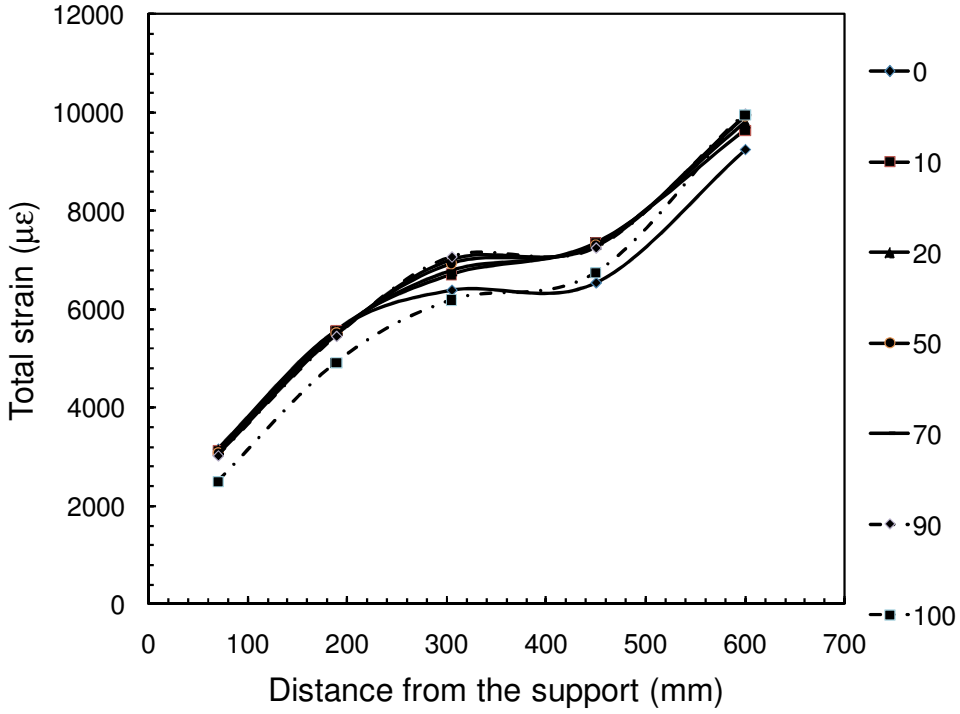

b-Total Strain in the CFRP rod at different load levels

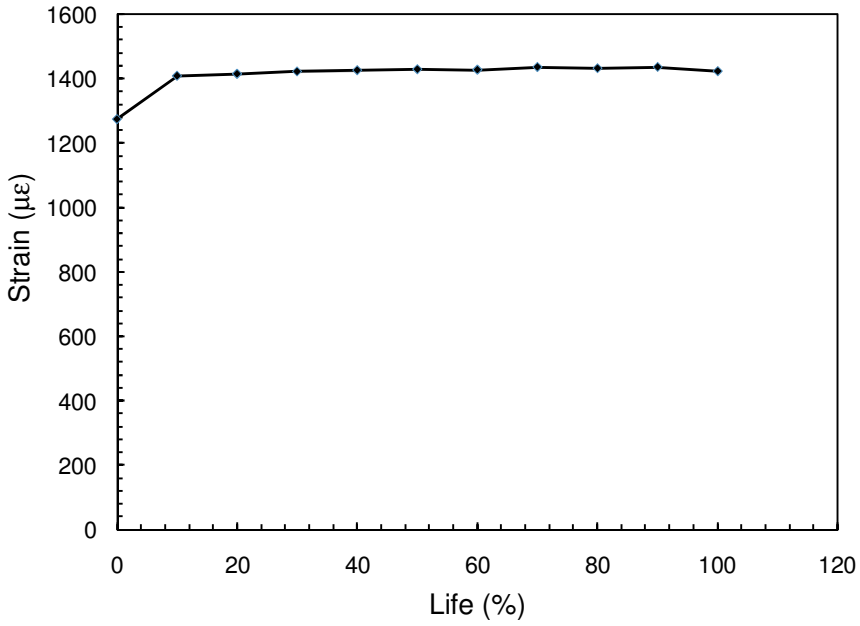

c-Mid-span concrete strain versus life

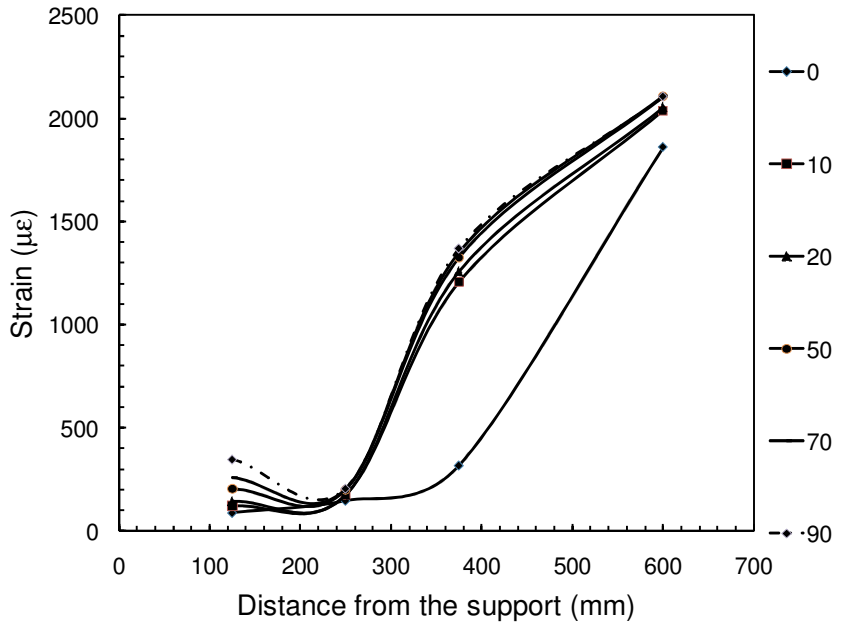

d- Strain in the steel rebar at different load levels

Figure B-15: Deflection and strains for Beam S-SC-40%-58% at different percentages of life

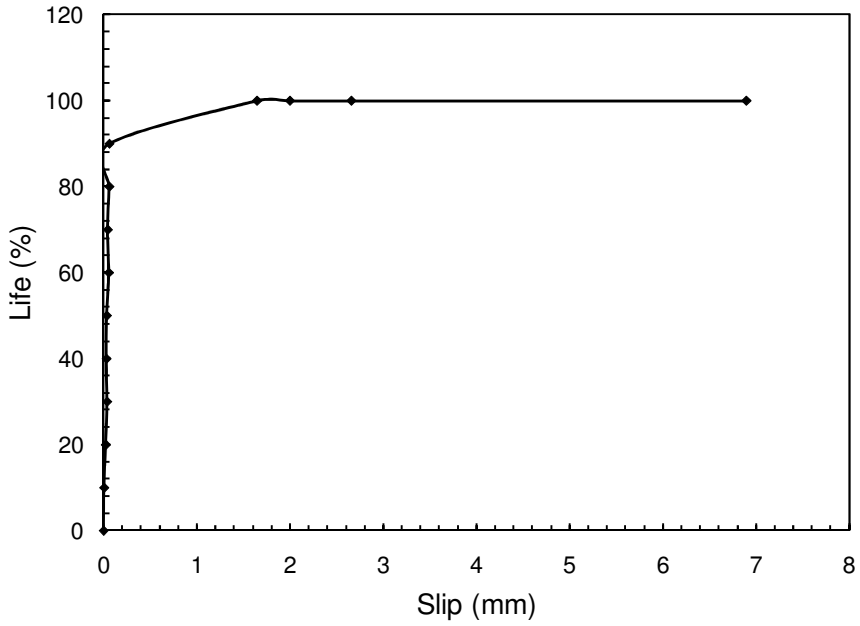

Figure B-16: Life versus CFRP rod end slip from epoxy for beam S-SC-40%-58%

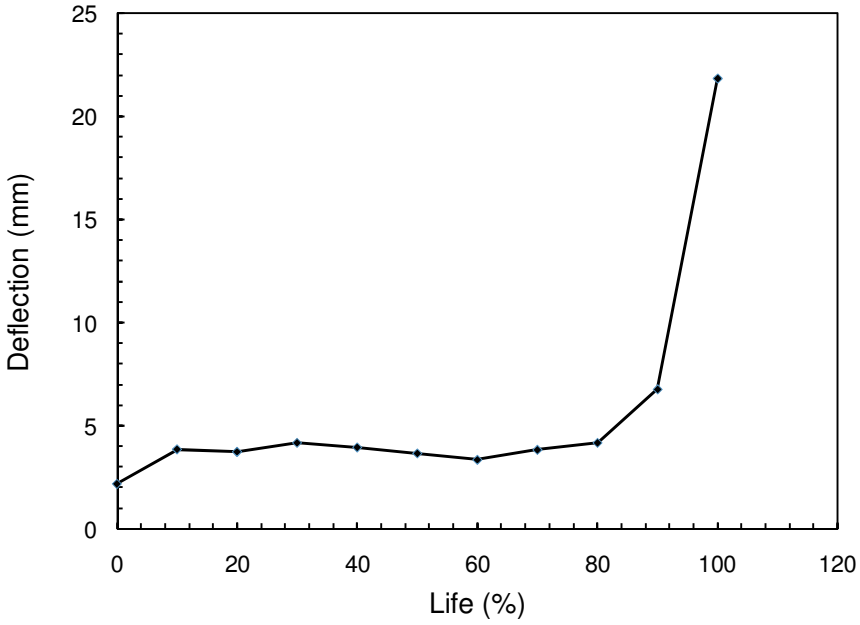

a-Mid-span deflection versus life

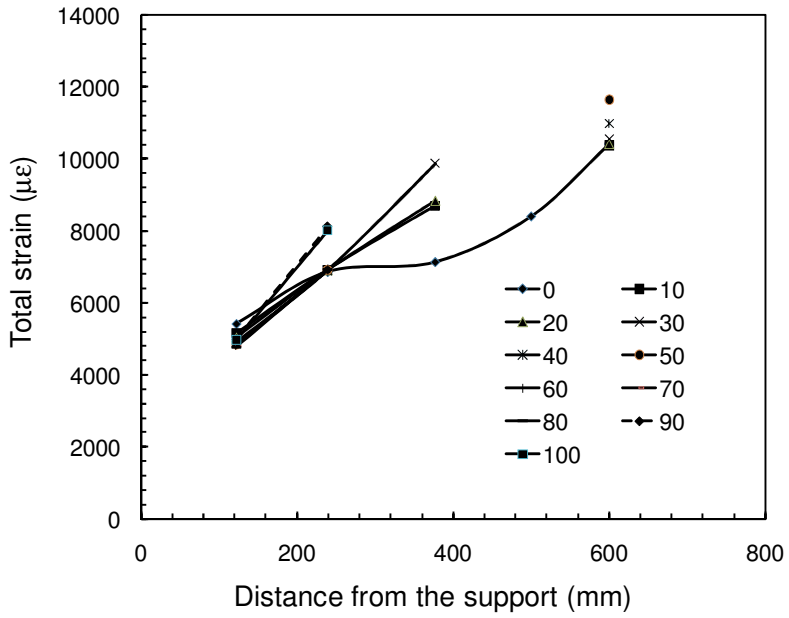

b-Total Strain in the CFRP rod at different load levels

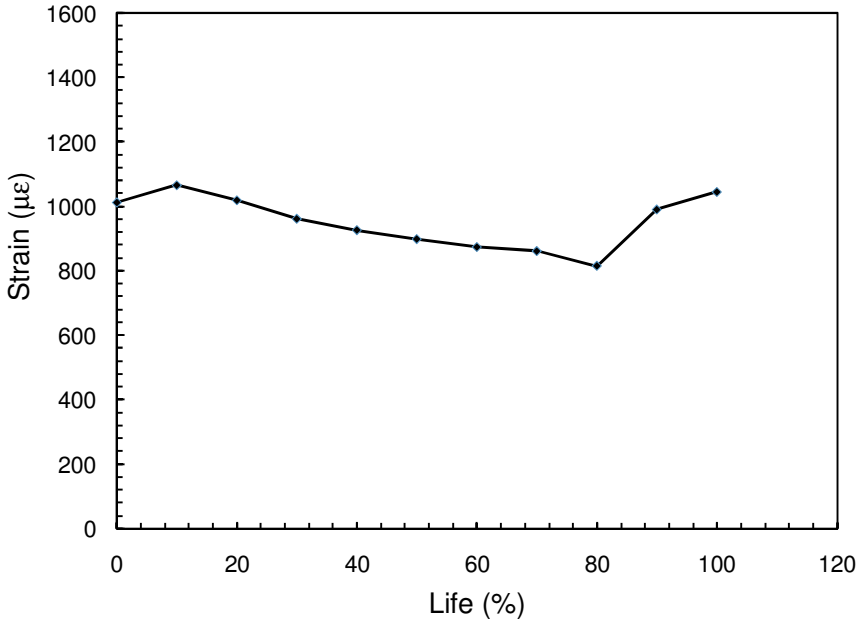

c-Mid-span concrete strain versus life

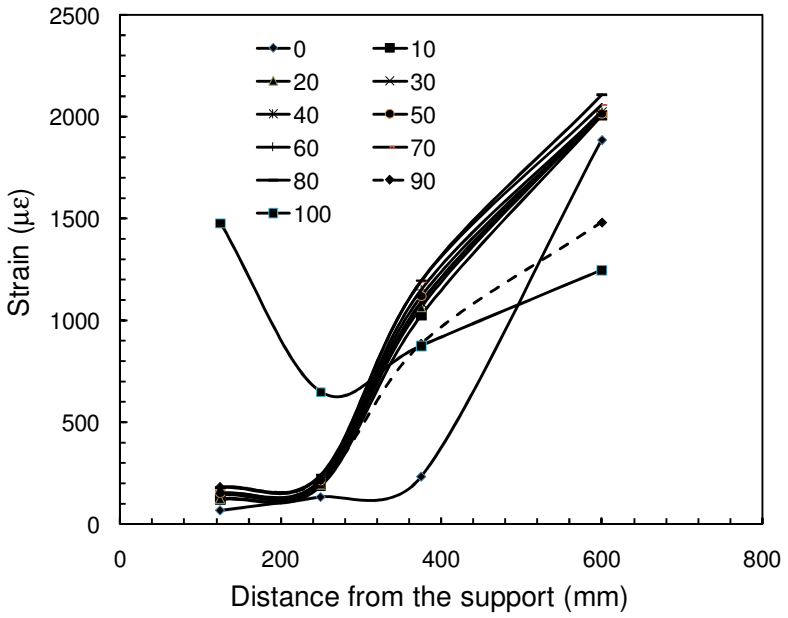

d- Strain in the steel rebar at different load levels

Figure B-17: Deflection and strains for Beam S-SC-40%-53%at different percentages of life

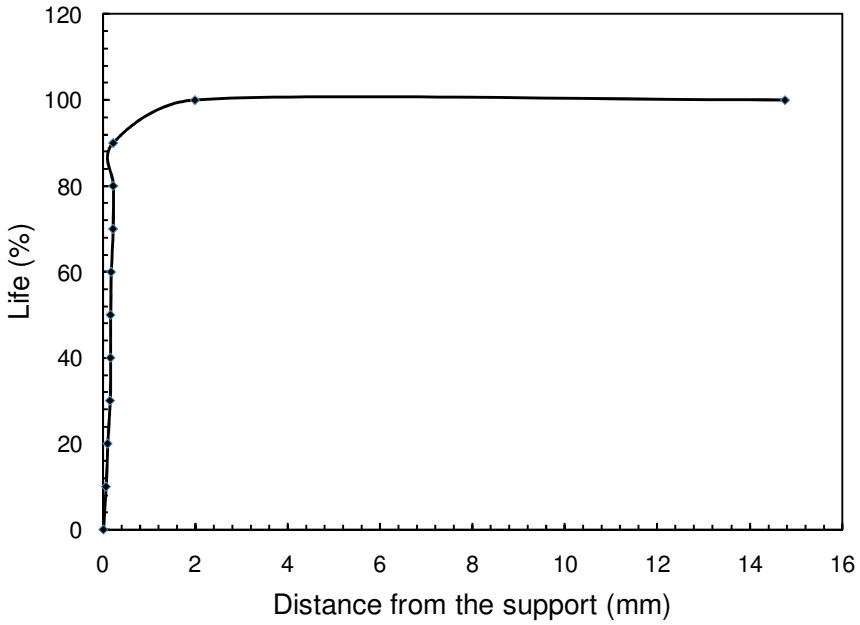

Figure B-18: Life versus CFRP rod end slip from epoxy for beam S-SC-40%-53%

Bibliography

ACI Committee 215, “Considerations for Design of Concrete Structures Subjected to Fatigue Loading, Manual of concrete Practice”, American Concrete Institute, 1997.

ACI Committee 440.2, “Guide for the Design and Construction of Externally Bonded FRP Systems for Strengthening Concrete Structures, Manual of concrete Practice”, American Concrete Institute, 2008.

ACI Committee 440.3, “Guide Test Methods for Fiber-Reinforced Polymers (FRPs) for Reinforcing or Strengthening Concrete Structures, Manual of concrete Practice”, American Concrete Institute, 2004.

Achintha P. M. M. and Burgoyne C. J., “Fracture Mechanics of Plate Debonding”, Journal of Composites for Construction, Vol. 12, No. 4, August 2008.

Aidoo J., Harries K.A., and Petrou M.F., “ Fatigue Behaviour of CFRP Strengthened Reinforced Concrete Bridge Girders”, ASCE Journal of Composites in Construction, Vol.7, No. 6, pp. 501-518, 2004.

Aidoo J., Harries K.A., and Petrou M.F., “ Full-Scale Experimental Investigation of Repair of Reinforced Concrete Interstate Bridge Using CFRP Materials”, ASCE Journal of Bridge Engineering, Vol.11, No. 3, pp. 350-358, 2006.

Al-Mahmoud F., Castel A., Francois R., and Tourner C., "Anchorage and Tension Stiffening Effect between Near Surface Mounted CFRP Rods and Concrete", Cement and Concrete Composites, 2010. (In press)

Al-Mayah A., "Interfacial Behaviour of CFRP-Metal Couples for Wedge Anchor Systems", PhD Thesis, University of Waterloo, Waterloo, Ontario, Canada, 2004.

Badawi M., "Monotonic and Fatigue Flexural Behaviour of RC Beams Strengthened with Prestressed NSM CFRP Rods", PhD Thesis, Department of Civil and Environmental Engineering, University of Waterloo, Canada, 2007.

Castro EK., Melo GS., and Nagato Y., "Flexural Strengthening of RC "T" Beams with Near Surface Mounted (NSM) FRP Reinforcements", In Proceedings of the FRPCS-8, ACI, 2007.

De Lorenzis L., "Strengthening of RC Structures with Near Surface Mounted FRP Rods", PhD Thesis, Department of Innovation Engineering, University of Lecce, Italy, 2002.

De Lorenzis L., Lundgren K., and Rizzo A., "Anchorage Length of Near Surface Mounted FRP Bars for Concrete Strengthening – Experimental Investigation and Numerical Modeling", ACI Structural Journal, Vol. 101, No. 2, Pp.269–278, 2004.

De Lorenzis L. and Nanni A., "Bond between NSM Fiber-Reinforced Polymer Rods and Concrete in Structural Strengthening", ACI Structural Journal, 99(2):123–32, 2002.

De Lorenzis L., Nanni A., and La Tegola A., "Flexural and Shear Strengthening of Reinforced Concrete Structures with Near Surface Mounted FRP Rods", In: Proceedings ACMBS III, Ottawa (Canada), 2000.

De Lorenzis L., Rizzo A., and La Tegola A. A., "Modified Pull-out Test for Bond of Near-Surface Mounted FRP Rods in Concrete", Composites-Part B: Engineering, Vol. 33, No. 8, pp. 589–603, 2002.

Dowling N., "Mechanical Behavior of Materials", Prentice Hall; 3rd edition, 2006.

De Lorenzis L. and Teng J.G., "Near-Surface Mounted FRP Reinforcement: An Emerging Technique for Strengthening Structures", Journal of Composites: Part B, Vol. 38, pp. 119-143, 2007.

Galati D. and De Lorenzis L., "Effect of Construction Details on the Bond Performance of NSM FRP Bars in Concrete", Advances in Structural Engineering, Vol. 12, No. 5, 2009.

Garrity SW., “Near-Surface Reinforcement of Masonry Arch Highway Bridges”, In: Proceedings of the 9th Canadian masonry symposium, Fredericton (Canada), CD-ROM, 2001.

Harries K.A., and Aidoo J., “ Debonding and Fatigue Related Strain Limits for Externally Bonded FRP”, ASCE Journal of Composites in Construction, Vol. 9, No. 1, pp. 87-90, 2006.

Harries K.A., Benjamin R. and Zorn A., “Experimental Evaluation of Factors Affecting Monotonic and Fatigue Behavior of Fiber-Reinforced Polymer-to-Concrete Bond in Reinforced Concrete Beams”, ACI Structural Journal, Vol. 104, No. 6, pp. 667-674, 2007.

Harries K.A., Aidoo J., Zorn A., and Quattlebaum J. “Deterioration of FRP-to-Concrete Bond Under Fatigue Loading”, Advances in Structural Engineering, Vol. 9, No. 6, pp. 779-789, 2006.

Harries, K.A., Richard, M. and Kim, Y. “Fatigue of CFRP Retrofitted Damaged Steel Beams”, Proceedings of the 2010 International Conference on Structural Faults and Repair, Edinburgh, June 2010.

Hassan T. and Rizkalla S., "Investigation of Bond in Concrete Structures Strengthened with Near Surface Mounted Carbon Fiber Reinforced Polymer Strips", ASCE Journal of Composites for Construction, Vol. 7, No. 3, pp. 248-257, 2003.

Hassan T. and Rizkalla S., "Bond Mechanism of Near Surface Mounted Fiber Reinforced Polymer Bars for Flexural Strengthening of Concrete Structures", ACI Structural Journal, Vol. 101, No. 6, pp.830-839, 2004.

Huang D. and Lyons J., " Numerical Stress Analysis of the Bond between a Reinforced Concrete T-Beam and FRP Sheets", Journal of Reinforced Plastics and Composites, Vol. 26, No. 12, 2007.

Kalayci A. S., Yalim B., and Mirmiran A., "Construction Tolerances and Design Parameters for NSM FRP Reinforcement in Concrete Beams", Construction and Building Materials, Vol. 24, pp. 1821-1829, 2010.

Mazzotti C., Savoia M., and Ferracuti B., "FRP – Concrete Delamination Results Adopting Different Experimental Pure Shear Set Ups", 11th International Conference on Fracture, Italy, March 2005.

Nordin H. and Taljsten B., "Concrete Beams Strengthened with Prestressed Near Surface Mounted CFRP", American Society of Civil Engineers (ASCE), Journal of Composites for Construction, Vol. 10, No. 1, pp. 60-68, 2006.

Novidis D., Pantazopoulou S.J., and Tentolouris E., "Experimental Study of Bond of NSM-FRP Reinforcement", Construction and Building Materials, Vol. 21, pp. 1760-1770, 2007 (online 5 October 2006).

Novidis D. and Pantazopoulou S.J., "Bond Tests of Short NSM-FRP and Steel Bar Anchorages", American Society of Civil Engineers (ASCE), Journal of Composites for Construction, Vol. 12, No. 3, pp. 323-333, 2008.

Oehlers, D.J., " FRP plates Adhesively Bonded to Reinforced Concrete Beams: Generic Debonding Mechanism", Advances in Structural Engineering, Vol. 9, No. 6, pp. 737-750, 2006.

Parretti R. and Nanni A., "Strengthening of RC Members using Near Surface Mounted FRP Composites: Design Overview", Advances in Structural Engineering, Vol. 7, No. 6, pp. 469-483, 2004.

Quattlebaum J.B., Harries K.A., and Petrou M.F., "Comparison of Three CFRP Flexural Retrofit Systems under Monotonic and Fatigue Loadings", ASCE Journal of Bridge Engineering, Vol. 10, No. 6, pp. 731-740, 2005.

Rosenboom O. and Rizkalla S., "Behavior of Prestressed Concrete Strengthened with Various CFRP Systems Subjected to Fatigue Loading", American Society of Civil Engineers (ASCE), Journal of Composites for Construction, Vol. 10, No. 6, pp. 492-502,

2006.

Soliman S.M., El-Salakawy E., and Benmokrane B., “Flexural Behaviour of Concrete Beams Strengthened with Near Surface Mounted Fibre Reinforced Polymer Bars”, Canadian Journal of Civil Engineering, Vol. 37, pp. 1371-1382, 2010.

Taljsten B., Carolin A., and Nordin H., “Concrete Structures Strengthened with Near Surface Mounted Reinforcement of CFRP”, Advances in Structural Engineering, Vol. 6, No. 3, pp. 201-213, 2003.

Teng JG., De Lorenzis L., Wang B., Rong L., Wong TN. and Lam L., “Debonding Failures of RC Beams Strengthened with Near-Surface Mounted CFRP Strips”, Journal of Composites for Construction, ASCE, Vol. 10, No. 2, pp. 92-105, 2006.

The International Federation for Structural Concrete (FIB), “Bond of Reinforcement in Concrete”, State-of-art report, August 2000.

Wahab N., Soudki K.A., and Topper T., "Bond of Carbon Fiber Reinforced Polymer Rods to Concrete in Near-Surface Mounted Application under Fatigue Loading," Proc. 2nd Canadian Conference on Effective Design of Structures, Hamilton, Ontario, Canada, pp.195-205, 2008.

Warren GE., Waterfront repair and upgrade, advanced technology demonstration site No. 2: Pier 12, NAVSTA San Diego. Site Specific Report SSR-2419-SHR, Naval Facilities Engineering Service Center, Port Hueneme (CA), 1998.

Yost J. R., Gross S. P., and Deitch M. J., " Fatigue Behavior of Concrete Beams Strengthened in Flexure with Near Surface Mounted CFRP", Proceedings of the 8th international symposium on Fiber Reinforced polymer reinforcement for concrete structures, Patras, Greece , July 16-18, 2007

Yun Y., Wu Y., Tang W. C., "Performance of FRP Bonding Systems under Fatigue Loading,", Engineering Structures, Vol.30, pp. 3129-3140, 2008.